HYDROTHERMAL SULFIDE DEPOSITS ON THE EAST PACIFIC RISE, 21°N

by

MARJORIE STYRT GOLDFARB

A. B., Harvard University

[1977]

SUBMITTED TO THE DEPARTMENT OF
EARTH AND PLANETARY SCIENCES
IN PARTIAL FULFILLMENT OF THE
REQUIREMENTS FOR THE
DEGREE OF

DOCTOR OF PHILOSOPHY

at the

MASSACHUSETTS INSTITUTE OF TECHNOLOGY

June 1982

Signature of Author: _____

Department of Earth and Planetary Sciences
May 21, 1982

Certified by: _____

Roger G. Burns, Thesis Supervisor

Accepted by: _____

Theodore R. Madden, Chairman
Departmental Committee on Graduate Students

HYDROTHERMAL SULFIDE DEPOSITS ON THE EAST PACIFIC RISE, 21°N

by

MARJORIE STYRT GOLDFARB

Submitted to the Department of Earth and Planetary Sciences on May 21, 1982 in partial fulfillment of the requirements for the Degree of Doctor of Philosophy in Earth and Planetary Sciences

ABSTRACT

Hydrothermal vents on the East Pacific Rise at 21°N, consisting of pipelike chimneys built on basal mounds, are actively venting fluid at temperatures up to 350°C. Samples taken from five of these vents revealed the presence of two different types of chimneys, Cu-rich and Zn-rich. Cu-rich chimneys consist of a pipe with a central channelway lined by a monomineralic layer of chalcopyrite or cubanite, with an exterior layer composed of varying proportions of pyrite, wurtzite, anhydrite, Mg-silicates, and Cu-Fe sulfides. Zn-rich chimneys vent slightly cooler fluid and are composed of multiple smaller fluid channels lined by wurtzite, with an exterior mass composed primarily of wurtzite, pyrite, anhydrite, and minor Cu-Fe sulfides. At any one point in any chimney, Zn and Fe sulfides precede and may be replaced by Cu-Fe sulfides.

The chimneys grow as a consequence of mixing between hot hydrothermal fluid, rich in metals and H_2S, and cold seawater. A framework of anhydrite + mixed sulfides formed by mixing is lined by a monomineralic sulfide layer when purer, hotter hydrothermal fluid is segregated in the chimney interior. The initial chimney structure is further developed by continued deposition of the inner lining from more pristine hydrothermal fluid and of the exterior layer by mixing between escaping hot fluid and inflowing seawater. Chalcopyrite and cubanite are deposited from hot, essentially unmixed hydrothermal fluid; Zn sulfides are deposited from cooler solutions after Cu in the fluid has been depleted. Purer hydrothermal fluid coming in contact with previously deposited Zn and Fe sulfides leads to Cu-Fe replacement of the earlier minerals. If the outward flow of hot fluid through the walls is inhibited and seawater comes in contact with massive chalcopyrite, a weathering rind of bornite-chalcocite can develop.

The vent structures may grow by alternations between open venting accompanied by chimney construction and sealed mounds with internal circulation of hot fluid. Periodic fracturing of the sealed mounds allows the chimneys to grow; sealing of the chimneys by precipitates recreates a sealed mound. The structures at a single vent may go through both Zn-rich and Cu-rich stages depending on the degree of mixing at depth and the initial temperature of the hot fluid. Internal circulation within a mound may also segregate Cu-Fe sulfides into the center of the mound and Zn sulfides into the exterior.

Dead vent structures are easily destroyed in ambient seawater by dissolution of anhydrite and oxidation of sulfides. Preservation of a deposit will occur only if it is covered over while it is still fresh or only partially oxidized.

Vents of the 21°N type could form ore deposits of considerable size, with variations in mineralogy depending on the specific setting. Both massive sulfide deposits in ophiolites and Kuroko-type ore deposits resemble preserved versions of the deposits at 21°N.

Thesis Supervisor: Dr. Roger G. Burns, Professor of Geochemistry

Table of Contents

List of Tables

List of Figures

Chapter 1

Introduction

In the spring of 1979, the RISE expedition to 21°N on the East Pacific Rise discovered an area of hot spring activity at the ridge crest. Large plumes of black and white precipitates formed where water at temperatures up to 350°C poured out of strange chimney-like edifices and mixed with seawater as it rose buoyantly through the water column. This discovery was a step forward in the development of the theory that circulation of seawater through hot crust at spreading centers is a major process worldwide. Another cruise to the same site in November 1979 provided hot water samples and samples of the solid material making up the vent structures, which form the subject of this study. The metal-rich nature of the vent materials suggested that the 21°N site provided a glimpse of an ore deposit in the process of formation, an event never before seen in progress. The study of the solid samples was undertaken with a dual aim: to explore the composition and creation of the hydrothermal deposits themselves, and to explore the relationship between the discoveries at 21°N and the formation of ore deposits.

Background

The concept that hot springs were formed by seawater

circulating through hot rocks at mid-ocean ridges became popular about ten years ago, as a likely solution to two particular problems. One of these was a direct consequence of plate tectonic theory. When mid-ocean ridges were recognized as spreading centers where hot new crust is created, high levels of heat flow at the ridge crests were predicted. However, actual measurements of heat flow were consistently lower than calculated. A number of authors proposed hydrothermal circulation as a means of dissipating the heat generated at the spreading centers (see, for example, Lister, 1972; Spooner and Fyfe, 1973; Williams et al., 1974). Wolery and Sleep (1976) combined data from ridge systems around the world and calculated that 32 - 42% of the heat produced at mid-ocean ridges was hydrothermally advected. They calculated a flow rate of $1.3 - 9 \times 10^{17}$ grams of seawater/year based on a mean exit temperature of the heated seawater of 150 - 300°C.

The second motivation for proposing hydrothermal circulation at mid-ocean ridges was the long-standing problem of magnesium balance in the oceans. Element residence times in the oceans are based on the assumption of a steady state, requiring the quantity of an element supplied to the oceans every year to be balanced by the amount removed. For magnesium, no satisfactory removal mechanism had been found. The quantity of Mg taken up by sediments was much smaller than the river input. Hydrothermal alteration provided an answer: Mg could be removed from seawater into altered

basalts. If all the Mg in seawater circulated through basalts was removed, then 1.5×10^{17} grams of seawater/year would have to cycle through the ridges in order to remove enough Mg to balance the river input (Holland, 1978). This figure is in line with Wolery and Sleep's (1976) estimate of the amount of seawater circulation necessary to account for the heat loss at ridges.

A growing belief in the likelihood of seawater circulation at ocean ridges led to a search for evidence. Hydrothermally altered basalts, serpentinites, and greenstones had been dredged from many mid-ocean ridges (see, for example, Melson and van Andel, 1966; Bonatti et al., 1970; Aumento et al., 1971; Humphris and Thompson, 1978). Similar mineral assemblages were found in basalts from the Reykjanes Peninsula in Iceland that had been altered by reaction with seawater at elevated temperatures (Tomasson and Kristmannsdottir, 1972). Hydrothermal brines on the Reykjanes Peninsula were found at temperatures up to 270°C (Mottl and Holland, 1978). Of particular interest for the ore-forming potential of seawater circulation was the discovery that hydrothermal solutions had leached metals from dredged pillow basalts. The crystalline interiors of the pillows alter more readily than the quenched exteriors, and contrasts in composition between the two parts indicated the loss of metals, in particular Fe, Mn, and Co (Corliss, 1971), but also Au and Ag (Keays and Scott, 1976).

Metal deposits associated with ocean ridges and known or presumed to have a hydrothermal origin have in fact been found along ridge systems around the world, although direct evidence of widespread hydrothermal venting at the open ocean ridges has only been accumulating since the discovery of the Galapagos warm springs in 1976. As early as 1966, Bostrom and Peterson noted that sediments from the crest of the East Pacific Rise were enriched in Fe, Mn, Cu, Cr, Pb, and Ni compared to normal pelagic sediments. A hydrothermal origin for the excess metals was proposed by several authors in the early 1970's (Bostrom et al., 1971; Piper, 1973; Dymond et al., 1973; Anderson and Halunen, 1974). When the Deep Sea Drilling Project was launched and sediment cores were obtained that extended down to the seafloor basalts, a basal layer of Fe- and Mn-rich sediment was discovered to exist throughout the Pacific basin (see, for example, Cook, 1971; Cronan et al., 1972; von der Borch and Rex, 1970; von der Borch et al., 1971). This basal layer is assumed to represent ridge crest sediments transported away from the ridge axis by seafloor spreading and buried by later sedimentation. Much of the Fe and Mn in the ridge crest sediments is still believed to be hydrothermal in origin, but many of the other metals are now recognized as a mixture of hydrogeneous deposits scavenged from seawater by the Fe-Mn sediments, and of biogenic deposits and detrital material mixed into the Fe-Mn sediments (Cronan, 1976; Heath and Dymond,

1977).

Hydrothermally deposited metalliferous sediments are also found, but in a different form, in the Atlantic Ocean, where thick crusts of very pure Mn oxides have been interpreted as hydrothermal deposits. Mn crusts were recovered by the French submersible Cyana from the FAMOUS region at 36°N near the axis of the Mid-Atlantic Ridge, where they occur as part of a mound-like deposit in a fracture zone. Although no temperature anomaly was detected anywhere in the FAMOUS region, the Mn crusts collected by the Cyana did come from an area of high heat flow (Thompson et al., 1975).

In 1976 an active hydrothermal field was located at 26°N on the Mid-Atlantic Ridge, where two small temperature anomalies were detected on the east wall of the rift valley (Cronan et al., 1979). This area, dubbed the TAG Hydrothermal Field, is characterized by extremely pure Mn oxide occurring as crusts on and veins in basalt fragments (Rona, 1976). Although metals other than Mn are rare in these deposits, local concentrations of Fe, Zn, and Cu have been found in the vicinity of the two temperature anomalies (Cronan et al., 1979). Similar hydrothermal deposits have been recovered underlying later hydrogenous deposits at distances of up to 60 km from the rift valley (Scott et al., 1975; Thompson et al., 1975). These deposits presumably formed at the ridge and were transported to their present

location by seafloor spreading.

Another significant type of hydrothermal deposit has also been recovered from the Mid-Atlantic Ridge. Cu-Fe and Fe sulfides have been found as disseminated mineralizations and in veins in metabasalts dredged from the Romanche and Vema fracture zones (Bonatti, Guerstein-Honnorez, and Honnorez, 1976), and pyrite concretions with a concentric structure have been dredged from the Romanche fracture zone (Bonatti et al., 1976). Both of these types of sulfide mineralizations are interpreted to be the result of hydrothermal solutions passing through the basalts. More recently, a hydrothermal quartz-sulfide assemblage has been recovered from the east wall of the Mid-Atlantic Ridge at 23.6°N, 10 km south of the Kane fracture zone. This is a brecciated sample showing signs of multiple stages of veining with both quartz and sulfides (Delaney et al., 1980). These mineralizations provide good evidence for the existence of circulating fluids capable of depositing sulfides along the Mid-Atlantic Ridge.

Intensive study of the first active warm water flow at a spreading center began in 1969 when hot brine pools were discovered along the central axis of the Red Sea. The Red Sea is a very young spreading center. Continental crust forms most of the seabed, with only a thin strip of oceanic crust along the ridge axis. Although a number of depressions containing brines have been located, only one, the Atlantis II Deep, shows an active inflow of hydrothermal solutions,

Figure I.1. Location of hydrothermal areas along spreading centers

1. Reykjanes Peninsula
2. Red Sea
3. FAMOUS area, Mid-Atlantic Ridge at 36°N
4. TAG hydrothermal field, Mid-Atlantic Ridge at 26°N
5. Galapagos Spreading Center, 86°W
6. East Pacific Rise, 21°N
7. Guaymas Basin, Gulf of California

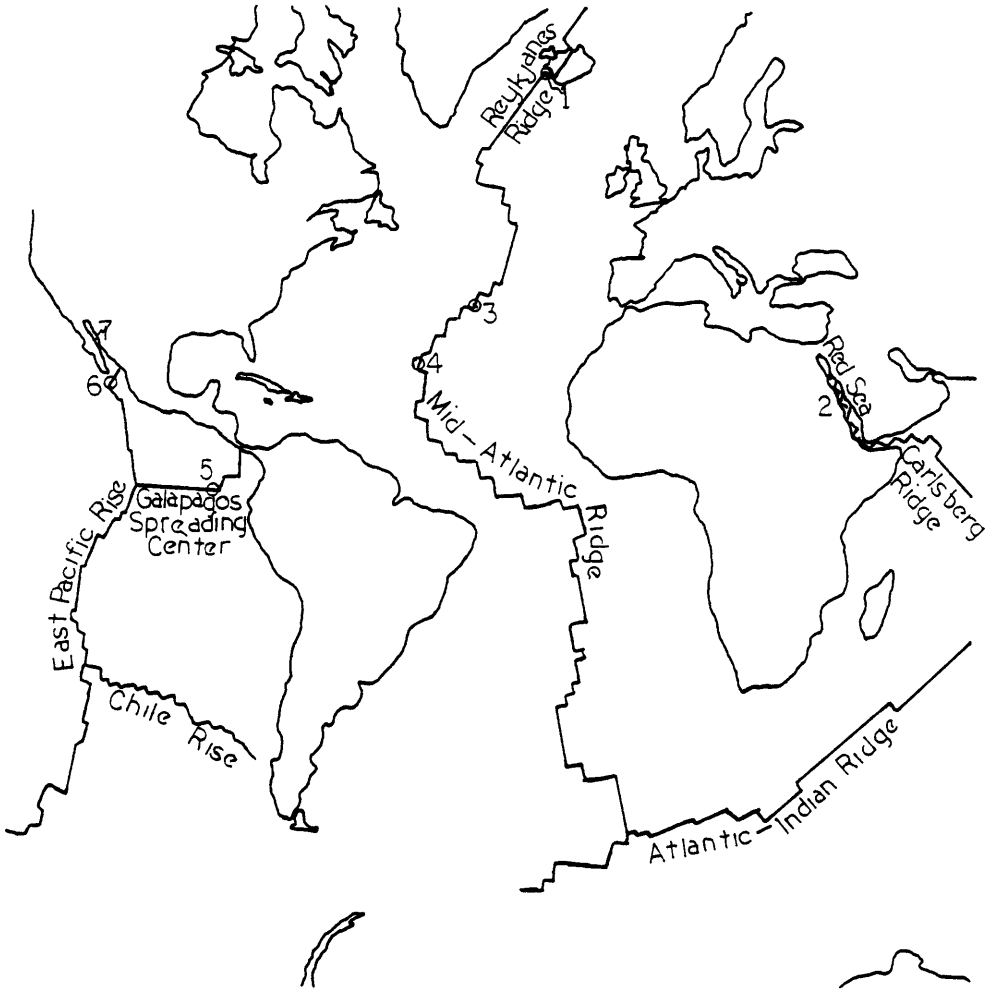
Reykjanes Ridge
1
6
5
Galapagos Spreading Center
East Pacific Rise
Chile Rise
3
4
Mid-Atlantic Ridge
Red Sea
2
Carlsberg Ridge
Atlantic-Indian Ridge

revealed by an increase in temperature with depth. The brines are trapped in the deeps by their density, which is greater than that of seawater.

The Atlantis II Deep contains two layers of brines, a pure hot brine at depth overlain by a layer in which the deep brine and Red Sea water mix (Craig, 1969; Turner, 1969). Sedimentation within the deep has been extensively studied (see, for example, Bischoff, 1969; Hackett and Bischoff, 1973). The sediments consist of units of metalliferous mud, including oxides, sulfides, and carbonates, in which Bischoff (1969) has defined 7 distinct facies.

The maximum temperature of the deep brine in the Atlantis II Deep is 60°C (Shanks and Bischoff, 1977). On the basis of a variety of geothermometers, a range of subsurface temperatures from 150°C to 250°C can be obtained (Schoell, 1976; Fournier and Truesdell, 1976; Sakai et al., 1970). Shanks and Bischoff (1977) have summarized actual observations and modeling of the geochemical system to produce the following sequence of events leading to formation of the Red Sea brines and precipitation of the metalliferous sediments: (1) Normal Red Sea water penetrates down into Miocene evaporates, forming a highly saline brine (156‰). (2) The saline brines are heated to 200 - 250°C and leach metals from hot basalts in the central rift zone. (3) Base metal sulfides are deposited from the cooling brines at the seafloor by reaction with sulfur reduced by interaction with

basalts. (4) Oxide minerals are deposited as the brine cools and slowly mixes with Red Sea water in the deeps.

The Red Sea hydrothermal system differs from circulation systems at open ocean ridges because the presence of evaporite beds leads to the formation of a highly saline brine. This brine is denser than seawater and so remains in the deeps instead of rising buoyantly as the 21°N hot springs do. Although it is an interesting occurrence, the Red Sea system cannot be used as a general case for the formation of hydrothermal deposits at an ocean ridge.

Active hot springs at an open ocean ridge were finally discovered in 1976 along the Galapagos Spreading Center at 86°W. Warm water at 3 - 20°C flows gently from vents swarming with unexpected and previously unknown organisms (Corliss and Ballard, 1977). The warm waters have been extensively studied (Edmond et al., 1979a, b), and will be discussed in connection with the 21°N hydrothermal fluid in the next section. Although basalts at the vents are coated by hydrothermal precipitates (Crane and Ballard, 1980), there are no extensive metal deposits presently forming. However, hydrothermal Mn crusts similar to those from the Mid-Atlantic Ridge have been found on young crust near the axial rift valley (Moore and Vogt, 1976), and a series of hydrothermal deposits have been found in the so-called mounds hydrothermal field located 20 - 30 km off the ridge axis. These deposits are aligned along fracture systems in

areas of high heat flow, roughly parallel to the spreading center. They consist of "mounds," actually, cones and ridges, connected by stripes of Mn crusts, overlying a sediment cover on the basalt floor (Lonsdale, 1977). The mounds are composed of an outer Mn oxide crust and an interior of "green clay" dominated by Al-poor Fe-nontronite (Corliss et al., 1978). When the Mn crust is punctured, warm water (4 - 10°C) flows out of the mounds, indicating the presence of hydrothermal discharge or circulation within the mounds (Corliss et al., 1979). A large scale hydrothermal circulation system for the Galapagos area has been proposed, involving discharge in areas of high heat flow along the ridge and in the mounds hydrothermal field, with recharge between the two areas (Lonsdale, 1977).

In the last several years discoveries of hydrothermal mineral deposits and/or active hot springs at oceanic spreading centers have multiplied. Besides the Galapagos and 21°N springs, hot water, sulfide and sulfate deposits have been found in the Guaymas Basin of the Gulf of California (Lonsdale and Elders, 1981; Lonsdale et al., 1980). Ferro-manganese crusts and nontronite resembling the deposits in the FAMOUS area and the Galapagos mounds have been found on the Explorer Ridge in the northeastern Pacific (Grill et al., 1981). Other evidence for widespread hydrothermal circulation comes from plumes of excess ^{3}He in deep ocean waters, which have their origin in hydrothermal vent waters.

^{3}He enrichments indicate hydrothermal activity in the TAG field (Jenkins et al., 1980), along segments of the East Pacific Rise between 15°N and 7°S (Boulegue et al., 1980), and near 12° - 15°S (Craig et al.,1980). Hydrothermal circulation of seawater at ridges is clearly a major process with immense ore-forming potential; the maximum size of any one area of hot spring activity is unknown, but almost certainly larger than any yet seen (Craig et al., 1980).

Hot Spring Composition

The fluid venting as hot springs at spreading ridges is naturally a subject of great interest. It is, in effect, an ore-forming solution that can be sampled and analyzed along with the deposits it forms, an opportunity not available in the case of most metal deposits.

The first hot water samples collected at 21°N in November 1979 were of uneven quality. All of them were mixed with seawater to some extent, and the composition of the pure fluid had to be deduced by extrapolating plots of composition against temperature to the temperatures measured in the chimney openings. Since precipitation occurs rapidly when the hot fluid mixes with seawater, and since precipitates were also trapped in the water samples, the possibility of inaccuracies remains, especially in the metal and reduced sulfur concentrations, which are of particular in-

Table I.1. Composition of Hydrothermal Fluids
(units = mmol/kg, except as noted)

	Clam-bake [a]	Garden of Eden	Dande-lions	Oyster Beds	Experi-mental 400°C [b]	Rey-kjanes [c]	21°N [d]
T°(c)	350	350	350	350	400	270	350
pH					3.6-4.1	5.0	3.4
Ca	40.2	34.3	34.3	24.6	29.1-52.0	39	~20
Mg	0	0	0	0	0.3-0.5	0.04	0
ΣS_{OX} [f]	2.23[e]	2.23[e]	2.23[e]	2.23[e]	2.71-6.19	0.31	<1
H_2S	~2.8	~6.7		~11	5.92-7.27 [g]	0.92	6.5-9
Si	21.88	21.88	21.88	21.88	25.1-28.7	10.2	21.5
Fe	scattered (variable)				78-118 ppm		~100 ppm
Na	487	451	313	259	470-514	354	~470
Cl	595	543	395	322		460	~540

[a] Edmond et al., 1979a, b (Galapagos vents); extrapolation

[b] Mottl and Holland, 1979; Mottl et al., 1978

[c] Ellis, 1979; Well 8 Reykjanes

[d] K. von Damm, personal communication; figures based on extrapolation from compositions of mixed solutions; H_2S obtained from pure hot solution.

[e] Extrapolates to zero at 380°C

[f] ΣS_{OX} = total oxidized sulfur

[g] ΣS_R = total reduced sulfur

terest for studying the sulfide deposits. Purer water samples were collected in November 1981, and should provide better data, but in the meantime some results of the original analyses are given in table I.1. The salinity of the fluid remains very similar to that of seawater, which is a major difference between this fluid and the Red Sea brines.

The Galapagos warm spring waters are the only other ridge crest springs studied to date. Analyses of the warm waters revealed that the concentrations of most elements showed a linear relationship with temperature (Edmond et al., 1979a, b). The linear trends are interpreted as the result of subsurface mixing between a pure hydrothermal solution and seawater. Since Mg is likely to be quantitatively removed from solution during the reaction of heated seawater with basalt, the temperature of the pure hydrothermal solution was estimated to be ~350°C, in order to be consistent with the Mg concentration, which extrapolates to zero at 344°C. Table I.1 gives extrapolated compositions of the solution at 350°C for each of the 4 Galapagos vents.

The similarity between the 21°N and Galapagos endmember fluids is almost certainly due to their similar formation from seawater circulating through basalts at elevated temperatures. The major characteristics of the solutions have been obtained in experimental studies of seawater-basalt interactions at temperatures between 200°C and 500°C (Bis-

choff and Dickson, 1975; Hajash, 1975; Mottl, Corr and Holland, 1974; Mottl, 1976; Mottl and Holland, 1978; Mottl, Holland and Corr, 1979). In all these experiments, Mg^{++} was rapidly removed from solution. The Ca^{++} concentration increased to over twice its initial value after a rapid decrease as a consequence of anhydrite precipitation as the seawater was heated. A rapid decrease in SO_4^{--} also resulted from anhydrite precipitation and from the reduction of SO_4^{--} during reaction with basalt. Fe and Mn increased with temperature over the entire range studied. The Fe:Mn ratio also increased, from about 1 at 300°C to about 7 at 500°C.

These particular experiments were conducted at water:rock ratios between 1 and 10, under rock-dominated conditions. At water:rock ratios of 50 or over, conditions in the system become water-dominated and the solution chemistry alters considerably (Mottl and Seyfried, 1980). Although a water:rock ratio cannot be determined as easily in a real system as in an experiment, Craig et al. (1980) have deduced a water:rock mass ratio close to 1 in the system at 21°N based on a $\delta^{18}O$ shift of +1.6‰ in the 350° solution. In a system with a low water:rock ratio, high concentrations of heavy metals and H_2S can only be obtained at temperatures in the 400° - 500°C range (Hajash, 1975; Seyfried and Bischoff, 1981). The composition of experimental solutions obtained in experiments with low water:rock ratios at 400°C

is given in Table I.1 for comparison to the composition of the 21°N and Galapagos hydrothermal fluids.

The similarity of the observed hydrothermal solutions to the solutions resulting from seawater-basalt reactions does not rule out contributions from "magmatic" fluids in the natural solutions. Some mantle contribution is indicated by high $^{3}He/^{4}He$ ratios in the vent waters (Craig et al., 1980).

Vent Descriptions

The active hydrothermal vents discovered at 21°N by project RISE occur in an area 6.2 km long and 100 - 200 m wide within the axial zone of the East Pacific Rise (see figure I.2). Twenty-five active vents emitting water at temperatures between 20°C and 350°C were identified from thermal anomalies and submersible observations (Spiess et al., 1980). The vent areas are usually located several hundred meters apart. Each vent area may contain one or more hot spring outlets. Samples from five different vent areas at the high end of the temperature spectrum were collected in November 1979; project RISE had previously taken samples from other hot vents in the area, and additional sampling was done in November 1981. In general, the hot springs are located in the southwestern part of the 21°N area, while warm springs are located farther to the north-

east.

The warm springs closely resemble the springs found at the Galapagos Spreading Center. They have a large biological population, and emit water at temperatures near 20°C (Spiess et al., 1980). The hot springs, however, form a new type of hydrothermal vent.

The hot spring waters enter the seawater environment at temperatures up to 350°C. Because the hydrothermal solution is close to seawater salinity but much hotter, it is less dense than the surrounding 2°C seawater, and so rises buoyantly, entraining seawater as it rises. The plume produced in this way is highly visible as the result of the formation of a cloud of fine-grained precipitates during mixing between the hot fluid and seawater. The hydrothermal fluid itself is clear and colorless (J. Edmond, personal communication). The precipitates in the cloud have been called "smoke," giving rise to the designation of the vent structures as "smokers" (see figure I.3).

The structures forming the vents consist of two parts, basal mounds and chimneys built on top of the mounds. The mounds form directly on basalt pillows or flows. They are up to 15 by 30 meters in plane section and 2 m or more in height. The mounds consist of two major types of material. One, described by Haymon and Kastner (1981), is an aggregate of Fe, Zn, and Cu sulfides crosscut by worm tubes up to 2 cm in diameter. Most of these worm tubes have been mineralized

Figure I.2. The vent field at 21°N on the East Pacific Rise, showing bathymetry, the zone of youngest volcanism, and the area of active vents. The area of dead vents discovered by the CYAMEX expedition is shown to the northeast. After Haymon and Kastner, 1981.

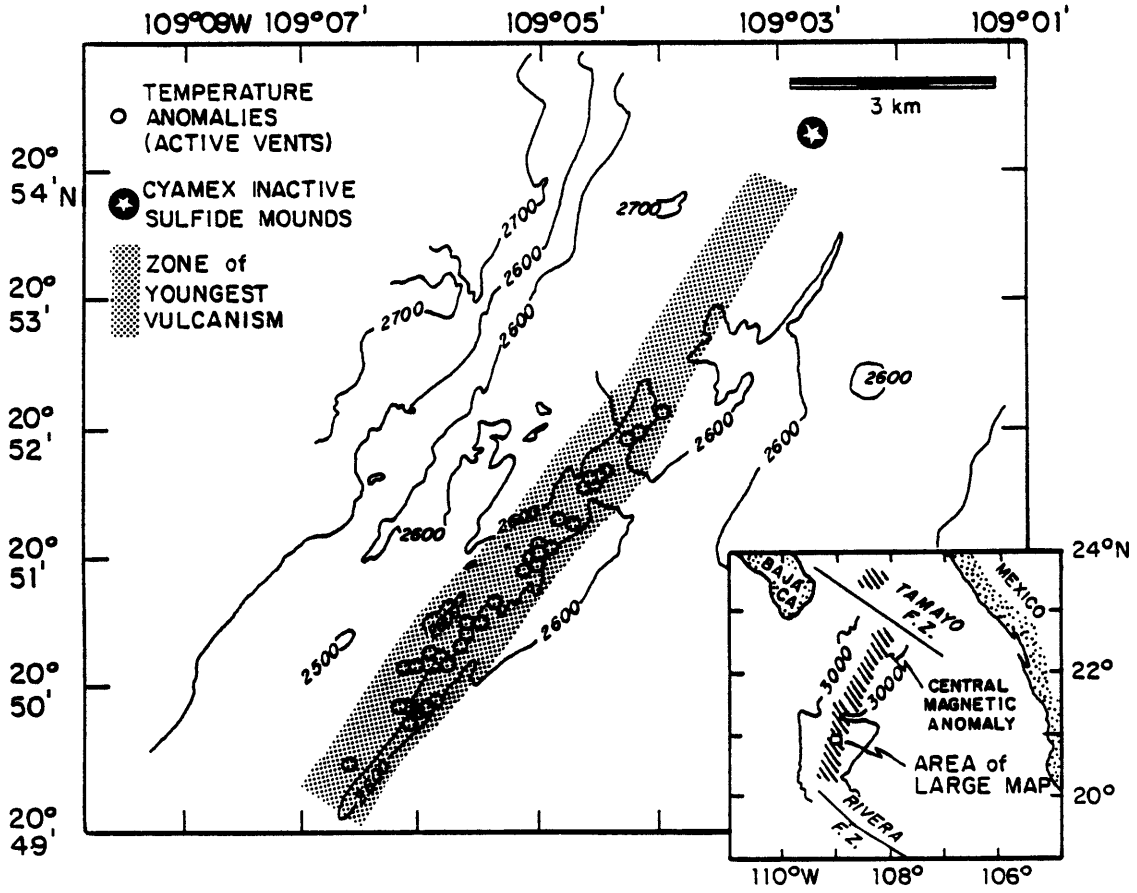
109°09W 109°07' 109°05' 109°03' 109°01'
TEMPERATURE ANOMALIES (ACTIVE VENTS)
CYAMEX INACTIVE SULFIDE MOUNDS
ZONE of YOUNGEST VULCANISM
3 km
20° 54'N
20° 53'
20° 52'
20° 51'
20° 50'
20° 49'
2700
2600
2500
BAJA CA.
TAMAYO F.Z.
MEXICO
CENTRAL MAGNETIC ANOMALY
AREA of LARGE MAP
RIVERA F.Z.
3000
24°N
22°
20°
110°W
108°
106°

and are coated with thin layers of sulfides, amorphous silica, barite, and sulfur (Haymon and Kastner, 1981), but some, which are unmineralized, still contained the remains of pompey worms which apparently were alive at the time the samples were taken. The second type of material making up the mounds is a soft sulfide mud, easily sampled with a scoop sampler (D. Converse, personal communication). The surfaces of the mounds are usually oxidized, and consequently appear ochre, orange, red, and black on the surface (Haymon and Kastner, 1981).

The chimneys surmounting the basal mounds are 1 to 5 meters in height. Both dead chimneys, which are no longer venting any water, and live or active chimneys are found in the area. Active chimneys are classed as "black smokers" or "white smokers" depending on the color of the precipitates in the plume above the chimney, but the division is not always clearcut.

Black smokers are generally pipelike in form, with pipes up to 30 cm in diameter (Spiess et al., 1980). They are not densely inhabited, although some organisms have been found on samples from black smokers. The fluid exiting from these vents is the hottest seen, and flows the most rapidly. The black smoke consists largely of hexagonal plates of pyrrhotite, with pyrite, sphalerite, and Cu-Fe sulfides. The pyrrhotite composition suggests a formation temperature near 300°C (Spiess et al., 1980). All the chimneys

Figure I.3. A black smoker at 21°N. The mechanical arm of Alvin is visible in the foreground. Photo by H. D. Holland.

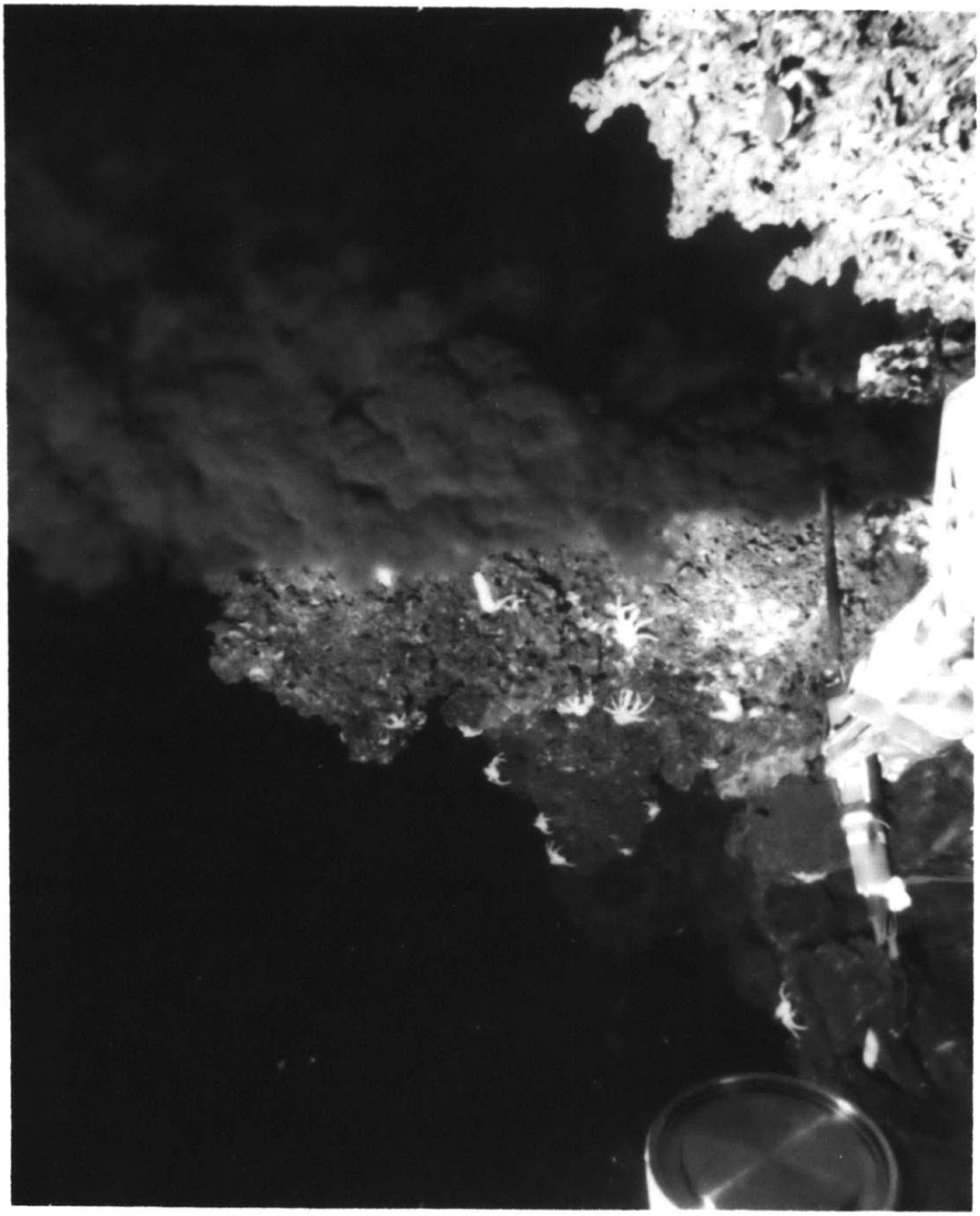

collected in November 1979 are from black smokers. The temperatures measured in the mouths of the sampled vents ranged from 270°C to 355°C.

White smokers are apparently slightly cooler than black smokers; Spiess et al. (1980) place the temperature of the exiting fluid at 32 - 330°C, which would overlap with the lower range of exit temperatures at black smokers. The flow rates are also slower, and the white smokers support a dense biota (Spiess et al., 1980). The structures of these vents vary from chimneys to a type known as a "snowball," which appears to be spherical as a result of an encrustation of white tubes of living polychaete worms (Haymon and Kastner, 1981). The white smoke for which the chimneys are named consists of amorphous silica, barite, and pyrite (Spiess et al., 1980).

The dense biota surrounding the hydrothermal vents both at 21°N and at the Galapagos is one of the unexpected bonuses of these discoveries. An entire population of new species of organisms lives on the vents. The larger, more obvious organisms at 21°N include unusual fish, the spectacular red and white tube worms that live in 3 - 23°C water, galatheid crabs, brachyuran crabs, and large clams with blood-red flesh (Ballard and Grassle, 1979). Among the smaller organisms are barnacles belonging to a new genus, three different archaeogastropod limpets, polychaete worms which may be a new family (Spiess et al., 1980), and pompey worms

whose tubes encrust the basal mounds of the vents. On the smallest scale, bacteria live at high temperatures in the vent waters (J. Baross, personal communication). Many of these new species of life are still unclassified. Certainly their contribution to the formation of mineral deposits at the vents has great but unknown potential.

Although the active vent areas present the most exciting new area of study, the first discoveries near 21°N were a group of extinct vents farther to the northeast and 700 - 800 meters west of the axis of the East Pacific Rise found by the CYAMEX expedition in 1978 (Francheteau et al, 1979; Hekinian et al., 1980). These deposits have been considerably altered and oxidized by exposure to ambient seawater, and provide valuable evidence of the destruction of the 21°N type of deposit after hydrothermal circulation through the vents ceases. A comprehensive description of the extinct vents is contained in Hekinian et al. (1980). In brief, the altered deposits consist of a sulfide material rich in pyrite and marcasite, accompanied by Zn and Cu-Fe sulfides, Fe-oxide phases, and silicates, but almost lacking in sulfates of any kind. A more detailed description will be given when the death of an active vent is discussed later.

Chapter II

Sample Collection and Analysis

Collection

Solid samples were collected from five hydrothermal vents situated within a 1.5 km long area along the ridge axis of the East Pacific Rise (figure II.1). On each of the five dives, chimney and mound samples were broken off using the mechanical arm on Alvin and collected in baskets on the front of the submersible. Samples from different vents were separated in different baskets. Temperature measurements were made with a thermocouple probe with a continuous readout.

After Alvin returned to the surface at the end of each dive, the solid samples were separated according to location and transported to R/V Gilliss for further examination. On board the Gilliss the samples were numbered and photographed immediately. The following morning, the samples were placed on deck to dry in the sun. To check on the effects of drying the samples as opposed to packing them damp, one sample, half of a larger piece, from the first dive was placed in a plastic bag while it was still damp. The damp sample quickly began to tarnish and oxidize, while the dry piece did not. Thereafter, all samples were allowed to dry thoroughly before being packed. When the rocks were dry, they were photographed again, and then were placed in plastic bags for tem-

porary storage.

At the end of the cruise the rocks were wrapped in paper towels and placed in plastic bags, which were then filled with nitrogen and sealed. When the samples arrived at Harvard, they were all intact. A few of the largest pieces collected on the last dive, which had been packed while they were still damp, were oxidized on the surface. The other samples all appeared to be unaltered. They have been stored in nitrogen since then, to maintain their original condition as closely as possible. A total of nearly 400 kg of solid samples was collected on the five dives, including chimney samples, a few mound samples, two scoop sediment samples from the base of the vents, and a small quantity of very fresh, unaltered basalt.

Shipboard Analysis

Hand samples were examined on board R/V Gilliss with the aid of a binocular microscope. Initial descriptions of the samples were made, and any features of particular interest noted for further examination. Many of the samples contained abundant evidence of organizms living in or on the chimneys, in the form of worm tubes or burrows, or actual worms. Gastropod shells were found on two samples during examination of the pieces. In addition, the samples smelled strongly of H_2S when first collected. In many cases H_2S was still de-

Figure II.1. Relative locations of the five vents sampled in November 1979; coordinates are from the transponder net used to navigate Alvin.

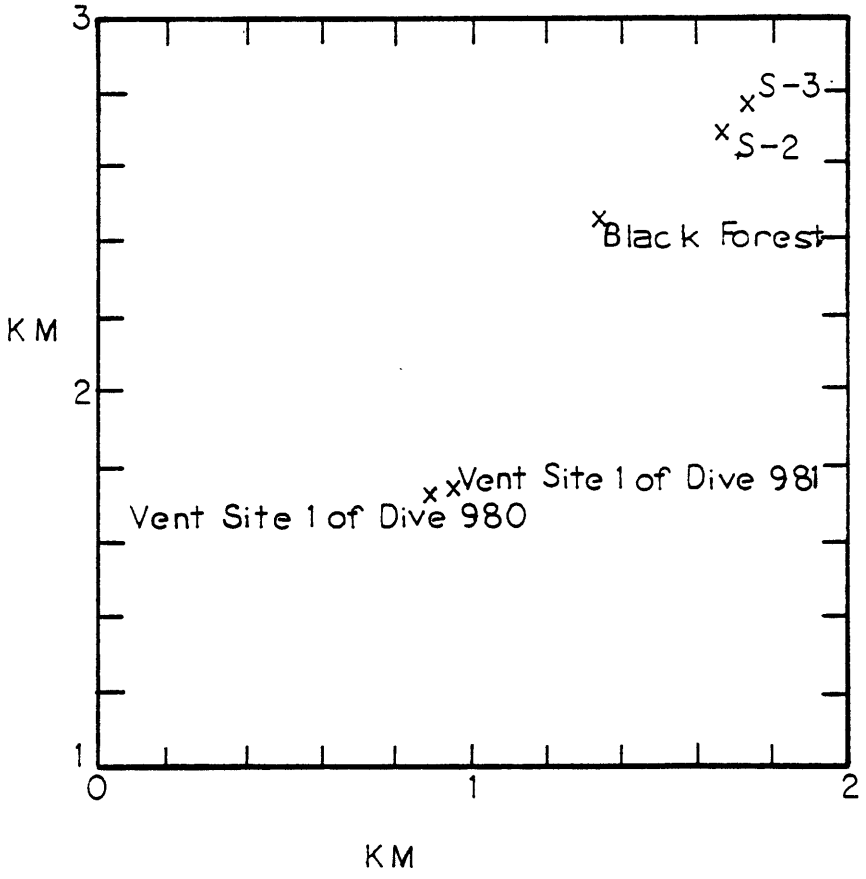
3
2
1
KM
0
1
2
KM
S-3
S-2
Black Forest
Vent Site 1 of Dive 981
Vent Site 1 of Dive 980

tectable several days later.

Semi-quantitative analyses of a number of samples were obtained with a portable X-ray fluorescence spectrometer, designed and operated by Benton C. Clark of Martin Marietta Aerospace. The spectrometer was originally designed for in situ analysis of fine regolith sediment on Mars (Clark et al., 1977). It uses radioisotope excitation sources (^{109}Cd and ^{55}Fe) and miniature proportional counters. No sample preparation is required. Detection limits vary from element to element and with matrix composition; for some elements, such as Sr, the detection limit is as low as 30 ppm. An area 1 cm in diameter is exposed to the counters for analysis.

X-ray fluorescence spectra were obtained from samples from each vent. Analyses were made on separate layers of one sample whenever possible. A semi-quantitative composition scale for the minerals in the samples was established by comparisons with spectra obtained from standard minerals, including sulfides, sulfates, and silicates. An example of the results obtained from the XRF analysis is shown in figure II.2.

With two exceptions, no peaks from trace elements were observed in any of the XRF spectra obtained on board ship. However, Sr was common at the parts per million level, usually accompanying Ca in anhydrite. Pb occurred rarely, and in irregular spots. Since the cruise, several samples have

examined with a high resolution detector at Martin Marietta Aerospace in Denver, and no additional trace elements were detected (B. C. Clark, personal communication).

Techniques of Analysis

Laboratory analysis of the 21°N samples has included studies using the scanning electron microscope (SEM), electron microprobe, and X-ray diffraction (XRD) powder camera. XRD work was carried out at MIT, using a Gandolfi camera with an Fe target and Mn filter. Samples were ground and packed in glass capillary tubes 0.3 mm in diameter for mounting in the camera. Exposures of 12 to 18 hours produced the optimal results. Some exposures of up to 24 hours were run, but no significant improvement in the quality of the lines was observed, nor was there any increase in the number of visible lines.

SEM analysis was performed at the Smithsonian Astrophysical Observatory, using a Cwikscan/100, Field Emission Scanning Electron Microscope at an operating voltage of 18 Kv. X-rays were collected from carbon-coated samples with a KEVEX X-ray energy spectrometer. The spectra produced gave qualitative analyses of the material, which were used in conjunction with the morphology of the crystals to deduce the mineralogy of the samples. To aid in the mineral identification, X-ray spectra were collected from standards of pyrite, pyrrhotite, chalcopyrite, cubanite, wurtzite, sphal-

Figure II.2. Typical XRF spectra, obtained from sample 980-R-12. (a) The outermost part of the mixed sulfide layer on the main chimney piece, rich in pyrite. (b) The inner part of the mixed sulfide layer, rich in ZnS. (c) The inner layer of the main chimney, rich in chalcopyrite. Spectra courtesy of B. C. Clark.

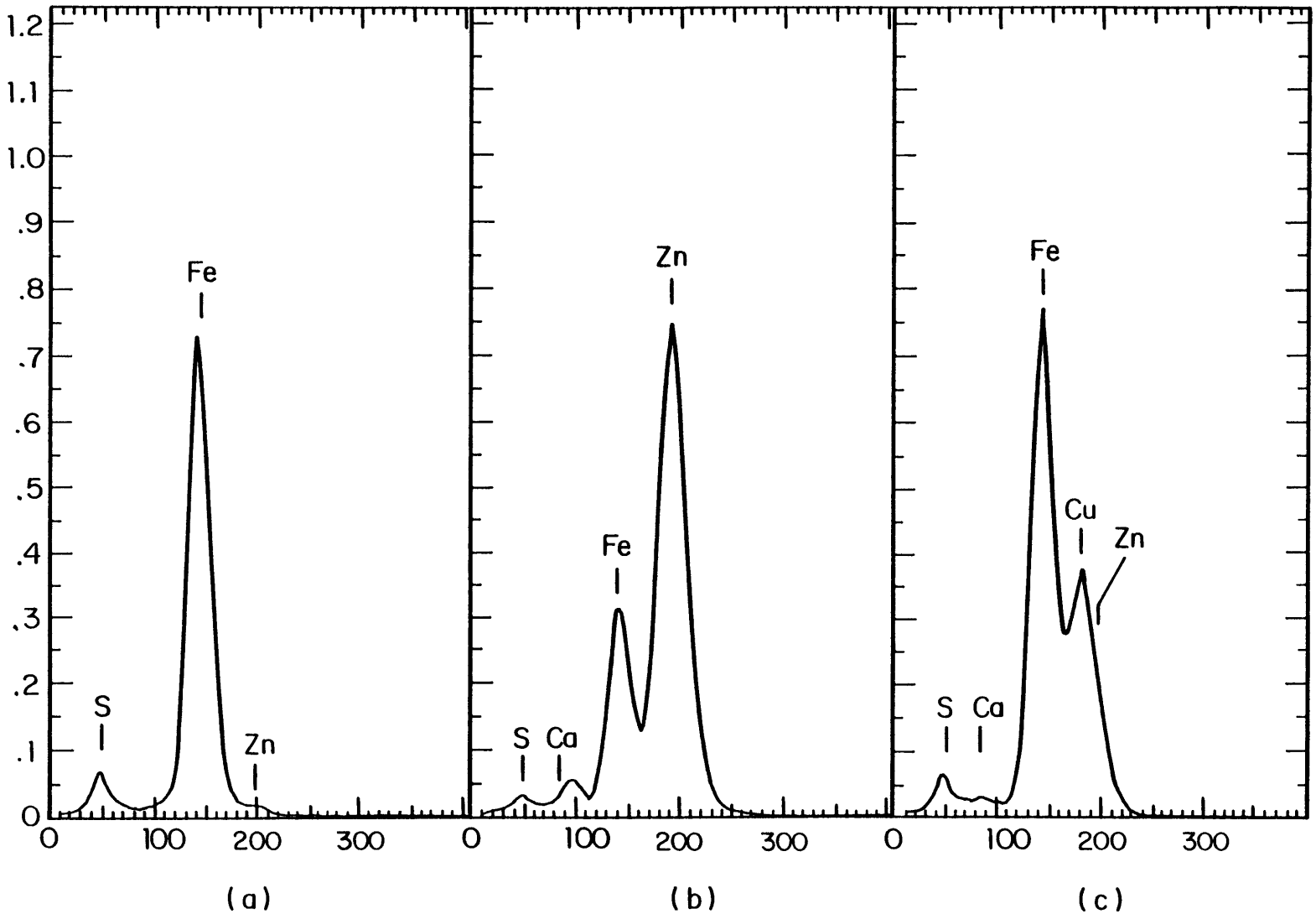
1.2
1.1
1.0
.9
.8
.7
.6
.5
.4
.3
.2
.1
0
S
Fe
Zn
S
Ca
Fe
Zn
S
Ca
Fe
Cu
Zn
0
100
200
300
(a)
(b)
(c)

erite, marcasite, talc and anhydrite. A consistent difference in the peak height ratio of Cu to S could be used to distinguish between chalcopyrite and cubanite. For pyrite and pyrrhotite, the peak height ratio of Fe to S varied linearly with dead time. When dead time was noted during analysis, pyrite and pyrrhotite could be distinguished on the basis of the Fe to S ratio.

Quantitative analyses of minerals were obtained primarily at Harvard University, using two electron microprobes. An ARL model E X-S electron microprobe was operated at an accelerating potential of 15 Kv, a sample current of 0.02 microamps, and a count time of 30 seconds up to a maximum of 60,000 counts. The Ziebold-Ogilvie correction scheme was used for analyses of sulfides and silicates, and Magic corrections for sulfates. Analyses were performed for Fe, Cu, Zn, Mn, Ni, Co, Cr, S, Ca, Ba, Sr, Al, Mg, and Si. Additional analyses were obtained using a Cameca electron microprobe with SEM capabilities and an X-ray spectrometer in addition to the quantitative analysis program. The Cameca microprobe was operated at an accelerating potential of 20 Kv and a sample current of 0.015 microamps. Analyses on this microprobe included Pb but omitted Mn, Ni, Co, and Cr from the sulfide analyses.

Polished thin sections and doubly polished thin sections of all the chimneys were studied in reflected and transmitted light. Mineral identifications were correlated

with the compositions obtained from microprobe analysis of the same sections, and textural relationships between minerals and across the chimneys were studied.

Hand Sample Descriptions

Even in hand specimen the samples from each of the five vents are at least slightly different. Within one vent area the samples generally exhibit minor variations but still allow the deduction of a coherent generalized chimney structure. For two vents in particular, vent site 1 of dive 981 and the Black Forest, the abundance and variety of samples permit the creation of a good chimney model. For the other three vents, a generalized chimney structure can be deduced, but the picture is much less complete. This is the consequence of the limited number of samples collected at vent S-2 and of the uncertainty of the location of the samples in the actual chimneys at vent S-3 and vent site 1 of dive 980. The large scale models based on the hand samples establish two classes of chimneys that will be retained throughout further analysis of the vents.

Vent S-2

Vent S-2 is represented by only five samples, collected during dive 978, the first of the five dives. The top of

this chimney had been sampled during the RISE expedition, and is also referred to as the National Geographic Vent. Since the upper part of the chimney had been broken off earlier, the samples collected in 1979 actually come from nearer the base of the chimney than any of our other samples. Three of the five samples were broken directly off the chimney; one was identified as coming from the uppermost edge of the structure. The other two apparently come from the upper part of the mound or the base of the chimney.

Sample 978-R-3, from the upper edge of vent S-2, consists of layers of golden sulfide, black sulfide, and white silicate and sulfate (see figure II.3). Most of the piece is composed, in hand sample, of four layers: a thin, very finely crystalline, sugary-looking black coating on an interior golden colored layer 3 - 8 mm wide, and an outer black band and white band which tend to intermingle. The exterior surface of the sample is altered to a rusty color. At the upper end of the sample another pair of bands separates from the main golden layer, producing an alternation of golden and black colors: the fine dusting of black on the interior surface is succeeded outward by a thin golden band 1 - 1.5 mm thick, then a narrow black band or line blending into the black coating on the principal layer of golden sulfide.

The dominant mineralogy of the piece and of the other two pieces from this chimney is straightforward, but unique

to this vent. The golden sulfide is cubanite, $CuFe_2S_3$, and the black sulfide layer consists of a mixture of pyrite and wurtzite. The white layer contains Sr-bearing anhydrite, and a Mg-silicate mixture to be discussed later. The exterior alteration is a limonitic Fe oxidation.

The other two samples from the chimney of vent S-2 are actually two halves of one piece: they can be fitted together perfectly. They consist of a brassy golden-colored interior layer of cubanite ranging in thickness from 1.5 mm to 1.5 cm. A very fine dusting of black sulfide (apparently wurtzite ± pyrite) covers the cubanite layer in these samples as in 978-R-3. A thicker exterior layer, also dark in color, consists of a fine-grained mixture of yellowish to silvery and black sulfides (pyrite and wurtzite) with white minerals, dominantly anhydrite. The anhydrite is intermeshed with the sulfides and also forms thin bands within the exterior layer. The outermost surface of these pieces is marked by the remains of pompey worm tubes, suggesting that the samples come from a location in the chimney below 978-R-3, which lacks worm tubes, but above the mounds, which are abundantly inhabited by the pompey worms.

The remaining two samples from vent S-2 apparently come from the top of the basal mound. One consists predominantly of a mass of pompey worm tubes, often with rusty orange surfaces containing Fe oxides. Between and around the worm tubes is a fine-grained black material consisting of wurt-

Figure II.3. Sample 978-R-3 from vent S-2. The sample is 9 cm long and up to 2 cm thick; it is composed of layers of cubanite, wurtzite, and anhydrite + mixed sulfides (see text). Photo A. Dionne.

zite, pyrite, and anhydrite. This black material makes up the bulk of the other sample, which is abundantly coated with worm tubes. Larger concentrations of anhydrite show as white patches in the pyrite-wurtzite mixture. There are also seams cutting the fine-grained sulfide mass, which are lined with hexagonal wurtzite crystals up to 1 mm across. This type of wurtzite mineralization is much more common in two of the other vent areas, S-3 and vent site 1 of dive 980.

The chimney structure at vent S-2 consists basically of a cubanite interior and a mixed sulfide, sulfate, and silicate exterior. Since there are so few samples from this vent, all the samples were studied, and were assumed to be representative of the chimney as a whole. In comparisons to other vent structures, the atypical location of these samples in the chimney compared to the samples from other vents must be kept in mind.

Vent Site 1 of Dive 981

A much larger number of samples was recovered from vent site 1 of dive 981: 23 chimney samples, 1 from dive 980 and the rest from dive 981, plus 1 scoop sediment sample from the base of the vent. The vent area includes two chimneys about 20 feet apart; pieces from the two chimneys were not separated during sampling. Most of the pieces conform to

one hand sample description, but two principal variations on the dominant type do occur, which probably reflects the inclusion of two chimneys in the sampling. One particular piece, 980-R-12, includes a chimney tip which was venting hot fluid at the time it was collected, and therefore merits special attention.

Most of the samples from this vent conform to a single pattern (see figure II.4). The inner wall of the chimney is composed of chalcopyrite, ranging in grain size from very fine to 1 - 2 mm across, in a layer up to 2 cm thick. The surface of the inner wall varies from a smooth curve with a faceted appearance resulting from the interlocking surfaces of chalcopyrite crystals, to a convoluted surface resulting from knobs of generally coarse chalcopyrite extending into the channelway. The knobs are infoldings of a chalcopyrite layer 1 - 2 mm thick and are usually hollow inside. Thin incursions of white anhydrite into the chalcopyrite layer are visible. Clumps of white material occur at irregular intervals on the inner surface of the wall. These clumps can be cleanly detached from the underlying chalcopyrite. They are composed of a mixture of anhydrite and Mg-silicates, and often appear fibrous when broken open. Dusty looking patches in the white material are caused by a coating of very fine-grained Fe and Zn sulfides.

To the exterior of the chalcopyrite layer in most of the samples is a dark-colored layer of mixed sulfides (py-

rite and wurtzite), anhydrite, and silicates. This layer may reach a thickness of several centimeters; it forms the most massive part of some samples from the chimney. Because the layer is dark in color, anhydrite concentrations appear as prominant white streaks and patches. On cut surfaces, pyrite-rich bands stand out as silvery reflective streaks.

A different outer layer occurs in many of the samples. This is a white-colored layer consisting of anhydrite and Mg-silicates with minor sulfides often imparting a dusty look to the material. Small patches of green chrysotile occur on the outermost surface of some pieces. The composition of this layer is very similar to that of the clumps on the interior wall of the chimney. Like the other outer layer, it reaches a thickness of several centimeters on some samples.

The major variations in samples from this vent involve the presence and absence of the two outer layers. In general, a chimney piece will have a thick outer layer of either the dark or the white material, but will have only a thin layer or none of the other. A few samples do not include complete cross-sections of the chimney; these invariably consist of broken-off pieces of the white anhydrite-dominated material.

Sample 980-R-12 is the most useful piece recovered from any vent. It consists of a small tube 12 cm long

Figure II.4. Sample 981-R-6, from vent site 1 of dive 981. The interior layer of this sample is composed of chalcopyrite, the exterior of anhydrite + mixed sulfides. The white material on the interior is a mixture of anhydrite and Mg-silicates. The piece is 10 cm across. Photo A. Dionne.

branching off a larger chimney cavity (figure II.5). At the time the sample was collected, hot water was venting through the small tube as a side vent off the main chimney. A detailed description of this specimen in hand sample reveals some of the complexity of a growing chimney.

At the uppermost edge of the tube part of 980-R-12, the active tip of the chimney, there is a narrow (< 1 mm) zone of very fine grained black material streaked with white. This is an area dominated by anhydrite coated and mixed with fine grained wurtzite and pyrite, which give the material its dark color. Just below the tip a very fine grained layer of chalcopyrite appears on the inner wall of the tube. Downward into the tube the chalcopyrite layer thickens and the grain size of the chalcopyrite increases; at the end of the tube adjoining the main chimney cavity the chalcopyrite layer is 1 cm thick and composed of grains 1 - 2 mm across. The black and white exterior layer, composed of anhydrite, silicates, wurtzite, and pyrite, also thickens downward in the tube, so that the total width of the tube walls increases from 1 mm to 3 - 5 cm. At the base of the tube a clump of the white anhydrite-silicate mixture described previously occurs on the inner wall of the tube. The exterior of the tube shows a rusty limonitic alteration on the outer surface of the mixed sulfide and sulfate layer.

The wall of the main chimney piece attached to the small

Figure II.5. Sample 980-R-12. Photos A. Dionne.

Upper photo: lower end of small tube, outside diameter = 7.3 cm

Lower photo: upper end of tube, maximum width = 5.3 cm

For mineralogy, see text.

tube is predominantly composed of the wurtzite-pyrite-anhydrite mixture, in a porous layer 3 - 4 cm thick. A certain degree of compositional layering is observable, as pyrite is more abundant towards the exterior of the layer and wurtzite is more abundant toward the interior. A thin layer of fine-grained chalcopyrite coats the interior wall of the cavity. The exterior is marked by pompey worm tubes and by yellow to white stains in linear arrays around the worm tube imprints in the black layer.

Sample 980-R-12 will be used extensively as a basis for constructing a model of chimney growth, because it presents a complete section from a new chimney tip to an apparently well-developed chimney wall. The other samples chosen to be "typical" of vent site 1 of dive 981 consist of an interior chalcopyrite layer and exterior layers varying from a thick mixed sulfide-sulfate layer (981-R-2) at one extreme to a thick anhydrite-silicate layer with very little intermixed sulfide (981-R-22) at the other. The "typical" samples were studied closely; a number of others were quickly surveyed to ensure that the conclusions reached on the basis of the study of the "typical" samples were in fact applicable to the full range of samples.

Black Forest Vent

The Black Forest vent was the most spectacular looking

vent visited; at least five separate chimneys rose from one basal mound. Twenty-one samples were collected, 3 on dive 979 and 18 on dive 982, plus one scoop sediment sample from the base of the chimneys. The samples from dive 982 are all pieces of one chimney, which broke into many pieces during the collection process. The 3 samples from dive 979 are probably from a different orifice, but no observable differences exist between the two sets of chimney pieces.

The Black Forest vent samples are remarkably constant in appearance and composition (figure II.6). The walls of these chimneys are very thin, only 2 mm to 1 cm wide. All but the outer 0.5 - 2 mm of the wall consists of a layer of chalcopyrite, varying in grain size from very fine to 1 mm across. As at vent site 1 of dive 981, the surface of the inner wall varies from smooth to convoluted, and has the same hollow infolded chalcopyrite knobs. The outer rim of the chimney is composed of a bornite-chalcocite solid solution up to 2 mm thick. This rim is usually visible as a dark, purple to blue edge on the chimney pieces, but occasionally it is sufficiently thin that it is invisible in hand sample. In a few rare areas it is entirely absent. The rim can be broken off quite cleanly from the interior chalcopyrite.

Anhydrite, silicates, wurtzite, and pyrite are all rare in the Black Forest samples. Masses of the white sulfate-silicate material found in vent site 1 of dive 981 do occur

Figure II.6. Sample 982-R-2 from the Black Forest. The chimney wall is composed predominantly of chalcopyrite, with a thin rim of bornite-chalcocite solid solution. The white material is a mixture of anhydrite and Mg-silicates. The sample is 22 1/2 cm long. Photo A. Dionne.

on the inner walls of some samples, and inside some of the chalcopyrite infoldings. This material also occurs rarely in the outer part of the chimney wall, but most of the samples contain no visible layer of sulfate, silicates, or sulfides other than chalcopyrite, bornite and chalcocite. In thin sections other minerals were found, as will be discussed later; these minerals are important in connecting the formation of this chimney complex to those at other vents.

One of the samples from the Black Forest was reported to be an active chimney tip when it was collected. It is a small side vent, unfortunately not as well preserved as sample 980-R-12, nor presenting as complete an evolutionary sequence as 980-R-12. However, it does exhibit some interesting features. The wall of the chimney at the uppermost tip is very thin (< 1 mm), thickening downward, but, like the other Black Forest samples, still remaining quite thin. The uppermost edge is black. A thin chalcopyrite inner coating appears just below the tip. Other than that, in hand sample this piece is very similar to all the other Black Forest samples. The microscopic textures are more revealing.

The scoop sediment sample collected at the Black Forest vent was examined by X-ray fluorescence on board the R/V Gilliss. The bulk sediment contained Fe and Cu in a ratio of 1.6:1, and S, but no Zn and essentially no other ele-

ments. After the sediment was rinsed and filtered, differences did appear among the different fractions. The finest sediment had an Fe:Cu ratio $\geq$ 2:1. The coarser fraction could be divided into a black material with an Fe:Cu ratio of 1:1 and a lighter-colored material with an Fe:Cu ratio about 1.5:1. No Zn and no trace metals were detected in any fraction (B. C. Clark, personal communication). The sediment is revealed, therefore, as a different material from the black smoke, which contains pyrrhotite and sphalerite (Spiess et al., 1980), and so the sediment cannot be ascribed to fallout from the vent plume. This clearly has a bearing on the process of formation of the basal mounds.

The chimney samples from the Black Forest vent exhibit an extremely consistent mineralogy. The chalcopyrite lining and thin bornite-chalcocite rim occur in virtually every sample. The scarcity of anhydrite and of silicates and non-Cu-bearing sulfides, is unique to this vent.

Vent S-3

The samples from vent S-3 are also very uniform in composition. Twenty-one samples were collected from a smoker several meters in height, 12 samples on dive 978 and 9 on dive 982. The samples are largely composed of a mass of friable, fine-grained black material with a large amount of white admixture; it is an intimate mixture of wurtzite,

pyrite, and anhydrite. The material is very porous and breaks easily when dry. Anhydrite is prominent throughout the samples, both mixed with the sulfides and as pockets of white crystals up to several centimeters long.

Many seams and cavities of varying widths cut through the fine-grained mass that makes up the bulk of the samples. These seams and cavities are lined with hexagonal black wurtzite crystals elongate perpendicular to the interior of each channel. The largest wurtzite crystals are 1 mm across. Just to the outside of the elongate wurtzite crystals there is a thin golden band containing chalcopyrite and intermediate solid solution. On many samples a very fine dusting of golden sulfides also occurs on the inner surface of the wurtzite crystals.

The exterior of the samples from vent S-3 often includes pompey worm tubes. The surfaces of both the worm tubes and the black sulfide mixture are coated by rusty oxidation and alteration minerals. In practice, the presence of worm tubes and oxidation is used to identify the exterior surface of these samples. Similarly, the center of the seams lined with elongate wurtzite crystals is assumed to be the site of fluid flow and therefore the interior of the chimney. These channels of fluid flow do not appear to have originated as worm tubes; their sizes, shapes, and configurations all argue against such an origin.

The cross-section of a chimney that the samples from vent

Figure II.7. Sample 978-R-16 from vent S-3. The mass of the sample consists of wurtzite, pyrite, and anhydrite. Pockets and seams of elongate wurtzite at the center of the upper edge and down the left-hand side of the piece appear to be darker and shinier. The sample is 14 cm long. Photo A. Dionne.

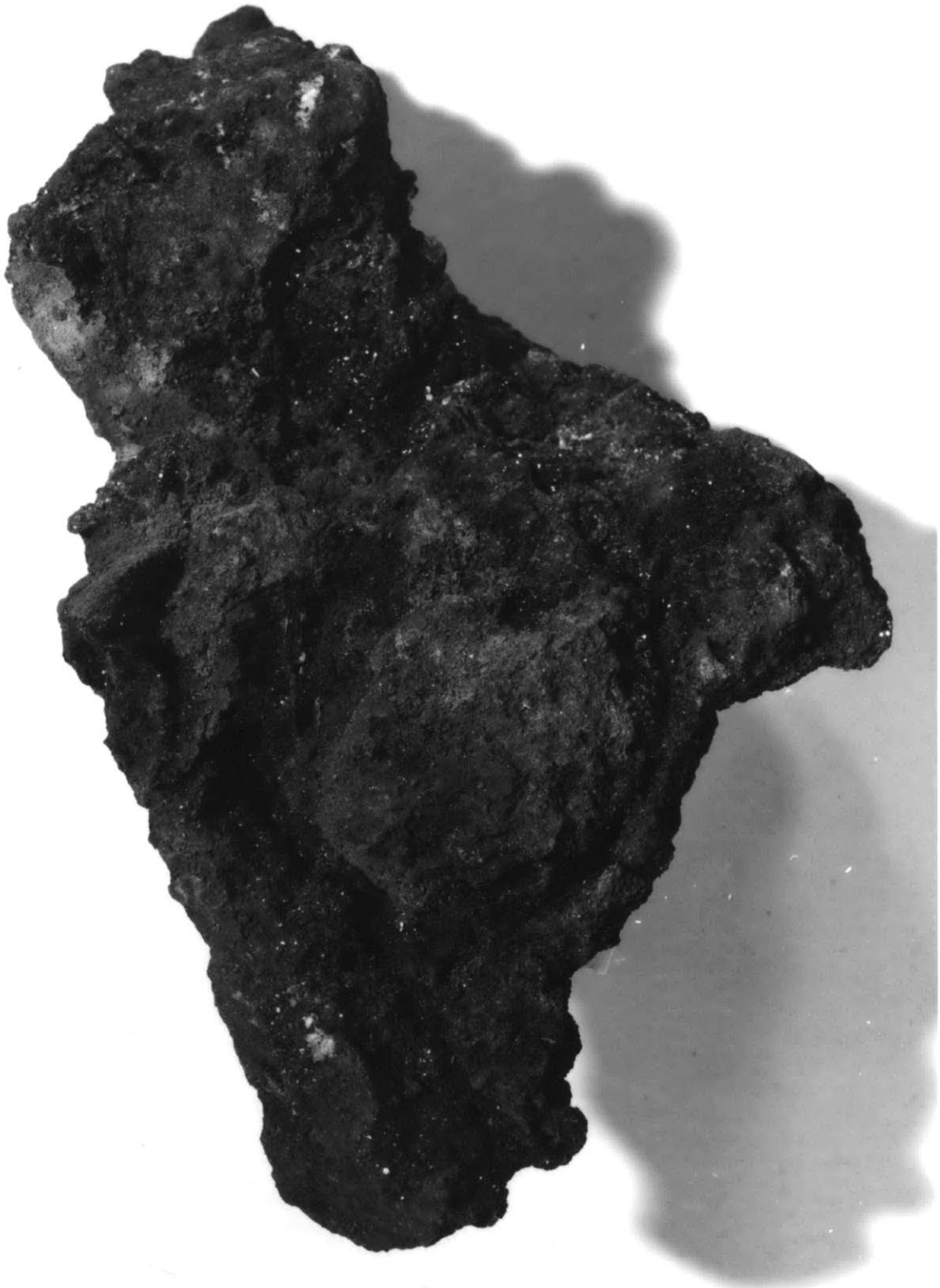

S-3 reveal is quite different from the previous chimneys. The chimney is primarily composed of a fine-grained mass of wurtzite, anhydrite, and pyrite, cut by many relatively narrow channelways lined with large wurtzite crystals, through which the hydrothermal fluid moved. The outer surface of this chimney is inhabited by pompey worms.

Vent Site 1 of Dive 980

The samples from vent site 1 of dive 980 present two distinct morphologies. Only ten pieces were collected at this vent site, and a complete picture of the chimney is not readily assembled. Most of the samples are small fragments and pieces that may have broken off the larger pieces during sampling. Of the three large samples, two are very similar to the samples from vent S-3. They consist predominantly of the fine-grained mixture of wurtzite, anhydrite, and pyrite just described. One (980-R-2) is cut by a relatively large single channelway lined with hexagonal wurtzite crystals. The same thin band of Cu-Fe sulfides lies just to the outside of the elongate wurtzite crystals. The major difference between the similar samples from this vent and vent S-3 is a comparative lack of small channelways in the samples from vent site 1 of dive 980.

The second type of sample from this vent is represented by 980-R-4 and a number of small pieces. Sample 980-R-4 is

a tube with one large and one small end but without a continuous central conduit (figure II.8). The tube is composed of large acicular anhydrite crystals up to 1 cm long, which appear on the surface to be black, but are light-colored below. A fine sulfide dust visible only under the microscope gives rise to the black color.

No single chimney model has been assembled for vent site 1 of dive 980, because the number of good samples is small and the variety among them does not allow the construction of a realistic model. All the major samples from this vent area were studied, since it was impossible to select "typical" samples.

Vent Classifications

Even the initial descriptions of the vent samples from 21°N indicate the existence of two classes of chimneys, one rich in Cu-Fe sulfides and the other rich in Zn sulfides. Vent S-2, vent site 1 of dive 981, and the Black Forest all have an essentially monomineralic interior lining of a Cu-Fe sulfide, either chalcopyrite or cubanite; they are grouped together as Cu-rich chimneys. Vent S-3 and vent site 1 of dive 980, in contrast, are almost devoid of Cu; the only trace of Cu is in thin bands and fine dustings of Cu-Fe sulfides around the elongate hexagonal wurtzite crystals that line the fluid channelways. The large wurtzite crystals

Figure II.8. Sample 980-R-4 from vent site 1 of dive 980. The tube is 8.5 cm in diameter. It is composed of long needles of anhydrite coated by fine-grained sulfides. Photo A. Dionne.

are characteristic of these two chimneys and lacking in the Cu-rich chimneys. Vent S-3 and vent site 1 of dive 980 are therefore classed as Zn-rich vents.

Different primary sulfides are not the only point of distinction between the two types of chimneys. The Cu-rich chimneys have a central fluid channelway that is easily identifiable in hand sample. They have one clear interior and one clear exterior surface. Many of the samples are clearly pieces of a tubular structure. The Zn-rich chimneys generally have multiple small fluid channels in a more massive wall. The samples are chunky and generally cannot be reconstructed to form a tube. Pompey worm tubes are much more abundant on the samples from Zn-rich chimneys than on those from Cu-rich chimneys.

There are observable differences in the temperature of hot water venting from the two groups of chimneys. The thermocouples held in the vent mouths at vent S-2, the Black Forest, and vent site 1 of dive 981 recorded steady temperatures close to 350°C. The maximum temperature recorded at vent site 1 of dive 980, however, was only 273°C. At vent S-3, a maximum temperature of only 260°C was recorded, but the probe was not placed directly in the vent mouth at any time. The reasons for the correlation between the temperature of the hot fluid exiting from the vent and the mineralogy of the vent structure will be discussed later; the basic cause is the rapid drop in the solubility of chalcopyrite

between 350°C and 250°C (Crerar and Barnes, 1976), leading to the deposition of most of the chalcopyrite at higher temperatures.

Microscopic/Textural Description

Direct observation and XRF analyses of the vent samples reveal the relative positions of different major minerals within the chimney walls, but provide no information on the relationships through time of the minerals. Study of polished and doubly polished thin sections of typical samples from each chimney allows these relationships to be deduced, and also reveals the presence of minor minerals and additional complexities in the chimney structures. A vent-by-vent review of the microscopic observations, from the interior of each chimney outward, will be followed by a general discussion of the significance of the observations.

Vent S-2

In polished section the inner layer of vent S-2 is pristine, solid cubanite through its entire thickness. At the outer edge of the cubanite there is a thin layer of cubanite grains mixed with pyrrhotite laths (figure II.9). The pyrrhotite is clean, and shows no sign of replacement. This is the only occurrence of unaltered, unreplaced pyrrhotite

Figure II.9. The cubanite-pyrrhotite-wurtzite layer of vent S-2, from sample 978-R-3. The dark grey mineral in the center is anhydrite, light grey on the right side is wurtzite. The dark yellow mineral is cubanite, which has been extensively rimmed by slightly lighter yellow chalcopyrite. The tan colored mineral is pyrrhotite within and on the edges of chalcopyrite/cubanite grains. Field of view 0.6 by 0.4 mm; reflected light.

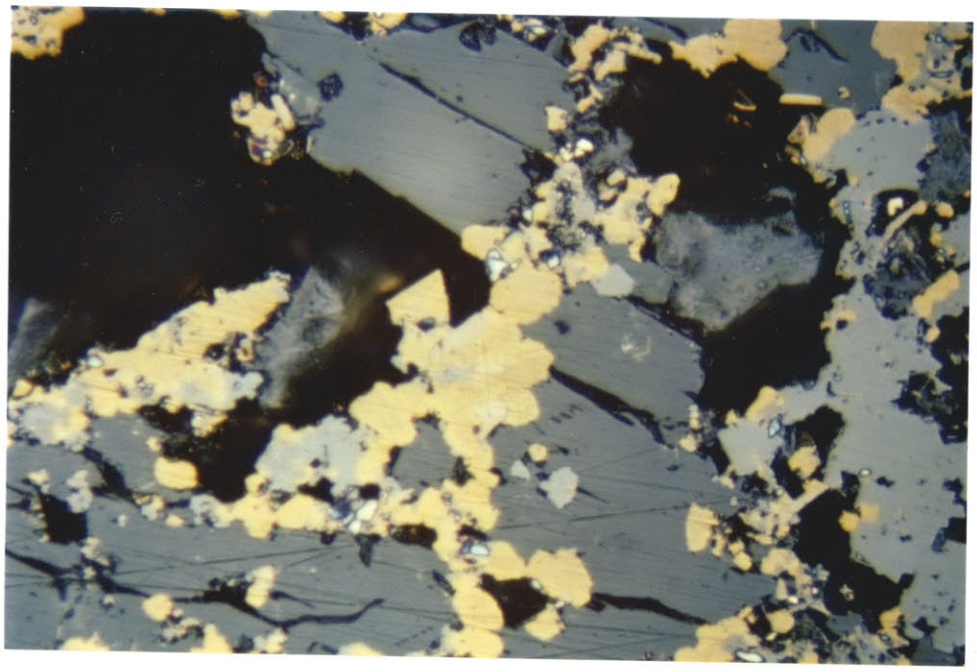

found in any of the chimneys. The cubanite in this layer, however, is rimmed by chalcopyrite at every edge touching pyrrhotite. The amount of chalcopyrite replacement, rimming and intruding into the cubanite grains, increases slightly to the exterior of the chimney, so that the cubanite grains on the exterior side of this layer are rimmed by chalcopyrite along all their edges regardless of the adjoining mineral grain, which may consist of more cubanite, pyrrhotite, or wurtzite.

On the outer edge of the cubanite-pyrrhotite layer, both wurtzite and anhydrite appear. Anhydrite in this layer and the next tends to fill interstices between the sulfides.

To the exterior of the pyrrhotite-bearing layer a wurtzite-dominated layer occurs. In hand sample, this layer forms a black band that appears to consist entirely of wurtzite. In polished section it contains noticeable quantities of cubanite, which occurs both as solid grains that appear to be primary and as replacements of wurtzite.

The wurtzite-rich layer is succeeded to the exterior by a curious, colloform or colloidal-looking layer of Mg-silicates, pyrite, and wurtzite. The silicates and sulfides appear to be growing in and around each other in globules (figure II.10). The pyrite in this layer is soft, yellow to brown in tint, and seems to contain a lot of water (figure II.11). It corresponds well to the pyritic material referred to as "melnikovite" by Ramdohr (1969). The Mg sili-

cates are poorly crystallized; their composition corresponds to a mixture of talc and chrysotile with a large amount of excess water. Anhydrite is also common in the outer part of this layer, in crystals of varying lengths, generally oriented perpendicular to the wall. The silicates and anhydrite often appear to have formed together, but to the extent that one does precede the other anhydrite seems to provide the basic framework inside which the other minerals have grown. The proportion of Mg-silicates decreases outward as the proportion of anhydrite increases. At the very exterior the chimney consists of coarse crystals of anhydrite oriented perpendicular to the chimney wall, with a sprinkling of fine-grained wurtzite and pyrite, which are minor in quantity but highly visible.

Vent Site 1 of Dive 981

Vent site 1 of dive 981 provided a variety of hand samples, and consequently a variety of polished sections. As was the case with the hand samples, two variations on one major trend were observed in the microscopic textures. Sample 980-R-12 again merits special attention, and reveals the fine details of chimney growth in its textural and mineralogical intricacies.

With the exception of 980-R-12, all the samples from vent site 1 of dive 981 have a solid chalcopyrite inner

Figure II.10. The colloidal-textured or colloform layer of vent S-2, from sample 978-R-3. The white mineral is pyrite; the grey mineral is Mg-silicate. The occasional grain of interstitial lighter grey is anhydrite. Field of view 0.6 by 0.94 mm; reflected light.

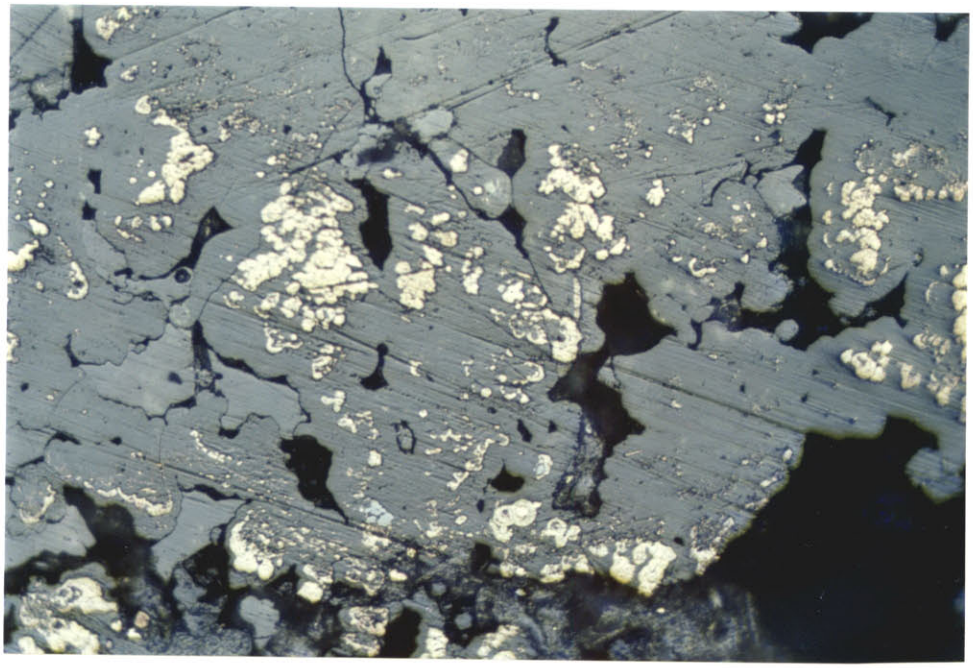

Figure II.11. "Melnikovite" showing original colloform structure, from vent S-2, sample 978-R-1. The darkness of the pyrite is accentuated by a small amount of tarnish; the spots of blue coloring are also tarnish. Field of view 0.6 by 0.94 mm; reflected light.

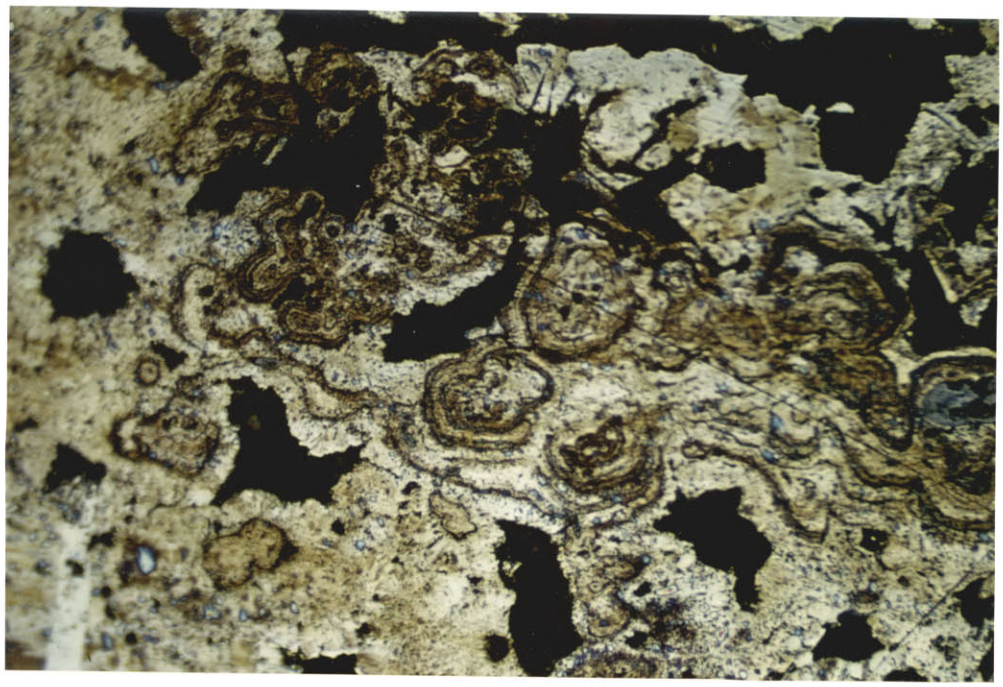

lining. In polished section occasional small grains of pyrite can be seen in void spaces between the chalcopyrite grains. There are also some small pockets within the chalcopyrite layer, visible to the naked eye as white patches, which contain an assemblage of anhydrite, wurtzite, pyrite, and chalcopyrite. The wurtzite in these pockets is extensively replaced by chalcopyrite, either as disseminated "chalcopyrite disease" like that described by Barton (1978), or as chalcopyrite replacement along individual bands of wurtzite crystals (figure II.12). Wurtzite, pyrite, and chalcopyrite in the pockets are all rimmed and replaced by anomalous bornite of a type which will be described later.

At the outermost edge of the chalcopyrite lining is a thin layer less than 1 mm wide which bears a resemblance to the anhydrite-rich pockets just described. This layer consists of sulfides surrounded by anhydrite. The sulfides are wurtzite, pyrite, chalcopyrite, and anomalous bornite. Both wurtzite and pyrite are replaced by chalcopyrite, wurtzite in the manner previously described and pyrite by invasion of chalcopyrite along cracks and at the edges of grains. The alternative bands of chalcopyrite and wurtzite on the outer edges of some wurtzite grains (e.g., figure II.12) have been described as re-

placement features because the amount of chalcopyrite present increases gradually across many of the wurtzite grains and because a continuous spectrum can be observed from disseminated chalcopyrite disease to chalcopyrite forming bands in wurtzite. The chalcopyrite bands could also form as intergrowths in wurtzite as a consequence of alternating precipitation of ZnS and $CuFeS_2$. Replacement of wurtzite by chalcopyrite implies a period of Zn-rich deposition followed by a period of Cu-rich deposition, while growth banding implies a fluctuation in the depositional conditions. Either explanation is possible; in the description of chimney formation it will be proposed that this layer forms in a zone of mixing between hot and cold solutions, in which the composition of the mineralizing solution could vary with time.

In this thin layer outside the inner lining, chalcopyrite, wurtzite, and pyrite are all replaced by anomalous bornite, which tends to replace pieces of previously formed grains rather than invading in the manner of chalcopyrite disease (figure II.13). Some grains of anomalous bornite do appear to be primary. These grains are smooth and unbroken, while replacement grains, even if they do not retain remnants of the original sulfide, are usually cracked. Along the cracks are occasional

patches and lines of highly visible covellite.

To the exterior of the layer containing anomalous bornite, two different layers occur, corresponding to the two different exterior layers observed in the hand samples. In those samples with an exterior layer of fine grained sulfides, the anomalous bornite-bearing layer loses its anomalous bornite and chalcopyrite and blends into a layer of wurtzite, pyrite, anhydrite, and Mg silicates. The sulfides in this mixture are similar to those in the colloidal Mg-silicate layer of vent S-2. In addition to the yellow-brown pyrite also found in vent S-2, ordinary pyrite and marcasite occur in this layer. The morphology of the FeS_2 and wurtzite varies from globular or colloidal forms like those in vent S-2 to very fine-grained crystals to masses that appear to have been built up by progressive overplating of sulfides on top of each other (figure II.14). Intermediate forms include "stringers" of connected grains of sulfides stretching across anhydrite or Mg-silicate (figure II.15). The wurtzite and pyrite apparently were precipitated essentially simultaneously, leading to rhythmic alteration of layers of the two sulfides along a stringer, and to mutual interfingering on the edges of grains (figure II.16). Pyrite and marcasite also seem to have been co-deposited, or at least no evidence to the contrary has been retained. The sulfides

Figure II.12. Sample 981-R-16 from vent site 1 of dive 981. Chalcopyrite (yellow) replacing wurtzite (grey) along selected bands. Disseminated chalcopyrite disease is also visible at top. Field of view 0.4 by 0.6 mm; reflected light.

Figure II.13. Sample 981-R-22 from vent site 1 of dive 981. Anomalous bornite (reddish-brown) replacing pyrite (white) and wurtzite (light grey). The dark grey material with internal reflections is anhydrite. Field of view 0.6 by 0.9 mm; reflected light.

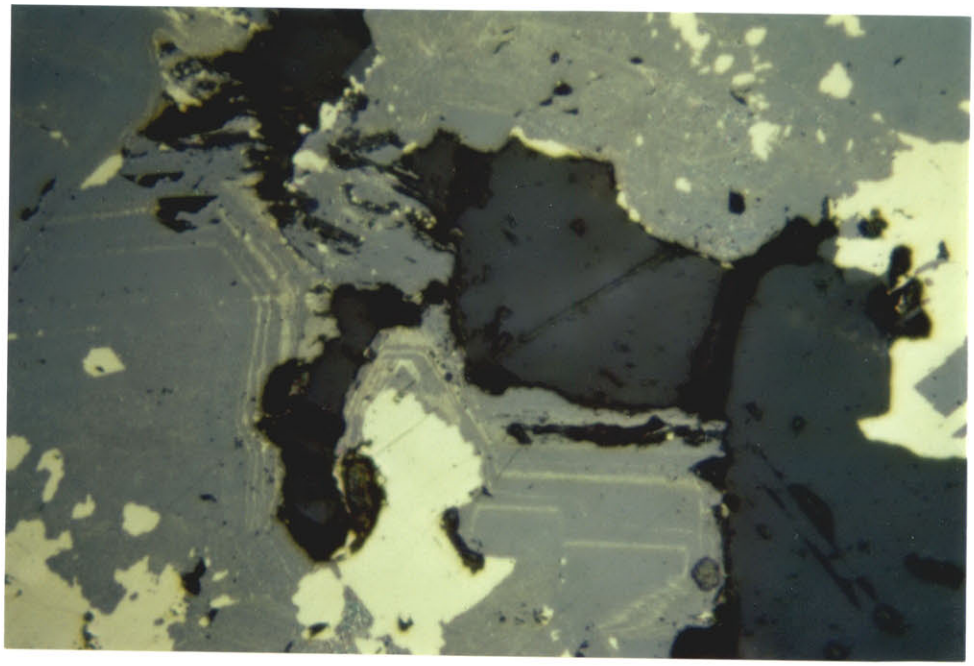

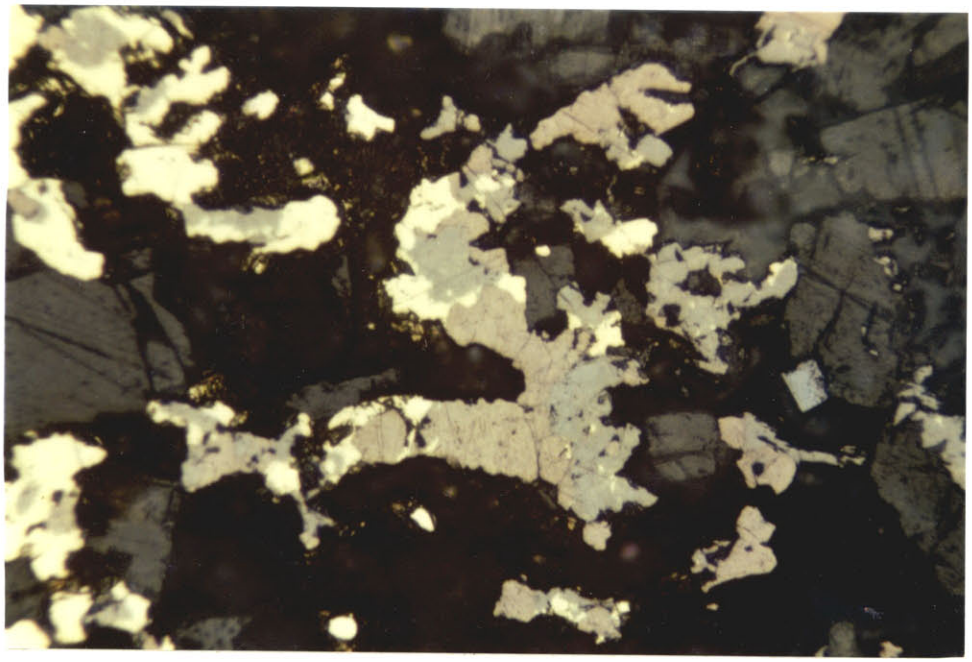

Figure II.14. Sample 978-R-1, outer layer. Pyrite overgrown by and intergrown with marcasite. Marcasite is slightly more blue in tint; pyrite is slightly yellower and often more euhedral. Field of view 0.4 by 0.6 mm; reflected light.

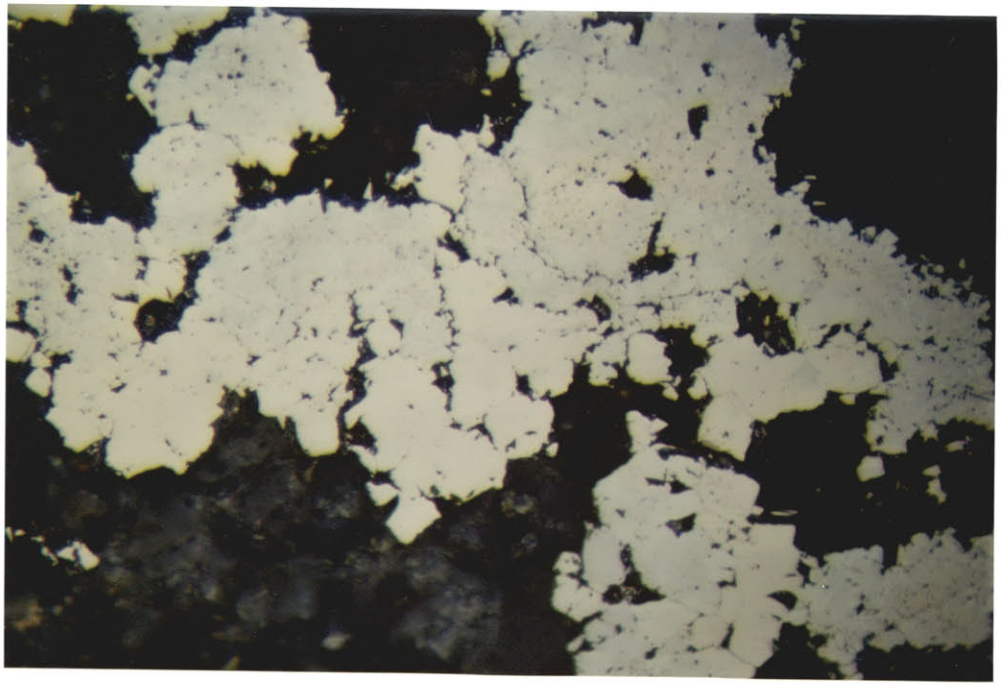

are often directly surrounded by Mg-silicates, but the underlying structure of the wall is provided by anhydrite, as in vent S-2. Some replacement of other sulfides by chalcopyrite is noticeable on the interior edges of the layer, but in general Cu is lacking. Towards the outer surface, the sulfides become scarcer and form smaller aggregates, while anhydrite becomes the predominant component of the chimney.

Other samples from this vent are lacking the fine-grained sulfide layer described above; the exterior layer of these samples is a white-colored layer dominated by anhydrite and Mg-silicates. Anhydrite forms the framework of this layer also; the Mg-silicates form between and along the edges of relatively coarse anhydrite crystals. Sulfides are not lacking, but they are much scarcer than in the previously described layer. Pyrite and wurtzite tend to be very fine-grained and associated with Mg-silicates, as they are in the fine-grained sulfide layer. Sulfides also appear as tiny specks scattered across and through anhydrite crystals, making the anhydrite cloudy in transmitted light. The difference between the anhydrite-dominated layer and the fine-grained sulfide layer is actually not in the mineralogy or in the relationships between sulfide and non-sulfide minerals, but in the relative abundances of the minerals present.

Sample 980-R-12 is especially interesting. In thin section the uppermost tip of 980-R-12 consists of anhydrite

Figure II.15. Sample 980-R-12 from vent site 1 of dive 981, outer layer. Reflected light; fields of view 0.4 by 0.6 mm.

(a) Pyrite "stringer" created by coalescence of many small grains. The rounded, very dark grey gangue is Mg-silicate; the lighter grey with internal reflections is anhydrite.

(b) A layered stringer of ZnS (light grey) and pyrite (white). Dark grey gangue in rounded forms, here showing some internal reflections, is Mg-silicate; medium grey gangue is anhydrite.

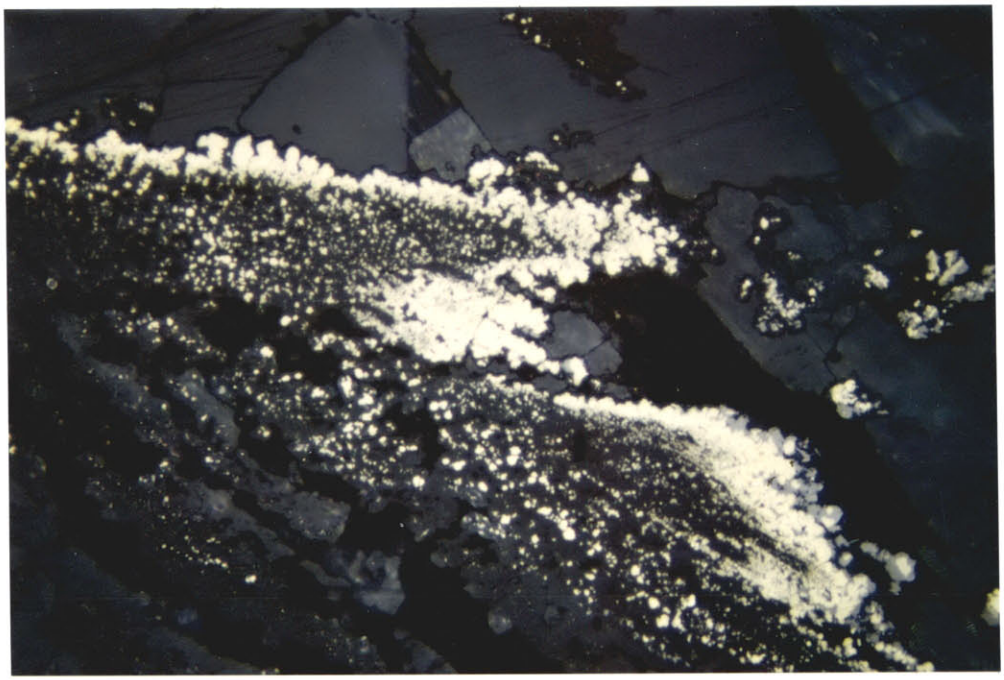

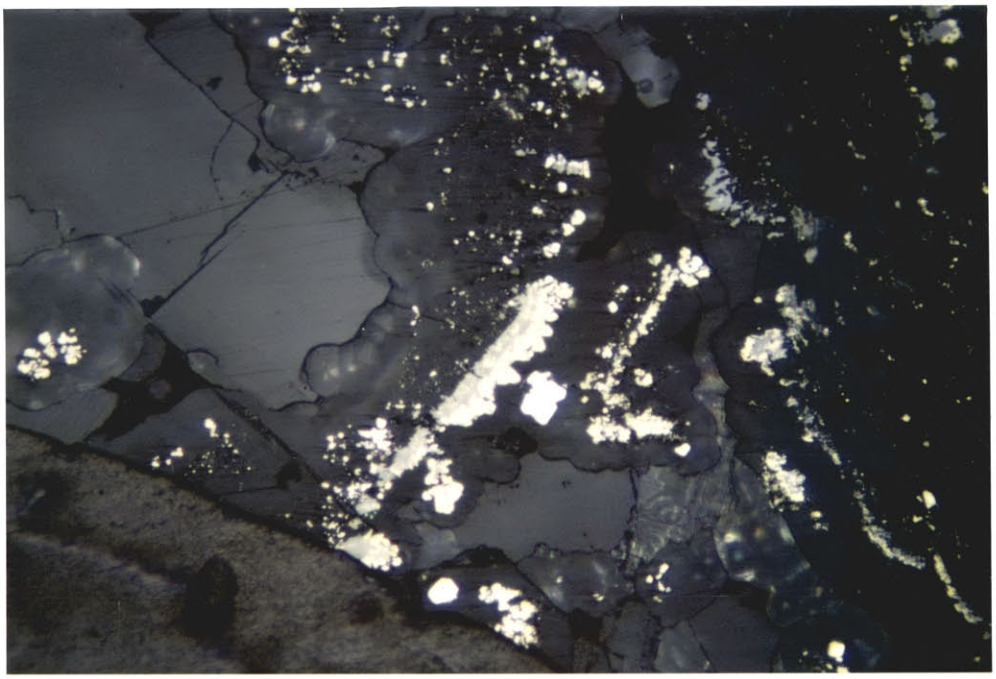

Figure II.16. Sample 980-R-12, fine-grained sulfides. Pyrite cubes (white) intergrown with wurtzite (light grey) at outer edge. Field of view 0.4 by 0.6 mm; reflected light.

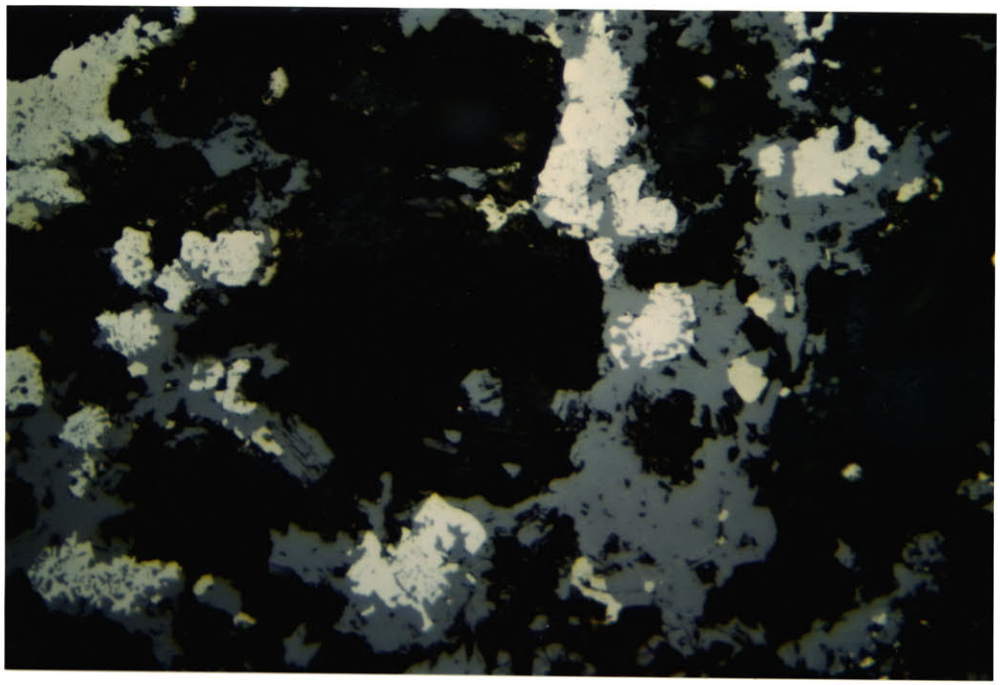

crystals oriented both horizontally and vertically, with a covering of abundant fine-grained pyrite and wurtzite. At this edge the interior and exterior are indistinguishable, and the chimney is composed basically of an anhydrite framework.

Just below the upper edge (< 1 mm below the tip) the first fine layer of chalcopyrite begins to coat the interior. In polished section this layer first appears as scattered grains of chalcopyrite in the inner edges of the anhydrite-sulfide structure, but the grains rapidly consolidate into a continuous layer of monomineralic chalcopyrite. The apparent size of the chalcopyrite increases downward in the chimney and the void space in the layer decreases, sugtesting both overplating on the initial chalcopyrite grains and progressive consolidation of small grains into larger ones.

Just below the appearance of the chalcopyrite lining in the tube, a series of changes is visible in polished section in the outer parts of the chimney wall. Two to three mm down in the tube, chalcopyrite disease begins to appear in the wurtzite grains remaining in and just outside the chimney interior. At approximately the same point, the first Mg-silicates appear in the anhydrite layer and just outside the chalcopyrite layer. The silicate-bearing part of the wall develops downward into the same colloidal or fine-grained layer of Mg-silicates, pyrite, wurtzite, and anhydrite

described in other samples from this vent, with some minor Cu-Fe sulfides. Although the transition from the anhydrite-sulfide mixture at the chimney tip to the "colloidal" silicate-sulfide layer is gradual, colloidal sulfides are definitely present 2 cm below the chimney tip. A well developed layer appears lower in the chimney walls and thickens downward, clearly by further deposition of both Mg-silicates and sulfides in situ. In the well developed silicate-sulfide layer, a limited amount of Cu-Fe sulfide replacement of wurtzite and pyrite takes place along the interior edge of the layer.

Another textural and mineralogical change occurs at depth of 3 - 3½ cm in the tube. There anomalous bornite develops within the chimney wall. It first appears replacing occasional grains of chalcopyrite and wurtzite, where the outer edge of the chalcopyrite layer and the inner edge of the anhydrite-silicate-sulfide layer meet. Downward in the chimney, anomalous bornite increases in abundance as a replacement mineral, and also apparently forms as a primary mineral. By about 5 cm depth it is sufficiently abundant to form a definable band between the inner and outer layers of the chimney.

At the base of the tube on 980-R-12, the chimney wall, from interior to exterior, consists of a chalcopyrite layer 1 cm wide, a narrow band of fine-grained sulfides and anhydrite with an abundance of anomalous bornite, and a layer

up to 3 cm wide consisting of Mg-silicates, fine-grained sulfides, and anhydrite. In this outer layer the dominant non-sulfide component varies from Mg-silicates in the inner part to anhydrite at the outer part. The sulfide fraction is richer in Zn towards the interior and in Fe towards the exterior. There is a small amount of Cu-Fe replacement of wurtzite at the inner edge of the outer layer. In polished section it is clear that all the layers grew by deposition in place during development of the chimney. The outer layer is not formed by precipitates from the plume settling onto the chimney. Several factors make this clear: (1) the orientation of anhydrite crystals is consistently perpendicular to the wall; (2) the anhydrite crystals are too long, and too coarse to be part of the fine-grained smoke; (3) the sulfide mineralogy is inconsistent with that of the smoke; (4) no evidence of recrystallization or of replacement except by Cu-Fe sulfides is visible; (5) Mg-silicates do not occur in the smoke. The development of the chimney that is visible in this sample is a valuable tool for reconstructing the process of chimney growth. The most important aspects of the development of the chimney wall in 980-R-12 are outlined in figure II.17.

Black Forest

The Black Forest vent yields the least complex of the

chimney samples when viewed in polished section. The chalcopyrite interior layer is succeeded to the exterior by a bornite - chalcocite solid solution. The boundary between chalcopyrite and bornite is sharp; there is little overlap of the two phases, but in places a clear replacement relationship is visible (figure II.18). Similarly, although the bornite-chalcocite transition is usually a continuous solid solution, replacement of bornite by chalcocite is also present in places (figure II.18). The beginnings of covellite replacement are visible on the outermost edges of the chalcocite.

There is a thin intermittent layer containing other sulfides at the boundary between the chalcopyrite lining of the chimney and the bornite-chalcocite solid solution. This layer, which is visible only in polished sections, contains small grains of wurtzite and pyrite, and an occasional rare instance of anomalous bornite replacing wurtzite, pyrite, or chalcopyrite. Otherwise, wurtzite and pyrite occur only as trace components of the white masses on the interior, as described in the hand samples. Anhydrite occurs in those clumps and occasionally on the outermost edge of the chimney. It also occurs, although very rarely, between the sulfide grains in the wurtzite + pyrite layer.

Polished sections of the upper end of the small tube serving as an active vent from the Black Forest, sample 979-R-1, reveal a gradual development of the chimney wall.

Figure II.17. Schematic view of the upper edge of sample 980-R-12, based on a composite of several sections; shown approximately to scale.

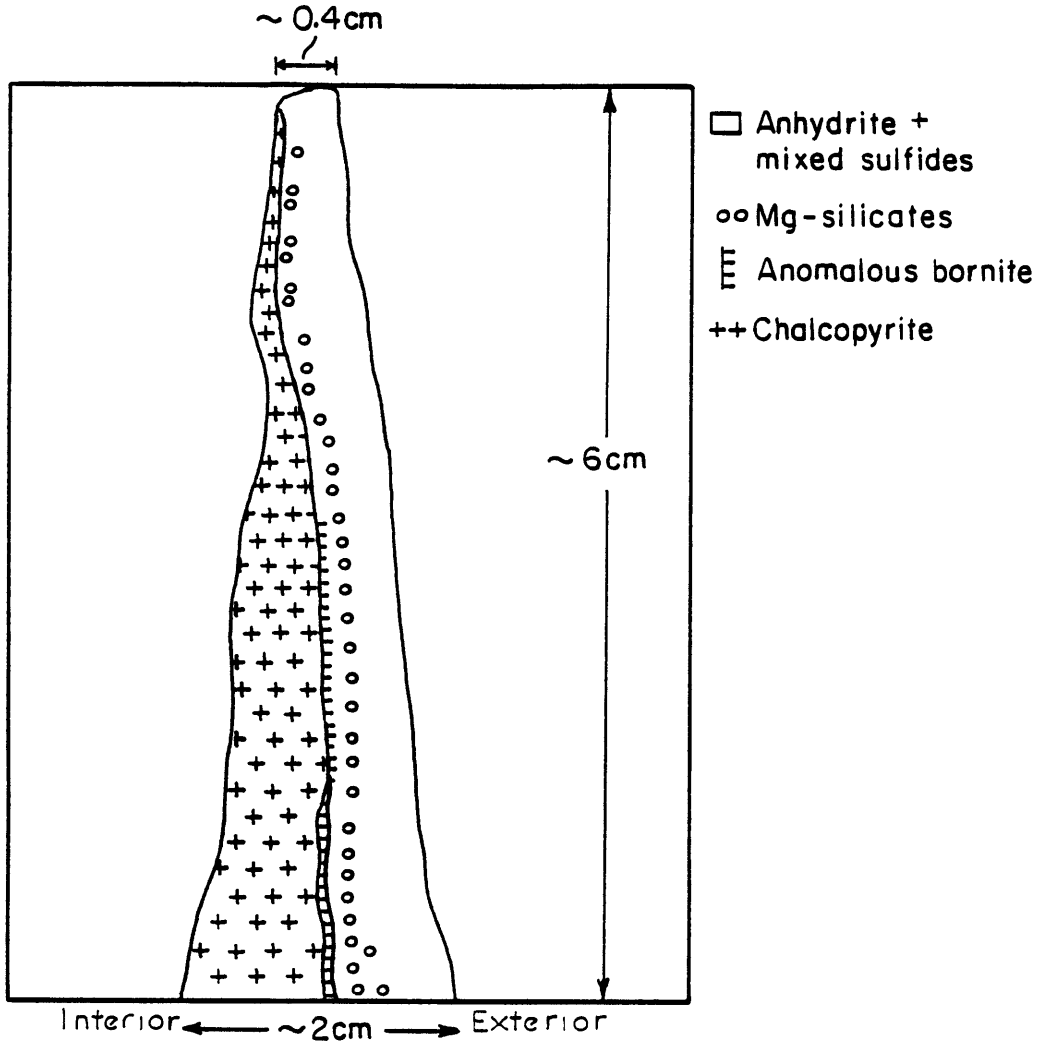
~ 0.4cm
~ 6cm
Anhydrite + mixed sulfides
Mg-silicates
Anomalous bornite
Chalcopyrite
Interior
~2cm
Exterior

Figure II.18. Sample 982-R-7, from the Black Forest. Replacement sequence: remnants of chalcopyrite (yellow), still rimmed by remnants of bornite (pinkish), mostly replaced by chalcocite (blue). Some bornite has completely replaced chalcopyrite before being replaced by chalcocite. Field of view 0.62 by 0.94 mm; reflected light.

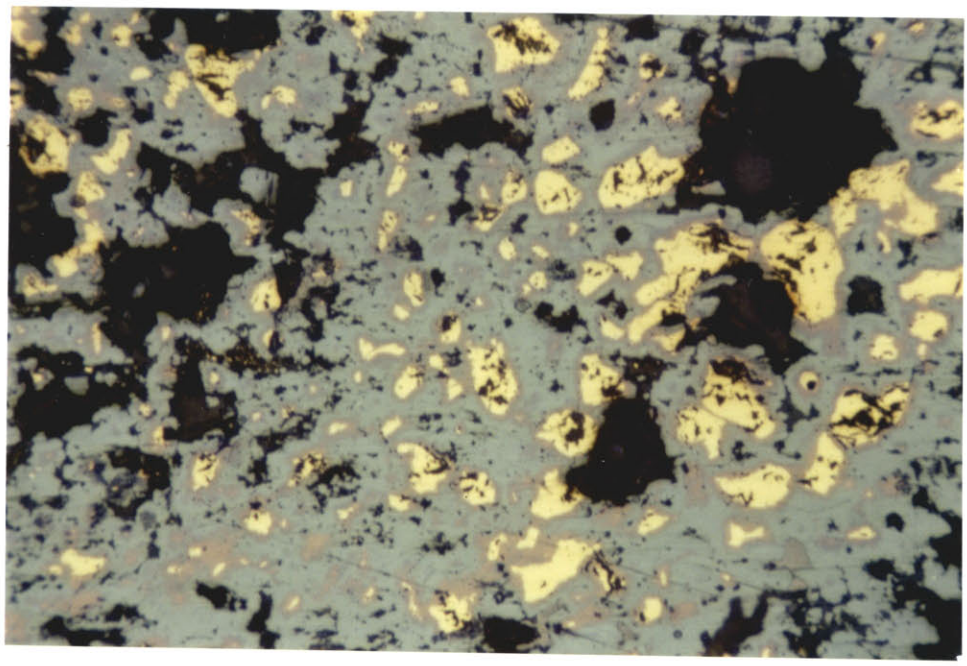

The uppermost edge of the tube has only a trace of chalcopyrite and is relatively rich in anhydrite, pyrite, and wurtzite. A chalcopyrite lining appears immediately below the tip and does thicken slightly downward, but the entire wall remains very thin throughout the length of the sample. The bornite-chalcocite rim develops gradually on the outer edge of the chalcopyrite layer, as anhydrite becomes less prominent in the chimney wall. Bornite first appears as scattered areas of replacement; in the upper part of the tube it does not form a continuous layer nor can it be separated from the interior chalcopyrite. The bornite-chalcocite rim appears to develop from the exterior after the chalcopyrite layer has formed.

Vent S-3

Vent S-3, as noted previously, is one of the Zn-rich vents. The elongate hexagonal wurtzite crystals that line the seams and cavities in the samples from this vent are dark red or black in thin sections when viewed in transmitted light. In plane view some color banding is present. Within this central lining, anhydrite sometimes fills the narrow cracks between wurtzite crystals.

The inner lining terminates against a mixture of sulfides and anhydrite. In a restricted band around the elongate wurtzite crystals, the mixed sulfides include a major quan-

Figure II.19. Sample 982-R-19, from vent S-3. Exsolution lamellae of cubanite (slightly darker) and chalcopyrite (slightly lighter) in a grain originally of iss composition. Field of view 0.4 by 0.6 mm; reflected light.

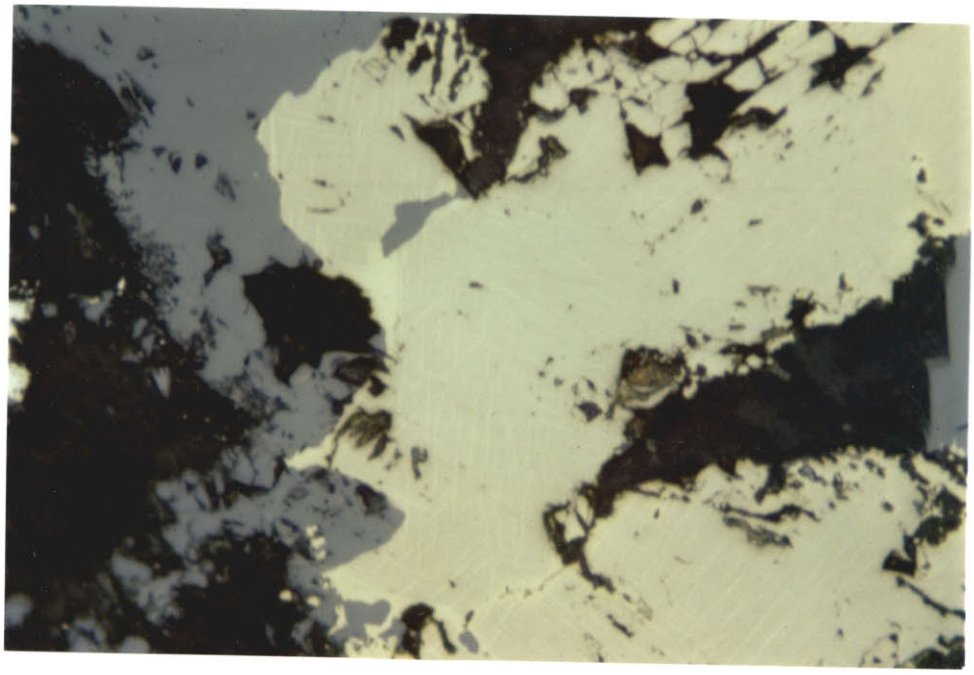

tity of intermediate solid solution (iss). This term as used here refers to a mineral that is presumed to have formed as homogenous grains corresponding to compositions within the intermediate solid solution field in the Cu-Fe-S system. It now appears as intergrown exsolution lamellae of cubanite and chalcopyrite, in varying proportions reflecting the original composition of the iss (figure II.19). Iss is the major Cu-Fe sulfide found in vent S-3; some chalcopyrite is also present.

The band of mixed sulfides that occurs just outside the central lining consists of wurtzite, iss, pyrite, pyrrhotite, chalcopyrite, and anhydrite. All of the sulfides occur as primary minerals; three of them also act as replacement minerals. Pyrite replaces pyrrhotite, forming bird's-eye textures (figure II.20). Iss replaces wurtzite, both in the mixed sulfides and in the ends of adjoining elongate crystals in the central lining (figure II.21). Chalcopyrite replaces pyrrhotite, wurtzite, pyrite, and possibly even iss. Pyrrhotite is never pristine, but is always replaced either by pyrite or by chalcopyrite. When replacing wurtzite, chalcopyrite has a similar form to iss replacing wurtzite. Replacements of pyrrhotite and pyrite are usually more massive, involving chalcopyrite rimming and invasion along cracks in the host grains. The exact relationship between chalcopyrite and iss is difficult to determine, because iss now appears as intergrown lamellae of chalcopyrite and

cubanite. However, there are places where a grain composed of lamellae appears to be entirely rimmed by chalcopyrite, and where the chalcopyrite lamellae are thickened adjacent to the rim, possibly indicating later chalcopyrite deposition over the iss.

To the exterior of the narrow band containing iss, the samples from vent S-3 consist of moderately fine to coarse anhydrite mixed with a large quantity of fine-grained wurtzite, pyrite, and pyrrhotite. The pyrrhotite is eroded and replaced by pyrite; the other sulfides show no sign of alteration or replacement. In one particular sample, minute grains of galena were detected using the SEM capability of the Cameca microprobe. In the same sample, barite was detected in polished section, associated with anhydrite around the galena. It is likely that small quantities of both galena and barite occur elsewhere in these samples. Pb and Ba were detected occasionally both by XRF and by electron microprobe, and barite was observed occasionally in thin section and on the SEM. Both phases occur only in traces, and may be present in similar layers of other chimneys.

Vent Site 1 of Dive 980

Vent site 1 of dive 980 yields two different types of samples, as noted in the hand sample description. One type is identical in thin section to the samples from vent S-3.

Figure II.20. Sample 982-R-19, from vent S-3. Pyrite and marcasite (white) replacing pyrrhotite (tan) in bird's eye texture. The grey mineral is wurtzite; the yellow mineral is cubanite. Field of view 0.4 by 0.6 mm; reflected light. Photo R. Loucks.

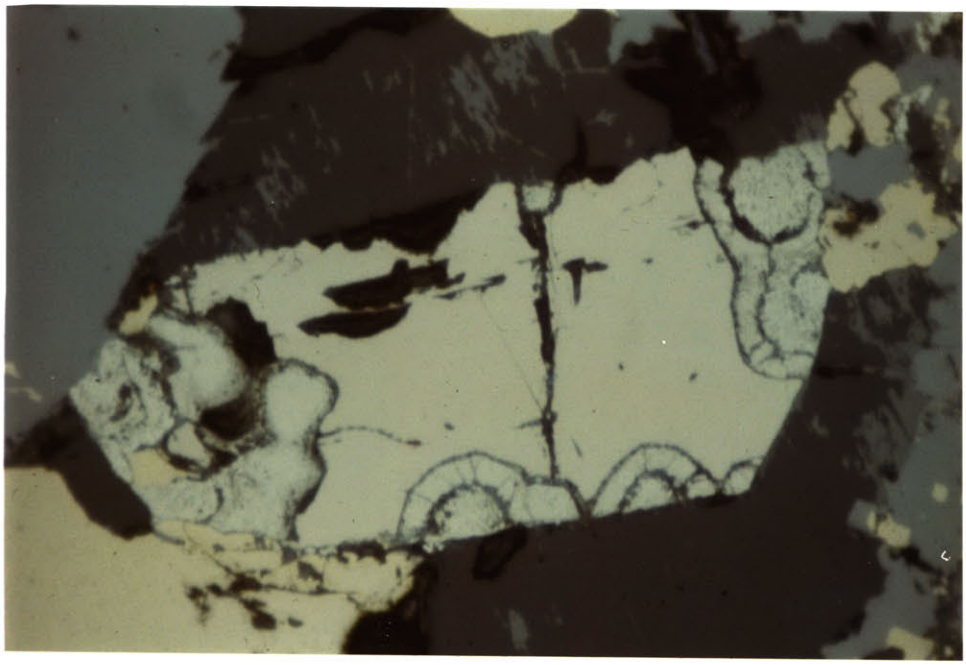

Figure II.21. Sample 982-R-12, from vent S-3. Iss (yellow) replacing wurtzite (grey) preferentially along selected layers, at the outer tip of an elongate crystal lining a channelway. The white mineral is pyrite. Field of view 0.62 by 0.94 mm; reflected light.

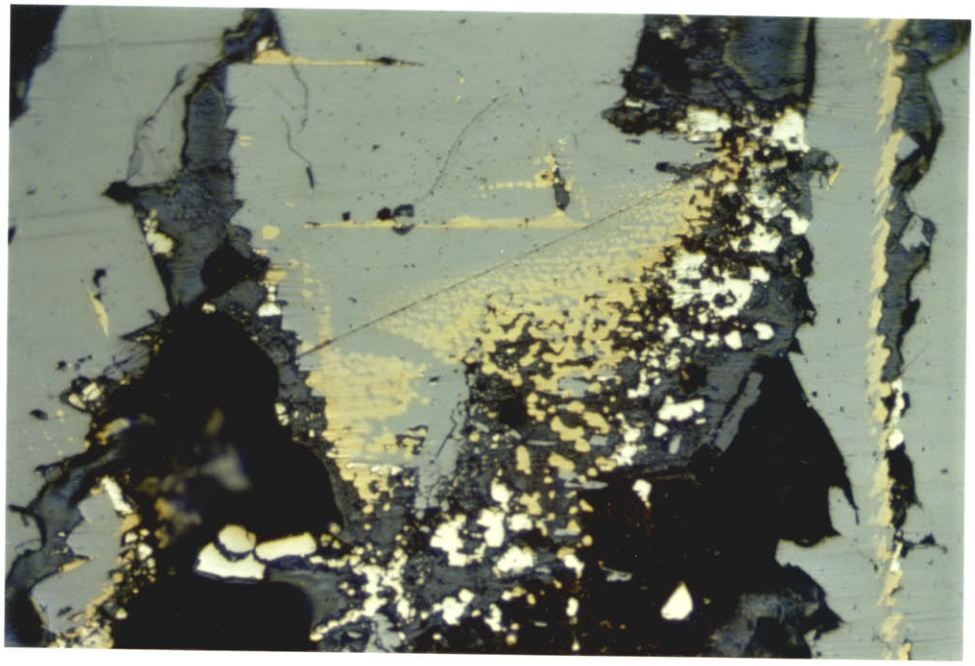

Some of the fine-grained wurtzite in these samples has exsolved chalcopyrite, creating a lattice texture different from the chalcopyrite "disease" created by Cu-Fe replacement of wurtzite (see figure II.22). The second type of sample from this vent consists of coarse acicular anhydrite crystals which look black in color. In polished section in both transmitted and reflected light it is evident that the large crystals are anhydrite. The surfaces of the anhydrite crystals are covered with a fine dust composed of wurtzite and pyrite, in tiny grains and dendritic forms, which imparts the black color to the samples.

Replacement Trends and Textures: Summary

Although there are differences in mineralogy and morphology from chimney to chimney, the general order of deposition and replacement of minerals is consistent in all of them. When the same minerals occur in two chimneys, the relationships between them are similar; for example, the replacement of wurtzite by Cu-Fe sulfides occurs in all the chimneys.

Sulfides in the chimneys are related to each other by a variety of replacement, intergrowth, and overgrowth textures. Minerals that occur as replacement minerals at one time or place may form as a direct precipitate at another. Three replacement sequences occur widely throughout the chim-

Figure II.22. Sample 980-R-2, from vent site 1 of dive 980. Wurtzite grains with yellow chalcopyrite exsolution blebs along crystallographic planes. Field of view 0.62 by 0.94 mm; reflected light.

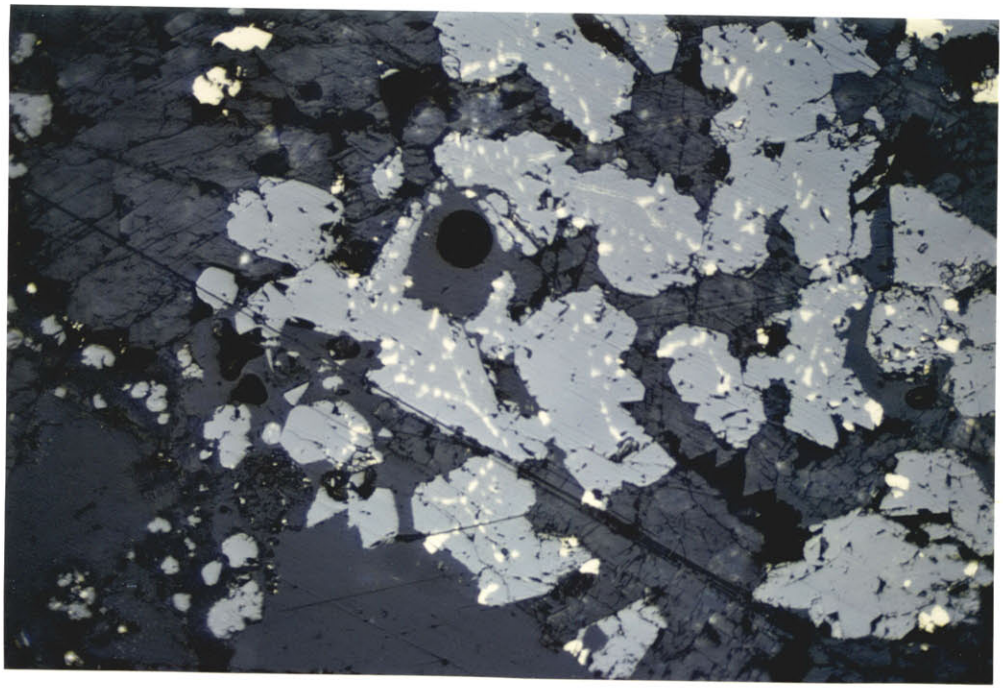

neys: (1) the replacement of pyrrhotite by later sulfides (pyrite and chalcopyrite), (2) the replacement of pyrite and wurtzite by Cu-Fe sulfides, and (3) the replacement of Cu-Fe sulfides by other Cu-Fe sulfides, generally poorer in Fe. Only in this last sequence are multiple levels of replacement visible, where a series of Cu-Fe sulfides forms by progressive incomplete replacement.

Textural similarities between chimneys extend beyond the replacement series among the sulfides. The general pattern of a coarsely crystalline, monomineralic inner lining at the fluid channelways and a more fine-grained sulfide mixture toward the exterior is observed in all the chimneys. The role of anhydrite as a framework for an outer fine-grained sulfide layer is common to all the chimneys except the Black Forest.

The sequence of mineral deposition deduced from polished sections of the chimneys is complicated by occasional reversed sequences of deposition. In general, at any one point in the chimney wall, the deposition of Zn sulfide precedes that of Cu-Fe sulfides, while Fe sulfides may be deposited throughout but are much more important early in the depositional sequence, during the deposition of Zn sulfide. Among the Fe sulfides, pyrrhotite is deposited only very early in the paragenesis, whereas pyrite may be deposited at any time. During the period of Cu-Fe sulfide deposition, chalcopyrite is earlier than bornite which is in turn earlier

than chalcocite and covellite.

Mineral Compositions

Quantitative analyses of sulfide, sulfate, and silicate minerals were obtained by electron microprobe analysis. In general, only major elements were included in the program: Fe, Cu, Zn and S for sulfides; Ca, Ba, Sr and S for sulfates; and Fe, Mg, Ca, Na, K, Al and Si for silicates. Qualitative or semi-quantitative X-ray scans from XRF or SEM analysis were used to check on the presence of minor elements. Some of the microprobe analyses also included Pb, Ni, Mn, Co, and Cd. Detectable levels of minor elements were rare. Sulfide analyses with totals of 100 ± 2% were considered good. However, only minor differences in element proportions were found between good analyses and those with high or low totals. Poor analyses could therefore be considered reliable indicators of mineralogy, even if they were not good guides to mineral composition. Sulfate analyses on an oxide basis also totaled 100 ± 2%. Silicate analyses yielded totals that were consistently low due to the presence of major amounts of water. A summary of the minerals present in the vents, with comments on their compositional ranges, is given in Table II.1. The actual analyses are listed in Appendix A.

Table II.1. Mineralogy of the hydrothermal vents

Vent	Major Minerals	Minor Minerals
Site 1 dive 981	Chalcopyrite Anhydrite Wurtzite Pyrite Mg-silicates	Iss Anomalous bornite Covellite
Black Forest	Chalcopyrite Bornite-chalcocite solid solution Anhydrite	Pyrite Wurtzite Anomalous bornite Covellite Mg-silicates
S-2	Cubanite Wurtzite Anhydrite Mg-silicates	Pyrrhotite Chalcopyrite
Site 1 dive 980 and S-3	Wurtzite Anhydrite Iss Pyrite	Chalcopyrite Cubanite Pyrrhotite Barite Galena (trace)

Compositions of the Sulfide Minerals

Mineral	Composition	Comments
Wurtzite	ZnS; (Zn,Fe)S	up to 33 mole % FeS
Pyrite	FeS_2	
Pyrrhotite	$Fe_{1-x}S$	
Chalcopyrite	$CuFeS_2$	
Cubanite	$CuFe_2S_3$	refers to cubic cubanite of $CuFe_2S_3$ somposition; identified by X-ray diffraction, electron microprobe, and polished section

(continued)

Mineral	Composition	Comments
Intermediate solid solution		refers to an original composition in the iss field; now appears as exsolved lamellae of chalcopyrite and cubanite composition
Bornite	Cu_5FeS_4	occur also as solid-solution phases with compositions continuous over the entire range
Chalcocite	Cu_2S	
Covellite	CuS	
Anomalous Bornite	$Cu_5Fe_1S_{4.6}$	essentially constant composition, identified by electron microprobe and by optical properties; see text

Fe Sulfides

Both $Fe_{1-x}S$ and FeS_2 occur in the vent deposits. Analysis of pyrrhotite was difficult and generally yielded totals between 93.37 and 98.09 wt%. Trace quantities of Cu and Zn were found in the pyrrhotite laths in vent S-2, but no trace metals were detected in pyrrhotite in vent S-3. The metal: sulfur atomic ratio of the analyses averaged 0.85:1 regardless of the total obtained. Pyrrhotite of $Fe_{0.85}S$ composition could be hexagonal or monoclinic, and suggests a relatively high temperature of formation; the presence of up to 0.31 wt% Cu in solid solution also implies an origin at high temperature. Pyrrhotite in the black smoke is hexagonal (Spiess et al., 1980).

FeS_2 occurs as both pyrite and marcasite. Pyrite is the dominant polymorph. Marcasite was found only in the well-developed fine-grained and colloidal-textured layer on the exterior of the chimney from vent site 1 of dive 981. Regardless of which polymorph is present, the chemical composition of FeS_2 is essentially stoichiometric. Since FeS_2 always occurs in small grains or as rounded masses in a water-rich layer, it also yields many low totals; just over 50% (35 out of 69) of the analyses were good. Some of the low totals are probably the result of the presence of water in the soft brown melnikovite. FeS_2 occurring in a colloidal mass with ZnS contains an average of about 2 wt% Zn. No

other metals were detected. The pyrite occurring in the interior chalcopyrite layer of vent site 1 of dive 981 is apparently slightly S-deficient. actually corresponding to $FeS_{1.92}$.

Cu-Fe Sulfides

Cu-Fe sulfides in the vent deposits consist of chalcopyrite, cubanite, and iss, all with a metal:S atomic ratio of approximately 1, and anomalous bornite, bornite-chalcocite solid solution, and covellite. Average compositions of chalcopyrite and cubanite are shown in figure II.23. Chalcopyrite is essentially stoichiometric $CuFeS_2$. The cubanite, identified optically, by XRD, and by comparison with standard cubanite on the SEM, is actually slightly Fe-rich and Cu-poor compared to stoichiometric $CuFe_2S_3$. Iss cannot be directly analyzed in the way that the other minerals can, because it now appears as a network of chalcopyrite and cubanite lamellae instead of as a homogeneous mineral. The proportions of the two types of lamellae give a rough indication of the original iss composition. More quantitative analyses were obtained using the SEM feature of the Cameca microprobe: performing a quantitative analysis with a relatively low power scanning beam gave a composition averaged over the area scanned, and so approximated the composition that would be obtained by homogenizing the grain. Composi-

Figure II.23. Compositions of chalcopyrite, cubanite, and iss.

Solid circle = average chalcopyrite from Black Forest.

Solid square = average chalcopyrite from vent site 1 of dive 981.

Solid triangle = average cubanite from vent S-3.

Open triangle = average cubanite from vent S-2.

Crosses = individual iss analyses from vent site 1 of dive 981.

Open squares = stoichiometric chalcopyrite (cp) ($CuFeS_2$) and cubanite (Cub) ($CuFe_2S_3$).

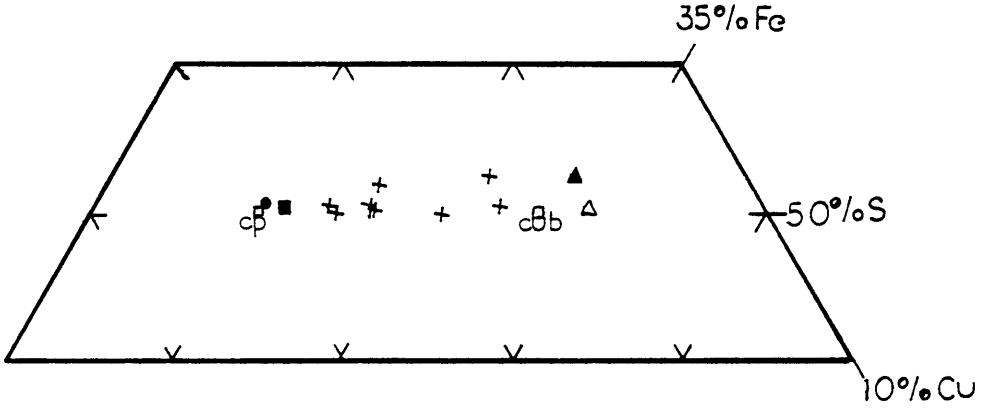
35% Fe
50% S
10% Cu

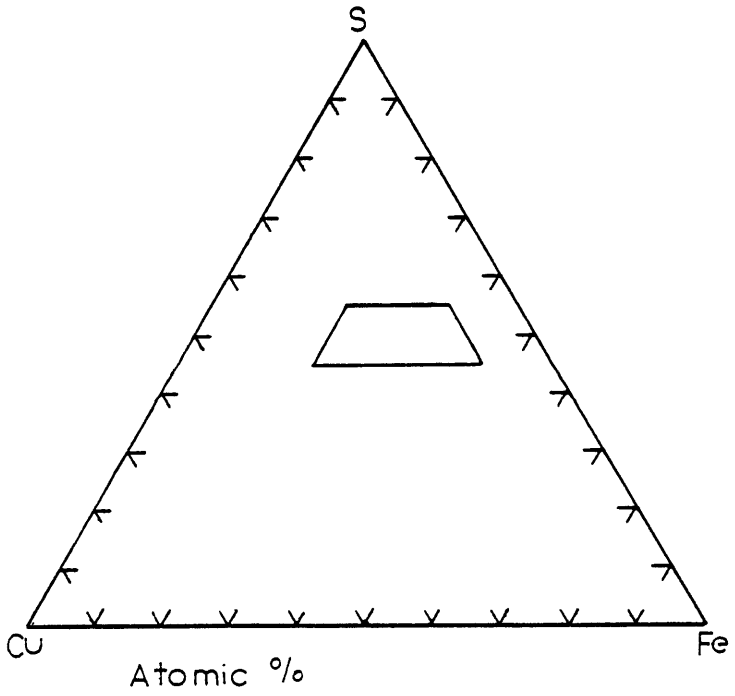
S
Cu
Fe
Atomic %

tions of individual iss grains obtained in this way are shown in figure II.23. The totals of the analyses ranged from 94.66 - 100.00 wt% and included 0.74 - 1.59 wt% Zn. The compositions span the entire range between chalcopyrite and cubanite, but none of them fall below 50 mole% S. Although the bulk of the iss field does fall below 50% S, very few compositions in the field are quenchable. The final appearance of iss as cubanite and chalcopyrite lamellae reflects the fact that those phases can be quenched, and so may in itself represent a modification of the original iss composition.

The compositions of the various forms of bornite, chalcocite, and covellite found in the vent deposits are depicted in figure II.24. Anomalous bornite has a composition of 60.81 wt% Cu, 10.81 wt% Fe, 0.03 wt% Zn, and 28.35 wt% S averaged over 27 analyses totaling 100 ± 2 wt%; this composition corresponds to $Cu_5FeS_{4.6}$. Zn is often present in trace quantities up to 0.15 wt%, but because it is not always present the "average" Zn content is very low. The anomalous bornite falls within Sillitoe and Clark's (1969) observed compositional range for anomalous bornite, although it contains more sulfur than any bornite synthesized experimentally by Yund and Kullerud (1966).

The bornite-chalcocite solid solution rim on the Black Forest chimney is the only known occurrence of ordinary bornite or of chalcocite in the vent samples. Analyses from a

Figure II.24. Compositions of bornite-chalcocite solid solution, anomalous bornite, and covellite.

Solid circles = analyses from a cross-section of the bornite-chalcocite rim on the Black Forest

Solid square = average composition of anomalous bornite.

Solid triangle = covellite analysis.

Open circles = stoichiometric bornite (bn) (Cu_5FeS_4), chalcocite (cc) (Cu_2S), covellite (cv) (CuS), chalcopyrite (cp) ($CuFeS_2$), cubanite (cub) (Cu_5FeS_4), and pyrrhotite (po) $Fe_{1-x}S$)

The area enclosed in the solid line is the bornite-chalcocite solid solution field at 400°C from Craig and Scott (1974).

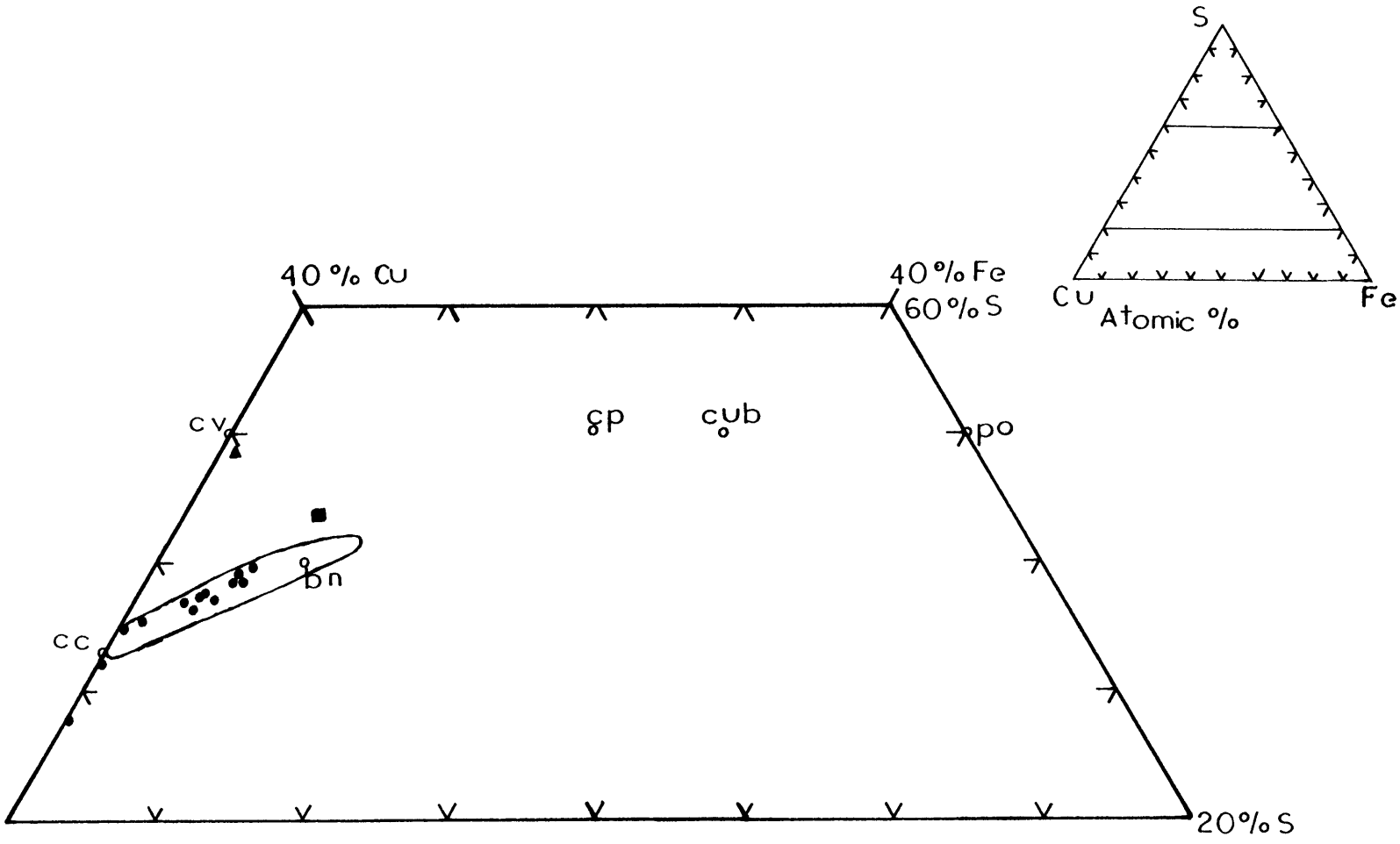
S
Cu
Fe
Atomic %
40 % Cu
40 % Fe
60 % S
cv
cc
bn
cp
cub
po
20 % S

cross section of the rim are shown in figure II.24. The Cu:Fe atomic ratio increases consistently across the 2.25 mm thick section of the rim. The outlined field is the bornite-chalcocite solid solution field at 400°C from Craig and Scott (1974). The agreement between the equilibrium solid solution field and the observed compositions is excellent.

Covellite in the vent samples is always associated with anomalous bornite or chalcocite. It usually occurs as fine lines and irregular patches; a good analysis of this material is almost impossible to obtain. The composition shown in figure II.24 is based on an analysis totaling only 92.70 wt%, of covellite replacing anomalous bornite. It is offered only as an indication of the presence of covellite, and not as a good quantitative analysis. Some anomalous bornite is almost certainly included in the analysis also, which accounts for the Fe content.

Zn Sulfide

ZnS is the most widespread sulfide in the vent deposits. It occurs in all samples to at least a minor extent. All the zinc sulfide samples studied by XRD were forms of wurtzite, and all the visible crystals are hexagonal. Analysis of XRD spectrometer tracings reveals the presence of a mixture of polymorphs, but 2H wurtzite is predominant (Brack-

mann, 1980). However, the possibility remains that some of the ZnS is in fact sphalerite, which is the form of ZnS in the black smoke (Spiess et al., 1980). ZnS in the fine-grained mixed sulfides has not been studied by XRD because the minerals could not be separated sufficiently to produce an XRD tracing from only one mineral. XRD patterns from the sulfide mixture are not useful for distinguishing wurtzite from sphalerite because the lines from pyrite overlap with those from both forms of ZnS.

Microprobe analysis of wurtzite yielded excellent results. All the ZnS contained Fe, generally in large amounts, up to 19.95 wt% Fe (32.99 mole% FeS). Figure II.25 presents average wurtzite compositions in the Zn-Fe-S system. Also included on the diagram are wurtzite analyses obtained on samples from vent S-3 by Brackmann (1980). Average compositions, however, can be misleading. In this case, they conceal a wide variation in Fe content within each sample, as shown in figure II.26, where the mean, standard deviation, and total range of Fe content in ZnS from a variety of chimney locations are depicted. The wurtzite crystals lining the channelways in vent S-3 have the most limited range of compositions. Variations in composition within separate crystals in the lining are comparable to variations among the different grains. Wider ranges and more scattered averages are found in the fine-grained mixture of sulfides forming the mass of the Zn-rich chimneys, but ZnS grains there

Figure II.25. Average wurtzite compositions.

Crosses = individual elongate wurtzite crystals lining channelways in vent S-3; this study and Brackmann (1980).

Open circles = fine-grained wurtzite from vent S-3.

Closed circle = concentric ZnS, with galena, from vent S-3.

Solid triangle = wurtzite from colloidal-textured layer of vent S-2.

Solid square = wurtzite from wurtzite-rich layer of vent S-2.

Open square = wurtzite from thin mixed sulfide layer, vent site 1 of dive 981.

Open triangle = wurtzite from thick mixed sulfide layer, vent site 1 of dive 981.

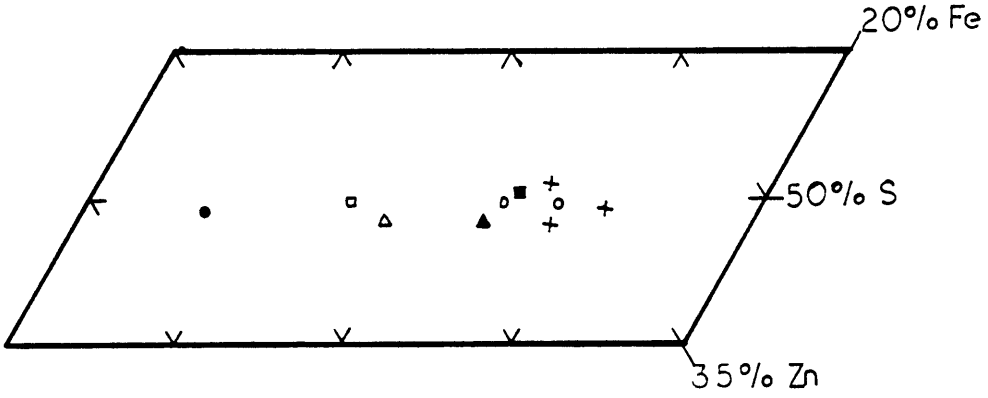
20% Fe
50% S
35% Zn

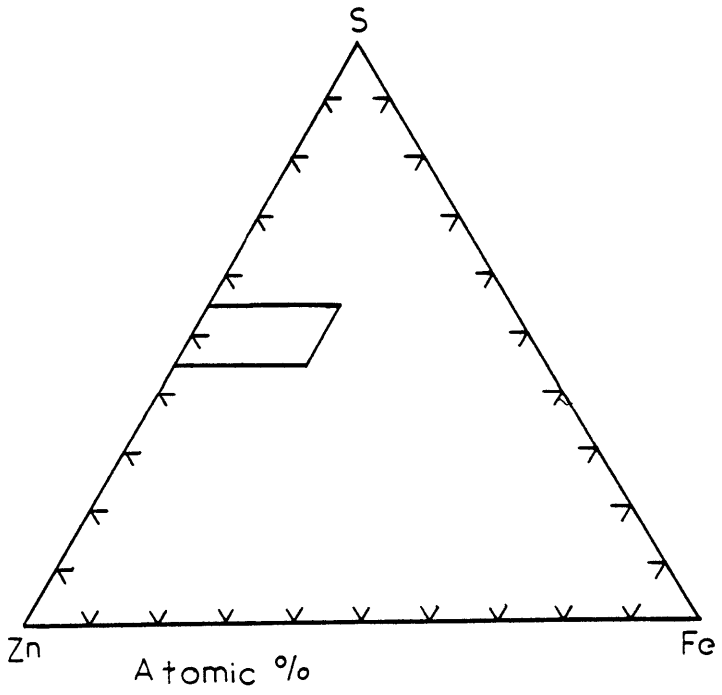
S
Zn
Fe
Atomic %

Figure II.26. Range of Fe (wt %) in ZnS.
Length of line = total range in Fe
Cross mark = average Fe
Ellipse = standard deviation

A: Elongate hexagonal prism from vent S-3.

B: Another elongate hexagonal prism from vent S-3; data from Brackmann (1980).

C: Same as (B), but a different crystal.

D: Wurtzite from mixed sulfide layer of vent S-3, with Mn and Cd in analyses.

E: Same location as (D), but with no Mn and Cd in analyses.

F: Concentric ZnS associated with galena from outer layer of vent S-3.

G: Wurtzite from colloform layer of vent S-2.

H: Wurtzite from thin mixed sulfide layer, vent site 1 of dive 981.

J: Wurtzite from thick mixed sulfide layer, vent site 1 of dive 981.

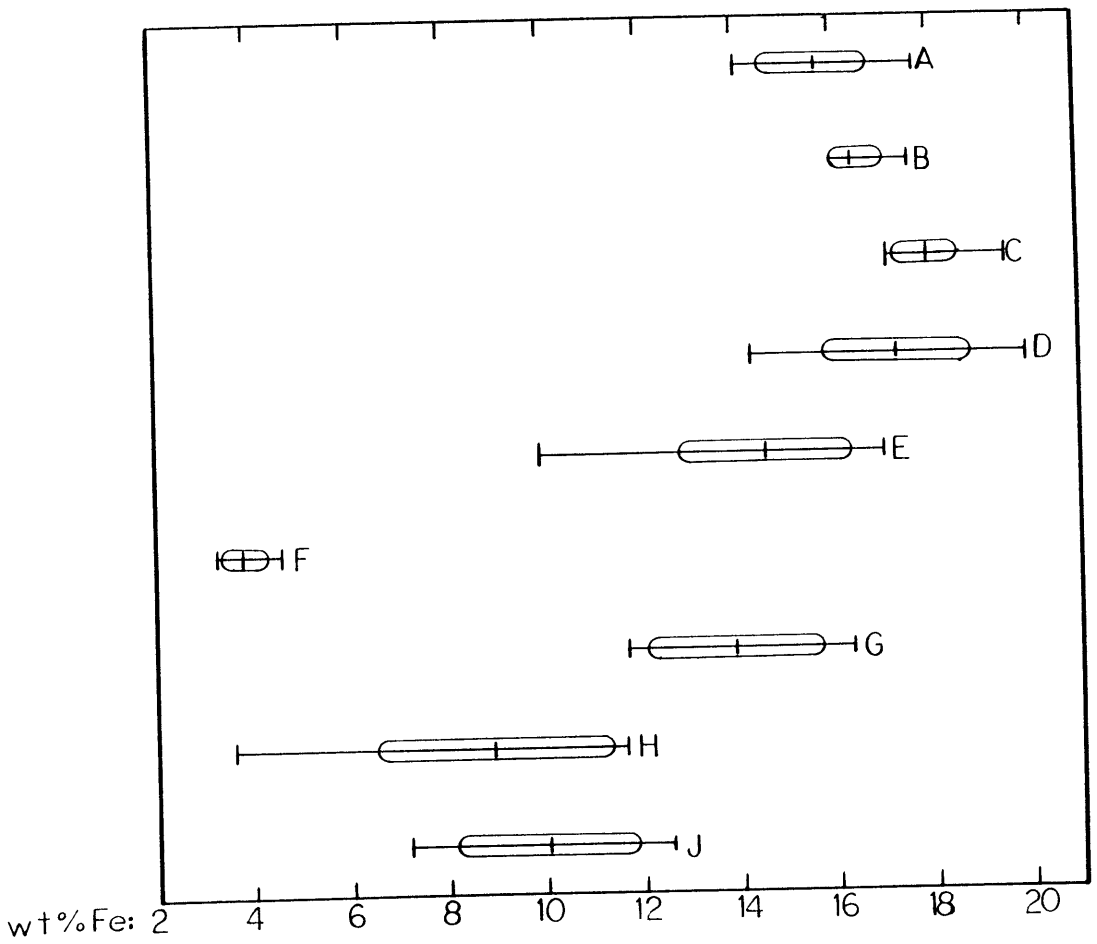
A
B
C
D
E
F
G
H
J
wt% Fe: 2 4 6 8 10 12 14 16 18 20

can be as rich in Fe as any in the interior. However, ZnS in the exterior layers of the chimneys may be much lower in Fe than any in the interior. Wurtzite in the elongate hexagonal crystals contains 14 or more wt% Fe; in the exterior of the chimney the Fe content drops as low as 3.33 wt%.

Taken as a whole, wurtzite in the Cu-rich chimneys spans a slightly smaller range of compositions than that in the Zn-rich chimneys. The high end of the range is not as Fe-rich (16.32 wt% Fe vs. 19.95 wt%), and although the low end of the range is almost identical (3.62 wt% vs. 3.33 wt%), it is represented by only 2 analyses below 6.43 wt% Fe. The difference between the two Cu-rich chimneys is interesting. In both cases the wurtzite comes from the fine-grained or colloidal outer layer, yet there is very little overlap in the Fe content of wurtzite in the two chimneys. Separately, the wurtzite in each of the Cu-rich chimneys exhibits a much more limited range of Fe content than the wurtzite in a Zn-rich chimney does.

The FeS content of wurtzite or sphalerite is a reflection of the conditions under which the mineral formed. Temperature, a_{FeS}, and f_{S_2}, are among the factors determining the degree of solid solution at equilibrium (Craig and Scott, 1974). The much wider range of (Zn,Fe)S composition in the Zn-rich chimney compared to the relatively restricted ranges in the Cu-rich chimneys suggests that wurtzite in the Zn-rich chimney formed under more widely varying conditions

than that in the Cu-rich chimneys. The different ranges of (Zn,Fe)S in the two Cu-rich chimneys also suggest different conditions of formation of the same mineral in the two chimneys.

Wurtzite contains the most extensive trace metal suite of any of the sulfides in the chimneys. All the elongate hexagonal crystals analyzed contained on the order of 0.1 wt% Mn and 0.25 wt% Cd. Similar levels of Mn and Cd were found in the finer-grained wurtzite in the mass of the Zn-rich samples, when those elements were included in the analysis. Although Pb was included in many of the analyses, it was detected in only two places. In one small spot on the outside of vent S-3, ca. 2.5 wt% Pb was detected in tiny grains and round globules of ZnS with a low Fe content (~ 3.84 wt%). These globules are perfectly round and concentrically banded in reflected light. Morphologically, they are unlike any other ZnS observed in the chimneys. Intimately associated with these globules and tiny wurtzite grains are minute inclusions of PbS, on a scale of 1 - 5 microns. The Pb content of the ZnS may be accounted for by sub-microscopic inclusions of PbS.

The second occurrence of detectable levels of Pb in wurtzite is in the colloidal layer of vent S-2. In this layer the analyses consistently reveal low levels of Pb (~ 0.2 wt%), which is apparently present in solid solution.

Cu is also present as a trace metal in wurtzite. Be-

cause disseminated Cu-Fe sulfide replacement is common in all the samples, analyses containing more than 1 wt% Cu were considered likely to be diseased and were omitted from these calculations. Often, disseminated chalcopyrite disease was visible in wurtzite grains containing several wt% Cu. This approach tends to minimize the estimates of Cu concentration in wurtzite, but it is not an unreasonable approach, because a limited solid solution of Cu in wurtzite has been achieved experimentally. Moh (1975), Wiggins and Craig (1980), and Hutchison and Scott (1981) found less than 1 wt% Cu in sphalerite at 600°C, in studies that imply that even less Cu should be present in sphalerite formed at lower temperatures. Wurtzite seems unlikely to contain much more Cu than sphalerite; Moh (1975) found less than 1% chalcopyrite in wurtzite at 1032°C, although sphalerite at the same temperature contained up to 2 wt% chalcopyrite. The effect of the high levels of Fe present in the wurtzite at 21°N on the solubility of Cu in ZnS is unknown.

In the Cu-rich chimneys, Cu is ubiquitous in ZnS at low levels. The highest concentration (0.65 wt%) occurs in the colloidal layer of vent S-2, accompanying Pb. In contrast, wurtzite in the predominantly wurtzite layer contains only 0.07 wt% Cu, just above the detection limit for Cu.

In vent site 1 of dive 981, wurtzite occurring in samples with only a thin mixed sulfide layer contains ~0.3 wt% Cu, while in the thick fine-grained to colloidal layer it

contains ~0.2 wt%. Analyses of wurtzite grains with chalcopyrite disease in this chimney revealed Cu contents from 1.31 wt% to 10.97 wt% Cu, plus one heavily replaced grain containing 27.94 wt% Cu.

Anhydrite

The sulfate component of the chimneys consists almost entirely of anhydrite. Both XRD patterns and microprobe analyses confirm that the predominant mineral is anhydrite, which is reasonable considering that anhydrite can be precipitated by simply heating seawater to ca. 120°C (Bischoff and Seyfried, 1977). Most of the microprobe analyses are excellent; some of the totals are slightly low as a result of inclusions of sulfide and silicate minerals within the anhydrite. Besides Ca and S, Sr, Ba, and Pb were included in the analyses. Ba appeared once, at a level of 0.09 wt%, but Sr is essentially the only minor element detected in the anhydrite. Sr is consistently present in anhydrite from the Black Forest vent, and in massive layered anhydrite from vent S-2. It is absent from the samples from vent S-3 and vent site 1 of dive 980, the two Zn-rich vents, and from the colloidal and mixed sulfide layers of vent S-2.

In anhydrite that is concentrated in almost monomineralic bands in vent S-2 and the Black Forest (where it occurs rarely), Sr occurs at levels up to 0.57 wt% SrO; the average

SrO content is 0.23 wt%. The isolated inclusions of anhydrite that occur within the sulfides in the Black Forest chimney are richer in Sr, containing from 0.18 to 0.93 wt% SrO, with an average of 0.53 wt%. The presence of Sr is very useful, because the isotopic composition of the Sr can reveal the relative proportions of seawater Sr and basalt Sr involved in formation of the anhydrite (Albarede et al., 1981).

Silicates

Silicates are the least abundant of the major mineral types in the vent deposits. Amorphous silica was detected on the X-ray spectra from the SEM. Silicates containing Mg were also detected, and these proved to be sufficiently abundant to be studied by microprobe analysis. XRD lines obtained from samples including Mg-silicates were generally confused or indeterminate. In thin sections the silicates generally appear as rounded globules associated with fine-grained or colloidal sulfides. They do not appear as identifiable crystals either in thin section or on the SEM.

Microprobe analyses of the Mg-silicates gave totals ranging from 67.14 to 92.60 wt%. Some of the missing weight is accounted for by water and some by minute inclusions of sulfides. Na, K, Al, Ca, and Fe were included in the analyses as well as Mg and Si, but only Fe was detected, in quan-

tities from 0.25 wt% FeO to 4.27 wt% FeO. Analyses were performed on samples from the Black Forest and vent S-2. The best development of silicates is in vent S-2, and the totals there are most consistent, at 75.27 ± 2.33 wt%. All the analyses are shown in figure II.27, plotted as though the low totals are entirely due to H_2O. The analyses plot within the area bounded by talc, chrysotile, and H_2O. The Mg:Si atomic ratio of the material falls between that of chrysotile and that of talc, saponite, and sepiolite. However, the composition seems to vary, and the water content is often very large. The Mg-silicate phase could not be identified with any particular mineral or mixture of minerals.

Other Minor Phases

Additional minor phases in the vent deposits were detected by SEM, in polished section, and, rarely, in microprobe analysis. Detection and identification of these minor phases is largely a matter of chance, since their distribution is so random that a specific section cannot be chosen intentionally to include them. Additional trace minerals of three types were found: native sulfur, oxides, and sulfate. Native sulfur was identified in sample 981-R-1. It was seen

Figure II.27. Composition of Mg-silicates. Open circles are stoichiometric compositions:

bru = brucite

fo = forsterite

en = enstatite

anth = anthophyllite

chrys = chrysotile

sep = sepiolite and palygorskite

sap = saponite

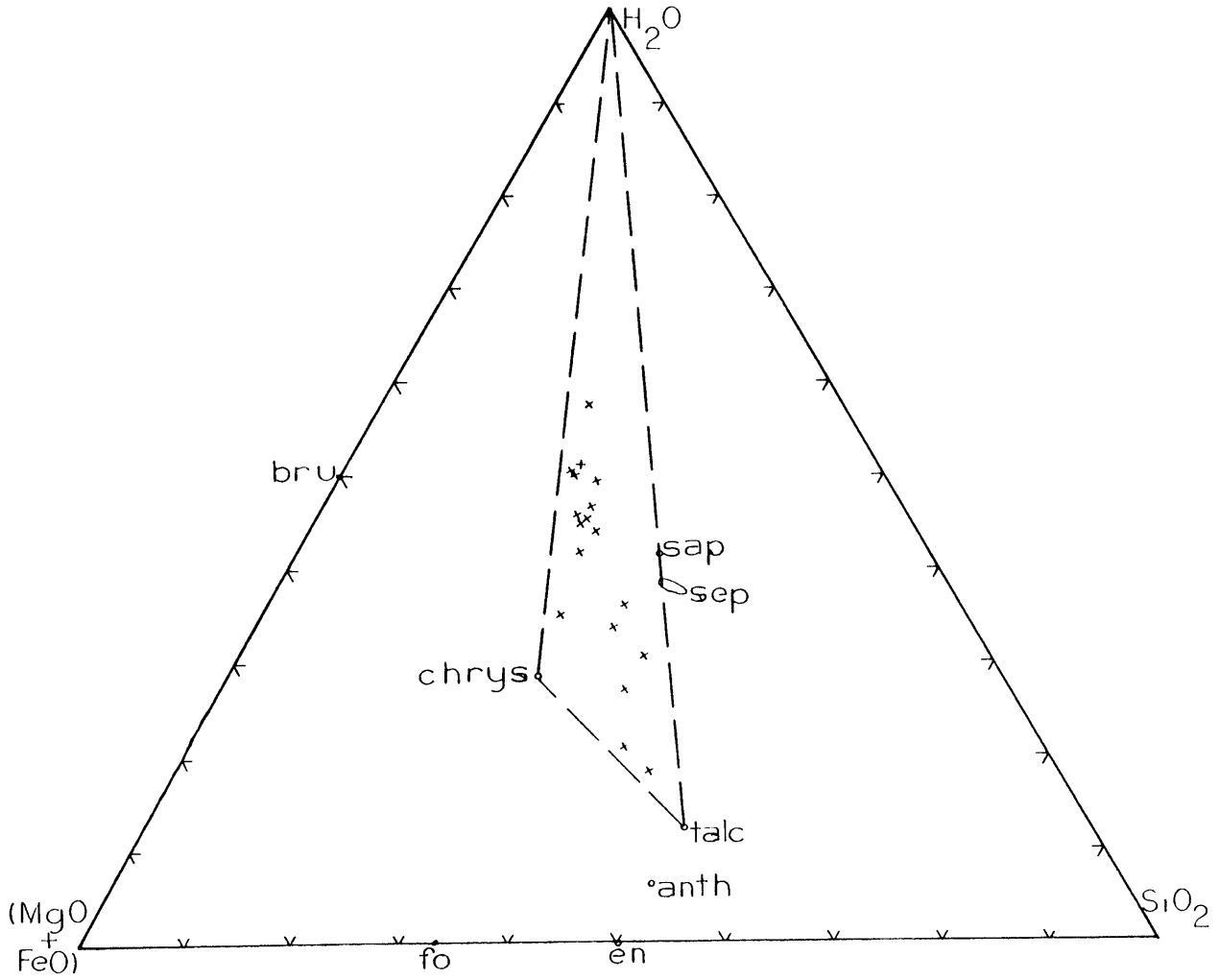
H_2O
bru
sap
sep
chrys
talc
anth
(MgO + FeO)
fo
en
SiO_2

as small blobs on the SEM, and identified by X-ray spectra showing only S. It has also been detected in samples from vent S-3 (Brackmann, 1980).

Iron oxides occur on the exterior surfaces of all the chimneys. They formed only a very thin, patchy shell on the outer surface of the chimneys when the samples were collected, and were identified by XRF analysis and visually on board ship. This thin shell is easily lost when cutting samples and making polished sections; the Fe oxides therefore are not generally seen in thin section. The problem also arises in the laboratory of differentiating between a limonitic outer shell formed on an active chimney, and one developed by oxidation after the samples were collected. A thin oxidation layer did form on some of the samples. In particular, samples from vent S-3 collected on dive 982 that had to be packed for shipping while they were still slightly damp developed a rusty alteration on their originally black surfaces. The dry samples did not oxidize in the same way. The distinction between dry and damp samples is important; a slight tarnish did form gradually on many of the dry samples, but the oxidation only penetrated into the damp samples.

Anhydrite is the major sulfate component of the chimneys, as previously noted. Barite, however, does occur in small quantities. It has been observed in samples from vent S-3 in thin section, on the X-ray spectrum of the SEM, and

on the X-ray spectrum of the Cameca microprobe. The barite seen on the SEM occurs as very fine blades coating anhydrite laths. In thin section barite was observed in the same section containing PbS, in the Pb-rich area. The X-ray spectra on the Cameca of blades in this area indicated the presence of barite containing small quantities of Pb. Attempts to obtain a quantitative analysis, however, were unsuccessful.

A wide variety of trace minerals has been reported in other vent samples from 21°N by Haymon and Kastner (1981) and Oudin (1982). All of these are very rare; some of them have been identified only once. The list includes native sulfur, barite, galena, and Fe oxides as reported here, as well as jarosite and Ag-bearing sulfides.

Summary

The five vent areas sampled on the November 1979 cruise to 21°N can be separated into two sets of vents, one Cu-rich and one Zn-rich. Each of the chimneys has its own peculiarities, reflecting differences in the particular environment and conditions under which the chimneys formed, but the similarities and differences among the chimneys permit a broader view of the process of formation of the vent structures than any one chimney does.

The Cu-rich chimneys from vent S-2, vent site 1 of dive 981, and the Black Forest vent are characterized by a major

central fluid channelway lined by a single Cu-Fe sulfide, either chalcopyrite or cubanite. The exterior part of the chimney wall consists of a melange of varying proportions of anhydrite, Mg-silicates, and a fine-grained and/or colloidal sulfide mixture. Anomalous bornite and bornite-chalcocite replacement sequences occur at the contact between the monomineralic Cu-Fe sulfide interior and the mixed sulfides. The temperature of the hydrothermal fluid exiting from these chimneys is very hot, close to 350°C. Vent S-2 is noticeably richer in Fe than the other two Cu-rich vents. It contains $CuFe_2S_3$ instead of $CuFeS_2$, and wurtzite with a large component of FeS. The Black Forest vent is unusual in its lack of anhydrite and silicates.

The Zn-rich chimneys from vent S-2 and vent site 1 of dive 980 are generally characterized by many small fluid channelways cutting through massive samples. The channelways are lined with elongate wurtzite crystals rich in Fe, surrounded by a thin layer rich in Cu-Fe sulfides which are beginning to replace the outer edges of the wurtzite crystals. The bulk of the samples consists of a mixture of anhydrite and fine-grained sulfides, but lacks the colloidal texture and the Mg-silicates that occur in the fine-grained sulfide layer of the Cu-rich chimneys. The fluid venting from the Zn-rich chimneys is cooler than that venting from the Cu-rich chimneys; the measured exit temperatures are less than 300°C.

There are similarities between the chimneys that relate the two types. A certain degree of likeness exists between the outer mixed sulfide layers. The replacement sequences are similar in the two sets of chimneys; in particular, the replacement of wurtzite by the Cu-Fe sulfides chalcopyrite, cubanite, and iss. Also of interest is the one mound sample collected at vent S-2: the patterns of channelways and overall mineralization in the mound sample are almost identical to those of the chimney samples from the Zn-rich vents.

Chapter III

Chimney Formation

The process of chimney formation reduces, at a basic level, to the precipitation of minerals from aqueous solutions. The composition of those solutions and the environment they encounter determine what minerals will be deposited, and when and where they will precipitate. The total system includes not only the hydrothermal fluid and ambient seawater, but also the pre-existing chimney structure through which the hot fluid rises.

It is important always to bear in mind that the development of the vent structures at 21°N is a dynamic process. Adjoining mineral grains in the samples were not necessarily deposited together. Even co-deposited minerals are not necessarily in equilibrium. Deposition may occur simultaneously under different conditions at different locations within the chimney walls. At any one location, conditions may change as the chimney develops. Finally, the temperature and composition of fluid rising through the vent may change over time. However, the chimneys do bear traces of their history, and the process of their growth can be reconstructed. The minerals themselves carry information about the environment in which they formed. This information will be examined, followed by a discussion of the mechanism of deposition of the minerals, the degree of equilibrium in the deposits, and

the construction of the vent structures.

Fe Sulfides

Pyrite is the only Fe sulfide present in most of the chimney samples. Its presence sets rather broad limits on the f_{S_2} and f_{O_2} of the environment at a given T. More useful information may be provided by the rare occurrences of pyrrhotite in the chimney. The presence of pyrrhotite and pyrite co-existing in equilibrium could be used to define f_{S_2} rather precisely at any given T. However, pyrrhotite in the Zn-rich chimneys precedes and is replaced by pyrite, implying a change in the environment of formation rather than implying equilibrium between the two minerals. In vent S-2 pyrrhotite occurs without pyrite, although the presence of pyrite in the chimney wall farther to the exterior implies a different environment of formation in the different layers of the chimney.

In general, the composition of pyrrhotite alone is not a useful indicator of the conditions under which it formed. However, the Cu content of pyrrhotite in vent S-2 can be used to infer a temperature of formation. The presence of a maximum of 0.31 wt% Cu in solid solution at equilibrium implies that the pyrrhotite coexisting with cubanite in vent S-2 was deposited at temperatures up to ca. 375°C (Hutchison and Scott, 1981) (see figure III.1). These temperatures agree

Figure III.1. The solubility of ZnS in iss at 1 bar and 5 kb, and of CuS in pyrrhotite at 1 bar, in the assemblage sphalerite + pyrite + pyrrhotite + iss. Data from Hutchison and Scott, 1981, except as noted. From Hutchison and Scott, 1981; figure 4.

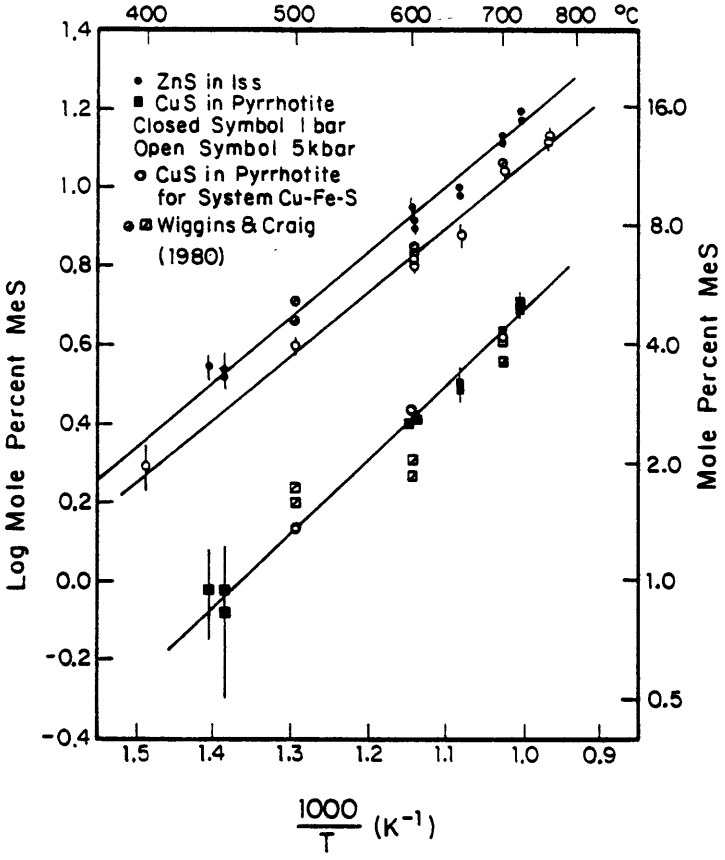
400
500
600
700
800
°C
1.4
1.2
1.0
0.8
0.6
0.4
0.2
0.0
-0.2
-0.4
16.0
8.0
4.0
2.0
1.0
0.5
• ZnS in Iss
■ CuS in Pyrrhotite
Closed Symbol 1 bar
Open Symbol 5kbar
o CuS in Pyrrhotite
for System Cu-Fe-S
Wiggins & Craig
(1980)
Log Mole Percent MeS
Mole Percent MeS
1.5
1.4
1.3
1.2
1.1
1.0
0.9
1000/T (K⁻¹)

with Spiess et al.'s (1979) estimation that pyrrhotite in the black smoke formed at ca. 300°C.

Zn Sulfide

ZnS in the vent samples permits three possible approaches to defining the conditions of formation of the deposits. One is to use the form of the ZnS itself, i.e., the occurrence of wurtzite rather than of sphalerite; another is to use the FeS content of the ZnS. The third alternative is to derive formation temperatures from fluid inclusions in wurtzite.

The relative stability of sphalerite and wurtzite under a variety of conditions is not well known, perhaps because wurtzite is uncommon compared to sphalerite. The standard view holds that sphalerite is the stable low-temperature form of ZnS, and wurtzite the stable high-temperature form (Barton and Skinner, 1979). The inversion temperature was determined by Moh (1975) to be 1031°C for S-rich ZnS and 1013°C for Zn-rich ZnS. If this is true for the zinc sulfides at 21°N, it implies the presence of a major quantity of metastable ZnS in the chimneys.

However, the wurtzite-sphalerite transition can be affected by variations in "ZnS" composition, including the presence of trace metals and possibly the metal:S atomic ratio. High concentrations of CdS or MnS in solid solution

($\geq$ 10 mole %) stabilize the wurtzite structure and therefore lower the inversion temperature of sphalerite to wurtzite (Craig and Scott, 1974; Tauson and Chernyshev, 1979; Barton and Skinner, 1979), but although both Cd and Mn are present in wurtzites from 21°N, they are never sufficiently abundant to affect the relative stability of the two ZnS phases. The presence of Fe may have a much smaller effect on the stability of the ZnS polymorphs; the evidence concerning its effect is contradictory. Craig and Scott (1974) state that FeS in solid solution in ZnS stabilizes the sphalerite structure; Tauson and Chernyshev (1979) and Moh (1975) found FeS to stabilize wurtzite.

The effect of non-stoichiometry on the Zn sulfides is also a matter of some debate. Barton and Skinner (1979) believe that the variation in stoichiometry of ZnS is too small to have a major effect on the stability of the phases, especially since Skinner and Barton (1960) found sphalerite at 900°C in equilibrium with either free S or free Zn. However, Scott and Barnes (1972) maintain that the wurtzite-sphalerite transition is a function of f_{S_2} as well as temperature, that the true metal:S atomic ratio is slightly less than 1 in sphalerite and slightly greater than 1 in wurtzite. Their conclusions are supported by Shalimova and Morozova (1965), who converted wurtzite to sphalerite in the presence of S and sphalerite to wurtzite in the presence of Zn. Pankratz and King (1965) found S/(Zn+Fe) mole ratios of 1.001 - 1.004

in sphalerite and 0.995 - 0.998 in wurtzite by making very precise analyses of synthetic crystals. Scott and Barnes (1972) defined the wurtzite-sphalerite transition as a function of f_{S_2} and T based on hydrothermal recrystallization and gas mixing experiments; their results are shown in figure III.2.

If the stability relations of sphalerite and wurtzite are determined by f_{S_2} as well as by T, then the presence of wurtzite as a stable phase in the chimneys could be a valuable indicator of the conditions prevailing in the chimneys. Microprobe analyses yielded values both slightly rich in S and slightly rich in Zn, although most were rich in Zn. Unfortunately, the uncertainty in the analyses is too great to define non-stoichiometry in the Zn sulfides with sufficient accuracy. The wurtzite-sphalerite boundary shown in figure III.2. might be taken as an upper limit on f_{S_2} at a given T, but the uncertainty in extrapolating the curve below 400°C makes this a rather flexible upper limit. An obvious difficulty for this interpretation arises from the observation that wurtzite and pyrite do not exist together stably above about 150°C if Scott and Barnes' version of the ZnS equilibrium is accepted, whereas wurtzite + pyrite is the most common assemblage in the chimneys.

The Fe content of ZnS co-existing with pyrite and/or pyrrhotite is also a function of f_{S_2} and T. All the studies of this solid solution have been made using sphalerite, which

Figure III.2. The wurtzite-sphalerite equilibrium as a function of f_{S_2} and tempersture, shown with the pyrite-pyrrhotite equilibrium. From Craig and Scott (1974).

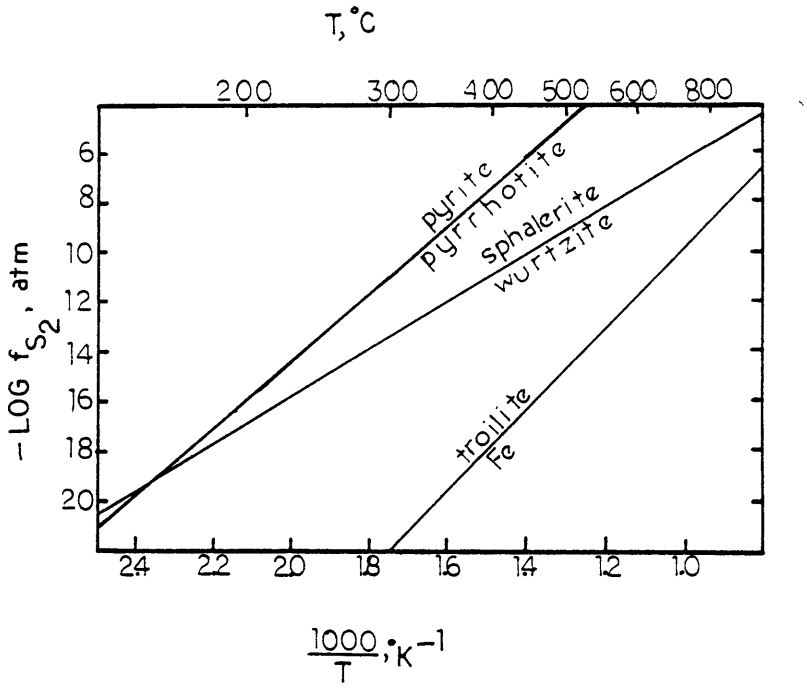
T, °C
200
300
400
500
600
800
6
8
10
12
14
16
18
20
$-\text{LOG } f_{S_2}$, atm
pyrite
pyrrhotite
sphalerite
wurtzite
troilite
Fe
24
22
20
18
16
14
12
1.0
$\frac{1000}{T}$, °K^{-1}

means that the application of the data to wurtzite introduces another source of uncertainty and error. The additional error may well be small, because the actual difference between the sphalerite and wurtzite structures involves only a small stacking difference and rotation of the layers in the two phases (Vaughan and Craig, 1978). The fact that FeS in solid solution probably has little effect on the relative stability of wurtzite and sphalerite also suggests that the data for the FeS content of sphalerite can be applied to wurtzite with little additional error.

The relationships among f_{S_2}, T, and the composition of (Zn,Fe)S coexisting with pyrite and/or pyrrhotite are shown in figure III.3. Once again, the uncertainty increases at low temperatures. The FeS content of ZnS coexisting with both pyrite and pyrrhotite remains essentially constant and close to 21 mole %FeS at temperatures below ca. 550°C (Scott and Barnes, 1972). Although the FeS content of ZnS cannot be used as a geothermometer in the temperature range applicable to the vents at 21°N, it can be used to infer an f_{S_2} value at a given T.

Wurtzite in the chimneys at 21°N can be found in four different relationships with Fe sulfides: (1) (Zn,Fe)S alone, accompanied by neither $Fe_{1-x}S$ or FeS_2, in the channel linings of Zn-rich chimneys; (2) (Zn,Fe)S co-precipitated with pyrite, in the mixed sulfide layers of all the chimneys; (3) (Zn,Fe)S co-existing with both pyrrhotite and pyrite;

Figure III.3. Relationships between the mole % FeS in sphalerite (light solid lines) and equilibria in the Fe-S and Cu-Fe-S systems, at 1 bar. Data points shown are from Czamanske (1974). From Czamanske (1974); figure 1.

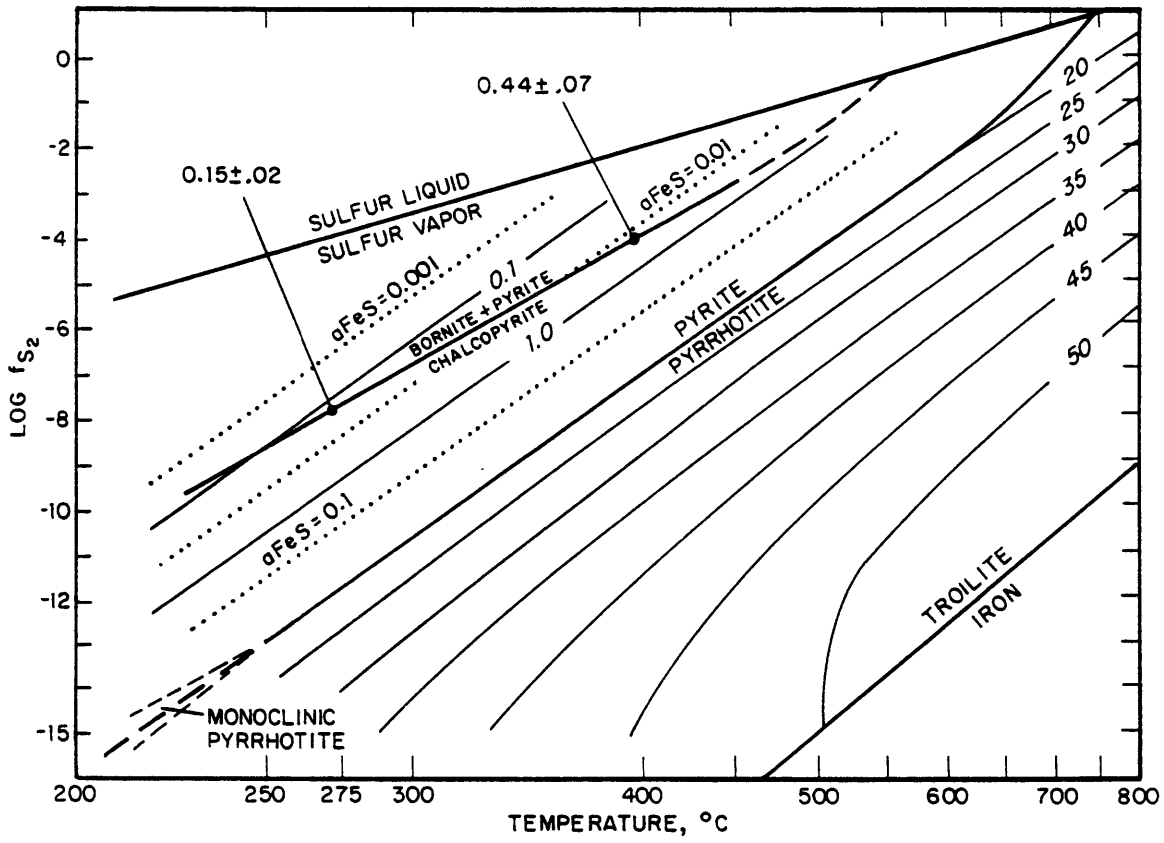
0.44±.07
0.15±.02
SULFUR LIQUID
SULFUR VAPOR
aFeS=0.001
aFeS=0.001
0.1
BORNITE + PYRITE
CHALCOPYRITE
1.0
aFeS=0.1
PYRITE
PYRRHOTITE
MONOCLINIC
PYRRHOTITE
TROILITE
IRON
20
25
30
35
40
45
50
0
-2
-4
-6
-8
-10
-12
-15
LOG f_{S_2}
200
250
275
300
400
500
600
700
800
TEMPERATURE, °C

(4) (Zn,Fe)S co-existing with and apparently co-precipitated with pyrrhotite in the pyrrhotite-bearing layer from vent S-2. In case (3), wurtzite co-precipitated with pyrite that replaced pyrrhotite, in the mixed sulfide layer of vent S-3; the wurtzite is therefore likely to be in equilibrium with pyrite, but not necessarily with pyrrhotite. The relationships between Fe and Zn sulfides are therefore probably similar in case (2) and case (3).

Wurtzite deposited as a monomineralic lining in the Zn-rich chimneys, case (1) above, coexists with no Fe sulfides and therefore is not subject to this particular analysis. The other occurrences of (Zn,Fe)S, however, display interesting and sometimes contradictory variations in FeS content. In vent S-3, a Zn-rich vent with occasional remnants of pyrrhotite in the wurtzite + pyrite mixed sulfide layer, cases (2) and (3) above, the f_{S_2} indicated by the minimum mole % FeS in ZnS lies along the pyrite-pyrrhotite boundary. As the mole % FeS increases to 32.99% the corresponding range in f_{S_2} values extends well into the pyrrhotite field. The only exception is the unusual concentric ZnS coexisting with galena and pyrite, but not with pyrrhotite. The FeS content of this ZnS (5.80 - 8.16 mole % FeS) plots within the pyrite field.

In the samples from vent S-2, wurtzite occurs either with pyrrhotite in a pyrrhotite-rich layer (case(4)) or with

pyrite in a mixed sulfide layer (case (2)); there is no significant difference in the FeS content of wurtzites in the two layers. The range in FeS contents (19.84 to 27.26 mole %) again indicates a range in f_{S_2} values from the pyrite-pyrrhotite boundary down into the pyrrhotite field.

Wurtzite from vent site 1 of dive 981 exhibits a very different range of FeS contents. In these samples, wurtzite coexists with pyrite in a mixed sulfide layer similar to that from vent S-2. However, the FeS values indicate a range in f_{S_2} from the pyrite-pyrrhotite boundary upward into the pyrite field, as FeS varies from 21.72 to 6.12 mole %.

The total range in f_{S_2} values indicated by the FeS content of ZnS in the chimneys at 21°N extends from within the pyrite field well into the pyrrhotite field; the precise values of f_{S_2} depend on the temperature of the minerals. An inconsistency exists, in many of the samples, between the presence of coprecipitated pyrite and wurtzite and the FeS content of the wurtzite, which indicates that wurtzite should coexist, at equilibrium, with pyrrhotite. Even if there is considerable uncertainty in all the phase boundaries and compositional contours, it is clear both that only approximate indications of f_{S_2} can be obtained by applying the above relationships to the chimneys at 21°N, and that extensive metastability and/or disequilibrium may occur in the deposits.

Fluid inclusions from wurtzite crystals lining the chan-

nelways in one sample from vent site 1 of dive 980 do yield useful temperature data. Four inclusions were found. The filling temperatures fell between 266 - 269°C (Styrt et al., 1981), implying formation temperatures of 285 - 289°C when a pressure correction for 260 bars is applied (Potter, 1977).

Iss

In the Cu-Fe-Zn-S system, the solubility of ZnS in iss can be a sensitive temperature indicator (Hutchison and Scott, 1981) (see figure III.1). It is useful in the low temperature ranges present in the hydrothermal vents because the levels of ZnS in iss are still relatively high at temperatures near 400°C. The iss grains analyzed are from the outer layer of vent site 1 of dive 981. They coexist and were apparently coprecipitated with wurtzite and pyrite. Their ZnS content ranged from 1.08 mole % to 2.30 mole %, with an average of 1.58 mole % ZnS. The corresponding temperatures of formation range from ~320°C to ~400°C; the average composition yields a temperature of formation of ~356°C. The agreement between this temperature and the exit temperature of hydrothermal fluid at the vent (350°C) is startling but gratifying. However, as a result of the shortcomings of the analytical technique used to obtain iss compositions are unlikely to reflect accurately the precise composition of the original iss. The error on the curves in

figure III.1 must also be taken into account. In consequence, a large uncertainty factor must be applied to the temperature estimates obtained from iss compositions.

Anomalous Bornite

The presence of anomalous bornite outside the monomineralic chalcopyrite lining of vent site 1 of dive 981 and the Black Forest implies a temperature limitation in the environment of deposition. Yund and Kullerud (1966) found that sulfur-rich bornite formed readily below about 140°C. Although the anomalous bornite in the chimneys is richer in S than any synthesized by Yund and Kullerud, the composition is within the range of composition observed by Sillitoe and Clark (1969) in anomalous bornites from the Copiapo mining district of Chile. These anomalous bornites occur with ordinary bornite, as does anomalous bornite in the Black Forest vent. Sillitoe and Clark observed that samples of their anomalous bornite exsolved chalcopyrite lamellae when heated in vacuo at 115°C for 7 days, similar to the behavior of natural and synthetic sulfur-rich bornites studied by Brett and Yund (1964). The most common natural occurrence of anomalous bornite is in red-bed Cu ores; its absence from hypogene ores has been interpreted to imply that it can be deposited directly only from low-temperature fluids (Brett and Yund, 1964); however, the mineral does also form as an oxidation product of hypogene bornite (Sillitoe and Clark,

1969). All the available evidence indicates that anomalous bornite forms only at low temperatures, less than ~150°C. This places a rather strong upper limit on the temperature within the chimney walls at the time of formation of anomalous barnite.

The preceding discussion concerned only those minerals that retain internal evidence of the T, f_{S_2}, or f_{O_2} at the time of their formation, but all the minerals present in the chimneys must be saturated or supersaturated in the mineralizing solution at the time of their deposition. Interaction between the hydrothermal fluid and its surroundings creates the conditions under which the fluid becomes saturated with particular minerals, and thereby controls the formation of the chimney structures. The major mechanism of mineral deposition at 21°N is the interaction that occurs between hydrothermal fluid and seawater.

Fluid Mixing

At 21°N, a hot fluid with a low pH, rich in H_2S and metals, emerges as a buoyant plume and mixes with cold seawater that has a much higher pH and is rich in SO_4^{--}. The changes in T, pH, and oxidation state of the solutions that occur during mixing provide obvious mechanisms for the precipitation of vent deposits.

Mixing of two fluids has been observed or deduced in

other natural geothermal systems and ore deposits (see, for example, Fournier and Truesdell, 1974; Fournier, 1977; Ripley and Ohmoto, 1977; Turner and Gustafson, 1978; Solomon and Walshe, 1979). Drummond (1981) verified quantitatively the effectiveness of mixing of two distinct fluids as a mechanism of ore deposition, using a computer program of mass action, charge balance, and mass balance equations to model the thermodynamics of the system. In a model of Kuroko ore deposition, he concluded that mixing between cold seawater and a hot (300°C) fluid at a pH of 4.5, similar in composition to the 21°N hydrothermal fluid, would result in essentially quantitative deposition of sulfides accompanied by significant sulfate and quartz deposition.

Abundant evidence of mixing between seawater and hydrothermal solutions can be found in the vent deposits at 21°N. The isotopic evidence is particularly compelling. Analyses of the isotopic composition of sulfur in samples from all five vents indicate that sulfate in anhydrite in the samples came directly from seawater (Styrt et al., 1981). Sulfur in sulfides from the same samples was derived primarily from basalts (Styrt et al., 1981; Arnold and Sheppard, 1981), and therefore must have been brought into the chimneys by the hydrothermal fluid. Simultaneous deposition of sulfates and sulfides requires mixing of the two fluids.

Isotopic analyses of strontium in anhydrite from the vent deposits provide direct evidence for deposition from

mixed solutions of seawater and hydrothermal fluid. Albarede et al. (1981) found that the hydrothermal fluid and seawater contain similar concentrations of Sr, but that the $^{87}Sr/^{86}Sr$ ratio in the two fluids is distinctly different. The $^{87}Sr/^{86}Sr$ ratio in present day seawater is 0.7091; in the hydrothermal fluid it is 0.7030. All the analyzed samples of sulfates from the vents at 21°N fall between these two extremes (Albarede et al., 1981; Vidal and Caluer, 1981). The observed isotopic ratios indicate that Sr in the anhydrite is derived from mixtures of seawater and hydrothermal fluid, which may contain as much as 2/3 hydrothermal fluid (Albarede et al., 1981). It is interesting to note that the $^{87}Sr/^{86}Sr$ ratio in samples from a single chimney may vary considerably; this indicates that anhydrite is deposited from mixed solutions with a wide range of ratios of seawater to hydrothermal fluid.

Anhydrite deposition from a wide range of mixed solutions is also indicated by the range of filling temperatures recorded for fluid inclusions in anhydrite from samples from vent site 1 of dive 981 and vent site 1 of dive 980 (Kusakabe et al., in prep., and this study). The filling temperatures are summarized in figure III.4. At each vent, a wide range of temperatures was observed. The maximum filling temperature exceeded the temperature that was actually measured at the mouth of the vent; this may simply be an insig-

Figure III.4. Filling temperatures of fluid inclusions in anhydrite.

A: Sample 980-R-2, from vent site 1 of dive 980; Kusakabe et al., in prep.

B: Sample 981-R-1, from vent site 1 of dive 981; Kusakabe et al., in prep.

C: Sample 981-R-22, from vent site 1 of dive 981; this study.

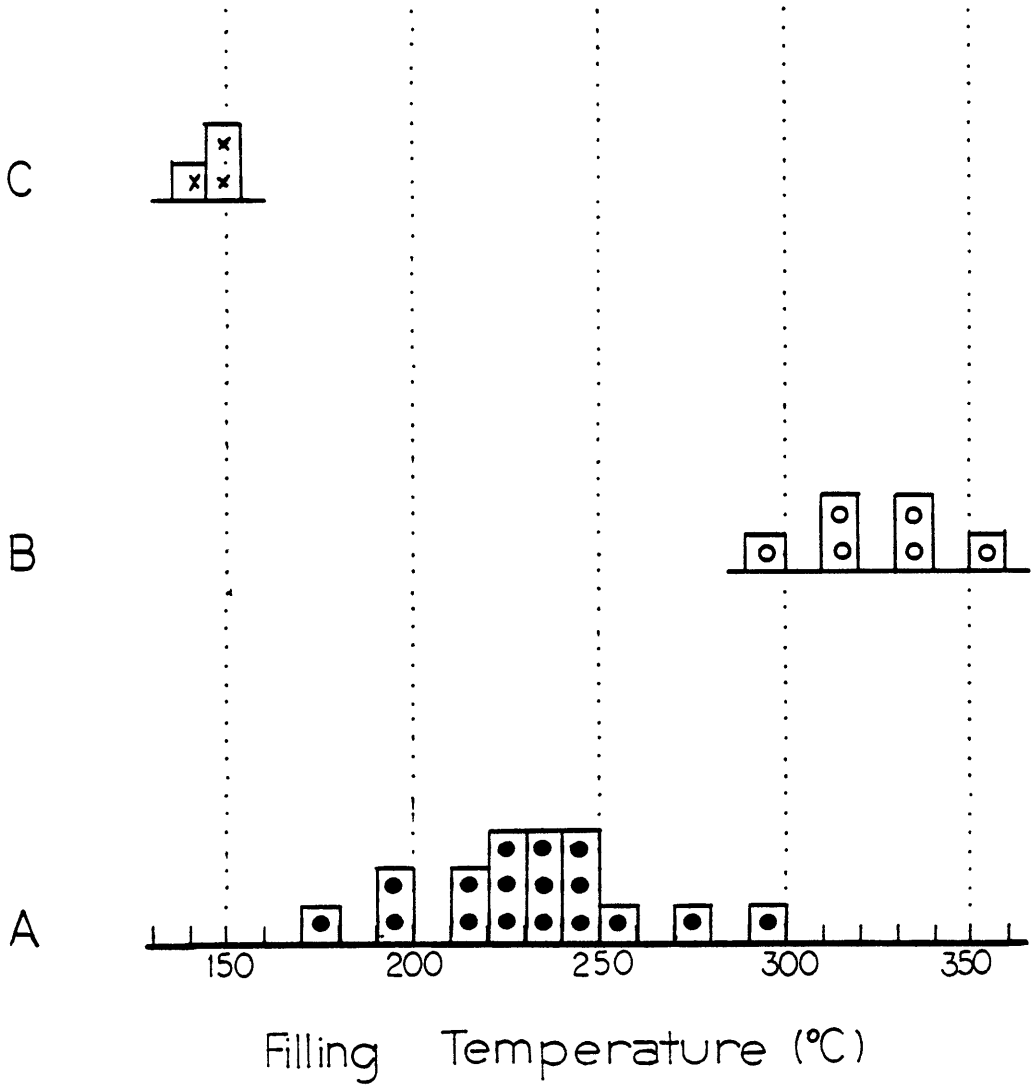
C
B
A
150
200
250
300
350
Filling Temperature (°C)

nificant difference between two methods of determining temperatures. It may also indicate that temperatures within the chimney structure have in the past exceeded those measured at the upper edge of the vent, or that previous solutions rising through the vents were hotter than those presently observed.

Since mixing between hydrothermal fluid and seawater contributes to the formation of the vent deposits, the characteristics of the mixed solutions as well as the pure endmembers become important. Figures III.5 - III.8 depict mineral stability fields in the Cu-Fe-S-O system at 350°C, 300°C, 200°C, and 100°C. Also shown on the diagrams are a variety of f_{S_2} - f_{O_2} values derived from the composition of the 350°C fluid and the mixed solutions. Details of the construction of the diagrams and the calculation of f_{S_2} and f_{O_2} values are presented in Appendix B.

At 350°C, the hydrothermal solution is probably in internal equilibrium. The f_{O_2} values derived from the CH_4 - CO_2 balance in the fluid (marked by triangles along the f_{O_2} axis) and from H_2 in the fluid (marked by circles along the f_{O_2} axis) agree well, falling in the range of $10^{-29.75}$ - $10^{-30.75}$. Because the pure hydrothermal fluid contains essentially no oxidized sulfur, a single f_{S_2} - f_{O_2} pair cannot be determined from the sulfur balance. However, f_{S_2} and f_{O_2} will fall along a line of constant total S, which is shown in figure

Figure III.5. f_{S_2} - f_{O_2} diagram for the Cu-Fe-S-O system at 350°C.

py = pyrite

po = pyrrhotite

mag = magnetite

hem = hematite

cc = covellite

bn = bornite

cp = chalcopyrite

S = condensed sulfur

Triangle, circle and dot-dash line through squares indicate f_{S_2} and f_{O_2} values calculated from fluid composition; see text and Appendix B.

Solid lines: equilibria in the Fe-S-O or Cu-S-O systems.

Long dashed lines: stable equilibria in the Cu-Fe-S-O system.

Short dashed lines: metastable equilibria in the Cu-Fe-S-O system.

For details of calculations, see Appendix B.

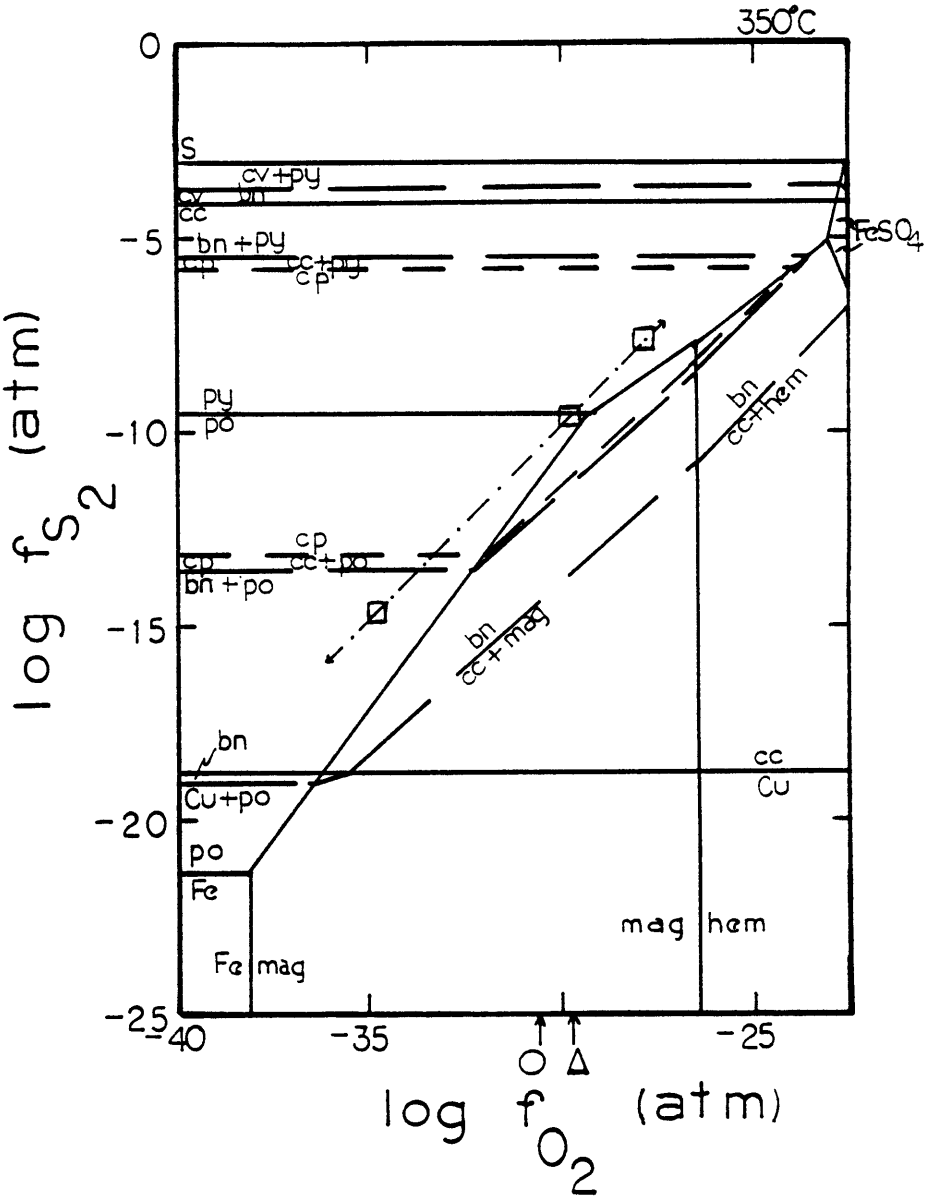
350°C
0
-5
-10
-15
-20
-25
S
cv+py
cv
bn
cc
bn+py
cp
cc+py
cp
FeSO4
py
po
cp
cp
cc+po
bn+po
bn
cc+mag
bn
cc+hem
bn
Cu+po
cc
Cu
po
Fe
Fe
mag
mag
hem
-40
-35
-25
O
Δ
log fS2 (atm)
log fO2 (atm)

Figure III.6. f_{S_2} - f_{O_2} diagram for the Cu-Fe-S-O system at 300°C. Open square indicates f_{S_2} - f_{O_2} derived from S_R/S_{OX} and ΣS; other symbols and abbreviations as in figure III.5.

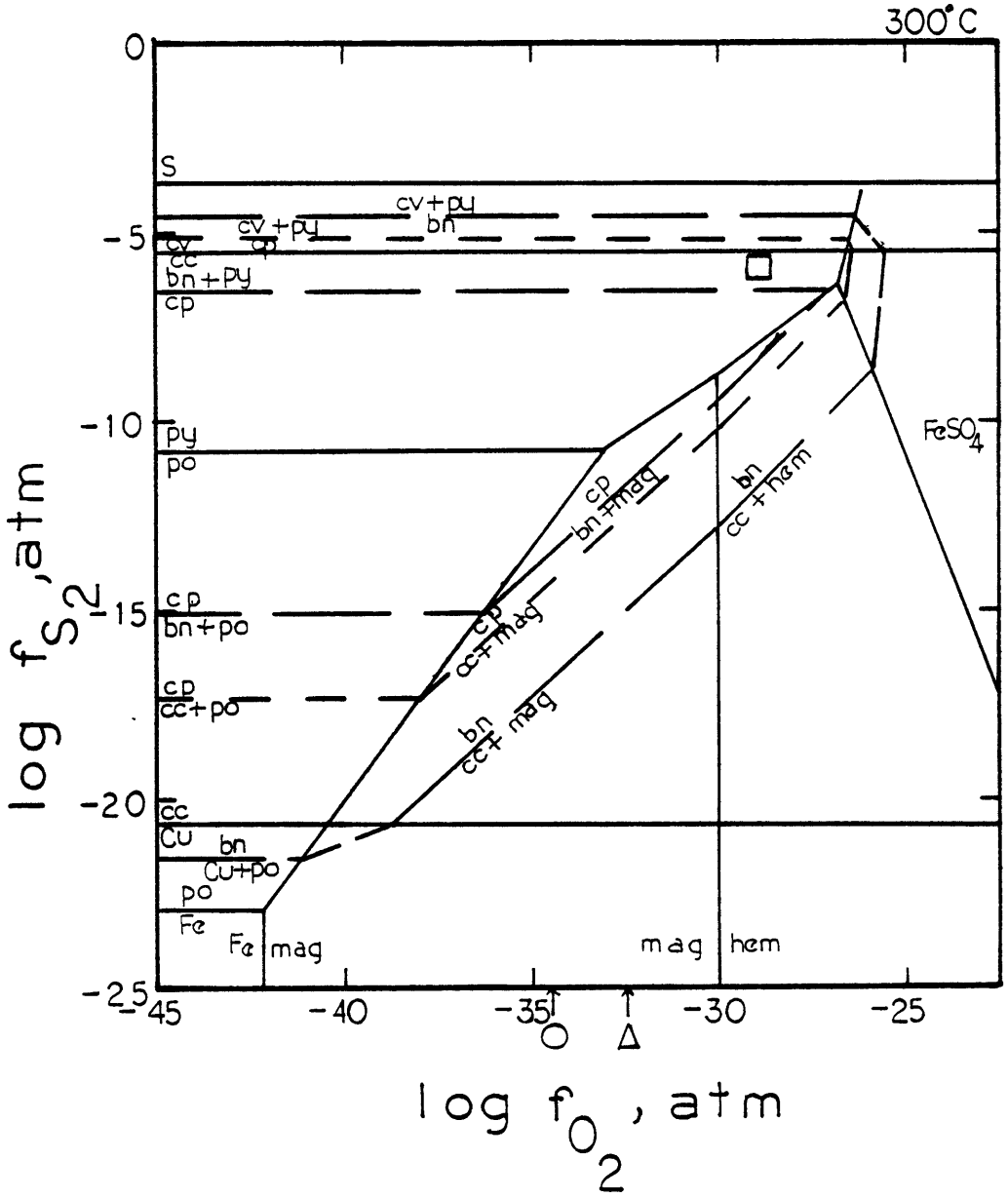
300°C
0
-5
-10
-15
-20
-25
S
cv+py
cv
cp
cc
bn+py
cp
py
po
cp
bn+po
cp
cc+po
cc
Cu
bn
Cu+po
po
Fe
Fe
mag
mag
hem
cp
bn+mag
cp
cc+mag
bn
cc+mag
bn
cc+hem
FeSO4
-45
-40
-35
-30
-25
O
Δ
log fS2, atm
log fO2, atm

Figure III.7. f_{S_2} - f_{O_2} diagram for the Cu-Fe-S-O system at 200°C; symbols and abbreviations as in figure III.6.

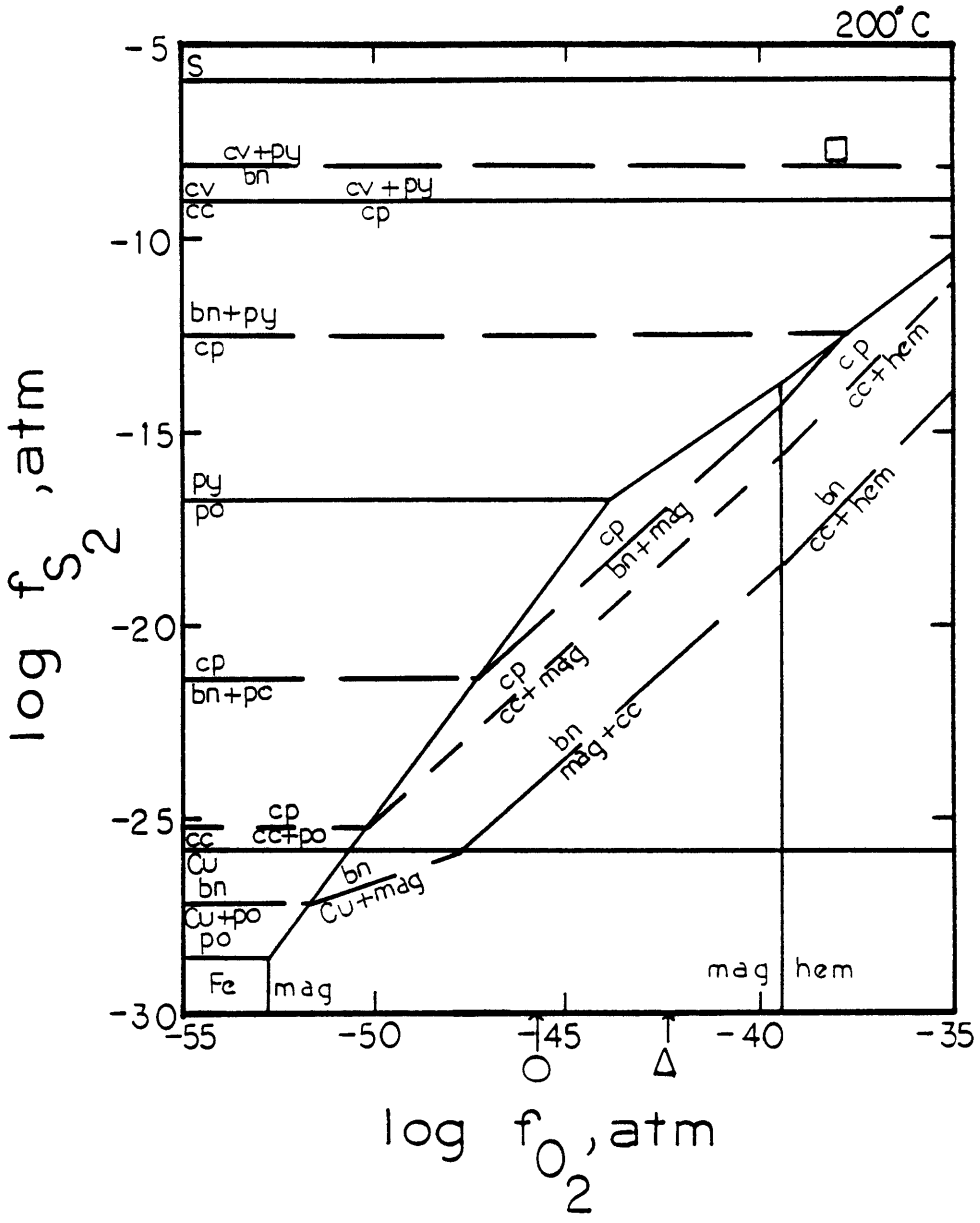
200°C
-5
-10
-15
-20
-25
-30
S
cv+py
bn
cv
cc
cv+py
cp
bn+py
cp
py
po
cp
bn+pc
cp
cc
cp
cc+po
Cu
bn
Cu+po
po
Fe
mag
cp
bn+mag
cp
cc+mag
bn
mag+cc
cp
cc+hem
bn
cc+hem
mag
hem
-55
-50
-45
-40
-35
O
Δ
log f_{S_2}, atm
log f_{O_2}, atm

Figure III.8 f_{S_2} - f_{O_2} diagram for the Cu-Fe-S-O system at 100°C; symbols and abbreviations as in figure III.6.

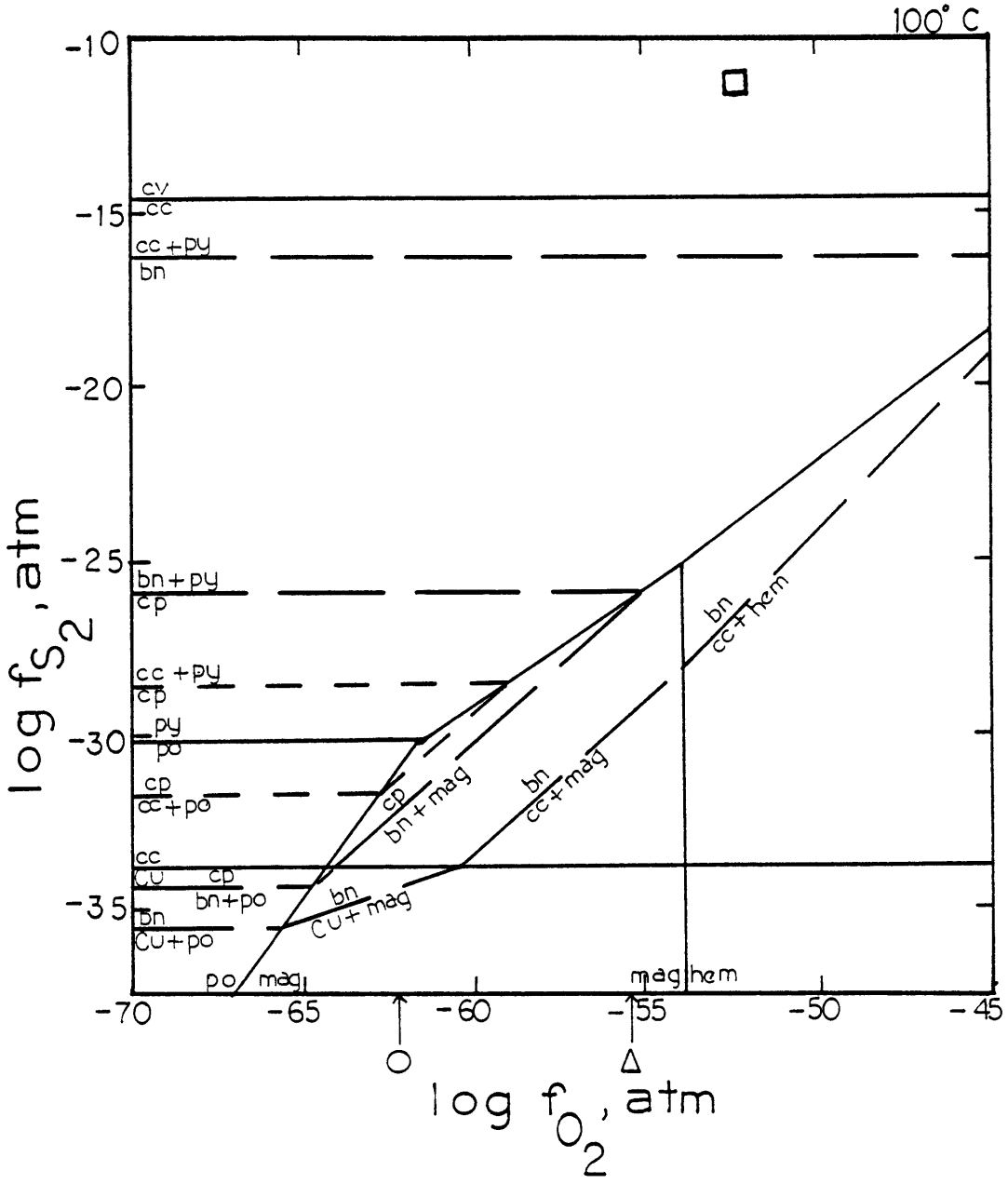
100° C
-10
-15
-20
-25
-30
-35
cv
cc
cc + py
bn
bn + py
cp
cc + py
cp
py
po
cp
cc + po
cc
cu
cp
bn + po
bn
cu + po
po
mag
cp
bn + mag
bn
cu + mag
bn
cc + mag
bn
cc + hem
mag
hem
-70
-65
-60
-55
-50
-45
O
Δ
log f_{S_2}, atm
log f_{O_2}, atm

III.5. At an f_{O_2} of ca. 10^{-30}, this line crosses the pyrite-pyrrhotite boundary. Since the fluid does precipitate both pyrite and pyrrhotite, conditions in the fluid might well correspond to those near the pyrite-pyrrhotite boundary. This rising fluid appears likely to be internally in equilibrium.

However, the calculation of a single f_{S_2} - f_{O_2} pair to characterize a mixed solution of seawater and hydrothermal fluid is complicated by the possibility of disequilibrium between reduced and oxidized species in the mixed solution. Mixing between the fluids takes place very rapidly; the establishment of equilibrium among species in the mixed solution depends on the speed of the chemical reactions relative to the residence time of the solution in the system. Reaction between reduced and oxidized species of sulfur occurs relatively slowly: at a $\Sigma S \sim 10^{-2}$ m, equilibrium between reduced and oxidized sulfur species requires on the order of 17 days to reach 90% completion at 350°C; the process takes much longer periods of time at lower temperatures (Ohmoto and Lasaga, 1980). However, equilibrium among the reduced and oxidized species separately is likely to be reached much more rapidly. The f_{S_2} - f_{O_2} values marked by squares in figures III.6 - III.8 were calculated from sulfur concentrations in the solutions before any precipitation occurred, assuming that equilibrium was attained among reduced and oxidized sulfur species, but that no reaction occurred between reduced and oxidized sulfur. In other words, total

reduced sulfur was taken from the H_2S in the hydrothermal solution (K. von Damm, personal communication), and total oxidized sulfur from the sulfate in seawater; f_{S_2} and f_{O_2} were calculated from S_R/S_{OX} and ΣS at each temperature, assuming linear mixing lines for both reduced and oxidized sulfur. Values for pH were taken from the measured composition of solutions collected in November 1979 and November 1981 (K. von Damm, personal communication).

The amount of reaction and degree of equilibrium among reduced and oxidized sulfur species in the mixed solutions is difficult to estimate. The proportion of sulfur reduced from seawater sulfate that is present in the sulfide minerals can be evaluated by isotopic analyses of sulfur. However, the presence of sulfide reduced from seawater sulfate does not necessarily imply that any reaction occurred in the mixed solutions. Another indication of the degree of reaction can be obtained from the isotopic composition of oxygen in the sulfate minerals. This does not directly reflect the reduction or oxidation of sulfur species, but it can reflect the degree of isotopic equilibrium and therefore of chemical equilibrium between deposited sulfate and a mixed solution at a particular temperature.

The $\delta^{34}S$ measurements obtained from sulfides in the vent deposits vary from +1.3‰ to +4.5‰ (Styrt et al., 1981; Arnold and Shepard, 1981; H. Nielsen, per. communication) (figure III.9). Since S in the hydrothermal fluid is dominated by H_2S, $\delta^{34}S_{H_2S}$ in the sulfides approximates $\delta^{34}S_{\Sigma S}$ in

Figure III.9. $\delta^{34}S$ measurements, in ‰, obtained on samples from the hydrothermal vents.
Solid circles: Styrt et al. (1981).
Crosses: Arnold and Sheppard (1981).
Triangles: H. Nielsen, personal communication.
Analyses from vent site 1 of dive 980 and vent S-3 are of wurtzite;
Analyses from Black Forest are chalcopyrite;
Analyses from vent S-2 are of cubanite;
Analyses by Styrt et al. (1981) and Nielsen from vent site 1 of dive 981 are of chalcopyrite, by Arnold and Sheppard (1981) are of chalcopyrite and/or pyrite.

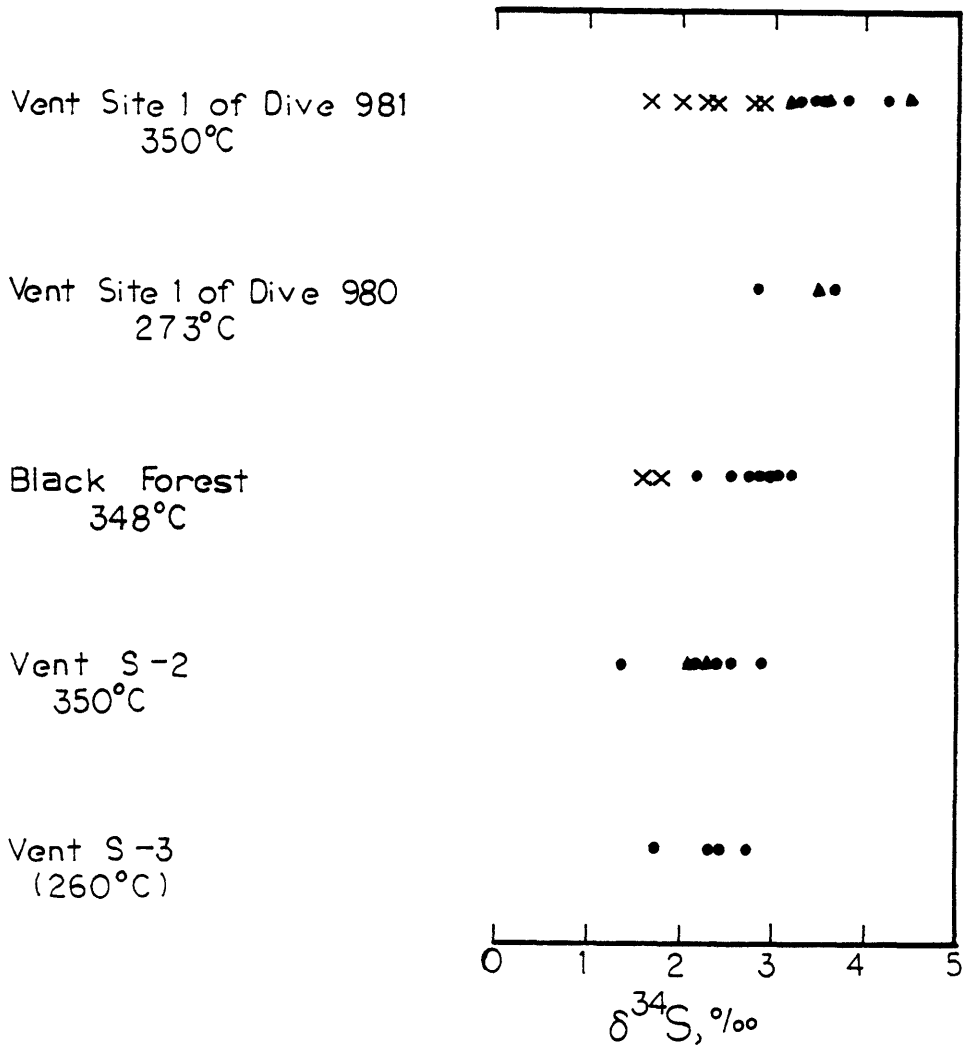
Vent Site 1 of Dive 981
350°C
Vent Site 1 of Dive 980
273°C
Black Forest
348°C
Vent S-2
350°C
Vent S-3
(260°C)
0
1
2
3
4
5
δ34S, ‰

the fluid (Styrt et al., 1981). If all the sulfur in the hydrothermal solution were derived from basalts, $\delta^{34}S$ should be identical to that of normal mid-ocean ridge basalts, in the range of 0 to +1.5‰ (Kanehira et al., 1973). Sulfide produced by reduction of seawater sulfate at 350°C will have a more positive value of $\delta^{34}S$. Some reduced sulfur of seawater origin must be present in the solutions at 21°N in order to raise $\delta^{34}S$ of sulfides above +1.5‰. The proportion of reduced sulfur derived from seawater sulfate and from basalts is difficult to determine in a dynamic system like that at 21°N. However, at least 10 - 20% H_2S of seawater origin is required to raise $\delta^{34}S$ of the sulfides into the range +2 to 4‰ (Styrt et al, 1981).

Reduced sulfate can be added to H_2S in the hydrothermal fluid either below the seafloor during creation of the fluid by the reaction of seawater with basalts, or during mixing between hot fluid and seawater either subsurface or within the chimneys. Sulfur of seawater origin that is reduced during reaction with basalts should appear equally in all sulfides deposited from the resulting hydrothermal fluid. However, variations may occur over time in the proportion of reduced seawater sulfate in the hydrothermal fluid, depending on local conditions within the circulatory system. Reduction of varying quantities of seawater sulfate during mixing with hot fluid can cause local variations in $\delta^{34}S_{H_2S}$,

and therefore in $\delta^{34}S$ in the sulfides. However, if a small quantity of hydrothermal fluid mixes with a large quantity of seawater, forming a low temperature mixed solution, some H_2S may be oxidized to $SO_4^{=}$, which will in effect lower $\delta^{34}S_{H_2S}$ and $\delta^{34}S$ in the sulfides.

In the chimneys at 21°N, $\delta^{34}S$ values obtained from sulfides from the monomineralic linings of the fluid channelways included the entire range of values from +1.3‰ to +4.5‰. The $\delta^{34}S$ composition was more constant within each chimney, usually exhibiting only a 1.5 - 2‰ variation (figure III.9). There is no correlation between $\delta^{34}S$ and the temperature of the hydrothermal fluid in the mouth of the vent, suggesting that variations in $\delta^{34}S$ among vents are related to differences in their local subseafloor circulatory system rather than to different degrees of mixing within the vents.

The extremely wide range of $\delta^{34}S$ values obtained from vent site 1 of dive 981 is unusual. In this chimney, $\delta^{34}S$ of the sulfides appears to be related to the position of the sulfide minerals within the chimney wall. Chalcopyrite from the monomineralic layer, analyzed by Styrt et al. (1981) and H. Neilsen, yields the highest $\delta^{34}S$ values. The lower $\delta^{34}S$ values were obtained by Arnold and Sheppard (1981); at least some of their samples consisted of fine-grained sulfides mixed with or subordinate to anhydrite. They did detect the

presence of sulfate inclusions in the sulfide samples, and consequently the sulfides were leached before the sulfur was extracted for analysis (Arnold and Sheppard, 1981). Sulfate contamination is unlikely to be a problem in the other analyses, since the samples analyzed by Styrt et al. (1981) and Nielsen were chosen carefully to avoid the presence of sulfate minerals. In this chimney, therefore, $\delta^{34}S$ appears to decrease outward through the chimney wall, although even the lower $\delta^{34}S$ values probably include ca. 10% sulfur of seawater origin (Arnold and Sheppard, 1981). There are four possible explanations for the $\delta^{34}S$ trend within this chimney: (1) seawater penetrated to the chimney interior, the sulfate was reduced to H_2S, and $\delta^{34}S$ of the interior sulfides thus increased; (2) the exterior sulfide + anhydrite layer formed when a small quantity of hot fluid mixed with a large quantity of seawater, some H_2S was oxidized during mixing, and $\delta^{34}S$ of the exterior sulfides decreased; (3) the interior and exterior sulfides were deposited from different solutions and the proportion of reduced seawater sulfate in the hydrothermal solutions varied with time; (4) a combination of the above. None of these explanations can at present be singled out as the correct one. The first two do require partial equilibrium to be attained among reduced and oxidized sulfur species.

Oxygen isotope data from anhydrite in the chimneys also suggest that partial equilibrium of a sort is attained in the

mixed solutions. In the pure hydrothermal fluid, $\delta^{18}O$ is ~ +1.6‰ (Craig et al., 1980), while seawater sulfate has a $\delta^{18}O$ of +9.6‰ (Kusakabe et al., in prep.). Analyses of anhydrite yield $\delta^{18}O$ values between +10.2‰ and +11.5‰ (Kusakabe et al., in prep.). These $\delta^{18}O$ values could be attained at equilibrium in mixed solutions between 180°C and 220°C (Kusakabe et al., in prep.); however, filling temperatures obtained from fluid inclusions in anhydrite from the same samples indicate that most of the anhydrite formed at temperatures above 220°C (Kusakabe et al., in prep.). One explanation of this disequilibrium is that the anhydrite precipitated from relatively hot mixed solutions in which only partial equilibrium was achieved, leaving the sulfate with high $\delta^{18}O$ values inherited from seawater. At least partial equilibrium must have been attained in the mixed solutions, or the $\delta^{18}O$ of the sulfates would be identical to that of seawater. It is interesting to note that $\delta^{34}S$ of the sulfates did remain identical to seawater, indicating that the sulfur species reached equilibrium more slowly than oxygen. The different rates of approach to equilibrium are related to the ease of exchanging oxygen and sulfur atoms in the sulfate molecule. In order to exchange an oxygen atom for a different oxygen atom only one sulfur-oxygen bond must be broken, whereas all four S - O bonds must be broken before the S atom can be replaced.

If reactions did occur among the reduced and oxidized

sulfur species, then the f_{S_2} - f_{O_2} values indicated by the squares in figures III.6 - III.8 would change slightly. A range of conditions might result from local variations in the extent of reaction. However, neither oxidation nor reduction is likely to occur to any significant extent. Reduction of $SO_4^=$ is a slow process because, as previously noted, all four S - O bonds must be broken. Oxidation of H_2S may occur more rapidly, but the available supply of oxygen is limited.

If the ΣS and the ratio of S_{OX}/S_R in the fluids accurately reflect the f_{S_2} - f_{O_2} conditions prevalent during deposition of the sulfides, then the mineral assemblages present in the chimneys should be compatible with the f_{S_2} - f_{O_2} conditions derived from the S balance in figures III.5 - III.8. At 350°C, at the top of the Cu-rich chimneys, these f_{S_2} - f_{O_2} conditions probably fall within the chalcopyrite field, along the pyrite-pyrrhotite boundary. At 300°C, the indicated composition is close to the chalcopyrite-bornite + pyrite boundary. At 200°C, it approaches the bornite-covellite + pyrite boundary and by 100°C it is within the covellite stability field. The chalcopyrite - bornite - (chalcocite) - covellite sequence is observed across the chimney wall at one vent, the Black Forest vent, but mainly as a replacement sequence. The Cu-rich sulfides other than chalcopyrite and cubanite form infrequently as primary minerals, probably because Cu is depleted in the hydrothermal fluid as a result of chal-

copyrite deposition.

The f_{S_2} - f_{O_2} conditions in the mixed solutions are compatible with pyrrhotite deposition only at 350°C. At lower temperatures the fluids plot firmly in the pyrite field. Since pyrrhotite occurs rarely in the chimney samples and is usually replaced by pyrite or chalcopyrite, that aspect of the fluid composition is consistent with the sample mineralogy. However, the compatibility between the fluid composition and pyrite deposition reemphasizes the apparent incompatibility between the conditions of mineral formation and the wurtzite present in most of the samples.

The presence of wurtzite with widely varying FeS contents in the chimneys implies that a mineralogy of the vent deposits does not reflect a single, stable f_{S_2} defined by the reduced and oxidized sulfur contents of the hydrothermal fluid. The FeS contents of the wurtzite, as discussed previously, imply that the ZnS formed over a wide range of f_{S_2} under conditions which were very different from those indicated by the sulfur content of the mixed solutions.

The local f_{O_2} conditions in the mixed solutions, although not directly reflected by the sulfide mineralogy, may also vary widely. Different oxidation-reduction pairs in the solutions reach equilibrium at different rates; the effective f_{O_2} locally within the chimney may be affected by all of the oxidation-reduction processes. In particular, the

f_{O_2} values implied by the CH_4 - CO_2 balance in and the H_2 content of the mixed solutions are shown in figures III.6 - III.8. The wide range in f_{O_2} indicated by these two values and that obtained from the sulfur balance in the solutions clearly indicate that no single f_{O_2} value can accurately represent conditions in the mixed solutions.

The widely varying f_{S_2} and f_{O_2} values indicated by the sulfur balance, the CH_4 - CO_2 balance, and the H_2 contents of the mixed solutions and by the mineralogy of the vent deposits implies that chimney formation must be considered as a non-equilibrium process. Disequilibrium in the solutions is reflected in a pervasive disequilibrium in the precipitates. Co-existing minerals that precipitated from the same solution still cannot be considered as equilibrium assemblages. Since all the thermodynamic data used to evaluate mineral deposition is based on equilibrium relationships, the disequilibrium state of these deposits requires a cautious approach.

Despite the ranges of f_{S_2} and f_{O_2} values in the mixed solutions, the f_{S_2} - f_{O_2} relations are useful for revealing the powerful effect of the hydrothermal solutions on the internal environment of the chimneys. Although seawater maintains a much higher f_{O_2} and lower f_{S_2} than the hydrothermal fluid, the f_{O_2} of the mixed solutions, derived from any of the previous sources, actually drops until the solutions become very cool, while the f_{S_2} apparently remains almost con-

stant to below 200°C and then drops slowly until the solutions consist almost entirely of seawater. The temperature drop is the major cause of this phenomenon; in the calculations based on sulfur, the reaction $H_2S + \frac{1}{2}O_2(g) = \frac{1}{2}S_2(g) + H_2O(\ell)$ proceeds farther to the right with falling temperature (Drummond, 1981; see equilibrium constants in Appendix B), resulting in a decrease in f_{O_2} and maintaining a high f_{S_2} in the mixed solutions. As a consequence, the sulfides in the chimneys are maintained by the internal environment of the vents even though they are far out of equilibrium with ambient seawater.

Mixing between hydrothermal fluid and seawater also provides an explanation of the black smoke precipitated in the plumes above the vents. Fe sulfides, which are deposited at the upper edges of the vent structures, are saturated in the hydrothermal solution. As the solution mixes with seawater the sulfides rapidly become supersaturated and therefore precipitate to form smoke. If essentially all the Fe, Zn, and Cu carried in the hot fluid precipitate as smoke, the dominant constituent of the smoke will be FeS or FeS_2, consistent with the reported composition of black smoke (Spiess et al., 1980). Anhydrite also becomes saturated when $SO_4^=$ is added to the hydrothermal fluid, but the quantity of anhydrite deposited is limited by the available $SO_4^=$. Solubility calculations for pyrite and pyrrhotite are given in Appendix C.

If mixing between hydrothermal fluids and seawater is the major mechanism leading to mineral deposition in the chimneys, then water must be able to penetrate the chimney walls. Since most of the material making up the vent structure is porous and contained considerable water at the time it was collected, this requirement presents no real problem. In particular, the uppermost tip of the active chimney opening from vent site 1 of dive 981 has a very thin wall composed of the fine-grained sulfide and anhydrite mix, which contained considerable water in all the chimney samples. Penetration of seawater through such material should proceed with little difficulty.

A more effective barrier to fluid penetration occurs where a thick lining of sulfides forms the inner wall of a more highly developed chimney. Although flow of water through such walls may be severely restricted, there is still evidence for seawater and hydrothermal fluid penetration through the walls of such chimneys. Replacement rims on sulfides in the center of chimney walls apparently form when fluid comes in contact with previously deposited minerals with which it is not in equilibrium. The most convincing evidence for seawater penetration through the entire thickness of well-developed chimney walls is the presence of Mg-silicates and anhydrite in mixtures forming clumps on the interior walls of the Cu-rich chimneys. Since the hydrothermal fluid contains virtually no Mg^{+2} and SO_4^{--}, the Mg-

silicates and anhydrite can only form when Mg^{+2} and SO_4^{--} of seawater origin reach the inner channel of the chimney. The sulfate-silicate clumps do form in place. They can be traced back into "veinlets" of anhydrite filling spaces between chalcopyrite grains. They were also found inside the active chimney tube on sample 980-R-12 at the end adjoining the main chimney cavity, where the chalcopyrite layer is thick and coarse-grained, but not at the actively forming tip.

Growth Tip

The progressive development of an active Cu-rich chimney can be observed in sample 980-R-12 from vent site 1 of dive 981. This particular piece has already been described in detail, but a summary emphasizing its most significant features follows (see also figure II.17). The uppermost tip of the chimney consists of a shell of anhydrite crystals, oriented both horizontally and vertically, coated with fine-grained sulfides. Just below the tip the beginning of a monomineralic interior layer appears as a very thin, fine-grained chalcopyrite lining.

Downward from the tip the inner chalcopyrite lining becomes thicker and more coarse grained, and the layer of anhydrite plus sulfides, now only an exterior layer, also thickens. The anhydrite develops a distinct orientation per-

pendicular to the chimney walls. Two to three mm down from the tip, chalcopyrite disease begins to appear in wurtzite grains remaining in and just outside the chimney interior. At the same level in the chimney, Mg silicates begin to form within the anhydrite layer just to the outside of the chalcopyrite layer. The silicate-bearing layer develops downward into a fine-grained and colloform layer of Mg-silicates, anhydrite, pyrite, wurtzite, and minor Cu-Fe sulfides.

The last significant change in the developing chimney appears 3 - 3½ cm down from the tip, where a layer of anomalous bornite appears, both as replacements in chalcopyrite and wurtzite and as grains that are apparently primary in origin. At the base of the small tube, where it joins a larger cavity, the chimney consists of a coarse-grained inner layer of chalcopyrite, a narrow band of mixed sulfides and anhydrite rich in anomalous bornite, and a thick, porous outer layer of anhydrite, Mg-silicates, and fine-grained and colloform sulfides. The innermost of the fine-grained sulfides exhibit Cu-Fe replacement in the wurtzite grains. Anomalous bornite is actually less abundant at this level than it is a little higher in the chimney.

Chimney Model

A model for the construction of a Cu-rich chimney can be created based on the development observed in sample 980-R-

12 combined with the mineralogy and textures seen in the other samples. The chimney develops as a result of mixing between hydrothermal fluid and seawater; the mixing is gradually modified and restricted by mineral precipitation in the chimney walls. After the general model is presented, differences in the formation of Zn-rich chimneys will be discussed.

At the uppermost tip of a growing chimney free mixing occurs between hot vent water and seawater. A fragile framework of anhydrite coated by fine-grained sulfides grows upward from the chimney edge as a result of mixing in contact with the edge of the chimney structure. This growth may be extremely rapid; in November 1981 a very delicate shell approximately 60 cm high appeared in place of a razed chimney in the space of only two days (Converse, personal communication; Goldfarb et al., in prep.). Because it was so fragile, this new growth could not be sampled, but it appeared to consist of the same material that formed a 0.5 - 1.0 cm rim of acicular "black" anhydrite on the upper parts of the black smokers observed on this cruise. This rim was not commonly seen in November 1979, and, as a consequence of its fragile nature, samples of it are rare. It is very porous, and consists of anhydrite needles oriented radially on the outside of the chimneys. A fine-grained coating of sulfides imparts the black color to the needles. The "black anhydrite" rim appears to be a more porous, more fragile version

of the outermost anhydrite and sulfide layer on the Cu-rich chimneys sampled in November 1979. The uppermost tip of sample 980-R-12 consists of material very similar to this "black anhydrite," with both a radial orientation and a vertical orientation, which may have served as points of attachment for a more fragile framework that was lost during sampling.

The first delicate anhydrite framework is very porous and allows mixing to occur freely through the shell. However, it does form the first barrier between seawater and hydrothermal fluid, and in so doing allows the temperature of the hydrothermal fluid to rise. As mixing through the shell continues, more anhydrite and sulfides are deposited, increasing the strength of the framework and its effectiveness as a barrier to mixing.

As more pristine hydrothermal fluid rises inside the initial anhydrite shell, the first thin interior lining beings to precipitate on the inner wall of the shell. This development is preserved in the first appearance of an inner chalcopyrite layer just below the uppermost edge of 980-R-12. Although mixing through the chimney walls is still extensive at this point, the development of the interior sulfide layer intensifies the restrictions on mixing. As a solid, interconnected monomineralic sulfide band forms, the void space in the inner layer is filled in. It becomes much less porous than the anhydrite layer and is therefore less amen-

able to fluid passing through it. As a consequence, the isolation of pure hydrothermal fluid in the chimney interior increases.

Two associated phenomena occur as the interior sulfide layer acquires the characteristics of a solid band. The presence of purer hydrothermal fluid in the chimney interior results in the overprinting of higher-temperature sulfides on lower-temperature sulfides; i.e., chalcopyrite disease appears in wurtzite remaining in the chimney interior. The restriction on free mixing through the chimney wall leads to the development of a mixing zone just outside the sulfide lining, where seawater drawn into the porous outer layer mixes with hot fluid escaping from the interior.

Outside the sulfide lining, Mg-silicates begin to form from Mg in the seawater and silica in the hydrothermal fluid. The Mg-silicates can only precipitate from mixtures of the two fluids. If heated seawater were the sole source of components, the Mg-bearing mineral should be an oxysulfate (Bischoff and Seyfried, 1978), but the addition of silica from the hydrothermal solution leads to amorphous silica saturation and the deposition of Mg-silicates. The mixing zone, then, can be identified with the colloform to fine-grained Mg-bearing layer that begins to develop 2 - 3 mm below the chimney tip. The formation of the very fine-grained sulfides that occur in this layer, predominantly pyrite and wurtzite, is similar to the formation of the black smoke:

hot fluid seeping outward from the chimney center encounters and mixes with seawater, leading to rapid precipitation of metal sulfides. The mineralogical evidence suggests that the average proportion of hydrothermal fluid in these mixed solutions is smaller than it is in the plume, and that the average temperature of the mixed solutions is accordingly lower. Anhydrite is usually the most abundant mineral in the mixing zone, which implies a higher proportion of seawater in the mixture. The only Fe sulfide deposited is pyrite, suggesting that the temperature of the mixture is lower than it is when the smoke precipitates. Lower average temperatures, however, can still include quite high local values: the filling temperatures of fluid inclusions in anhydrite from the anhydrite-dominated layer of vent site 1 of dive 981 range from 143°C to 350 - 360°C (see figure III. 4); the corresponding formation temperatures range from 172°C to ca. 372°C.

As the interior sulfide lining of the chimney grows thicker, the isolation of hydrothermal fluid in the center of the chimney increases, and its composition approaches that of the endmember fluid. The coexistence of a hot interior with limited seepage of fluid outward through the walls, adjoining a porous, water-logged outer layer allowing easy penetration of seawater to the outer edge of the sulfide lining probably results in a rapid drop in temperature in the mixing zone. An indication of temperature in the vicin-

ity of the mixing zone is given by the appearance of anomalous bornite between the chalcopyrite layer and the silicate-bearing anhydrite layer. Since anomalous bornite only forms below about 150°C, the temperature in the mixing zone must be near or below 150°C. However, in order to precipitate anhydrite, the temperature cannot fall below about 50°C even though the outflowing hydrothermal solution is richer in Ca than seawater. Fluid inclusions from three anhydrite crystals in the outer layer of sample 981-R-12 from vent site 1 of dive 981, were studied in order to test the formation temperature of anhydrite spacially associated with anomalous bornite. The fluid inclusions in two anhydrite grains immediately adjoining anomalous bornite yielded formation temperatures of 177 - 178°C, after a pressure correction (Potter, 1977), about 25°C higher than the upper stability limit of anomalous bornite. The third inclusion, located 1½ cm away, at the outer edge of the sample, gave a formation temperature of ~172°C. Unfortunately, the relationship in time of the two minerals cannot be truly determined. The anhydrite may well predate the anomalous bornite, which does form within a pre-existing anhydrite layer in sample 980-R-12.

Once a solid inner lining has been deposited in a chimney, fluid flow through the walls probably decreases. Clumps of anhydrite and Mg-silicates on the interior walls of the chimneys attest to the continued penetration of seawater to the chimney center. In situ deposition of Mg-sili-

cates and fine-grained sulfides in the exterior layer requires the outward flow of hydrothermal fluid. However, it seems likely that at depth in the chimneys the walls are largely sealed, and the chimney interior and exterior behave as two separate regions. The presence of anhydrite clumps on the inner walls of chimneys does not imply that seawater can penetrate the chimney wall at all points; on the contrary, the fact that these masses form only where anhydrite deposition can be traced back through the chalcopyrite inner lining implies that once the inner lining is in place seawater reaches the chimney center only along a few restricted paths.

Once the chimney interior and exterior are essentially segregated, the temperature rises inside the chimney, because the rate of heat loss by conduction is slow compared to the upward flow rates of 80 - 235 cm/sec (Converse, et al., in prep.). The composition of the fluid in the interior approaches a purely hydrothermal composition. If, as a result of some heat loss by conduction, a rise in temperature spreads outward gradually through the chimney wall, temperatures in the outer fringes of the inner lining and at the edges of the former mixing zone might rise. This could account for the observed occurrence of iss replacement of wurtzite in the inner edges of the anhydrite-silicate-sulfide layer at the base of sample 980-R-12. The replacement occurs to the outside of the anomalous bornite layer but ap-

pears after the anomalous bornite layer. Since the iss is unlikely to have formed at 150°C, a later rise in temperature is implied. This temperature increase may also destroy some of the previously formed anomalous bornite, which is less abundant in this area than in the section of chimney just above it. Destruction of the anomalous bornite may also provide some of the metals necessary to make the Cu-Fe replacement minerals.

In the exterior, seawater cools the chimney, but flow velocities are low (D. Converse, unpublished calculations), and the convective heat loss is therefore very slow. The persistence of anhydrite on the chimney exteriors suggests that the outer surface of the chimneys may actually be kept warm by heat loss from the interior that maintains them at a higher temperature than ambient seawater. However, during the cruise in November 1981 a suggestion of a decrease in the amount of sulfate was observed towards the base of the chimneys (D. Converse, personal communication); this implies that the disequilibrium between anhydrite and seawater does result in dissolution of exterior anhydrite from the lower parts of the chimneys.

The fluid inclusion filling temperatures obtained from anhydrite in the Cu-rich chimneys also suggest that anhydrite on the chimney exterior dissolves when it comes in contact with ambient seawater. Kusakabe et al. (in prep.) determined formation temperatures, corrected for pressure, of 314 - 372°C

from sample 981-R-1-2-2. This sample cannot be located precisely in the chimney wall, but it is composed of anhydrite and silicates with minor pyrite and wurtzite, and in appearance as well as in composition seems to be a chunk broken off the outer chimney wall. The high temperature of formation of this piece that is indicated by the fluid inclusion filling temperatures strongly suggests that the anhydrite originally formed just outside the inner chalcopyrite lining and that it was exposed by later dissolution of anhydrite farther to the exterior.

Although the major replacement process implied in this model of chimney formation involves higher-temperature sulfides replacing lower-temperature sulfides, this is not the only possible mechanism for generating replacement sequences in the chimneys. Pyrite replacement by chalcopyrite, which occurs contemporaneously with wurtzite replacement, can take place at constant temperature. Brimhall (1980) provides three possible mechanisms leading to chalcopyrite replacement of pyrite at 300°C: (1) an increase in f_{H_2S} and f_{O_2} and a_{Fe}/a_{Cu}^2, (2) a decrease in f_{O_2} at constant f_{H_2S} and a_{Fe}/a_{Cu}^2, and (3) a decrease in a_{Fe}/a_{Cu}^2 at constant f_{O_2} and f_{H_2S}. In the hydrothermal vents, the final replacement sequence could result from a combination of the first two factors. As the interior of the chimney becomes isolated from

seawater, and as the fluid composition approaches that of the pure hydrothermal endmember, f_{H_2S} should increase, and f_{O_2} may decrease, but a_{Fe}/a_{Cu}^2 is unlikely to undergo much change unless the composition of the fluid changes with time. Although the earlier and later sulfides are primarily associated with lower and higher temperatures respectively, resulting from different degrees of mixing with seawater, the replacements may also be the consequence of other changes in conditions that occur as the chimney interior becomes segregated from the exterior.

As the chimney interior becomes more isolated, the chimney exterior is more affected by ambient seawater. The effect on anhydrite has already been noted, but the sulfides are also out of equilibrium with seawater; alteration and replacement sequences can therefore be expected in the outer layer of sulfides. Oxidation on the outer surface of the chimneys was commonly observed, as red and ochre patches of Fe oxides, but the oxidation did not penetrate into the chimney wall. However, one replacement sequence does occur in a manner that suggests it may have developed from the exterior of the chimney inward, progressing in the opposite direction from most of the observed replacements.

This sequence is the replacement of chalcopyrite by a narrow rim of bornite-chalcocite solid solution on the exterior of the Black Forest samples. The rim develops after the

Figure III.10. Different stages of growth represented in idealized sections of active chimneys. From Goldfarb et al., in prep.

(a) During the initial growth stage, the chimney is composed dominantly of anhydrite and minor quantities of sulfides precipitated during mixing of seawater and hydrothermal fluid. The wall at this stage is highly permeable.

Figure III.10. (b) Continued mixing and consequent mineral precipitation within the chimney wall reduce the permeability. Temperature of the fluid inside the chimney rises, leading to the deposition of an inner Cu-Fe sulfide layer. Mg-silicates precipitate in a mixing zone between the Cu-Fe sulfide layer and the dominantly anhydrite layer. The upper part of this chimney is identical to the young chimney shown in figure III.10(a).

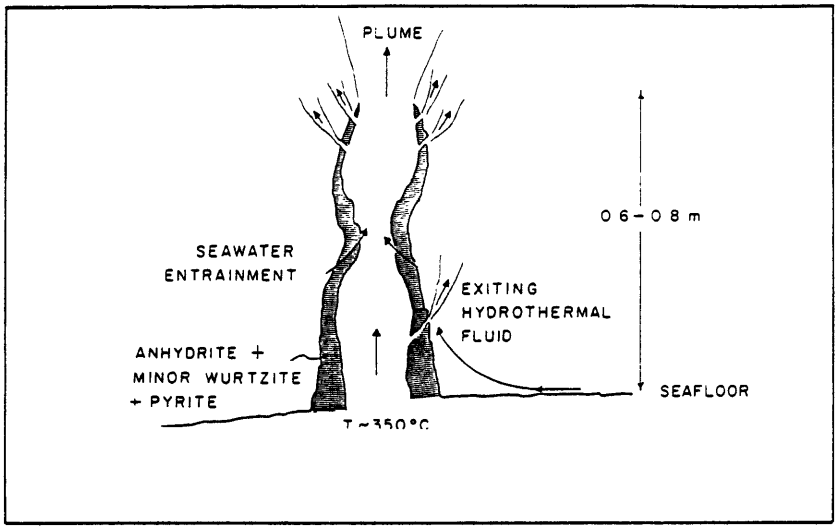
PLUME
0 6 – 0 8 m
SEAWATER
ENTRAINMENT
EXITING
HYDROTHERMAL
FLUID
ANHYDRITE +
MINOR WURTZITE
+ PYRITE
SEAFLOOR
T ~ 350°C

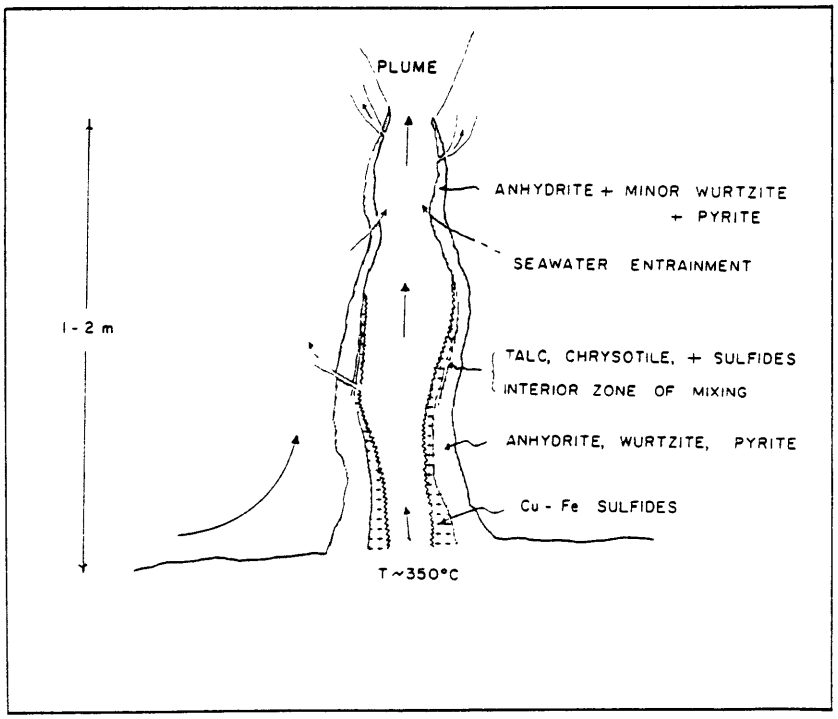
PLUME
1 - 2 m
ANHYDRITE + MINOR WURTZITE
+ PYRITE
SEAWATER ENTRAINMENT
TALC, CHRYSOTILE, + SULFIDES
INTERIOR ZONE OF MIXING
ANHYDRITE, WURTZITE, PYRITE
Cu - Fe SULFIDES
T ~ 350°C

formation of the chalcopyrite lining, as the replacement relations between the minerals implies, and it is not present at the upper edges of the small side tube from this vent. A gradual replacement of chalcopyrite by bornite, and then a gradual development of the bornite-chalcopyrite solid solution is visible in polished sections cut from this small tube. The observations suggest that seawater solutions penetrated inward and reached saturation progressively with the series of Cu-Fe sulfides from chalcocite through bornite. Essentially, this is a process of weathering analogous to the formation of supergene Cu-Fe sulfides by groundwater alteration, which forms similar sulfides (Blain and Andrew, 1977). The temperature at which the rind forms need not be particularly low, but occasional grains of anomalous bornite are found at the bornite-chalcopyrite boundary, suggesting a temperature at that point near or below 150°C.

The formation of a sulfide weathering rind only on the Black Forest vent may be related to the lack of anhydrite in the outer layer of this chimney. Only at this vent is there direct access of seawater to the massive sulfides. The replacement rim develops after the formation of the massive chalcopyrite layer, and does show an inverse relationship with anhydrite in the chimney. At the upper tip anhydrite dies out as the bornite rim appears. In other pieces from the chimney, the bornite rim is generally well developed, but it is absent in the comparatively rare areas

in which abundant anhydrite is present in the outer edge.

Formation of Zn-rich Chimneys

The process outlined above was based on the development of a Cu-rich chimney. There are clearly some differences between Cu-rich and Zn-rich chimneys, but the general method of formation is much the same. The fluid venting from the Zn-rich chimneys is cooler than that venting from the Cu-rich chimneys. If the composition of the original hydrothermal fluid is similar in all the chimneys, then Cu sulfides must be deposited deeper in the Zn-rich chimneys where the temperature is higher, possibly below the seafloor. The early depletion of the hydrothermal solutions in Cu as a result of mixing with seawater at depth is probably responsible for the major differences in mineralogy between the Zn-rich and the Cu-rich chimneys.

The Zn-rich chimneys probably form in a manner similar to that of the Cu-rich chimneys. Although no active chimney tips were collected from Zn-rich vents, a tubular sample and assorted fragments from vent site 1 of dive 980 are composed of a coarser version of the black anhydrite framework described as the initial framework of the Cu-rich chimneys. After the formation of an initial anhydrite framework above a Zn-rich chimney, a temperature rise occurs inside the shell just as it does in a Cu-rich chimney. The heated in-

terior does not foster chalcopyrite deposition, because the rising fluid is still depleted in Cu. Instead, the protected interior allows the growth of elongate wurtzite crystals which develop into the linings of the fluid channelways. The wurtzite linings are not as tightly interlocked as the chalcopyrite linings; more anhydrite and more void space are visible in polished sections between the wurtzite crystals in the Zn-rich chimneys than between the chalcopyrite or cubanite grains in Cu-rich chimneys. This provides more fluid access through the inner linings of Zn-rich chimneys.

Most of the mixing between solutions occurs in the outer mass of the Zn-rich chimneys, which is composed of large anhydrite crystals and fine-grained wurtzite and pyrite. Pyrrhotite remnants in the outer layer are probably relicts from mixing early in the chimney development before the inner lining formed. Two notable differences between the fine-grained sulfide layers in Zn-rich and Cu-rich chimneys may be consequences of the different degrees of mixing in the walls of the two chimneys. In the Zn-rich chimneys, the anhydrite + mixed sulfide layer shows no colloform textures and contains no Mg-silicates, both of which occur in this layer in Cu-rich chimneys. An examination of silica saturation in and Mg-silicate deposition from mixed solutions of seawater and hydrothermal fluid may reveal the reasons for these differences.

A series of stability diagrams for the MgO-SiO_2-H_2O

system is shown in figures III.11 - III.13. The concentration of Mg^{++} and H_4SiO_4 in the mixed solutions were calculated based on linear mixing between Mg^{++} and SiO_2 in seawater and hydrothermal solutions; pH was taken from measurements made on mixed solutions collected in November 1979. Details are given in Appendix C. Although the pure hydrothermal solution lacks Mg^{++} and is therefore undersaturated with respect to any Mg-silicate, any mixed solution plots within the talc stability field on these diagrams, and within the field of metastable chrysotile. At high temperatures, however, too little Mg^{++} would be present to form any significant quantity of Mg-silicates. The factor that apparently may control silicate deposition is the concentration of silica in the mixed solutions. Solutions below ~300°C rapidly become supersaturated with respect to quartz, but saturation with respect to amorphous silica is not attained until below ~200°C. It is possible that when a mixed solution forms at temperatures below ~200°C, a Mg-silicate mixture is precipitated, whereas both silica and Mg are retained in solution at higher temperatures. Fluctuations in pH within the walls of the chimney may also affect the stability of the Mg-silicates, but an increase in pH, like that which occurs in the mixed solutions, results in a higher degree of Mg-silicate supersaturation.

If deposition of Mg-silicates does in fact depend on temperature in this way, then the mixed sulfide layer in the Zn-rich chimneys should be deposited from mixed solutions

Figure III.11. The MgO-SiO_2-H_2O system at 300°C. Talc, chrysotile, and brucite data from Hemley et al. (1977); amorphous silica solubility from Chen and Marshall (1982); quartz solubility from Holland (1979).

Am SiO_2 = amorphous silica, Qtz = quartz. indicates the composition of a mixed solution at 300°C at 21°N. Details of the calculations are in Appendix C.

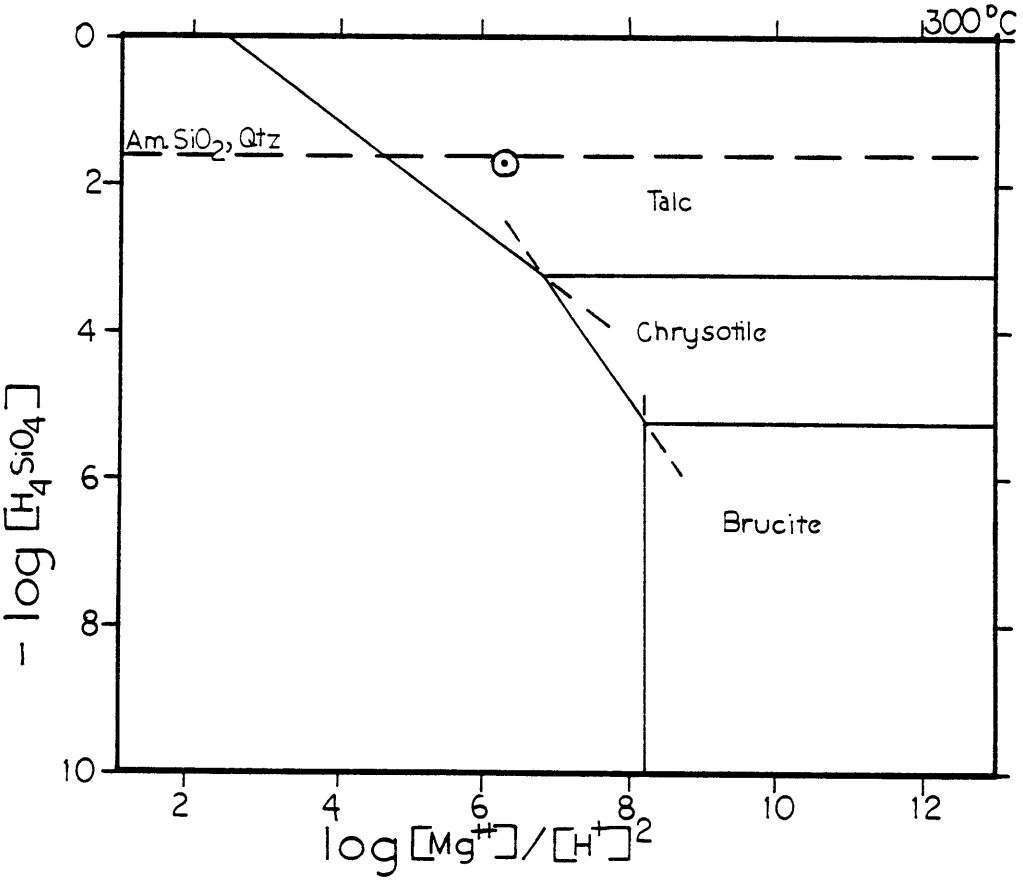
300°C
Am. SiO2, Qtz
Talc
Chrysotile
Brucite
0
2
4
6
8
10
2
4
6
8
10
12
- log [H4SiO4]
log [Mg++] / [H+]2

Figure III.12. The $MgO-SiO_2-H_2O$ system at 200°C; symbols and abbreviations as in figure III.11.

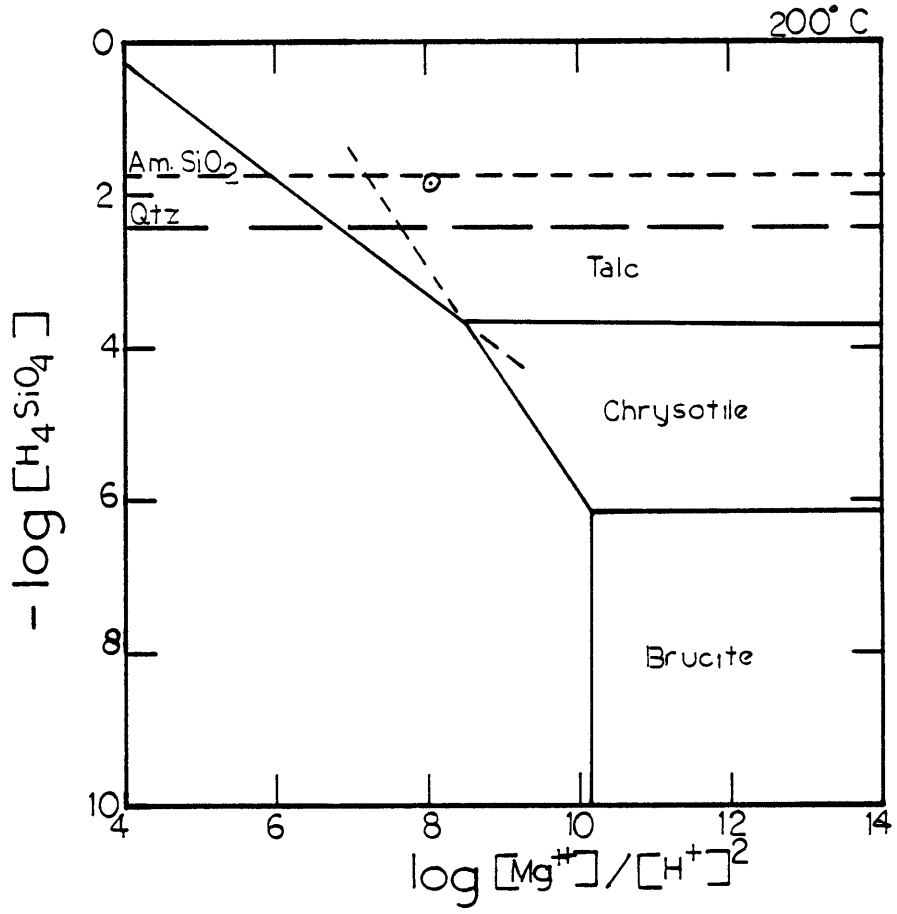
200° C
0
2
4
6
8
10
Am. SiO2
Qtz
Talc
Chrysotile
Brucite
4
6
8
10
12
14
- log [H4SiO4]
log [Mg++] / [H+]2

Figure III.13. The $MgO-SiO_2-H_2O$ system at 100°C; symbols and abbreviations as in figure III.11.

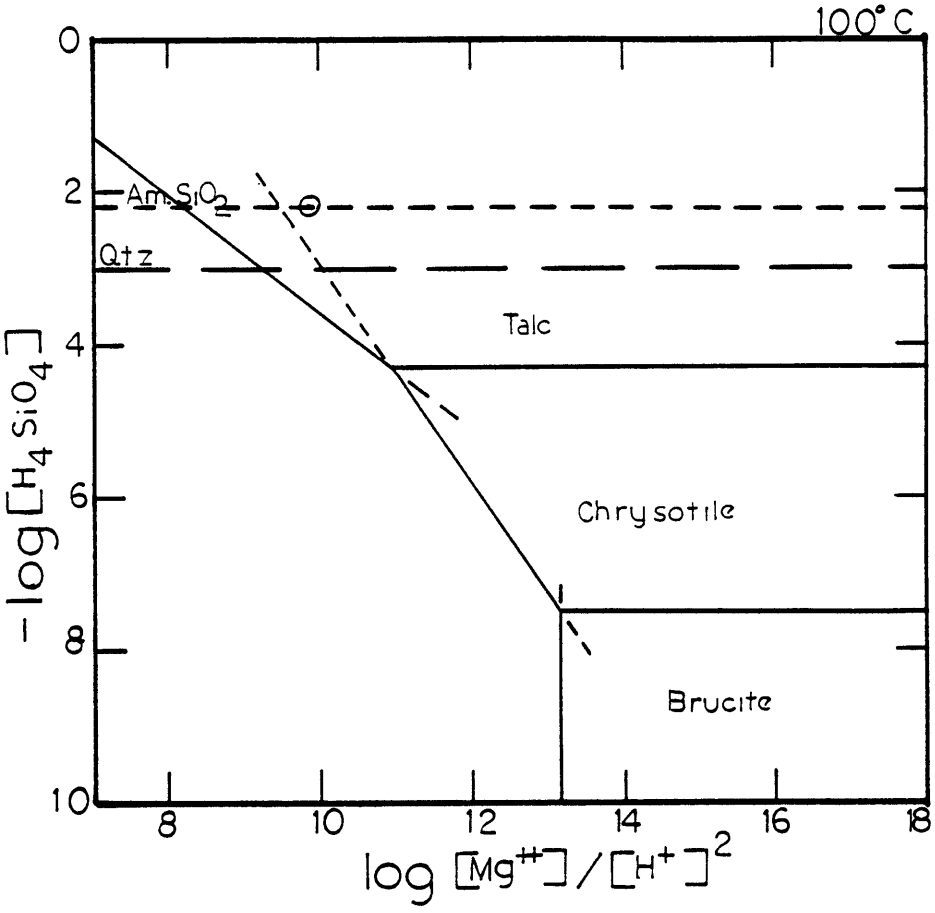
100° C
0
2
4
6
8
10
Am. SiO2
Qtz
Talc
Chrysotile
Brucite
8
10
12
14
16
18
- log [H4 SiO4]
log [Mg++] / [H+]2

at temperatures above ~200°C. The colloform layer in the Cu-rich chimneys should be formed at lower temperatures. If more hot fluid does escape from the interior of Zn-rich chimneys, such a difference in the formation of the outer layers might indeed exist.

There are some temperature data from fluid inclusions to support this theory. Fluid inclusions in anhydrite from the mixed sulfide masses of one Zn-rich vent, vent site 1 of dive 980, yielded a wide range of formation temperatures, corrected for pressure, from 200°C to 314°C (Kusakabe et al., in prep.; see figure III.4). The agreement with a postulated temperature of deposition above ~200°C is excellent.

The temperature of deposition of Mg-silicates in the Cu-rich chimneys is more difficult to determine. The Mg-silicates were deposited before, during, and after the formation of anomalous bornite in the adjoining layer. The temperature of formation therefore must have included temperatures of ~150°C or below. There is, unfortunately, no way of determining the maximum temperature at which the Mg-silicates formed.

The major mass of the Zn-rich chimneys, then, probably forms by mixing of seawater with a relatively large proportion of hydrothermal fluid seeping outward from the chimney interior. As the Zn-rich chimneys develop, the lower walls must eventually be sealed to fluid mixing by mineral deposition in all the available spaces. More pristine hydrothermal

solutions can then rise higher in the chimneys, and fluid still retaining Cu can come in contact with the previously deposited Zn sulfides. The presence of a late, Cu-bearing solution is implied by a fine dusting of Cu-Fe sulfides on the interior surface of some of the wurtzite-lined channels, and by Cu-Fe replacement of the outer edges of the elongate wurtzite crystals. If this does occur, then the lower levels of a Zn-rich chimney may contain considerable Cu.

The differences in the morphology of samples from Zn-rich and Cu-rich chimneys are related to the different mixing patterns in the vents. Hydrothermal solutions rising in a single large pipe, as in a Cu-rich chimney, will be relatively unaffected by inflow of small quantities of seawater; the temperature in a Cu-rich chimney will thus remain close to that of the hydrothermal endmember. Hydrothermal fluid rising in many small channels like those in Zn-rich chimneys may be more affected by small quantities of seawater penetrating through the chimney walls, and may even permit the penetration of a greater total quantity of seawater. The vent may therefore maintain a lower temperature fluid in the channelways. The narrow fluid channels in a Zn-rich vent may be more easily filled in by mineral deposition, creating a structure which contains hot fluid inside but which is sealed on the outside; this in turn creates a possibility that a new vent may form on the same site if the sealed structure is fractured. Both of these possibilities will be explored further in the next chapter.

Chapter IV

Life Cycle of a Vent

The process of chimney formation just described represents one facet of the construction of a hydrothermal vent structure. The basal mounds on which the chimneys form must also be considered as part of the formation process, although observations of and mineralogical data obtained from the mounds are scant. In addition, the samples taken from each vent can be used to describe its development at only one moment in time, during one phase in the life cycle of the vent. During that life cycle, the structure at any one vent may undergo changes. Because only one vent has been positively identified on more than one cruise the opportunities to observe changes in the structure of a single vent have been limited. Presentation of an evolving vent structure is therefore speculative, but if these active submarine hydrothermal deposits are to be compared to any extinct deposits, then the differences between what we see in progress and what is likely to be preserved to form an extinct deposit must be identified.

Mound Characteristics

Very little is known about the internal structure of the mounds beneath the chimneys, due to their inaccessibility

to sampling. Exterior samples have been described by Haymon and Kastner (1981) and Spiess et al. (1980), and observers in the Alvin on all three cruises have described the appearance of the mounds on the seafloor. In November 1981, a series of small depressions was made in the basal mound of the then inactive National Geographic vent (vent S-2) when the Alvin landed. Small black smokers quickly appeared in the depressions, suggesting for the first time that active hydrothermal circulation at high temperatures occurs within the mounds (Goldfarb et al., in prep.).

Samples collected from the outer surfaces of the mounds consist of aggregates of pyrite and sphalerite accompanied by minor chalcopyrite. The sulfides are crosscut by fossilized pompey worm tubes ½ to 2 cm in diameter, which are coated with alternating layers of sulfides, and an amorphous silica-barite-native sulfur assemblage. These honeycombed aggregates often enclose or are accompanied by areas of massive sulfides, which may contain channelways with mineralized linings (Haymon and Kastner, 1981). A few mound samples were collected from vents S-2 and S-3, which were very similar to those described above but which were also coated with the tubes of living worms. As seen from the Alvin, the mounds appear to consist primarily of fallen chimney blocks and fragments which have been oxidized on the surface, and which presumably have been colonized by pompey worms after falling.

A second component of the mounds was observed in November 1981, when fine sandy sulfides that could be easily sampled with a scoop sampler were collected from the mounds. One such sample was taken from the Black Forest vent in November 1979, but the common occurrence of such a sediment was not observed until the 1981 cruise. The sample taken at the Black Forest contained Fe and Cu in a ratio of about 1:1 and little or no Zn, a composition unlike that of the black smoke.

Although the mound surfaces are able to support an abundance of pompey worms, the water discovered inside the National Geographic mound in November 1981 can be deduced to be quite hot, from the escape of water as black smokers. Spiess et al. (1980) concluded that black smoke formed from venting of water at temperatures above ~275°C. The measured temperatures at the five vents examined in this study indicate that black smoke can form down to at least ~250°C. The National Geographic vent thus provides evidence that a mound which appears no longer to be an active vent can maintain high-temperature fluid circulation beneath an impermeable sulfide-oxide crust of unknown thickness. If the maximum temperature of fluid inside the mound is high enough, Cu-Fe sulfides could be deposited in the mound interior, and a layered structure could be created, composed of Cu-Fe sulfides in the center overlain by Zn sulfides and possibly anhydrite as the temperature drops in the zone between the

convecting fluid and ambient seawater.

Chimney-Mound Cycle

The life cycle of a sulfide vent structure begins when hot hydrothermal fluid emerges onto the seafloor in a terrain that allows it to reach the seawater-basalt interface in a relatively pristine condition, largely unmixed with seawater. When the first hot spring water mixes with seawater, it probably forms a plume of precipitates consisting of sulfides, sulfates, and silicates. The first deposit on the basalt floor then would be a blanket of the sediment formed by mixing at the seafloor, through which the hydrothermal fluid could continue to move upward. From the slightly protected environment created by the first sediment layer, a more extensive vent structure could develop. The deposit may be built by a series of chimney-mound cycles, which will be described here starting with an initial small mound capped by an impermeable crust.

Within a mound covered by an impermeable sulfide-oxide crust, internal circulation develops in the rising hydrothermal fluid. However, the fluid cannot escape to form a chimney, nor can the mound increase appreciably in size. There is little deposition onto the mound from above, and although the circulation within the mound can alter the mineralogy and fill in any empty space with precipitates, the

presence of the outer crust limits enlargement of the mound from within.

In order to build more of a vent structure, the impermeable crust on the mound must be fractured so that fluid can escape. Such fracturing should not be hard to induce. Small earthquakes, which could easily disrupt a mound, are common occurrences along active spreading ridge segments. If deposition does occur during the internal circulation of hydrothermal fluid, a volume increase of solids within the mound might also force fracturing, depending on the strength and thickness of the outer crust.

When the impermeable crust on the mound is broken, hydrothermal fluid escaping from all the cracks will immediately mix with the overlying seawater. If the fracturing of the crust is extensive, the effect will be a diffuse venting of hot fluid over the entire surface of the mound. Rapid mixing with seawater at the surface will result in the deposition of a layer of sediment which may quickly clog the smallest of the fractures. Many small chimneys may begin to form from fluid escaping at multiple fractures, but the smaller chimneys are likely to clog quickly with precipitates, leaving a limited number of larger chimneys growing over the largest cracks in the mound.

Once hydrothermal fluid is flowing out of fractures on the mounds, chimneys can be built up as described in the previous chapter. The internal diameter of the chimneys is

not large, and over time they may gradually be filled in by deposition on the interior walls. Eventually the chimneys do seal off and active venting of hydrothermal fluid ceases, as it did at the National Geographic vent between November 1979 and November 1981. When the vent is closed off, internal circulation within the mound can develop under the outer crust, as observed at the National Geographic vent.

If another episode of fracturing breaks open the new outer crust on the mound, another cycle of chimney building can take place. If the chimneys clog quickly with precipitates, and the impermeable crusts on the mounds fracture easily, more than one cycle of chimney-mound development may occur during the active life of a single hydrothermal vent. Each time a sealed mound forms, the internal circulation of high-temperature fluid will tend to redistribute metals within the sealed structure. In consequence, the exterior samples of all the mounds will tend to be similar and to be Zn-rich, regardless of the chimney composition. The interiors of the mounds may be Cu-rich, and may retain traces of more than one episode of layering, but since they cannot be sampled, their composition and structure remain unknown. The possible construction history of a vent structure is illustrated in figure IV.1.

Precipitation within the chimney pipes is not the only possible way of periodically cutting off the active flow of hydrothermal fluid from a vent. Sealing and re-fracturing

Figure IV.1. Schematic evolution of a mound-chimney cycle. From Goldfarb et al., in prep.

Stage 1: Small plumes of hydrothermal fluid flow out of fractures in the seafloor. Precipitation of sulfates and sulfides around the small vents leads to the construction of an embryonic basal mound.

Stage 2: Most of the small fractures are clogged; chimneys develop above the larger fractures. An impermeable cap forms on the basal mound.

Stage 3a: The impermeable cap of the second stage breaks, allowing the escape of hydrothermal fluid in many small plumes. Precipitation of sulfides and sulfates around the vents adds to the thickness of the basal mound. Chimney fragments are probably incorporated into the mound during this stage.

Stage 3b: Smaller vents rapidly plug with precipitates and form a new impermeable crust on the basal mound. A redistribution of minerals may occur within the new sealed mound.

Stage 4: Decay of the hydrothermal system causes temperatures to drop within the mound. High-temperature mineral assemblages may re-equilibrate with falling temperatures. Eventually flow through the system will cease.

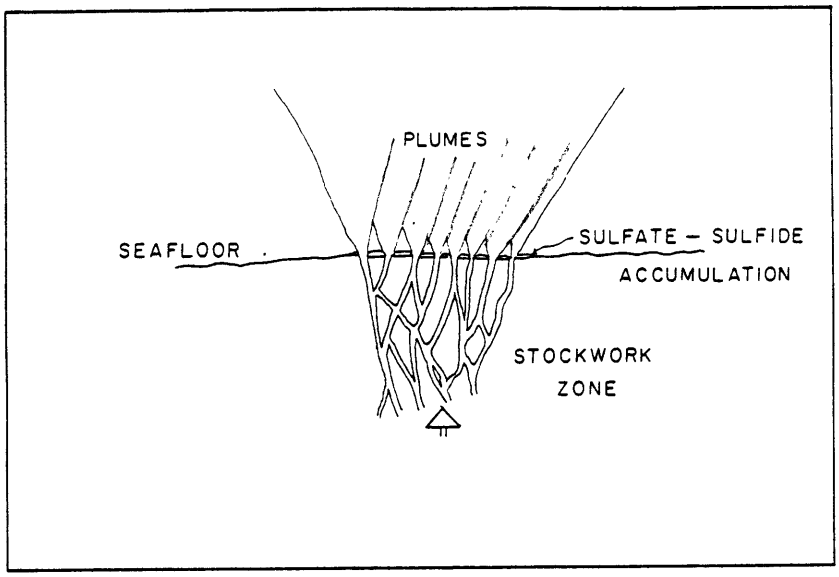
PLUMES
SEAFLOOR
SULFATE – SULFIDE
ACCUMULATION
STOCKWORK
ZONE

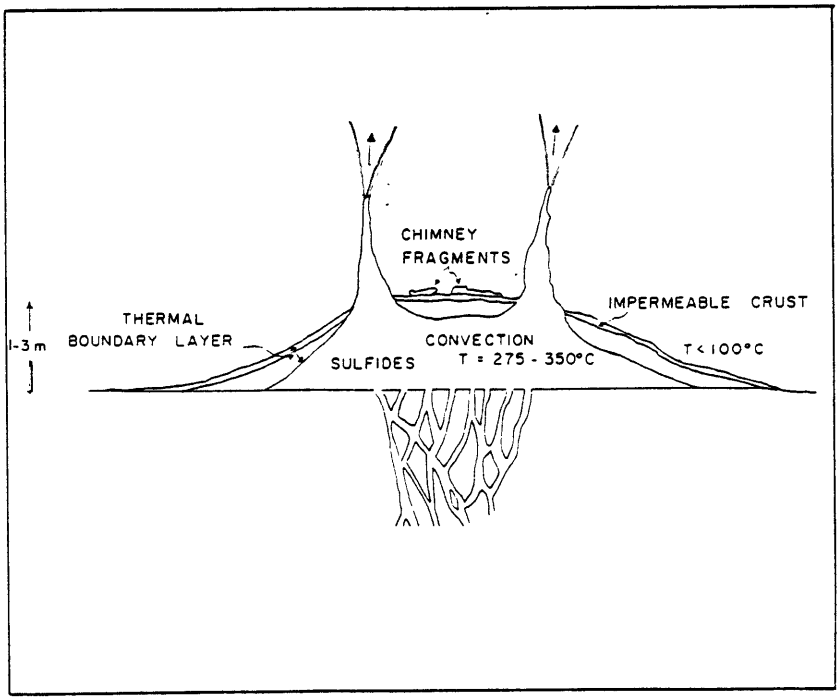
CHIMNEY
FRAGMENTS
IMPERMEABLE CRUST
1-3 m
THERMAL
BOUNDARY LAYER
CONVECTION
T = 275 - 350°C
SULFIDES
T < 100°C

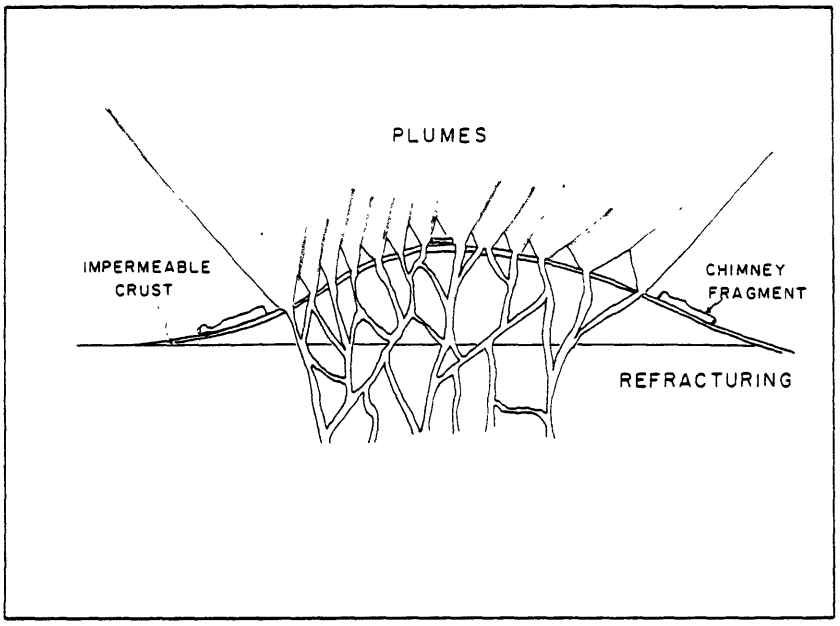
PLUMES
IMPERMEABLE CRUST
CHIMNEY FRAGMENT
REFRACTURING

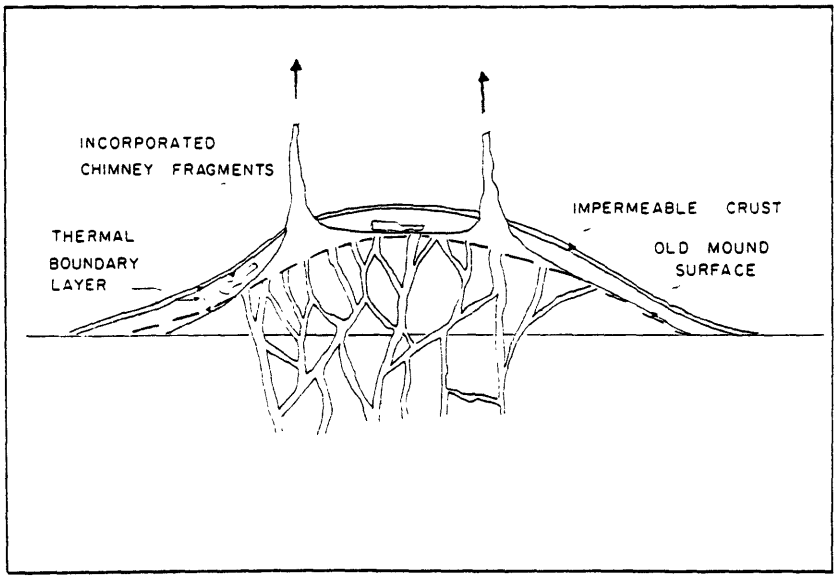
INCORPORATED CHIMNEY FRAGMENTS
IMPERMEABLE CRUST
THERMAL BOUNDARY LAYER
OLD MOUND SURFACE

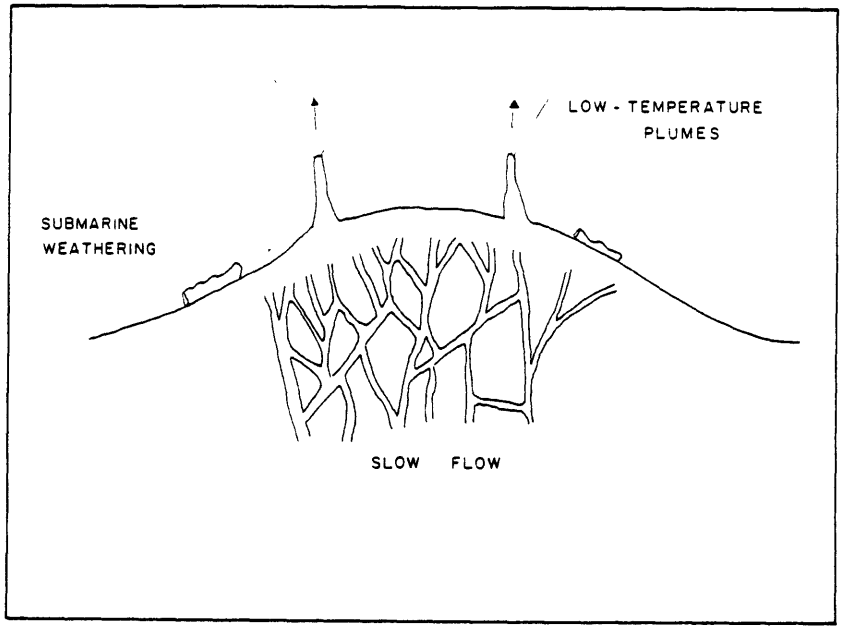
LOW - TEMPERATURE
PLUMES
SUBMARINE
WEATHERING
SLOW FLOW

may also occur in the fluid paths within the mound or below the seafloor. Alternatively, if the flow of fluid is itself episodic instead of constant then the vent chimneys may periodically be inactive. Episodic fluid flow, or periodic cooling and reheating, could occur as a consequence of new basalt eruptions or intrusions which intensify or revitalize an existing circulation system.

Although not explicitly noted in the outline given above, this repetitive process of vent development does allow for the enlargement of the mounds by the addition of both chimney blocks and sedimentary sulfides. Chimney pieces may be dislodged and fall onto the mound during several stages of development. While the chimney is growing, pieces can break off, but the chimneys appear to be relatively stable while they are active, so pieces are not likely to fall from an active area of the vent. Two other stages are likely to produce fallen chimney blocks. When the chimney has been sealed off, chimney pieces may fall, especially if they are weakened as a result of alteration by seawater. In addition, the disruptive mechanisms that fracture the impermeable crust on the mounds could also topple any chimney pipe remaining on top of a mound.

The sedimentary component of the mounds may also be created by a combination of processes at different stages in the vent development. One has already been noted: after the crust on a mound is fractured, when the first rapid mix-

ing between hot fluid and seawater occurs, a layer of sediment is likely to be deposited on the broken surface of the mound. Sediments can also be deposited on the surface of a mound during the chimney-building stage. The exterior of the chimneys generally consists of a layer of anhydrite and fine-grained mixed sulfides. If the anhydrite is gradually dissolved from the lower portions of a chimney, the sulfides will be released and fall to form a sediment layer on the mound. Some of the sulfides may be oxidized as the anhydrite dissolves, but the mineralogy of dead vent deposits indicates that anhydrite dissolution occurs more rapidly than sulfide oxidation. A small amount of black smoke may also drift down onto the mound as sediment, but this contribution is apparently relatively minor, judging from two facts: (1) most of the black smoke is carried away from the vents and does not visibly rain down on the mounds, and (2) the composition of the sediment on the mounds, where it has been analyzed, differs from that of the black smoke. Sediment from the Black Forest mound is rich in Cu but very poor in Zn, as the sulfides in the chimney are, whereas black smoke is fairly rich in Zn and contains very little Cu. The composition of sediment on all the mounds may turn out to be closely linked to the individual chimney compositions.

A repetitive pattern of chimney and mound formation also provides a means of accommodating changes over time in

the temperature and degree of mixing of the hydrothermal fluid and in the composition of the associated chimney. A possible evolution in the temperature of the hydrothermal fluid beneath the seafloor, over time, is presented schematically in figure IV.2, along with the sequence of chimney types that might occur over the life of the vent. The basic temperature variation is provided by heating fluid in the seafloor circulation system that creates the hydrothermal solutions to a maximum, and then cooling it as the circulation dies down. The effect on mineralogy in the vent deposits may be accentuated by sealing within the basal mound or in a stockwork zone below the seafloor between the Zn-rich and Cu-rich stages, resulting in a smaller admixture of cold seawater below the Cu-rich chimneys. The phase indicated as ZnII represents the infilling of a dying circulation system. It is not a separate type of chimney, but simply a late stage of mineralization. Sphalerite is found in the center of dead chimneys at extinct vents at 21°N (Haymon and Kastner, 1981). The National Geographic vent may have been in the ZnII phase when the vent S-2 samples were taken in November 1979, since those samples have an overlay of Zn sulfide on the interior of the massive cubanite lining. By November 1981 the vent consisted of a sealed mound.

The progression suggested above implies that Zn-rich deposits are succeeded by Cu-rich deposits over time at one vent, but not necessarily in one chimney. The Zn-rich chim-

Figure IV.2. Schematic view of the evolution of temperature within a hydrothermal vent system through time. The most likely occurrence of Zn-rich and Cu-rich stages are indicated; ZnII indicates a last episode of Zn-rich mineralization in a waning hydrothermal system. The time and temperature scales are relative; temperature refers to temperature at the base, not the mouth, of the vent, as the system as a whole develops and then declines.

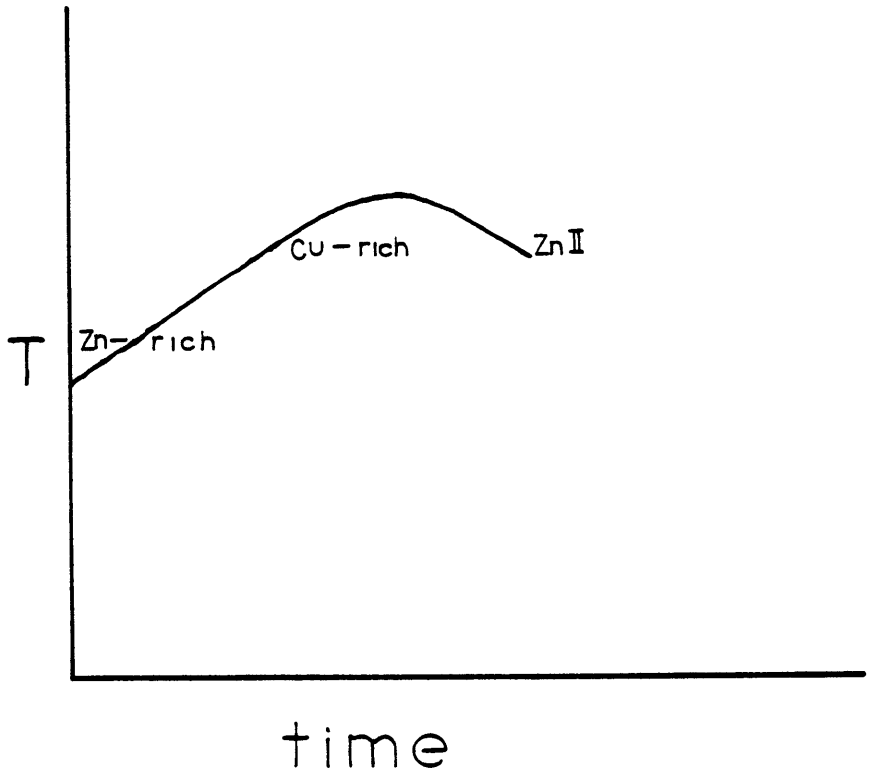
T
Zn-rich
Cu-rich
Zn II
time

neys sampled at 21°N seem unlikely to be transformed directly into the Cu-rich chimneys. There is too much difference between the general form of the two types of samples for that to occur. However, the bases of Zn-rich chimneys do appear to be sealing, since late Cu-Fe mineralization is present, and if another set of chimneys were to be constructed later on the same sites they might be Cu-rich instead of Zn-rich.

This version of the development of the hydrothermal vent deposits does permit explanation of a few additional observations made at 21°N. The model allows the mounds to grow in size periodically, resulting in mounds up to several meters high, all with oxidized exteriors and lacking freshly deposited material. Of particular interest is the fact that all mound samples from black smokers studied so far are similar and Zn-rich, regardless of the composition of the chimney above (Haymon and Kastner, 1981; this study). In the pattern of development just presented, all the exterior mound samples would tend to be similar, because they all formed in similar boundary zones between seawater and a hot mound interior containing circulating hydrothermal fluid. The particular mound sample from vent S-2 that resembles a Zn-rich chimney piece could have formed in such a boundary zone, or it could be a fallen piece from a previous, Zn-rich chimney. Finally, the observed variations in degrees of mixing and temperature among the vents are more logically

formed as a progression among different stages of vent development than as basic differences among a closely clustered group of vents all located on seafloor of essentially identical age and physical characteristics.

Death and Alteration

Since one of the aims of reconstructing the life of the hydrothermal vents at 21°N is to visualize how these vent structures might look if they were preserved as mineral deposits, the transformations accompanying the death of a vent and the subsequent alteration of the structures must be considered. Well preserved extinct vents in the same area as the active vents have been sampled and described by Haymon and Kastner (1981). A series of altered dead vents 700 - 800 m west of the ridge axis farther to the north, which were the first evidence of hot spring activity discovered in the area, has been described by Francheteau et al. (1978) and Hekinian et al. (1980). A comparison between the active vent deposits and the altered dead vents has been presented in Styrt et al. (1981). The differences in mineralogy between the active and dead vent deposits provides useful evidence of the gradual destruction of vent structures left unprotected in ambient seawater.

The "death" of a hydrothermal vent occurs when the flow of hydrothermal fluid ceases. The final precipitates filling

the center of chimneys from dead vents at 21°N consist primarily of sphalerite, together with native sulfur and pyrite, and minor wurtzite, marcasite, barite, amorphous silica, and chalcopyrite (Haymon and Kastner, 1981). This clogging material represents the last deposition from a waning flow of cooling hydrothermal fluid, the ZnII stage of the vent. The ZnII stage is probably a short-lived period of mineralization, in the final development of which seawater may actually move into the chimney from the top, leading to cooler conditions and more mixing lower in the chimney, and facilitating complete filling of the chimney channel.

The dead vents discovered by Francheteau et al. (1978) off the ridge axis north of 21°N reveal a multitude of differences, when compared with active vent structures, which result from alteration in the deposits after the death of the vents. The dead vents formed roughly cylindrical hills of varying sizes, up to 10 m in height with an average diameter of about 5 m, all located on a band of fissured and faulted terrain about 1.5 km wide. Samples taken from the hills consisted of two types of material: (1) dark grey massive sulfides with surfaces honeycombed by tubular structures of 0.5 mm to 3 cm in diameter, and (2) oxidized equivalents of the sulfide samples, yellow to red-brown in color and friable, identified as "gossans." The massive sulfide mixture includes sulfides rich in Zn, Fe, and Cu. The walls

of the tubes crosscutting the sulfide mass are coated with lamellae of pyrite, hydrated amorphous silica, and sphalerite and wurtzite. Layers of hydrous Fe oxides occur between the silica and sulfide layers in the more oxidized samples. Some of the tubes are clearly fossilized worm tubes, while others may have originated as channelways for fluids, but it is clear that all have served as conduits for mineralizing solutions (Hekinian et al., 1980).

Analyses of the samples by Hekinian et al. (1980) reveal the extent of the alteration effected by seawater. Sulfates are almost lacking from the dead vents. Minor Cu-Fe and Zn sulfates, barite, gypsum, and jarosite can be found, of which only barite and possibly gypsum have been found in more than one sample from the active vents. The major quantities of anhydrite characterizing the active vent deposits are entirely absent.

Among the sulfide phases, pyrite and marcasite make up ~50% of the bulk material, sphalerite and wurtzite ~34%, and Cu-rich sulfides ~16%. Cu-bearing sulfides include chalcopyrite, cubanite, bornite, digenite, and covellite, the last two of which occur as replacements of chalcopyrite. The crystallinity of the material varies from pyrite and ZnS similar to the "colloidal" sulfides in the active vents to well crystallized pyrite, sphalerite, chalcopyrite, and cubanite. Pyrite and sphalerite are the two most abundant minerals. The Zn sulfides are high in Fe, and a progression

can be observed from ~6 mole % FeS in gel-like wurtzite through ~15 mole % FeS in crystalline sphalerite associated with pyrite and chalcopyrite, to ~21 mole % FeS in sphalerite occurring as inclusions in pyrite. Wurtzite in the dead vents apparently is recrystallizing to sphalerite; incipient sphalerite crystallization can be detected within wurtzite gels. All the sulfides are gradually being replaced by hydrous Fe oxides, primarily goethite and limonite, which are common constituents of the dead vent material.

Silicates are also common in the dead vents, particularly in the oxidized gossan samples. Hydrated amorphous silica occurs primarily as one individual layer in the linings along tube walls. Crystalline silicates are widespread in association with both amorphous silica and Fe oxides. Nontronitic clays high in Si and Fe and low in Al are the major silicates; very minor quantities of zeolites and muscovite were also found.

The descriptions and mineralogy of the least altered samples from the dead vents are similar to those of mound pieces collected from the active vents. The extinct structures are conical in shape, a form that could result from a chimney-mound combination sealed off under a crust when the vent died. The major differences in mineralogy between the dead and active vent deposits are in the non-sulfide minerals. The unaltered sulfide component of the two vents is similar, as expected, although not identical. The sul-

fate, silicate, and oxide phases are significantly different.

The sulfates in the dead vents are completely different from those in the active vents. Anhydrite is undersaturated in normal seawater. It is therefore readily dissolved from a dead vent. Indeed, it has already been suggested that it may begin to dissolve from the lower parts of active vents. The sulfates that remain or form in the dead vents -- such as barite, Cu-Fe sulfates, and Zn sulfates -- are only a minor component of the deposits. Since the remaining sulfates are also out of equilibrium with seawater, it appears that they are more resistant to dissolution than anhydrite.

Iron oxides, on the other hand, are rare in the active vent structures, occurring only on the outer surfaces, but are abundant in the dead vent deposits. They form, obviously, from the oxidation of sulfides under the influence of seawater. The gossan samples are composed predominantly of Fe oxides, and even in the sulfide samples oxides can be seen replacing the sulfide phases (Hekinian et al., 1980). Most of the Zn and Cu in the sulfides is apparently lost during oxidation, although some is retained in the oxides, some is incorporated as minor metals in the silicate phases, and some is incorporated into minor Cu-Fe and Zn sulfates.

The silicate component of the deposits undergoes major transformation during the alteration process. The Mg-silicates present in the active Cu-rich chimneys do not occur in

the dead vents, either because they never were present in these particular vents or because the Mg has been removed by reaction with cold seawater. However, Fe-bearing nontronitic clays are abundant. Their association with amorphous silica and Fe oxides suggests that they form by reaction between the silica and Fe released during the oxidation of sulfides, to form stable crystalline silicates.

The dissolution and oxidation of minerals in the deposits, if allowed to continue unchecked, will eventually destroy the original mineralogy of the deposits. The preservation of the vent deposits in a recognizable form therefore becomes a problem of some concern.

Preservation

The preservation of hydrothermal deposits like those forming at 21°N will depend on how rapidly the vents are covered over. Basically, three apparently different types of deposits could be preserved in the geologic record under particular circumstances: (1) an oxidized deposit, (2) a sulfide deposit with an oxidized capping, and (3) a layered sulfide deposit.

Under "normal" circumstances, in which a dead vent deposit is left undisturbed and uncovered on the seafloor, the oxidation observed in the extinct vents at 21°N will proceed to completion. Essentially none of the original sulfide de-

posit will remain. The friable Fe oxide-silicate mound that replaces it will probably crumble and be scattered over the surrounding seafloor. When later detrital sediments accumulate over the remains of the mounds, the only preserved remnant of the original vent deposit will be an Fe oxide-silicate facies at the base of the sediment cover. If a later lava flow covers a completely oxidized deposit, a discontinuous layer of intercalated, baked sediment would appear within the volcanic sequence. Preservation of this type of deposit in the geologic record will not reveal the original presence of a potential ore deposit, although a stockwork zone of hydrothermal alteration should still be visible in the underlying basalts.

A different appearance will be preserved under special circumstances if the oxidation process is interrupted before it is complete, and the deposit is protected from complete alteration. A likely scenario for these special circumstances would be the eruption of basalts on the flanks of a spreading ridge, which covered and thereby preserved a partially oxidized mound. In this case, the deposit seen in the record would have a massive sulfide center overlain by an oxidized capping. The composition of the sulfide center would depend on the original composition of the mound interior and the extent to which the exterior had been destroyed by oxidation. In the case of a Cu-rich interior overlain by a Zn-rich exterior in the original deposit, a

relatively small amount of oxidation would produce a layered structure with a Cu-rich massive sulfide center overlain by a thin Zn-rich sulfide layer in turn overlain by an Fe-oxide gossan. More extensive oxidation would produce a Cu-rich massive sulfide directly overlain by a gossan. The preserved form of such a deposit bears a strong resemblance to the ophiolite-hosted massive sulfide ores in Cyprus.

Another set of special circumstances could result in the preservation of a virtually unaltered vent deposit, if a fresh pulse of basalt eruption at the spreading center covered an active or a newly extinct vent. In this case, the deposit revealed in the geological record would show a Cu-rich sulfide core surrounded by Zn-rich sulfides and anhydrite. Capture within the basalts of a sealed mound would produce a layered structure of Cu-rich sulfides overlain by Zn-rich sulfides probably overlain by sulfate-rich material. An active vent covered by later basalts might show more of an actual chimney structure with a Cu-rich core extending almost to the top of the deposit. Capture of an active Zn-rich chimney would show Cu-rich sulfides in the center only at depth, much the way a sealed mound might. However, if the vent were covered over before the hydrothermal circulation had ceased, then the sulfide deposit could well be rearranged by continuing internal circulation below the basalt cap. Hydrothermal alteration would also probably be visible in the base of the overlying basalts. A basalt

eruption pouring over an active chimney would be likely to knock over part of the chimney, thereby preserving sulfide chimney debris around a deposit organized into a layered structure by the continuing hydrothermal circulation. The basic form of this type of preserved deposit is similar to both the Kuroko ores of Japan and a number of ophiolite-hosted massive sulfide deposits.

Two particular characteristics of the hydrothermal vent structures at 21°N, which might logically be looked for in a preserved ore deposit, are a main vent outlet, and the fossilized worm tubes that are so abundant on the mounds and on the Zn-rich chimneys. Evidence of a vent outlet would be modified by circulation within a mound, so that the upper outlet might not be retained at all. However, indications of hydrothermal outflow should be retained in the basalts underlying the vent, in the form of alteration in a feeder zone. Quartz and sulfide deposition would also occur within the basalts if some cooling occurred below the seafloor.

The fossilized worm tubes, on the other hand, one would expect to be quite evident in almost any preserved deposit. The worm tubes are abundant on all the vents. They are not destroyed by circulation within a mound, because they grow only on the outside and in fact grow on mounds within which circulation is taking place. Finally, the tubes are still identifiable in gossan samples after oxida-

tion (Hekinian et al., 1980). Since traces of them are visible for so long, they seem to be one of the most persistant characteristics of the vents and therefore a possible mark of the origin of a preserved ore or sediment deposit.

Organic Contribution

With the exception of the mention of fossilized worm tubes, the possible organic contribution to the creation of the hydrothermal vent deposits has not been included in the preceding discussion. The extensive biota supported by the vents has been mentioned. Sulfur- and metal-oxidizing bacteria do inhabit the vent waters, although the maximum temperatures at which they live are unknown. The contribution of organisms to the construction of the vent structures appears to be minor, but the potential for destroying the structures seems to be large. The possibility exists that the sulfide deposits are eaten away by bacteria while the vents are active, and are also disassembled by inorganic oxidation after the vents die. At present, however, too little is known about the functioning of the living community at the vents to allow an assessment of the organic contribution to either the creation or the destruction of the vent structures.

Summary

The life cycle of a hydrothermal vent includes more than just the construction of a chimney. Looking at only the most obvious feature of each vent, a chimney usually sampled on only one cruise, essentially means looking at an ongoing process frozen at one point in time. Trying to expand the development of a vent to include its entire growth, evolution over time, death, and preservation leads to a series of conclusions extending beyond the chimney formation processes described in the previous chapter:

(1) The basal mounds below the chimneys grow through the addition of fallen blocks from chimneys, sediment deposited from direct fluid mixing through cracks in the mound crust and from dissolution of the outer layers of the chimneys, and internal deposition of sulfides from hot solutions.

(2) An apparently inactive mound can maintain an internal hydrothermal circulation at high temperature, below an impermeable sulfide-oxide crust. This will result in a reorganization of minerals within the mound into Cu-rich sulfides at the center, surrounded by Zn-rich sulfides and sulfates. As a consequence of this mound structure of a hot interior and a crust forming a boundary next to seawater, exterior samples from mounds at all the vents should be similar regardless of the chimney composition at the vent.

(3) The vent as a whole probably grows through a mound-chimney cycle in which the crust on a sealed mound is fractured, leading to escape of hydrothermal fluid. The largest cracks are not immediately plugged by precipitates. Above these outlets in the mound the chimney structures grow as described in the previous chapter. When escape of hydrothermal fluid through the chimney is blocked, another sealed mound develops. The cycle may be repeated many times at any one vent, depending on how readily the chimneys seal off and how easily the crusts on the mounds crack.

(4) During the life of a vent, the chimney structures at the vent may go through stages of Zn-rich and Cu-rich compositions, as the basic temperature of the hydrothermal fluid rises and then falls, and as the degree of seawater mixing in the vent structure changes.

(5) After the hydrothermal circulation at a vent ceases, the deposits become vulnerable to alteration by ambient seawater. Dissolution of anhydrite is accompanied by oxidation of sulfides and the formation of stable silicates, leading eventually to the replacement of a sulfide-sulfate facies by an oxide-silicate facies.

(6) The preservation state of the vent deposits depends on when they are covered and removed from contact with seawater. If the deposits are completely altered, only oxidized debris will remain at the base of a sediment column or sandwiched between basalt flows. If basalt eruptions

cover a partially oxidized deposit, a massive sulfide overlain by an oxide cap will be preserved. If an active vent is covered by fresh basalt, a complete, layered sulfide-sulfate deposit may be preserved. The upper vent outlet may not be retained in any deposit, if the minerals are redistributed by internal circulation below a sealed cap. However, a hydrothermal feeder zone should be recognizable in the underlying basalts. Remnants of the fossilized worm tubes that are so abundant on the vents should also remain, even in an extremely oxidized deposit. Identification of the remains of mineral deposits similar to those forming at the 21°N hydrothermal vents is not entirely straightforward, and requires at least a certain amount of reconstruction from any preserved form of deposit.

Chapter V

Comparison with Ore Deposits

Ore-Forming Potential

The ability of the hydrothermal fluid venting at 21°N to transport metals, and the efficiency of fluid mixing as a depositional mechanism, needs no further proof. However, it is quickly evident that the mounds and chimneys at 21°N are very small. Even if they were preserved before any destruction of sulfides took place, the resulting "ore deposits" would be miniscule in size. A single vent structure of an average size, with a mound 15 by 30 m in plan and 2 m high supporting a chimney 5 m tall and 2 m in average diameter contains less than 1000 m^3 of material. If 50% of the material consists of sulfides, with equal proportions of FeS_2, ZnS, and $CuFeS_2$, only about 16 tons of sulfides would be contained in the mass unless an extensive subsurface deposit also exists. A change in the proportions of the minerals present does not alter the conclusion: only a very large cluster of vents of this size could form an exploitable ore deposit.

However, although the particular vents observed at 21°N are small, the process operating there could serve to form larger deposits. Although such larger deposits might differ in some ways from these smaller ones, it is the larger de-

posits that may show up as workable ore deposits. Workable ore deposits that can be compared to the 21°N deposits do occur, confirming the importance of the system of mineral deposition at 21°N. Two types of stratiform massive sulfide ores in particular are most closely comparable to the 21°N deposits: those occurring in the extrusive layers of ophiolite complexes, and those comprising the Kuroko ores of Japan and Kuroko-type ores worldwide.

Ophiolite-Hosted Massive Sulfides

If hydrothermal vent deposits of the type found at 21°N are preserved through time, the setting in which they are most likely to be found is in segments of old ocean crust now accessible on land. Since this is the accepted interpretation of ophiolite complexes, the basaltic upper levels of ophiolite complexes provide a suitable setting, and the pyritic Cu- or Cu- and Zn-bearing massive sulfide deposits found in many of them are gcod candidates for the preserved vent structures.

The best studied of the ophiolite-hosted massive sulfide deposits are in the Troodos Complex in Cyprus. There, the deposits occur between two generations of extrusive basaltic lavas, at either the Basal Group-Lower Pillow Lava contact (Searle, 1972) or the Lower Pillow Lava-Upper Pillow Lava contact (Constantinou and Govett, 1973). The Upper

Pillow Lavas are unmineralized. Regardless of which of the two contacts is considered to be crucial, the sulfide deposits formed after one generation of lava extrusion and were subsequently covered by a later eruption. There is ample evidence, from studies of stable isotopes, Sr isotopes, alteration mineralogy, metamorphic facies, and basalt leaching, that a hydrothermal circulation system operated in the Basal Group Lavas and Lower Pillow Lavas, with major areas of outflow centered under the massive sulfides (Heaton and Sheppard, 1977; Spooner, 1977; Constantinou, 1977; Chapman and Spooner, 1977).

The massive sulfides in the Troodos ophiolite clearly did form as a consequence of hydrothermal circulation in oceanic basalts. The deposits take the general form of a stockwork zone leading upward to massive compact ore, overlain by conglomeratic ore and a cap of oxidized ochre (Constantinou and Govett, 1972; Searle, 1972). The great mass of the sulfides apparently formed at the basalt-seawater interface, contrary to early interpretations of the sulfides as replacements of basalts (Searle, 1972).

The ochres overlying the massive sulfides in the Troodos complex are Fe-rich oxy-hydroxide sediments containing variable amounts of sulfides, interbedded with cherts, tuffaceous material, and, in one location, limestone (Constantinou and Govett, 1972; Robertson, 1976). The precise composition and appearance of the ochres are variable, but

the major Fe oxide is usually goethite, sometimes maghemite. Sedimentary structures, including graded bedding and slump textures, are common, and the appearance of the ochres varies from massive to finely banded. The proportion of interbedded sulfides increases from the lower levels of the ochres down into the underlying conglomeratic ore. The upper contact with overlying basalt is generally sharp, as expected if the ochres formed before the next eruption (Constantinou and Govett, 1972).

The conglomeratic ore forming the upper levels of the massive sulfide deposit is composed of blocks of solid sulfide in a matrix of friable, sugary sulfides. The proportion of solid blocks and the size of the individual blocks increases downward, creating a gradual transition to compact ore. The sulfide blocks consist of fine-grained pyrite with colloform and banded textures, accompanied by chalcopyrite, sphalerite, and smaller amounts of covellite, other Cu sulfides, quartz, and sulfates. The other sulfides occur interstitially and as coatings on fractures in pyrite. The matrix consists largely of a soft, discolored variety of pyrite. The conglomeratic ore is highly porous. The sulfide blocks contain the most porous, youngest of three generations of pyrite found in the Troodos massive sulfides. The proportion of conglomeratic ore and the thickness of the ochre cap both vary among the deposits. Generally, the thinner conglomeratic ore zones are overlain by the more

poorly developed ochres (Searle, 1972; Constantinou and Govett, 1972, 1973).

The compact ore is composed of large blocks of solid pyrite with minor matrix fillings of sugary sulfides in fractures between the blocks. Chalcopyrite and covellite occur as coatings on fractures in the pyrite and on the faces of pyrite crystals. The compact ore consists mainly of two generations of pyrite. The first generation forms alternating euhedral and collomorphic zones, and the second occurs as grains with smooth, curved edges (Constantinou and Govett, 1972, 1973).

Chalcopyrite and, in smaller quantities, sphalerite and marcasite, are concentrated in the upper levels of the massive sulfides. Chalcopyrite and sphalerite occur within the last generation of pyrite and cementing earlier corroded pyrite. Chalcopyrite is often partially or completely replaced by covellite. Sphalerite also rims chalcopyrite, although occasionally the two are intergrown. Marcasite appears to form after the last generation of pyrite; it usually appears as fracture fillings. Pyrrhotite occurs rarely, in zones rich in chalcopyrite and sphalerite (Constantinou and Govett, 1972, 1973).

The stockwork zone underlying the massive sulfides consists primarily of coarser pyrite crystals and crusts in cavities and fractures in altered basalts, associated with quartz and jasper. The stringers are most extensive and

largest just below the ore bodies, where pods of sulfides form within the basalts (Searle, 1972).

The connection between the thickness of the ochres and the conglomeratic ore has already been mentioned. The formation of these two zones and the concentration of Cu and Zn in the upper levels of the ore bodies have been related to a single continuous process (Constantinou and Govett, 1972, 1973; Robertson, 1977). The ochres form as a result of submarine oxidation and leaching of the massive sulfides. The ochres thus develop originally as submarine gossans, but faulting and tilting of the sulfides lead to redeposition of the loose material, and the formation of sedimentary structures in the ochres. Since Cu and Zn sulfides, unlike pyrite, do not occur within the ochre, they are probably less stable or less resistant than the pyrite. The leaching process continues downward into the massive sulfides and forms the conglomeratic ore by preferential leaching along joints and fractures. The massive ore itself is partly a secondary development, as solutions penetrating down from the alteration zone redeposit sulfides in the upper part of the massive ore. The colloform pyrite in the conglomeratic ore and the Cu- and Zn-sulfides lining fractures in the upper levels of the deposits may all have been precipitated in this way, from low-temperature solutions, after the hydrothermal minerals had been leached and oxidized.

A broader look at the range of ophiolite-hosted massive sulfide deposits of the Troodos type reveals an interesting point. These deposits are all rich in pyrite, but chalcopyrite and sphalerite are generally more abundant than they are at Troodos. They are important components of massive sulfides in ophiolites in Newfoundland (Duke and Hutchinson, 1974; Upadhyay and Strong, 1973) and in the northern Apennines (Ferrario and Garuti, 1980; Bonatti et al., 1976). Deposits in the ophiolites from both of these localities show a noticeable zonation from sphalerite-rich massive sulfide lenses to chalcopyrite-rich stringer zones in the basalts. They also lack the ochre and the uppermost oxidation zone present in the Troodos deposits.

The general description of the ophiolite-hosted massive sulfides corresponds well to a deposit like those at 21°N, which was covered by basalts either just after its death or after some oxidation took place. The deposits in Newfoundland in particular have the Zn-rich upper levels and Cu-rich lower levels that would be produced by hydrothermal circulation inside a mound. Evidence of brecciation and sedimentary structures in the deposits (Duke and Hutchinson, 1974; Upadhyay and Strong, 1973) could be related to post-depositional events that modified the original structures. The lack of anhydrite in deposits that lack an oxidation layer may indicate that anhydrite dissolution occurred sufficiently rapidly that the oxidation products of the sulfides were

scarce and not preserved during the basalt eruption that subsequently buried the ores.

The partially oxidized Troodos deposits do differ from the anticipated results of burying a partially oxidized structure of the type at 21°N. The general sequence of an oxidized layer merging downward through a partially leached zone to compact ore is compatible with the submarine weathering of a mound. Oudin et al. (1981) have described some similar microscopic textures in samples from the dead and active vent structures at 21°N and samples from Troodos. However, the extreme preponderance of FeS_2 over Zn and Cu sulfides in the Troodos ores is difficult to explain. Zn and Cu sulfides may be lost from the inactive vent structures more rapidly than FeS_2; the dead vents at 21°N have either been depleted in Zn and Cu or were never as rich in those elements as the active vents are. If the Troodos ores were originally similar to the deposits at 21°N and to the Newfoundland Cu-Zn ores, then a considerable amount of Cu and Zn has been lost from the deposits. Extensive leaching and oxidation, possibly accompanied by additional secondary precipitation of pyrite below the oxidation crust, could lead to a concentration of pyrite in the massive sulfide body. However, the scarcity of chalcopyrite and sphalerite even in the stockwork zone suggests that most of the Troodos deposits never contained as high a proportion of these minerals as the other deposits do.

The different proportions of Fe, Cu, and Zn sulfides in the Troodos ores may be related to the size of the deposits. The smallest of the Troodos mines still produced almost 1½ times as much sulfide ore as the largest of the Newfoundland mines: Agrokipia B orebody at Troodos produced 50,000 tons of ore (Searle, 1972), while the largest of the York Harbor deposits in Newfoundland is estimated at 37,000 tons (Duke and Hutchinson, 1974). Agrokipia B is also rich in Cu and Zn sulfides; the other Troodos orebodies contained up to more than 15,000,000 tons of ore (Searle, 1972). However, there is no direct connection between the Cu and Zn content of the Troodos mines and the amount of ore produced. Interpretation of the Troodos deposits is also complicated by the fact that ancient mining operations removed considerable quantities of ore from the mines long ago. Since Cu and Zn are enriched at the upper levels of the visible ore, greater concentrations of chalcopyrite and sphalerite may simply be missing from the larger, previously worked mines.

The similarity between the ophiolite-hosted massive sulfides and the deposits at 21°N is sufficiently great to suggest strongly that these ores did form by the same process as the hydrothermal vents. Most of the ore deposits are on a much larger scale than the actively precipitating sulfide deposits at 21°N. Sulfide deposits on a scale similar to those at Troodos have recently been reported

from the Galapagos Spreading Center, 12°S on the East Pacific Rise, and the Juan de Fuca Ridge (Converse, personal communication), so size alone does not seem to be a problem. However, one characteristic is noticeably lacking from the ophiolite massive sulfides: there are no signs of life in or around any of the ores.

Kuroko Deposits

The Kuroko deposits of Japan are a particularly interesting group of ore deposits to compare to the hydrothermal vents at 21°N because they are relatively young, well preserved, undeformed, unmetamorphosed, and generally unaltered, which makes the task of working backward from the preserved deposits comparatively easy.

The Kuroko deposits are stratiform massive sulfide deposits exhibiting consistent compositional zoning. They are found in the Miocene Green Tuff sequences in Japan, which formed during a period of active volcanism of predominantly felsic composition, but which included some basalts. The ores are closely associated with so-called white rhyolite domes, which have been intensely hydrothermally altered (Lambert and Sato, 1974). There is evidence for resurgent caldera activity during the period of Green Tuff volcanism (Ohmoto et al., in press), and also for rifting activity at the time of Kuroko ore deposition, which subse-

quently died out when the rift failed to form completely (Cathles, in press). The presence of deep-sea foraminifera in associated sediments implies that the water depth at the time of ore deposition was greater than ca. 3000 m (Guber, 1979 and in press), a conclusion that is consistent with fluid inclusion data (Pisutha-Arnond et al., in press).

The ordinary form of the Kuroko ore bodies is shown in figure V.1. The following basic description can be found in many articles: Lambert and Sato (1974) is a good, easily available summary, and a variety of summary articles as well as more detailed studies can be found in The Geology of Kuroko Deposits, edited by Ishihara (1974). Generally a single locality contains at least two ore bodies; the individual ore bodies vary considerably in size, from deposits too small to be mined economically to ones about 700 x 300 x 500 m. The ore is divided, from the stockwork zone upward, into siliceous ore or keiko, gypsum ore or sekkoko, pyrite ore or ryukako, yellow ore or oko, black ore or kuroko, barite ore, and a chert zone referred to as tetsusekiei. Not all of the zones occur in each locality. The individual ore bodies vary from only one or two zones, as in deposits of stockwork or gypsum ore, up to the entire sequence. Siliceous ore consists of pyrite, chalcopyrite, and quartz as disseminated and stringer mineralization within a roughly funnel-shaped area in the white rhyolite and associated pyroclastics. Gypsum ore is generally stratabound and may

Figure V.1. A general section through a Kuroko ore body, after Lambert and Sato (1974).

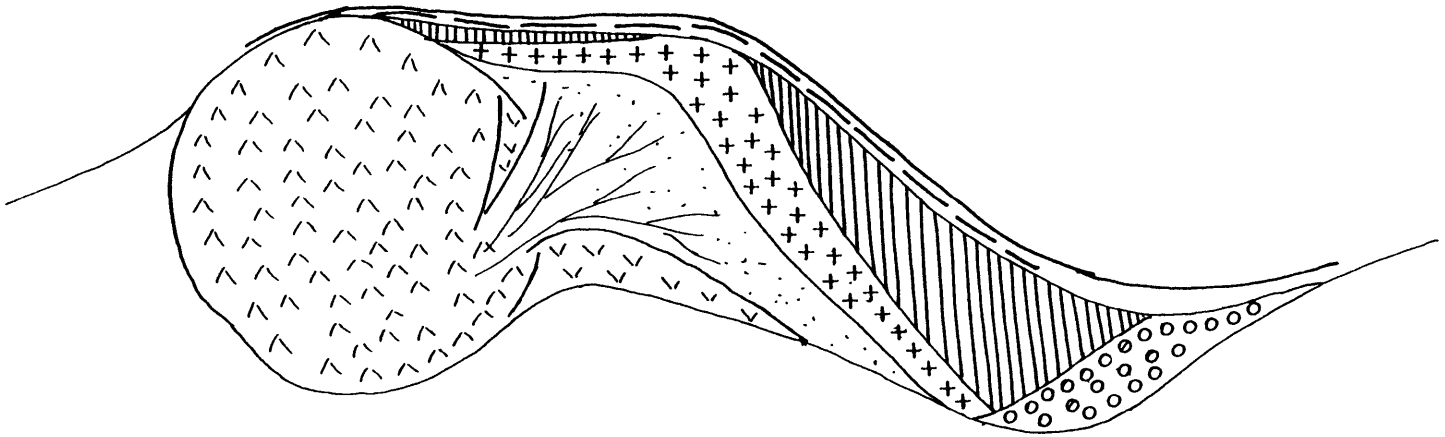

white rhyolite

rhyolite breccia

siliceous ore

yellow ore

black ore

barite

chert

gypsum ore

occur either vertically above the siliceous ore or adjacent to siliceous ore or yellow ore. It consists of gypsum and anhydrite with small amounts of sulfides (pyrite, chalcopyrite, sphalerite, and galena), quartz, and clay minerals.

Pyrite ore forms the lowest stratigraphic level of the massive sulfides. It is usually stratiform but may also form veins or disseminated mineralization. Small quantities of chalcopyrite and quartz occur with the pyrite. Yellow ore is composed of pyrite and chalcopyrite, accompanied by sphalerite, barite and quartz, and minor amounts of Cu, Pb, Bi, and Sb sulfosalts, fluorite, and bornite in some deposits. Black ore is a polymetallic mixed sulfide ore containing sphalerite, galena, chalcopyrite, and pyrite, with barite, bornite in some deposits, and, at the top of the zone, tennantite-tetrahedrite. A wide variety of minor minerals is found in black ore in different deposits, including silver-bearing sulfides and sulfosalts, native silver and electrum, Cu-bearing sulfosalts, and Ni sulfides.

Above the massive sulfides are three more zones of ore or of alteration. Barite ore consists of thin-bedded barite sometimes containing minor quantities of calcite, dolomite, and siderite. The tetsusekiei bed is a thin ferruginous chert, containing hematite often accompanied by pyrite and clay minerals, and sometimes by manganite and braunite (MnOOH and Mn_7SiO_{12}). The tetsusekiei zone is the last bed in the ore deposit proper, and is developed within clastic

material at the base of the hanging wall (Kaleogeropoulos and Scott, in prep.) However, hydrothermal alteration does continue into the hanging wall rocks, were quartz, sericite, and chlorite are common.

Ore textures and the paragenesis of the sulfides in the Kuroko deposits have been closely studied by Eldridge (1981) and Eldridge and Barton (in press). The major sulfides reveal four steps in the ore paragenesis: (1) precipitation of fine-grained sphalerite, pyrite, galena, tetrahedrite, and minor chalcopyrite in a "primitive" ore, (2) recrystallization of primitive ore to form coarser, growth-banded sphalerite and coarser and/or more euhedral pyrite, galena, and tetrahedrite, (3) replacement of early sulfides by chalcopyrite, (4) a minor period of deposition of sphalerite, galena, and tetrahedrite. Fluid inclusions in sphalerite and quartz from the four stages of the paragenesis have been studied by Pisutha-Arnond et al. (in press). The filling temperatures indicate a warming trend from stage 1 through stage 3 following by cooling in stage 4.

Certain other pertinent observations have been made about the Kuroko deposits by Eldridge and Barton (in press). Black ore usually occurs above and on the edges of yellow ore. Yellow ore veins have been observed to crosscut black ore. The yellow ore is more coarse-grained and more porous than the black ore. Although pyrite in the yellow ore may

be euhedral it is usually replaced and corroded by chalcopyrite. Sphalerite and galena in the yellow ore are always replaced and corroded by chalcopyrite. Finally, much of the ore consists of earlier, lithified clastic fragments, which bring together a variety of sulfides and gangue at a variety of stages. The finer classes may show graded bedding. Clearly, multiple brecciating events have occurred during the formation of Kuroko deposits.

One comparatively unknown feature of the Kuroko deposits is also of considerable interest in comparisons with 21°N. This is the existence of cylindrical masses of concentrically zoned sulfides and sulfates, up to 10 cm in diameter, occurring within the massive sulfide bodies and overlying mudstones. At the Matsumine and Matsuki mines, such structures consist of fine-grained pyrite and chalcopyrite on the exterior, succeeded inward by chalcopyrite with coarse, bladed, or dendritic textures, fine-grained sphalerite, galena, and barite and a small barite core (Scott, 1981). At Uwamuki No. 2 deposit, pipe structures exist with chalcopyrite-rich fillings and pyrite-rich exteriors (Eldridge, 1981). These concentrically zoned sulfide masses strongly resemble cross-sections of small clogged chimneys similar to those at 21°N, which have been broken off and preserved in the ore deposits. The sphalerite, galena, and barite filling of the structures at Matsumine and Matsuki suggest that these pipes were plugged by late-stage precip-

itates at a dying vent, while the chalcopyrite-filled pipe at Uwamuki No. 2 might have been clogged while the circulation system was still active.

Major similarities between the Kuroko ores and the deposits forming at 21°N are abundant. The sequence of mineral formation and replacement is almost identical to that inferred from 21°N. The overall form of the Kuroko deposits, a stockwork overlain by a Cu-rich massive sulfide formed by replacement and a surrounding Zn-rich massive sulfide, is just the pattern expected after hydrothermal circulation within a sealed mound. The presence of gypsum and anhydrite to the side of the massive sulfide bodies is appropriate, even if its precise location could not be predicted. The deposition of PbS and barite late in the paragenesis would be a logical extension of the trends observed at 21°N; although barite was never observed as a major precipitate, it was supersaturated in the water samples collected at 21°N (von Damm, personal communication). Hydrothermal alteration extending into the unmineralized hanging wall rocks indicates the continued existence of a circulation system after the ore deposits were buried. The parallel between the Kuroko deposits and deposits of the 21°N type which were buried while still active is excellent. A process of formation for the Kuroko ores developed by Eldridge and Barton (in prep.) resembles the 21°N vents, and is in fact partly based on the strong similarities between the two types of

deposits.

The comparison between the Kuroko ores and the 21°N deposits is not perfect, of course. The Kuroko ores contain appreciable quantities of Pb and Ag sulfides, which occur only rarely as minor minerals in the vent deposits at 21°N. This is a consequence of the difference in the host rocks of the two types of deposits. Isotopic studies of Pb in the Kuroko ores and the associated volcanics and basement rocks do not yield a mathematically precise origin for the Pb, but do indicate that some mixture of Pb from volcanics, the underlying Sasahata formation, and Paleozoic basement provides the best fit to the ore leads (Doe, Fehn, in press). At 21°N, in contrast, Pb isotopes in the basalts and the sulfides are identical (Vidal and Clauer, 1981). Clearly, the difference in the rocks penetrated by hydrothermal circulation has made a difference in the ore deposited from the hydrothermal solution. The reason for the greater abundance of Ag sulfides and of sulfosalts of all kinds in the Kuroko ores may be similar.

The other major difference between the Kuroko deposits and the vent structures at 21°N also appeared as a difference between the 21°N vents and ophiolite-hosted massive sulfides: a lack of life. There are foraminifera in sediments of the same age as the Kuroko ores, but no signs of the unique organisms abundant around the 21°N vents. Many of the foraminifera present are species living in the oceans

today (Guber and Merill, in prep.). They are specifically not organisms linked to hydrothermal vents. Since the similarity between the deposits is strong, it is hard to imagine that the Kuroko vents were barren. So the question remains unanswered: why is there no evidence of life in these deposits?

Another difference between the deposits at 21°N and both Kuroko deposits and ophiolite-hosted massive sulfides is the preponderance of wurtzite at 21°N as opposed to sphalerite in the ores. Although wurtzite in the dead vents at 21°N is being converted into sphalerite (Hekinian et al., 1980), it seems quite unlikely that all the ZnS in the two types of ore deposits originated as wurtzite and has recrystallized to sphalerite. There is certainly no evidence of such a transformation. It seems more likely that sphalerite is the usual, and stable, form of ZnS and that the wurtzite in the 21°N deposits is metastable and unusual. The presence of wurtzite may then be related to the degree of chemical disequilibrium in the fluid from which it precipitated.

The strong similarities between the Kuroko ores and the deposits forming at 21°N suggest that visible features of the Kuroko ore bodies might be used to model the inaccessible regions of the 21°N deposits. For example, the presence of a pyrite zone underlying the chalcopyrite-rich yellow ore suggests that a pyrite-rich zone might occur at depth in

or below the vent structures at 21°N. This, in turn, might help explain the dominance of pyrite in ophiolite-hosted massive sulfides of the Troodos type. The pyritic ore could have formed in the base of a vent system, from which the Cu- and Zn-rich zones have been lost by oxidation.

Summary

Two types of massive sulfide ores bear a close resemblance to vent deposits of the kind forming at 21°N, but on a much larger scale. The ophiolite-hosted pyritic Cu-Zn deposits formed at the seawater-basalt interface at the outlet of an extensive hydrothermal circulation system. In most deposits, Cu- and Zn-rich sulfides occur in the upper parts of the ore bodies, while at Troodos, in Cyprus, the uppermost layer of the ores is an oxidized gossan.

The Kuroko deposits were deposited as a consequence of hydrothermal circulation in predominantly felsic volcanics. They are layered ore bodies with chalcopyrite in the center and lower parts of the deposit and sphalerite in the upper and outer parts. Sulfate layers, both gypsum/anhydrite and barite, are preserved in the Kuroko deposits, usually above and peripheral to the sulfides.

Neither of these types of deposits is identical to the vent deposits at 21°N. The ophiolite-hosted ores appear to contain less Cu and Zn then expected, and a heavier concen-

tration of pyrite. The Kuroko ores contain relatively high levels of Pb and Ag, as a consequence of the different host rocks. In neither type of deposit is there any evidence of the abundant specialized biota that inhabits the vents at 21°N.

The occurrence of large sulfide deposits similar to those at 21°N implies that the hydrothermal process at 21°N can operate on a much larger scale. The differences between the ores and the vent structures suggest that some of the inaccessible parts of the chimneys and mounds do differ from the visible parts. The concentration of monomineralic pyrite deep in both the Kuroko ores and the massive sulfides in ophiolites suggests that a pyrite-rich zone may exist within the mounds at 21°N. The widespread evidence of brecciation, slumping, and sedimentary rearrangement of broken ore within the ore deposits provides indirect support for the idea that the structures at 21°N may be repeatedly built up, sealed, and fractured, and rebuilt over the life of each vent.

Interestingly, with the exception of the deposits at Troodos, all the preserved ores created by these hydrothermal systems seem to have been buried before any destruction of the sulfides took place. Either this is a reflection of the particular pieces of crust that have been preserved, or, more likely, some special circumstances are required to preserve a deposit after it has begun to decay. It appears

that the deposits are most likely to be covered over soon after they form, by a new phase of volcanic eruptions at the same site. Partially oxidized deposits covered by later lavas may be an unusual occurrence, just as Troodos is not a "typical" ophiolite from a mid-ocean ridge setting.

The generation of ore deposits by the hydrothermal circulation process operating at 21°N is clearly not limited to mid-ocean ridge settings. However, both Kuroko and ophiolite ore deposits were formed in spreading environments. Ophiolites can be created at either mid-ocean ridges or back-arc spreading centers, the alternative suggested setting of the Troodos ophiolite. The Kuroko deposits were created in an area where a rift may have been developing but did not form. It appears that the large scale hydrothermal circulation and concomitant leaching necessary to form a sizeable ore deposit can only develop in an environment where large quantities of hot new rock exist to maintain the circulation and provide ingredients for the hot solution. The submarine environment provides an effective solution for leaching (seawater), which will still be buoyant when it reaches the seafloor as hydrothermal fluid. Highly saline brines such as the Red Sea brines are not buoyant in seawater even when hot, and consequently produce a different type of deposit. Ore deposits formed on the model of the 21°N vents thus are associated with submarine spreading environments of some sort, but different settings

will produce different ores. The hydrothermal vents at 21°N, while not economically important in themselves, outline a process of ore formation that is widespread in occurrence and richly productive.

Chapter VI

Conclusions

A review of the preceding discussion of the mineralogy of the samples collected from the hydrothermal vents at 21°N, their implications for the growth and development of the structures created at the vents, and the relationship of these structures to the formation of ore deposits, yields conclusions in four major categories: (1) the classification of samples from the active chimneys, their mineralogy and relationships among the minerals; (2) the process of vent development, the construction and evolution of the vent structures over the life of the hot springs; (3) the possibilities for preservation of mineral deposits formed at such hydrothermal vents, and the alteration and destruction of structures lacking a protective cover; (4) comparisons between the potential deposits at 21°N and economic ore deposits, revealing the ore-forming potential of the hydrothermal circulation process and its applicability in a range of environments.

Chimney Types

The chimneys sampled at 21°N in November 1979 can be classified into Cu-rich chimneys venting fluid at tempera-

tures near 350°C and Zn-rich chimneys venting fluids at temperatures below 300°C. The Cu-rich chimneys are characterized by a central channelway lined by a monomineralic layer of chalcopyrite or cubanite and exterior layers composed of varying amounts of anhydrite, Mg-silicates, and Fe, Zn, and Cu-Fe sulfides. Samples from the Zn-rich chimneys consist of a mass of fine-grained material cut by multiple narrow channelways lined by elongate wurtzite crystals. The mass of the samples consists of a mixture of fine-grained wurtzite and pyrite, rare pyrrhotite, and anhydrite. Just to the outside of the wurtzite channel linings is a band rich in Cu-Fe sulfides forming as primary precipitates and as replacements of the other sulfides.

The replacement sequences in all the chimneys are similar, when the same minerals are present. Four replacement trends occur throughout the chimneys. Pyrite replaces pyrrhotite in the Zn-rich chimneys. Chalcopyrite and intermediate solid solution replace wurtzite, pyrite, and pyrrhotite. Anomalous bornite replaces chalcopyrite, pyrite, and wurtzite. Finally, in the Black Forest vent, bornite replaces chalcopyrite and is in turn replaced by chalcocite. The general order of deposition deduced from the sulfide relationships indicates early deposition of Fe and Zn sulfides followed by replacement by and later deposition of Cu-Fe sulfides.

Vent Construction

The basic mechanism of deposition at the hydrothermal vents is mixing between hot, H_2S-rich hydrothermal fluid and cold, $SO_4^=$-rich seawater. Mixing between the two fluids is so rapid that equilibrium is not maintained in the mixed solutions, nor between the solutions and the precipitated mineral assemblages.

The vent structures grow in a series of mound and chimney phases. A mound of sulfide sediment and solid fragments sealed by a cap of sulfides and oxides preventing the escape of hot fluid is subjected to fracturing. The smaller cracks are quickly plugged by precipitation, but the larger cracks persist as vents for the rising hydrothermal solution.

Over these outlets chimneys are constructed. The chimneys grow through the gradual development of a wall restricting mixing between the hydrothermal solution and seawater. A framework of anhydrite coated by fine-grained sulfides forms at the upper edge of a chimney, where complete mixing occurs. This shell begins to isolate the chimney interior; as the temperature inside rises the monomineralic sulfide lining begins to form inside the chimney.

Outside the monomineralic sulfide lining a mixing zone develops in which hot fluid seeping out from the chimney interior mixes with seawater. Fine-grained sulfides are deposited when this mixing occurs, just as they are in the

plume above the chimney. A relatively cool mixed solution can also precipitate Mg-silicates. Anhydrite is precipitated from almost any mixture of seawater and hydrothermal fluid, and consequently may be present throughout the chimney wall. Where the outer anhydrite-rich layer is missing, a weathering rim can develop where the massive sulfide lining is in contact with seawater.

As the chimney matures, both the inner lining and exterior layer continue to grow. The interior of the chimney is increasingly isolated from the exterior; hotter, purer hydrothermal fluid rises through the chimney, leading to the overprinting of late, high-temperature minerals on early, relatively low-temperature mineral assemblages.

The construction of a Zn-rich chimney varies only slightly from the construction of a Cu-rich chimney. One major difference is a greater degree of mixing at depth in a Zn-rich chimney, resulting in cooler, less pristine fluid in the chimney interior. Cu-sulfides are probably deposited at depth at Zn-rich vents; consequently, wurtzite forms the inner lining of the many smaller fluid channelways. The outward flow of hot fluid is less restricted, and deposition in the mixing zone can take place at higher temperatures. The walls of Zn-rich chimneys do eventually seal off. Cu-rich sulfides are then deposited higher in the chimney from purer hydrothermal solutions.

When the fluid passageways in either a Cu-rich or a Zn-

rich chimney are blocked by mineral deposition, an inactive sealed mound develops. However, under the impermeable crust of the mound hydrothermal circulation continues. This can lead to a rearrangement of minerals within the mound, by replacement and redeposition, so that the hot center and lower parts of the mound become rich in Cu-Fe sulfides and the periphery rich in Zn sulfides. If the crust of the mound is fractured, hot fluid can escape and build new structures provided that the fundamental hydrothermal circulation system is still active.

The mineral deposit at a single vent may go through a series of chimney-mound cycles during the life of the vent. Such a cycle allows periodic enlargment of the mounds, by the addition of chimney fragments and sulfide sediment. A repetitive building cycle also allows an evolution in the form and composition of the vent structures, particularly in chimneys, over time. A gradual increase in the temperature of the rising fluid, coupled with sealing of the system at depth and therefore a decrease in mixing lower in the structure, may lead to a Zn-rich chimney being succeeded by a Cu-rich chimney. The final phase of the vent evolution may be a slight cooling trend as the hydrothermal circulation system dies down, resulting in Zn sulfide deposition within a chalcopyrite chimney lining.

Preservation and Alteration

The preservation of a mineral deposit forming at 21°N will depend heavily on the speed with which it is protected from contact with seawater after the hydrothermal circulation ceases. An unaltered sulfide-sulfate assemblage can be preserved only if the deposit is covered by a new basalt eruption while the vent is still active or just after its death. A partially altered and oxidized structure, with sulfides below a weathered layer, could be preserved if a later eruption or a flank eruption covered an aging deposit. However, if the deposit is left uncovered in open seawater, it will be completely destroyed by oxidation and only an Fe-oxide and silicate sediment will remain.

As soon as seawater comes in contact with the sulfides and sulfates at an extinct vent, the process of destruction begins. Anhydrite is rapidly dissolved by seawater, and diaappears from the deposits long before the sulfides. The sulfides are both oxidized to Fe-oxy-hydroxides and react with amorphous silica to produce Fe-rich nontronitic clays.

Ore Formation

The ore-forming potential of vents like those at 21°N is large. Similar hydrothermal circulation and the creation of a mineral deposit by mixing of the resulting hot

fluid and seawater can occur in any location having the necessary prerequisites: a large supply of hot, new rock material to provide heat and material and run the circulation system, seawater as the circulatory fluid and leaching agent, and a seafloor permeable to circulation. Ore deposits have formed in the past under such conditions. The two types of ore bodies that most closely resemble the 21°N deposits and must have formed in a similar way, ophiolite-hosted massive sulfides and Kuroko deposits, clearly indicate that the process is widely applicable. These ore deposits, in turn, suggest that pyrite-rich zones may be concealed and inaccessible in the active vent structures at 21°N, as well as demonstrating the feasibility of building deposits like those at 21°N on a larger scale.

References

Albarede, F., Michard, A., Minster, J. F. and Michard, G., 1981. $^{87}Sr/^{86}Sr$ ratios in hydrothermal waters and deposits from the East Pacific Rise at 21°N. Earth Planet. Sci. Lett. 55, 229-236.

Anderson, R. N. and Halunen, A. J., Jr., 1974. Implications of heat flow for metallogenesis in the Bauer Deep. Nature 251, 473-475.

Arnold, M., and Sheppard, S. M. F., 1981. East Pacific Rise at latitude 21°N: isotopic composition and origin of the hydrothermal sulphur. Earth Planet. Sci. Lett. 56, 148-156.

Aumento, F., Loncarevic, B. D. and Ross. D. I., 1971. Hudson geotraverse: geology of the mid-Atlantic Ridge at 45°N. Philos. Trans. R. Soc. Lond. A268, 623-650.

Barton, P. B., Jr., 1978. Some ore textures involving sphalerite from the Furutobe Mine, Akita Prefecture, Japan. Mining Geology 28, 293-300.

Barton, P. B. and Skinner, B. J., 1979. Sulfide mineral stabilities, in: Barnes, H. L., ed., Geochemistry of Hydrothermal Ore Deposits, 2nd ed. John Wiley & Sons, New York, pp. 404-454.

Bischoff, J. L., 1969. Red Sea geothermal brine deposits: their mineralogy, chemistry, and genesis, in: E. T. Degens and D. A. Ross, eds., Hot Brines and Recent Heavy Metal Deposits in the Red Sea, New York, Springer-Verlag, pp. 368-401.

Bischoff, J. L. and Dickson, F. W., 1975. Seawater-basalt interaction at 200°C and 500 bars: implications for origin of sea-floor heavy-metal deposits and regulation of seawater chemistry. Earth Planet. Sci. Lett. 25, 385-397.

Bischoff, J. L. and Seyfried, W. E., 1977. Seawater as a geothermal fluid: chemical behavior from 25°C to 350°C. Proceedings (of the) Second Int. Sym. Water-Rock Interaction, I. A. G. C., Strasbourg, France, pp. IV 166-IV 172.

Bischoff, James L. and Seyfried, William E., 1978. Hydro-

thermal chemistry of seawater from 25° to 350°C. Am. J. Sci. 278, 838-860.

Blain, C. F. and Andrew, R. L., 1977. Sulphide weathering and the evaluation of gossans in mineral exploration. Minerals. Sci. Engng. 9, 119-150.

Bonatti, Enrico, Guerstein-Honnorez, Beatriz-Melba and Honnorez, Jose, 1976. Copper-iron sulfide mineralizations from the equatorial Mid-Atlantic Ridge. Econ. Geol. 71, 1515-1525.

Bonatti, E., Honnorez, J. and Ferrara, G., 1970. Equatorial Mid-Atlantic Ridge: Petrologic and Sr isotopic evidence for an Alpine-type rock assemblage. Earth Planet. Sci. Lett. 9, 247-256.

Bonatti, Enrico, Honnorez-Guerstein, M. B., Honnorez, J. and Stern, C., 1976. Hydrothermal pyrite concretions from the Romanche Trench (equatorial Atlantic): Metallogenesis in oceanic fracture zones. Earth Planet. Sci. Lett. 32, 1-10.

Bonatti, E., Zerbi, M., Kay, R. and Rydell, H., 1976. Metalliferous deposits from the Apennine ophiolites: Mesozoic equivalents of modern deposits from oceanic spreading centers. Geol. Soc. Amer. Bull. 87, 83-94.

Bostrom, K., Farquharson, B. and Eyl, W., 1971. Submarine hot springs as a source of active ridge sediments. Chem. Geol. 10, 189-203.

Bostrom, K. and Peterson, M. N. A., 1966. Precipitates from hydrothermal exhalations on the East Pacific Rise. Econ. Geol. 61, 1258-1265.

Brackmann, A. J., 1980. The occurrence of wurtzite in the hot active vents at 21°N, EPR. A. B. Thesis, Harvard University, 80 pp.

Brett, R. and Yund, R. A., 1964. Sulfur-rich bornites. Amer. Mineral. 49, 1084-1098.

Brimhall, G. H., Jr., 1980. Deep hypogene oxidation of porphyry copper potassium-silicate protore at Butte, Montana: a theoretical evaluation of the copper remobilization hypothesis. Econ. Geol. 75, 384-409.

Chapman, H. J. and Spooner, E. T. C., 1977. ^{87}Sr enrichment of ophiolitic sulphide deposits in Cyprus confirms ore formation by circulating seawater. Earth Planet. Sci.

Lett. 35, 71-78.

Chen, C.-T. A. and Marshall, W. L., 1982. Amorphous silica solubilities IV. Behavior in pure water and aqueous sodium chloride, sodium sulfate, magnesium chloride, and magnesium sulfate solutions up to 350°C. Geochim. Cosmochim. Acta 46, 279-287.

Clark, B. C., III, Baird, A. K., Rose, H. J., Jr., Toulmin, P., III, Christian, R. P., Kelliher, W. C., Castro, A. J., Rowe, C. D., Keil, K. and Huss, G. R., 1977. Viking X-ray fluorescence experiment: analytical methods and early results. J. Geophys. Res. 82, 4577-4594.

Constantinou, G., 1977. Hydrothermal alteration of the basaltic lavas of the Troodos Ophiolite Complex associated with the formation of the massive sulphide deposits. From Volcanic Processes in Ore Genesis, p. 77.

Constantinou, G. and Govett, G. J. S., 1972. Genesis of sulphide deposits, ochre and umber of Cyprus. Inst. Mining Metallurgy Trans., sec. B., v. 81, p. B34-46.

Constaninou, G. and Govett. G. J. S., 1973. Geology, geochemistry and genesis of Cyprus sulfide deposits. Econ. Geol. 68, 843-858.

Cook, H. E., 1971. Iron and manganese rich sediments overlying oceanic basaltic basement, equatorial Pacific, Leg 9, D. S. D. P. G. S. A. Abstr. Progr. 3, 530.

Corliss, John B., 1971. The origin of metal-bearing submarine hydrothermal solutions. J. Geophys. Res. 76, 8128-8138.

Corliss, J. B. and Ballard, R. D., 1977. Oases of life in the cold abyss. Nat. Geographic 152, 440-453.

Corliss, J. B., Dymond, J., Gordon, L. I., Edmond, J. M., von Herzen, R. P., Ballard, R. D., Green, K., Williams, D., Bainbridge, A., Crane, K, van Andel, T. H., 1979. Submarine thermal springs on the Galapagos Rift. Science 203, 1073-1083.

Corliss, J. B., Lyle, M., Dymond, J. and Crane, K., 1978. The chemistry of hydrothermal mounds near the Galapagos Rift. Earth Planet. Sci. Lett. 40, 12-24.

Craig, H., 1969. Geochemistry and origin of Red Sea brines, in: Hot Brines and Recent Heavy Metal Deposits in the Red Sea, E. T. Degens and D. A. Ross, eds. Springer-Verlag, New York, 208-242.

Craig, H., Lupton, J. E. and Chou, C. C., 1980. East Pacific Rise study: Geochemistry of mantle volatiles. Proposal for research to NSF, March, 1980.

Craig, J. R. and Scott, S. D., 1974. Sulfide phase equilibria, in: Sulfide Mineralogy, P. H. Ribbe, ed., Mineralogical Society of America Short Course Notes, Volume 1, November 1974, pp. CS-1 - CS-110.

Crane, K. and R. D. Ballard, 1980. The Galapagos Rift at 86°W, 4.Structure and morphology of hydrothermal fields and their relationship to the volcanic and tectonic processes of the Rift Valley. J. Geophys. Res. 85, 1443-1454.

Crerar, D. A. and Barnes, H. L., 1976. Ore solution chemistry V. solubilities of chalcopyrite and chalcocite assemblages in hydrothermal solution at 200° to 350°C. Econ. Geol. 71, 772-794.

Crerar, D. A., Susak, N. J. Borcsik, M. and Schwartz, S., 1978. Solubility of the buffer assemblage pyrite + pyrrhotite + magnetite in NaCl solutions from 200 to 350°C. Geochim. Cosmochim. Acta 42, 1427-1437.

Cronan, D. S., 1976. Basal metalliferous sediments from the eastern Pacific. GSA Bull. 87, 928-934.

Cronan, D. S., van Andel, T. H., Heath, G. R., Dinkelman, M. G., Bennett, R. H., Bukry, D., Charleston, S., Kaneps, A., Rodolfo, K. S. and Yeats, R. S., 1972. Iron-rich basal sediments from the eastern equatorial Pacific: Leg 16, Deep Sea Drilling Project. Science 175, 61-63.

Cronan, D. S., Rona, P. A. and Shearme, S., 1979. Metal enrichments in sediments from the TAG hydrothermal field. Marine Mining 2, 79-89.

Czamanske, G. K., 1974. The FeS content of sphalerite along the chalcopyrite-pyrite-bornite sulfur fugacity buffer. Econ. Geol. 69, 1328-1334.

Delaney, J. R., Mogk, D. W. and Mottl, M. J., 1980. High-temperature, sulfide-bearing hydrothermal system on the Mid-Atlantic Ridge at 23.6 North. GSA Abstr. Progr. 12, 411.

Drummond, S. E., Jr., 1981. Boiling and mixing of hydrothermal fluids: chemical effects on mineral precipatation. Ph.D. Thesis, Penn. State Univ., 380 pp.

Duke, N. A. and Hutchinson, R. W., 1974. Geological relationships between massive sulfide bodies and ophiolitic volcanic rocks near York Harbor, Newfoundland. Can. J. Earth Sci. 11, 53-69.

Dymond, J., Corliss, J. B., Heath, G. R., Field, C. W., Dasch, E. J., Veeh, H. H., 1973. Origin of metalliferous sediments from the Pacific Ocean. GSA Bull., 84, 3355-3372.

Edmond, J. M., Measures, C., McDuff, R. E., Chan, L. H., Collier, R., Grant, B., Gordon, L. I. and Corliss, J. B., 1979. Ridge crest hydrothermal activity and the balances of the major and minor elements in the ocean: The Galapagos data. Earth Planet Sci. Lett. 46, 1-18.

Edmond, J. M., Measures, C., Mangum, B., Grant, B., Sclater, F. R., Collier, R., Hudson, A., Gordon, L. I. and Corliss, J. B., 1979. On the formation of metal-rich deposits at ridge crests. Earth Planet. Sci. Lett. 46, 19-30.

Edmond, J. M., von Damm, K. and McDuff. R., 1982. The chemistry of the hot springs on the East Pacific Rise and the dispersal of their effluent. Nature, in press.

Eldridge, C. S., 1981. Ore textures and paragenesis in Kuroko deposits. M. S. Thesis, Penn. State Univ.

Ellis, A. J., 1979. Explored geothermal systems, in: Geochemistry of Hydrothermal Ore Deposits, Barnes, H. L., ed., John Wiley & Sons, New York, 632-683.

Ferrario, A. and Garuti, G., 1980. Copper deposits in the basal breccias and volcano-sedimentary sequences of the eastern Ligerian ophiolites (Italy). Min. Dep. 15, 291-303.

Fournier, R. O., 1977. Chemical geothermometers and mixing models for geothermal systems. Geothermics 5, 41-50.

Fournier, R. O. and Truesdell, A. H., 1974. Geochemical indicators of subsurface temperature 2: Estimation of temperature and fraction of hot water mixed with cold water. U. S. G. S. Jour. Res. 2, 263-270.

Francheteau, J., Needham, H. D., Choukroune, P., Juteau, T., Seguret, M., Ballard, R. D., Fox, P. J., Normark, W., Carranza, A., Cordoba, D., Guerrero, J., Rangin, C., Bougault, H., Cambon, P. and Hekinian, R., 1979. Massive deep-sea sulphide ore deposits discovered on the East Pacific Rise. Nature 277, 523-528.

Goldfarb, M. S., Converse, D. R., Holland, H. D. and Edmond, J. J. The genesis of hot spring deposits on the East Pacific Rise, 21°N. In preparation.

Grill, E. V., Chase, R. L., MacDonald, R. D. and Murray, J.W., 1981. A hydrothermal deposit from Explorer Ridge in the northeast Pacific Ocean. Earth Planet. Sci. Lett. 52, 142-150.

Guber, A. L., 1979. Foraminifera help fathom the origin of the Kuroko ore deposits. Earth and Min. Sci. 49, 13-20.

Hackett, J. P. and Bischoff, J. L., 1973. New data on the stratigraphy, extent and geological history of the Red Sea geothermal deposits. Econ. Geol. 68, 553-564.

Hajash, Andrew, 1975. Hydrothermal processes along mid-ocean ridges: an experimental investigation. Contrib. Min. Petrol. 53, 205-226.

Haymon, R. M. and Kastner, M., 1981. Hot spring deposits on the East Pacific Rise at 21°N: preliminary description of mineralogy and genesis. Earth Planet. Sci. Lett. 53, 363-381.

Heath, G. R. and Dymond, J., 1977. Genesis and transformation of metalliferous sediments from the East Pacific Rise, Bauer Deep, and Central Basin, northwest Nazca plate. GSA Bull 88, 723-733.

Heaton, T. H. E. and Sheppard, S. M. F., 1977. Hydrogen and oxygen isotope evidence for seawater-hydrothermal alteration and ore deposition,Troodos complex, Cyprus. From Volcanic Process in Ore Genesis, pp. 42-57.

Hekinian, R., Fevrier, M., Bischoff, J. L., Picot, P. and Shanks, W. C., 1980. Sulfide deposits from the East Pacific Rise near 21°N. Science 207, 1433-1444.

Hemley, J. J., Montoya, J. W., Christ, C. L. and Hostetler, P. B., 1977. Mineral equilibria in the MgO-SiO_2-H_2O system: I. Talc-chrysotile-forsterite-brucite stability relations. Am. J. Sci. 277, 322-351.

Holland, H. D., 1978. The Chemistry of the Atmosphere and Oceans. John Wiley & Sons, New York.

Holland, H. D. and Malinin, S. D., 1979. The solubility and occurrence of non-ore minerals, in: H. L. Barnes, ed., Geochemistry of Hydrothermal Ore Deposits. New York, John Wiley & Sons, 461-508.

Humphris, S. E. and Thompson, G., 1978. Hydrothermal alteration of oceanic basalts by seawater. Geochim. Cosmochim. Acta 42, 107-125.

Hutchison, M. N. and Scott, S. D., 1981. Sphalerite geobarometry in the Cu-Fe-Zn-S system. Econ. Geol. 76, 143-153.

Ishihara, S., ed., 1974. Geology of Kuroko Deposits. Mining Geology Special Issue No. 6, The Society of Mining Geologists of Japan.

Jenkins, W. J., Rona, P. A. and Edmond, J. M., 1980. Excess ^{3}He in the deep water over the Mid-Atlantic Ridge at 26°N: evidence of hydrothermal activity. Earth Planet. Sci. Lett. 49, 39-44.

Kanehira, K., Yui, S., Sakai, H. and Sasaki, A., 1973. Sulfide globules and sulfur isotope ratios in the abyssal tholeiite from the Mid-Atlantic Ridge near 30°N latitude. Geochem. J. 7, 89-96.

Keays, R. R. and Scott. R. B., 1976. Precious metals in ocean-ridge basalts: implications for basalts as source rocks for gold mineralization. Econ. Geol. 71, 705-720.

Kinkel, A. R., Jr., 1966. Massive pyritic deposits related to volcanism, and possible methods of emplacement. Econ. Geol. 61, 673-694.

Kusakabe, M., Chiba, H. and Ohmoto, H. Stable isotopes and fluid inclusion study of anhydrite from the East Pacific Rise at 21°N. In preparation.

Lambert, I. B. and Sato, T., 1974. The Kuroko and associated ore deposits of Japan: a review of their features and metallogenesis. Econ. Geol. 69, 1215-1236.

Lister, C. R. B., 1972. On the thermal balance of a mid-ocean ridge. Geophys. J. R. astr. Soc. 25, 515-535.

Lonsdale, P., 1977. Deep-tow observations at the Mounds Abyssal hydrothermal field, Galapagos Rift. Earth Planet. Sci. Lett. 36, 92-110.

Lonsdale, P. F., Bischoff, J. L., Burns, V. M., Kastner, M. and R. E. Sweeney, 1980. A high-temperature hydrothermal deposit on the seabed at a Gulf of California spreading center. Earth Planet. Sci. Lett. 49, 8-20.

Lonsdale, P. and Elders, W., 1981. Hydrothermal sulfide formation at the seabed, Guaymas Basin, Gulf of California. GSA Abstr. Progr. 13, 68.

Melson, W. G. and van Andel, T. H., 1966. Metamorphism in the Mid-Atlantic Ridge, 22°N latitude. Marine Geol. 4, 165-186.

Moh, G. H., 1975. Tin-containing mineral systems: Part II. Phase relations and mineral assemblages in the Cu-Fe-Zn-Sn-S system. Chemie der Erde 34, 1-61.

Moore, W. S. and Vogt, P. R., 1976. Hydrothermal manganese crusts from two sites near the Galapagos Spreading Axis. Earth Planet. Sci. Lett. 29, 349-356.

Mottl, M. J., 1976. Chemical exchange between sea water and basalt during hydrothermal alteration of the oceanic crust. Ph.D. Thesis, Harvard University.

Mottl, M. J., Corr. R. F. and Holland, H. D., 1974. Chemical exchange between sea water and mid-ocean ridge basalt during hydrothermal alterations: an experimental study. Geol. Soc. Am. Abstr. Programs 6, 879-880.

Mottl, M. J. and Holland, H. D., 1978. Chemical exchange during hydrothermal alteration of basalt by seawater - I. Experimental results for major and minor components of seawater. Geochim. Cosmochim. Acta 42, 1103-1115.

Mottl, M. J., Holland, H. D. and Corr, R. F., 1979. Chemical exchange during hydrothermal alteration of basalt by seawater - II. Experimental results for Fe, Mn and sulfur species. Geochim. Cosmochim. Acta 43, 869-884.

Mottl, M. J. and Seyfried, W. E., 1980. Sub-seafloor hydrothermal systems: rock- vs. seawater-dominated, in: P. A. Rona and R. P. Lowell, eds., Seafloor Spreading Centers: Hydrothermal Systems, Stroudsburg, PA, Dowden, Hutchinson & Ross, Inc., pp. 66-82.

Ohmoto, H., Cole, D. R. and Mottl, M. J., 1976. Experimental basalt-seawater interaction: sulfur and oxygen isotope studies. E⊕S 57, 342.

Ohmoto, H. and Lasaga, A. C., 1980, Kinetics of isotopic exchange and chemical reactions between sulfides and sulfates in hydrothermal solutions. GSA Abstr. Progr. 12, 494.

Oudin, E., Picot. P. and Pouit, G., 1981. Comparison of sulphide deposits from the East Pacific Rise and Cyprus. Nature 291, 404-407.

Pankratz, L. B. and King. E. G., 1965. High-temperature heat

contents and entropies of two zinc sulfides and four solid solutions of zinc and iron sulfides. U. S. Bureau of Mines, Rep. Invest. 6708.

Piper, D. Z., 1973. Origin of metalliferous sediments from the East Pacific Rise. Earth Planet Sci. Lett 19, 75-82.

Potter, R. W., II, 1977. Pressure corrections for fluid-inclusion homogenization temperatures based on the volumetric properties of the system NaCl-H_2O. J. Res. U. S. Geol. Surv. 5, 603-607.

Ramdohr, P., 1969. The Ore Minerals and Their Intergrowths. Oxford, Pergamon Press, 1174 pp.

Riley, J. P. and Skirrow, G., 1975. Chemical Oceanography. New York, Academic Press.

Ripley, E. M. and Ohmoto, H., 1977. Mineralogic, sulfur isotope, and fluid inclusion studies of the stratabound copper deposits at the Raul Mine, Peru. Econ. Geol. 72, 1017-1041.

Robertson, A. H. F., 1976. Origin of ochres and umbers: Evidence from Skouriotissa, Troodos Massif, Cyprus. Trans. Inst. Min. Metall. 85, Sec. B, B245-B251.

Rona, P. A., 1976. Pattern of hydrothermal mineral deposition: Mid-Atlantic Ridge crest at latitude 26°N. Mar. Geol. 21, M59-M66.

Sakai, H. and F. W. Dickson, 1978. Experimental determination of the rate and equilibrium fractionation factors of sulfur isotope exchange between sulfate and sulfide in slightly acid solutions at 300°C and 1000 bars. Earth Planet. Sci. Lett. 39, 151-161.

Sasaki, H., Osaki, S. and Tsukagishi, M., 1970. Sulfur and oxygen isotopic geochemistry of sulfate in black ore deposits of Japan. Geochem. J. 4, 27-39.

Sasaki, A., 1972. Variation of sulfur isotopic composition of oceanic sulfate. 24th Int. Geol. Congr., Sect. 10, 342-345.

Schoell, M., 1976. Heating and convection within the Atlantis II Deep geothermal system of the Red Sea, in: Proceedings Second United Nations Symposium on the Development and Use of Geothermal Resources 1, 583-590.

Scott, R. B., Malpas, J., Udintsev, G. and Rona, P. A., 1975. Submarine hydrothermal activity and seafloor spreading at 26°N, MAR. GSA Ann.Meet., Abstr. w/ prog., Vol. 7, p. 1263.

Scott, S. D. and Barnes, H. L., 1972. Sphalerite-wurtzite equilibria and stoichiometry. Geochim. Cosmochim. Acta 36, 1275-1295.

Scott, S. D., 1981. Contributed discussion to seminar on sea-floor hydrothermal systems. Geosci. Can. 8, 103-104.

Searle, D. L., 1972. Mode of occurrence of the cupriferous pyrite deposits of Cyprus. Inst. Mining Metallurgy Trans., sec. B., Vol. 81, p. B189-B197.

Seyfried, W. E., Jr. and Bischoff, J. L., 1981. Experimental seawater-basalt interaction at 300°C, 500 bars, chemical exchange, secondary mineral formation and implications for the transport of heavy metals. Geochim. Cosmochim. Acta 45, 135-147.

Shalimova, K. V. and Morozova, N. K., 1965. Effect of excess zinc on the crystal structure of ZnS. Sov. Phys.-Crystallog. 9, 471-472.

Shanks, W. C., III and Bischoff, J. L., 1977. Ore transport and deposition in the Red Sea geothermal system: a geochemical model. Geochim. Cosmochim. Acta 41, 1507-1519.

Sillitoe, R. H. and Clark, A. H., 1969. Copper and copper-iron sulfides as the initial products of supergene oxidation, Copiapo Mining district, northern Chile. Am. Miner. 54, 1648-1710.

Skinner, B. J. and Barton, P. B., Jr., 1960. The substitution of oxygen for sulfur in wurtzite and sphalerite. Am. Mineral. 45, 612-625.

Solomon, M. and J. L. Walshe, 1979. The formation of massive sulfide deposits on the seafloor. Econ. Geol. 74, 797-813.

Spiess, F. N., MacDonald, K. C., Atwater, T. Ballar, R., Carranza, A., Cordoba, D., Cox, C., Diaz Garcia, V. M., Francheteau, J., Guerrero, J., Hawkins, J., Haymon, R., Hessler, R., Juteau, T., Kastner, M., Larson, R., Luyendyk, B., MacDougall, J. D., Miller, S., Normark, W., Orcutt. J. and Rangin, C., 1980. East Pacific Rise: Hot springs and geophysical experiments. Science 207, 1421-1433.

Spooner, E. T. C., 1977. Hydrothermal model for the origin of the ophiolitic cupriferous pyrite ore deposits of Cyprus. From Volcanic Processes in Ore Genesis, pp. 58-71.

Spooner, E. T. C. and Fyfe, W. S., 1973. Sub-sea-floor meta-

morphism, heat, and mass transfer. Contrib. Mineral. Petrol. 42, 287-304.

Styrt, M. M., Brackmann, A. J., Holland, H. D., Clark, B. C., Pisutha-Arnond, V., Eldridge, C. S. and Ohmoto, H., 1981. The mineralogy and the isotopic composition of sulfur in hydrothermal sulfide/sulfate deposits on the East Pacific Rise, 21°N latitude. Earth Planet. Sci. Lett. 53, 382-390.

Sugaki, A., Shima, H., Kitakaze, A. and Harada, H., 1975. Isothermal phase relations in the system Cu-Fe-S under hydrothermal conditions at 350°C and 300°C. Econ. Geol. 70, 806-823.

Tauson, V. L. and Chernyshev, L. V., 1978. The sphalerite-wurtzite transition in isomorphous mixtures of the system ZnS-MnS-CdS-FeS. Geochem. Internat. 15, No. 5, 33-41.

Thompson, G., Woo, C. C. and Sung, W., 1975. Metalliferous deposits on the Mid-Atlantic Ridge. GSA Abstr. Progr. 7, 1297.

Tomasson, J. and Kristmannsdottir, H., 1972. High temperature alteration minerals and thermal brines, Reykjanes, Iceland. Contrib. Mineral Petrol. 36, 123-134.

Turner, J. S., 1969. A physical interpretation of the observation of hot brine layers in the Red Sea, in: Hot Brines and Recent Heavy Metal Deposits in the Red Sea, E. T. Degens and D. A. Ross, eds., Springer-Verlag, New York, 164-173.

Turner, J. S. and Gustafson, L. N., 1978. The flow of hot, saline solutions from vents in the sea floor -- some implications for exhalative sulfide deposits. Econ. Geol. 73, 1082-1100.

Upadhyay, H. D. and Strong, D. F., 1973. Geological setting of the Betts Cove Copper Deposits, Newfoundland: an example of ophiolite sulfide mineralization. Econ. Geol. 68, 161-167.

Vaughan, D. J. and Craig, J. R., 1978. Mineral Chemistry of Metal Sulfides. Cambridge University Press, Cambridge, U. K., 493 pp.

Vidal, Ph. and Clauer, N., 1981. Pb and Sr isotopic systematics of some basalts and sulfides from the East Pacific Rise at 21°N (project RITA). Earth Planet. Sci. Lett. 55, 237-246.

von der Borch, C. C., Nesteroff, W. D. and Galehouse, J. S., 1971. Iron-rich sediments cored during Leg 8 of the Deep Sea Drilling Project, in: Initial Reports of the Deep Sea Drilling Project, v. VIII, J. I. Tracy et al., eds., Washington, DC. U. S. Govt Printing Office, 829-835.

von der Borch, C. C. and Rex, R. W., 1970. Amorphous iron oxide precipitates in sediments cored during Leg 5, Deep Sea Drilling Project, in: Initial Reports of the Deep Sea Drilling Project, Vol. V, D. A. McManus et al., eds. Washington, DC. U. S. Govt Printing Office, 541-544.

Whittaker, E. J. W. and Wicks, F. J., 1970. Chemical differences among the serpentine "polymorphs": a discussion. Am. Min. 55, 1025-1047.

Wiggins, L. B. and Craig, J. R., 1980. Reconnaissance of the Cu-Fe-Zn-S system: sphalerite phase relationships. Econ. Geol. 75, 742-751.

Williams, D. L., von Herzen, R. P., Sclater, J. G. and Anderson, R. N., 1974. The Galapagos spreading centre: lithospheric cooling and hydrothermal circulation. Geophys. J. R. astr. Soc. 38, 587-608.

Wolery. T. A. and Sleep. N. H., 1976. Hydrothermal circulation and geochemical flux at mid-ocean ridges. J. Geol. 84, 249-275.

Yund, R. A. and Kullerud, G., 1966. Thermal stability of assemblages in the Cu-Fe-S system. J. Petrol. 7, 454-488.

Appendix A: Mineral Analyses (Wt. %)

" -- " indicates element concentration is below detection limit.

All averages are recalculated to 100%.

"Other elements" lists other elements included in the analysis but not detected.

"n. d." indicates an element not included in the analysis.

$Fe_{1-x}S$

Vent S-2

Sample No.	Fe	Cu	Zn	S	Total
978-R-3	57.54	0.17	0.18	38.11	96.00
	57.04	0.24	--	38.53	95.81
	55.85	0.31	0.07	37.25	93.54
	54.99	0.30	0.04	38.04	93.37
	54.71	0.07	--	38.69	93.47
Average	59.33	0.23	0.06	40.37	

Vent S-3

Sample No.	Fe	Cu	Zn	S	Total
982-R-19	58.35	--	--	39.36	97.71
	57.39	--	0.11	38.65	96.15
	58.44	--	--	38.46	96.90
	57.89	--	--	38.77	96.66
	58.21	--	--	39.63	97.84
	58.72	--	--	38.88	97.60
	58.16	--	--	38.92	97.08
	57.61	--	0.08	38.39	96.08
	57.74	--	--	38.36	96.10
	57.98	--	--	38.86	96.84
	58.03	0.07	0.08	39.11	97.29
	57.78	--	--	39.64	97.42
	57.88	--	--	39.17	97.05
	58.57	--	--	39.52	98.09
	57.77	--	0.13	39.43	97.33
	57.47	0.16	--	38.70	96.33
	57.19	--	--	39.05	96.24
	55.55	--	--	38.67	94.22
	55.55	--	--	37.66	93.75
Average	59.72			40.28	

FeS_2

Vent S-3

Sample No.	Fe	Zn	S	Total	Other elements
982-R-19	48.14	1.18	53.91	103.23	Cu, Co,Ni,Cd
	42.67	--	51.56	94.23	Cu, Pb
	45.08	--	51.90	96.98	Cu, Pb
	46.47	--	52.63	99.10	Cu, Pb
	43.29	0.20	52.80	96.29	Cu, Pb
Average	46.21		53.79		

FeS_2

Vent S-2

Sample No.	Fe	Cu	Zn	S	Total	Other elements
978-R-1	45.87	--	--	52.52	98.39	Pb
	45.52	--	0.11	52.96	98.59	"
	46.08	--	--	52.98	99.06	"
	43.26	--	--	53.15	96.41	"
	45.80	--	--	53.73	99.53	"
	46.12	--	--	53.65	99.77	"
	45.67	--	--	53.80	99.47	"
	46.23	--	--	52.38	98.61	"
	46.29	--	--	53.02	99.31	"
	44.96	0.07	0.04	52.55	97.62	"
	43.24	--	0.09	52.51	95.84	"
	43.31	0.06	0.12	51.58	95.07	"
	46.78	--	0.11	53.16	100.05	"
	46.08	--	0.05	52.85	98.98	"
	46.59	--	--	52.35	99.11	Pb=0.17
	46.19	0.08	--	52.34	98.61	Pb
	45.57	--	--	52.16	97.73	"
	45.63	--	--	52.91	98.54	"
	46.40	--	--	51.05	97.45	"
	44.78	--	0.07	51.92	96.77	"
	45.44	--	--	52.65	98.09	"
	44.11	--	--	51.32	95.57	Pb=0.14
	44.51	--	0.09	52.16	96.98	Pb=0.22
	44.31	--	--	52.18	96.49	Pb
978-R-3	45.95	--	--	53.14	99.09	Pb
Average	46.31			53.69		

Vent site 1 of dive 981: FeS_2 in interior of chimney

Sample No.	Fe	Cu	Zn	S	Total	Other elements
981-R-3	47.82	--	--	51.41	99.23	Mn,Co,Ni,Cd
	46.79	0.47	--	51.09	98.35	"
	47.95	--	--	52.90	100.85	"
	46.90	0.11	--	51.76	98.77	"
	47.23	0.75	--	52.42	100.40	"
	46.56	1.00	--	51.66	99.22	"
	46.72	0.45	--	49.05	96.22	"
	47.31	0.43	--	51.42	99.16	"
	48.77	--	--	47.07	95.84	"
	47.76	0.11	--	48.70	96.57	"
	45.96	--	--	50.34	96.30	"
	47.76	--	--	52.46	100.22	"
	47.19	--	--	51.15	98.34	"
	47.63	0.16	--	51.48	99.27	Co=0.15, Ni=0.12, Cd=0.13, Mn
981-R-16-3	45.85	0.52	0.61	52.60	99.78	Co=0.21,Mn,Ni,Cd
	45.34	0.43	0.63	52.29	98.82	Co=0.13, Mn,Ni,Cd
Average	47.96			52.04		

FeS_2

Vent site 1 of dive 981: FeS_2 containing Zn, exterior

Sample No.	Fe	Cu	Zn	S	Total	Other elements
981-R-3	46.70	0.43	0.48	50.92	98.53	Co, Cd, Ni, Mn
980-R-12	40.10	0.23	9.32	48.79	98.44	Pb
	43.55	--	2.21	50.27	96.03	"
	44.36	--	2.75	50.62	97.95	Pb=0.23
	41.56	--	4.95	50.22	97.03	Pb=0.30
981-R-2	44.06	--	1.22	50.04	95.32	Pb
981-R-22	46.21	0.26	0.17	52.25	98.89	"
	44.89	0.07	1.09	52.98	99.27	Pb=0.25
	45.75	--	0.08	52.48	98.31	Pb
	44.77	--	0.17	51.67	96.61	"
	45.21	--	0.14	50.93	96.28	"
	44.58	0.07	0.07	50.21	94.93	"
Average	45.61	--	1.95	52.44		

Vent site 1 of dive 981: exterior FeS_2, not containing Zn

Sample No.	Fe	Cu	S	Total	Other elements
980-F-12	45.76	--	52.55	98.31	Pb, Zn
	45.98	0.36	51.14	97.48	"
	45.66	--	52.19	98.37	Pb=0.52, Zn
981-R-2	44.92	--	49.77	94.69	Pb, Zn
	45.09	0.07	50.96	96.12	"
981-R-22	46.12	--	52.15	98.27	"
	46.98	--	53.33	100.31	"
	45.81	--	52.52	98.33	Pb, Zn
	46.37	--	52.58	98.95	"
Average	46.80		53.20		

$CuFeS_2$

Black Forest

Sample No.	Cu	Fe	S	Total	Other elements
982-R-4	34.23	30.34	34.87	99.44	Co, Ni, Cd, Mn, Zn
	34.28	30.10	34.43	98.91	"
	29.48	23.39	31.01	83.88	"
	33.21	29.61	34.11	96.93	"
	34.23	30.43	35.09	99.75	"
	34.04	29.77	35.33	99.14	"
	33.67	29.53	34.95	98.15	"
	34.59	29.27	34.73	98.59	"
	34.05	30.46	33.15	97.66	"
	31.99	30.15	34.95	97.09	"
	33.44	30.11	33.66	97.21	"
	34.18	30.36	34.29	98.83	"
	33.39	30.51	33.63	97.53	"
	33.57	31.25	34.33	99.15	"
	33.27	30.99	33.75	98.01	"
	33.31	31.05	34.55	98.91	"
	32.62	30.29	35.23	98.14	"
	33.35	30.02	35.61	98.98	Co, Ni, Cd, Mn, Zn
	32.73	30.83	33.98	97.54	"
	34.86	30.01	36.33	101.20	"
	34.39	29.95	36.13	100.47	"
Average	34.20	30.57	35.23		

Vent site 1 of dive 981

Sample No.	Cu	Fe	Zn	S	Total	Other elements
981-R-2	32.02	30.00	0.53	34.31	96.86	Pb
	31.27	28.44	0.80	33.01	93.65	Pb=0.13
	31.58	28.64	0.76	33.58	94.56	Pb
	32.00	29.19	0.55	33.33	95.07	"
	32.32	29.68	0.21	33.58	95.79	"
981-R-22	33.45	28.81	0.20	33.73	96.19	"
	33.86	27.88	0.98	33.39	96.11	"
	34.37	29.16	0.24	34.76	98.53	"
981-R-16	33.82	30.40	--	35.43	99.66	Mn, Co, Ni,Cd
	34.13	31.05	--	35.85	101.33	"
	32.68	31.21	--	34.71	98.60	"
	34.54	30.87	--	35.43	100.83	Mn, Co, Ni,Cd
	33.93	30.98	--	35.40	100.31	"
	34.23	31.00	--	35.27	100.49	"
	33.88	30.79	--	35.36	100.03	"
	34.16	31.04	--	35.46	100.65	"
	34.05	31.02	--	35.56	100.62	"
	34.26	31.45	--	35.45	101.16	"
	33.80	31.64	--	35.40	100.84	"
	34.06	31.14	--	35.63	100.83	"
	34.01	31.77	--	35.42	101.20	"
	34.14	31.87	--	35.34	101.36	"

Vent S-2

Sample No.	Cu	Fe	Zn	S	Total	Other
978-R-3	29.41	30.03	0.77	34.02	94.02	Pb
	29.76	30.51	0.84	33.64	94.75	Pb

Vent site 1 of dive 981

Sample No.	Cu	Fe	Zn	S	Total	Other Elements
980-R-12	33.90	29.49	0.06	33.92	97.37	Pb
	34.31	29.31	0.18	33.84	97.64	"
	33.28	28.84	0.10	33.52	95.74	"
	33.74	28.87	0.21	34.29	97.11	"
	33.74	29.54	0.24	33.89	97.41	"
	33.91	27.18	0.14	34.70	95.93	"
	33.26	29.22	0.12	34.60	97.20	"
	34.07	29.10	0.18	34.17	97.52	"
	33.59	29.12	0.36	33.98	97.05	"
	33.79	29.07	--	34.13	96.99	"
	33.94	29.18	0.16	34.38	97.66	"
	33.70	28.97	0.22	34.44	97.33	"
	33.10	28.85	0.16	34.48	96.59	"
	33.47	29.23	0.14	33.95	96.79	Pb
	33.76	29.19	0.22	34.21	97.38	"
	33.61	29.27	--	33.65	96.53	"
	33.66	29.48	--	33.95	97.09	"
	33.79	29.68	--	34.55	98.02	"

Vent site 1 of dive 981

Sample No.	Cu	Fe	Zn	S	Total	Other Elements
981-R-3	33.30	31.91	--	35.77	100.98	Mn, Co, Cd, Ni
	33.12	32.27	--	35.50	100.89	"
	33.37	32.02	--	35.56	100.95	"
	33.46	32.22	--	35.67	101.35	
	33.37	31.88	--	35.36	100.61	"
	33.32	32.13	--	35.35	100.80	"
	33.46	32.21	--	35.58	101.25	"
	33.06	31.77	--	35.30	100.13	"
	33.13	31.81	--	35.52	100.46	"
	33.60	31.74	--	35.47	100.81	"
	33.65	31.36	--	35.44	100.45	"
	34.31	31.99	--	35.98	102.28	"
	33.81	32.04	--	35.93	101.78	"
	33.96	31.96	--	33.17	99.63	Co=0.16, Ni=0.19, Cd=0.19, Mn
Average	34.02	30.75		35.23		

Cubanite

Vent S-2

Sample No.	Cu	Fe	Zn	Co	S	Total	Others
978-R-3	20.89	41.77	--	0.09	35.27	98.02	Ni,Cd,Mn
	21.08	42.58	--	0.08	35.28	99.02	"
	20.96	42.63	--	0.11	35.42	99.12	"
	21.34	42.59	--	0.10	35.46	99.49	"
	20.88	42.14	--	0.12	34.78	97.92	"
	20.84	42.14	--	0.13	34.99	98,10	"
	21.19	42.53	--	0.09	35.71	99.52	"
	20.80	41.76	--	--	35.03	97.59	"
	20.41	41.11	--	0.10	33.28	94.90	"
	20.98	42.16	--	0.14	34.85	98.13	"
	20.89	42.28	--	0.09	34.75	98.01	"
	21.36	42.44	--	0.12	34.99	98.91	"
	21.32	42.83	--	0.08	35.77	100.00	"
	20.10	39.25	--	0.08	32.99	92.42	"
	20.45	42.24	--	0.09	34.50	97.28	"
	20.33	42.54	--	0.09	34.97	97.93	"
	20.77	40.94	--	0.10	33.61	95.42	"
	20.53	41.99	--	0.11	34.28	96.91	"
	20.77	42.33	--	0.09	34.46	97.65	"
	21.33	37.44	0.67	n.d.	34.82	94.26	Pb
	20.91	38.53	0.88	n.d.	34.49	94.81	"
	21.41	38.09	0.74	n.d.	34.23	94.47	"
	21.49	39.59	0.78	n.d.	34.01	95.87	"
	21.07	38.82	0.78	n.d.	33.72	94.39	"
	20.82	38.94	0.77	33.91	94.43	Pb	
	20.89	38.38	0.72	33.61	93.59	"	
Average	21.65	42.50		35.78		Co=0.07	

Vent S-3

Sample No.	Cu	Fe	Zn	S	Total	Other elements
982-R-19	21.59	39.85	0.82	34.85	97.11	Pb
	21.46	39.77	1.77	35.14	98.14	"
	21.68	38.86	0.99	34.72	96.25	"
	20.92	40.64	0.83	34.42	96.81	"
	21.70	37.57	1.26	34.62	95.15	"
	20.52	40.89	0.63	35.12	97.16	"
	20.31	40.01	0.87	34.48	95.67	"
	20.87	39.49	0.95	34.36	95.67	"
	20.46	40.34	0.94	34.97	96.71	"
	20.28	43.71	--	36.45	100.44	Mn, Co, Cd, Ni
	21.08	42.62	--	36.54	100.24	"
	20.73	43.02	--	36.41	100.16	"
	21.23	42.94	--	36.50	100.67	"
	21.45	43.07	--	36.10	100.62	"
	21.29	43.43	--	36.95	101.67	"
	20.91	42.86	--	36.85	100.62	"
	21.80	42.78	--	36.75	101.33	"
	21.05	41.75	--	36.13	98.93	"
	21.18	41.29	36.29	98.76	Zn, Co., Ni, Cd, Mn	
	21.11	41.52	36.20	98.83		"
Average	21.22	42.88	35.89			

Bornite-Chalcocite

Black Forest

Sample No.	Cu	Fe	Zn	S	Total	Other elements
982-R-4	74.91	2.87	0.19	21.87	99.59	Cd, Ni, Mn, Co
	49.40	13.55	0.40	35.64	98.99	"
	70.12	8.06	0.06	24.98	103.22	"
	69.87	7.60	0.10	24.62	102.19	"
	69.34	7.74	--	24.48	101.56	"
	68.77	7.82	--	24.26	100.85	Cd, Mn, Ni, Co
	70.54	7.33	--	23.57	101.44	"
	70.99	6.99	--	24.52	102.50	"
	73.70	6.04	--	23.96	103.70	"
cross section of rim: inner edge	67.64	7.59	--	23.89	99.12	"
	62.35	7.45	--	23.21	93.01	"
	68.63	7.44	--	24.60	100.67	"
	69.43	7.05	--	24.21	100.69	"
	70.53	5.98	--	23.02	99.53	"
	71.81	5.21	--	23.27	100.29	"
	80.05	0.10	--	19.30	99.45	"
	73.75	4.23	--	22.73	100.71	"
	79.40	--	--	15.55	94.95	"
outer edge	78.43	1.03	--	20.97	100.43	"
	73.44	4.63	--	23.10	101.17	"
	72.16	5.10	--	23.55	100.81	"
	77.28	1.58	--	22.21	101.07	"

Intermediate Solid Solution

Vent site 1 of dive 981

Sample No.	Cu	Fe	Zn	S	Total	Other elements
981-R-3	31.20	32.45	0.96	35.39	100.11	Cd=o.11, Ni, Co, Mn
980-R-12	28.08	32.50	0.82	33.26	94.66	Pb
	27.56	32.44	1.45	34.45	95.90	"
	25.99	35.63	1.26	33.94	96.82	"
	30.28	31.93	0.74	33.85	96.80	"
	28.57	32.81	1.00	33.99	96.37	"
	23.16	36.09	1.59	34.79	95.63	"
981-R-2	23.70	37.31	0.98	33.98	95.97	"

Anomalous Bornite

Vent site 1 of dive 981

Sample No.	Cu	Fe	Zn	S	Total	Other elements
981-R-22	60.03	10.84	0.06	26.11	97.04	Pb
	59.39	10.97	--	26.28	96.64	"
	58.19	11.06	--	26.88	96.13	"
	58.58	10.94	0.11	26.84	96.47	"
	61.09	11.39	0.04	26.86	99.38	Pb
	60.31	11.45	0.09	27.30	99.15	"
	60.76	11.10	0.06	25.83	97.75	"
	59.94	10.98	0.08	26.77	97.77	"
	60.56	11.12	0.15	27.37	99.36	"
	61.05	10.90	0.08	26.30	98.33	"
	61.59	11.00	0.07	27.19	99.85	"
	59.42	11.27	--	27.49	98.35	Pb=0.17
	59.74	11.12	0.09	27.86	98.81	Pb
	61.78	9.84	--	26.78	98.40	"
	61.08	11.02	--	26.13	98.23	"
	61.09	11.39	--	26.86	99.34	"
	60.31	11.45	--	27.30	99.06	"
	60.56	11.12	--	27.37	99.05	"
	61.59	11.00	--	27.19	99.78	"

Anomalous Bornite

Vent site 1 of dive 981

Sample No.	Cu	Fe	Zn	S	Total	Other elements
981-R-16	61.22	9.14	--	30.57	100.93	Mn, Ni, Cd, Co
	60.20	8.85	--	30.33	99.38	"
	59.62	9.91	--	30.59	100.12	"
	60.01	10.03	--	30.61	100.65	"
	60.23	10.32	--	30.77	101.33	"
	60.13	10.17	--	30.77	101.61	"
	60.24	10.52	--	30.67	101.57	"
	58.08	11.84	--	31.38	101.30	"
	58.58	11.28	--	30.70	100.57	"
	59.98	10.38	--	30.72	101.08	"
	61.85	10.93	0.11	24.75	97.64	Pb
	60.63	10.56	0.07	26.03	97.29	"
	60.34	10.06	--	25.30	95.70	"
	60.69	10.61	--	25.73	97.03	"
	60.75	10.33	0.07	26.27	97.42	"
	60.88	10.61	--	26.01	97.50	"
	59.24	10.30	0.10	25.54	95.18	"
	60.59	10.79	0.12	25.62	97.12	"
	60.47	10.81	0.10	25.13	96.51	"
	61.16	10.66	0.13	24.71	96.66	"
	62.25	10.92	--	25.35	98.52	"
	61.08	11.17	0.11	25.94	98.30	"
	62.23	10.55	0.08	25.03	97.89	"
	62.08	10.73	0.13	25.70	98.78	Pb=0.14
	61.30	10.98	0.16	26.17	98.94	Pb=0.33
Average, 980-R-12	62.61	11.11	0.10	26.18		
Average, all others	60.67	10.88	0.03	28.43		
Average, all good analyses	60.81	10.81	0.03	28.35		

Covellite

Vent site 1 of dive 981

Sample No.	Cu	Fe	S	Total	Other elements
981-R-22	61.53	1.71	29.46	92.70	Zn, Pb

PbS

Vent S-3

Sample No.	Pb	Fe	S	Total	Otherelements
982-R-19	83.83	0.56	12.28	96.67	Zn, Cu
	82.56	0.37	12.14	95.07	"
	87.59	--	12.90	100.56	Zn=0.07, Cu
	85.63	0.33	12.92	98.88	Zn, Cu

(Zn,Fe)S

Vent S-3: One single elongate hexagon from interior lining

Sample No.	Zn	Fe	Mn	Cd	S	Total
982-R-19	51.14	14.04	0.10	0.21	34.76	100.25
	51.11	15.66	--	0.22	35.01	102.00
	51.59	15.62	0.13	0.19	34.66	102.19
	50.66	15.65	0.13	0.29	34.79	101.52
	49.50	16.97	0.14	0.21	34.76	101.58
	48.60	17.72	0.14	0.27	34.52	101.25
	50.32	15.98	0.12	0.30	34.92	101.64
	51.18	15.48	0.10	0.29	34.94	101.99
Average	49.73	15.65	0.11	0.25	34.27	

All analyses include Co, Ni, Cu.

Vent S-3: mixed sulfides, analyses including Mn and Cd

Sample No.	Zn	Fe	Mn	Cd	S	Total
982-R-19	49.23	15.76	0.10	0.29	34.94	100.32
	47.48	18.60	0.14	0.32	35.39	101.93
	48.16	17.47	0.12	0.34	35.28	101.37
	49.94	16.07	0.13	0.27	35.33	101.74
	47.18	18.85	0.13	0.34	34.97	101.47
	48.82	16.93	0.14	0.34	34.70	100.93
	47.14	18.67	0.13	0.27	35.09	101.30
	47.80	18.02	0.12	0.27	34.92	101.13
	52.34	14.28	0.11	0.25	34.56	101.54
	48.90	17.07	0.10	0.30	34.81	101.18
	49.88	16.85	0.10	0.31	35.39	102.53
	46.28	19.95	0.14	0.33	35.11	101.81
	45.79	19.87	0.14	0.34	34.96	101.10
	47.50	18.19	0.15	0.36	34.84	101.04
	49.84	15.99	0.13	0.29	34.79	101.04
	48.24	17.82	0.14	0.36	35.32	101.88
Average	47.74	17.28	0.13	0.31	34.55	

All analyses include Co, Ni, Cu.

Vent S-3; mixed sulfides, analyses not including Cd, Mn

Sample No.	Zn	Fe	S	Total	Other elements
982-R-19	52.11	13.78	33.20	99.19	Cu=0.10, Pb
	49.73	16.57	32.97	99.27	Cu, Pb
	49.71	15.05	33.43	98.19	"
	52.41	13.19	33.05	98.65	"
	51.16	15.01	33.22	99.39	"
	53.60	13.55	33.21	99.36	"
	52.55	13.64	33.84	100.03	"
	48.46	16.42	33.35	98.33	Cu=0.10, Pb
	53.49	12.39	32.36	98.24	Cu, Pb
	48.29	16.63	33.86	98.95	Cu=0.17, Pb
	56.36	9.94	32.95	99.25	Cu, Pb
	54.18	12.13	34.10	100.41	"
	54.24	12.42	33.70	100.36	"
	54.93	12.57	33.31	100.93	Cu=0.12, Pb
	49.37	16.59	33.40	100.40	Cu=1.04, Pb
	52.13	14.49	33.65	100.52	Cu=o.25, Pb
	54.71	12.58	32.87	100.16	Cu, Pb
	51.62	13.96	33.17	98.75	"
	51.64	13.14	32.38	97.16	"
	50.63	14.59	32.63	97.85	Cu,Pb
	48.13	15.73	32.27	96.13	"
	50.01	15.42	33.62	99.05	"
	50.24	15.07	33.46	98.77	"
	50.98	14.04	33.15	98.17	"
	48.80	16.51	33.78	99.09	"
	50.55	15.32	33.68	99.55	"
	49.89	15.69	33.27	98.85	"
	48.23	17.01	33.94	99.18	"
	49.92	16.12	34.39	100.53	"
Average	51.75	14.60	33.65		

Vent S-3: concentric ZnS, with PbS

Sample No.	Zn	Fe	Pb	Cu	S	Total
982-R-19	59.03	4.64	1.59	0.32	32.83	98.41
	57.51	5.70	1.39	--	30.66	95.26
	61.16	4.42	1.74	0.31	32.27	99.90
	61.20	3.47	2.55	0.53	32.15	99.90
	60.81	3.53	3.10	0.41	32.40	100.25
	63.58	3.23	2.04	0.13	31.98	101.06
	59.88	3.72	3.30	0.49	31.27	98.66
	59.02	3.64	3.05	0.75	31.60	98.06
	59.12	3.10	3.41	0.58	31.50	97.71
Average	60.88	4.00	2.49	0.39	32.24	

(Zn,Fe)S

Vent S-2: colloidal layer

Sample No.	Zn	Fe	Cu	Pb	S	Total
978-R-1	53.73	13.83	0.24	0.22	34.74	102.74
	55.70	11.69	0.34	0.37	32.98	101.08
	51.85	14.32	1.09	--	33.59	100.85
	56.29	10.71	0.85	0.41	34.30	102.56
	49.71	16.32	1.07	--	34.10	101.20
	53.75	12.76	0.17	--	32.51	99.19
	51.77	14.87	0.56	0.70	33.08	100.98
	62.96	5.02	0.10	2.94	33.06	104.08
	64.44	4.39	0.20	3.20	32.09	104.32
978-R-3	40.25	20.82	0.09	--	32.78	93.94
	46.13	17.52	0.09	--	33.38	97.12
	51.22	13.95	--	--	32.80	97.97
Average	52.89	12.96	0.40	0.65	33.11	

Vent S-2: wurtzite + pyrrhotite layer

Sample No.	Zn	Fe	Cu	S	Total	Other elements
978-R-3	49.04	15.15	0,11	33.20	97.49	Pb
	51.59	12.82	--	32.65	97.05	"
	46.99	16.47	--	33.18	96.66	"
	50.76	13.84	0.13	32.62	97.35	"
	47.27	15.89	--	32.14	95.30	"
	46.40	16.77	0.10	33.37	96.64	"
	49.18	13.58	0.08	32.82	95.66	"
	50.56	12.70	0.08	33.11	96.45	"
	48.86	13.46	0.34	33.31	95.97	Pb=0.13
	47.03	16.18	0.58	33.34	97.13	Pb
	51.65	11.99	0.83	33.50	97.97	"
	48.61	16.23	0.08	33.10	98.02	"
	51.70	13.33	0.06	33.55	98.64	"
	50.47	14.11	--	33.01	97.59	"
	52.20	12.13	--	32.45	96.78	"
Average	51.03	14.76	0.16	34.05		

Vent site 1 of dive 981: thin mixed sulfide layer

Sample No.	Zn	Fe	Cu	S	Total	Other
981-R-22	55.78	10.53	--	33.90	100.21	Pb
	54.26	11.42	0.68	33.23	99.59	"
981-R-16	55.39	8.46	0.24	33.71	97.94	Mn=0.13
	54.50	9.36	0.24	33.71	97.86	Mn=0.13
	54.27	9.55	0.46	33.86	98.26	Mn=0.11
	55.48	8.39	0.14	33.90	98.04	Mn=0.13
	54.90	10.04	--	33.96	99.02	Mn=0.13
	55.56	8.86	--	33.64	98.16	Mn=0.09
	54.78	9.74	--	33.95	98.59	Mn=0.13
	55.05	9.58	--	34.16	98.95	Mn=0.16
981-R-22	55.41	10.31	0.16	32.53	98.56	Pb
	55.78	10.53	0.07	33.90	100.28	"
	56.20	9.85	0.19	32.75	98.99	"
	54.26	11.42	0.68	33.23	99.59	Pb
981-R-2	60.80	7.39	0.23	31.90	100.32	"
	60.76	6.43	0.10	32.34	99.63	"
	59.62	7.85	0.12	32.43	100.02	"
	56.35	11.07	0.42	33.23	101.07	"
980-R-12-B	57.43	7.38	0.66	33.83	99.30	"
	53.48	10.06	0.96	33.26	97.76	"
	58.81	6.91	0.67	32.86	99.25	"
	63.09	3.62	0.48	34.07	101.26	"
	61.87	3.80	0.50	32.89	99.06	"
980-R-12-D	57.64	9.73	0.11	33.19	100.67	"
	55.95	10.84	0.34	32.97	100.10	"
	58.51	8.36	0.13	33.23	100.23	"
	57.69	9.99	0.33	33.88	101.89	"
	54.07	11.63	0.12	32.98	98.80	"
	61.83	6.89	0.50	33.46	102.68	"
	57.47	11.60	0.33	33.92	103.32	"
Average	57.31	9.00	0.34	33.35		

Analyses with Mn also include Cd, Co, Ni.

Vent site 1 of dive 981: thick mixed sulfide layer

Sample No.	Zn	Fe	Cu	S	Total	Other elements
980-R-12-N	58.92	8.51	0.33	33.37	101.13	Pb
	55.12	11.49	0.09	33.29	99.99	"
	52.56	13.12	0.44	32.95	99.07	"
	56.17	11.94	0.36	32.32	100.79	"
	57.46	10.92	0.25	32.46	101.09	Pb
	56.66	11.12	0.20	32.62	100.60	"
	53.56	12.59	0.19	32.58	98.92	"
	60.89	7.22	0.37	33.39	101.87	"
	57.01	10.51	0.09	33.06	100.67	"
	56.98	10.41	0.12	33.34	100.85	"
	61.97	6.98	0.26	33.39	102.91	Pb=0.31
	60.77	6.97	0.45	33.47	102.34	Pb=0.68
	58.29	9.25	0.93	33.81	102.28	Pb
	59.78	9.18	0.78	33.34	103.08	"
	57.99	8.30	0.27	32.77	99.33	"
	54.73	11.60	0.57	33.25	100.15	"
	57.52	9.70	0.07	33.09	100.38	"
	57.37	10.80	--	33.45	101.62	"
	56.90	11.22	0.10	33.62	101.84	"
Average	56.24	10.55	0.31	32.90		

Vent site 1 of dive 981: wurtzite with Cu-Fe sulfide replacement

Sample No.	Zn	Fe	Cu	Mn	S	Total
981-R-16	54.87	4.96	4.76	0.12	33.84	98.56
	45.43	9.95	9.81	0.11	33.96	99.25
	54.32	4.79	5.39	0.11	33.80	98.40
	52.75	10.09	1.31	0.14	34.00	98.29
	53.17	9.01	2.23	0.13	33.96	98.51
	53.41	9.20	1.52	0.13	33.95	98.21
	50.00	8.64	5.72	0.14	33.54	98.05
	51.29	7.63	5.77	0.15	33.56	98.40
	50.01	7.56	7.34	0.13	33.80	98.85
	52.00	8.30	4.06	0.13	33.83	98.31
	42.53	10.89	10.97	0.14	33.91	98.45
	45.12	10.07	9.55	0.13	33.91	98.77
	52.53	9.96	1.61	0.17	34.13	98.39
	50.48	10.39	2.85	0.12	34.24	98.08
	50.60	7.93	5.83	0.13	33.91	98.39
	44.97	10.32	8.13	0.16	33.79	97.36
	51.04	9.45	4.31	0.14	33.88	98.81
	55.04	9.04	1.84	0.11	34.34	100.76
	52.51	7.50	5.60	0.11	33.98	100.08
	48.56	11.73	6.41	0.12	34.34	101.48
	52.93	5.95	6.77	0.14	34.13	100.26
	54.53	8.30	3.40	0.12	34.51	101.18
	44.81	10.86	10.95	0.09	34.36	101.35

All analyses include Cd, Co, Ni.

(Zn,Fe)S

Vent site 1 of dive 981: wurtzite with Cu-Fe replacement

Sample No.	Zn	Fe	Cu	S	Total	
980-R-12	57.93	2.24	8.57	32.33	101.07	
	60.16	6.73	1.66	33.90	102.45	
	51.57	13.09	2.40	32.95	100.01	
	60.63	6.33	1.61	33.15	101.72	
	52.43	10.54	1.49	33.03	97.49	
	53.97	8.73	3.18	33.07	98.95	
	56.05	11.09	1.36	33.45	101.95	
	49.83	13.68	3.82	33.16	100.49	
	50.76	12.06	3.05	33.78	99.65	
	60.47	7.05	1.41	33.12	102.50	Pb=0.45
	54.50	9.59	1.66	32.52	98.27	
	55.93	9.54	1.79	33.79	101.05	
981-R-2	51.36	10.65	2.82	32.20	97.03	
981-R-22	50.34	13.66	1.31	33.26	98.57	
	53.61	10.59	1.31	33.03	98.54	
	50.91	10.31	6.45	33.79	101.46	
981-R-16	36.25	6.14	27.94	31.30	101.69	

All analyses include Pb.

Anhydrite

Vent S-2: massive anhydrite

Sample No.	CaO	SrO	SO_3	Total	Other elements
978-R-3	41.58	0.46	57.15	99.19	Ba, Pb
	42.21	0.34	58.78	101.33	"
	41.46	0.38	58.45	100.29	"
	41.54	0.21	58.45	100.20	"
	41.54	0.30	58.25	100.09	"
	41.15	0.57	57.78	99.50	"
	41.28	0.27	58.13	99.68	"
	41.36	0.32	58.08	99.76	"
	38.41	0.35	53.11	91.87	"
	41.09	0.25	57.15	98.49	Ba, Pb
	40.81	0.40	58.28	99.49	"
	41.68	0.24	57.83	99.75	"
	41.99	0.19	58.63	100.81	"
	40.59	0.31	58.13	99.03	"
	32.87	0.39	53.41	86.67	"
	41.05	--	58.08	99.13	"
	38.58	0.22	59.30	98.10	"
	40.44	0.12	58.68	99.24	"
	38.41	0.27	59.13	97.81	"
	41.31	--	59.44	100.85	BaO=0.09, Pb
	39.74	--	57.45	97.19	Ba, Pb
	40.49	--	57.69	98.18	"
	41.03	--	58.99	100.02	"
Average	41.06	0.24	58.70		

Vent S-2: anhydrite in wurtzite-cubanite mixture

Sample No.	CaO	SO_3	Total	Other elements
978-R-3	40.08	59.37	99.45	Sr, Ba, Pb
	40.34	59.79	100.13	"
	39.26	58.23	97.49	"
	38.71	57.27	95.98	"
	39.58	58.73	98.31	"
	40.27	59.55	99.82	"
	39.82	60.34	100.16	"
Average	40.22	59.78		

Vent S-2: anhydrite in colloidal layer

Sample No.	CaO	SO_3	Total	Other elements
978-R-3	38.13	57.35	95.48	Ba, Sr, Pb
	37.21	55.89	93.10	"
	36.70	56.41	93.11	"
	37.90	56.24	94.14	"
	35.86	55.19	91.05	"
	38.59	58.23	96.82	"
	38.08	56.64	94.73	"
Average	39.87	60.13		

Vent S-3

Sample No.	CaO	SO_3	Total	Other elements
982-R-19	35.72	53.54	89.33	BaO=0.07, Sr, Pb
	37.09	53.22	92.31	Ba, Sr, Pb
	37.36	55.75	93.12	"
	37.52	56.35	93.87	"
	33.92	51.52	85.49	"
	36.21	54.26	90.47	"
Average	40.15	59.85		

Vent site 1 of dive 980

Sample No.	CaO	SO_3	Total	Other elements
980-R-7	29.10	45.39	75.21	SrO=0.72, Ba, Pb
	29.37	45.17	74.54	Sr, Ba, Pb
980-R-7	30.48	47.40	77.88	Sr, Ba, Pb
	31.29	46.97	78.26	"
	28.65	46.99	75.64	"
	24.79	41.18	65.97	"
Average	38.87	61.13		

Black Forest: massive anhydrite

Sample No.	CaO	SrO	SO_3	Total	Other elements
982-R-2	41.23	0.26	57.78	99.27	Ba, Pb
	41.35	0.27	57.75	99.37	"
	41.42	0.21	57.78	99.41	"
	41.00	0.48	57.88	99.36	"
	41.04	0.13	58.10	99.27	"
	41.54	0.13	57.68	99.35	"
	41.42	0.13	57.80	99.35	"
Average	41.56	0.23	58.20		

Black Forest: anhydrite inclusions in sulfide layers

Sample No.	CaO	SrO	SO_3	Total	Other elements
982-R-2	41.19	0.46	57.70	99.35	Ba, Pb
	40.38	0.59	57.15	98.12	"
	40.87	0.51	58.13	99.51	"
	40.35	0.93	57.78	99.06	"
	40.67	0.45	57.13	98.25	"
	41.22	0.18	57.53	98.93	"
Average	41.25	0.53	58.23		

Mg silicates

Vent S-2

Sample No.	FeO	MgO	SiO_2	Total	Other elements
979-R-3	0.54	34.02	38.49	73.05	Na, K, Ca, Al
	0.25	34.92	41.83	77.00	"
	1.40	32.18	38.88	72.46	"
	0.31	31.58	41.77	73.66	"
	0,25	33.11	42.29	75.65	"
	4.27	32.19	40.18	76.64	"
	0.60	33.85	42.42	76.87	"
	3.29	32.65	36.99	72.93	"
	0.49	35.45	43.20	79.14	"

Black Forest

Sample No.	FeO	MgO	SiO_2	Total	Other elements
982-R-2	3.33	31.13	43.53	77.99	Na,K, Ca, Al
	2.66	30.32	50.44	83.42	"
	1.80	30.26	54.45	86.51	"
	2.20	32.60	53.67	88.47	"
	1.99	32.51	58.10	92.60	"
	2.30	34.24	54.88	91.42	"
	1.46	38.32	43.67	83.45	"
	3.80	27.59	35.75	67.14	"

Appendix B: f_{S_2} - f_{O_2} diagrams

Mineral stability fields

Mineral stability fields in the Cu-Fe-S-O system were constructed using equilibrium constants for the following equilibria fromDrummond (1981) (reference 1) and Barton and Skinner (1979) (reference 2)

Reaction	Reference
$1/3\ Fe_3O_4(xl)+2H^+=Fe^{++}+H_2O(l)+1/6O_2(g)$	1
$FeS(xl)+2H^+=Fe^{++}+H_2S$	1
$FeS_2(py)+2H^++H_2O(l)=Fe^{++}+2H_2S+1/2O_2(g)$	1
$CuFeS_2(xl)+H^++1/4O_2(g)=FeS_2+1/2H_2O(l)+Cu^+$	1
$1/4Cu_5FeS_4(xl)+H^+=1/4CuFeS_2(xl)+1/2H_2S+Cu^+$	1
$4Cu+S_2(g)=2Cu_2S$	2
$2Cu+S_2(g)=2CuS$	2
$2Cu_2S+S_2(g)=4CuS$	2
$Cu+Fe+S_2(g)=CuFeS_2$	2
$5/2Cu+1/2Fe+S_2(g)=1/2Cu_5FeS_4$	2
$3/2Fe+O_2(g)=1/2Fe_3O_4$	2
$4Fe_3O_4+O_2(g)=6Fe_2O_3$	2
$8/13Fe_2O_3+S_2(g)=10/13FeS_2+6/13FeSO_4$	2
$H_2S+1/2O_2(g)=1/2S_2(g)+H_2O(l)$	1
$1/2S_2(g)=S(xl)$ or $S(l)$	1

f_{S_2} - f_{O_2} calculations: (1)□

S_R, = total reduced sulfur, is assumed to equal H_2S from the hot endmember

S_{ox}, = total oxidized sulfur, is assumed to equal $SO_4^=$ from seawater

both S_R and S_{OX} are calculated based on linear mixing between the two endmembers

then an ideal f_{S_2} - f_{O_2} is calculated assuming equilibrium among sulfur species, as follows:

$$\Sigma S = H_2S + HS^- + S^= + H_2SO_4 + HSO_4^- + SO_4^=$$

$$\Sigma S_{OX} = H_2SO_4 + HSO_4^- + SO_4^=$$

$$\Sigma S_R = H_2S + HS^- + S^=$$

$H_2S = HS^- + H^+$ K1 } S_R

$HS^- = S^= + H^+$ K2

$H_2SO_4 = HSO_4^- + H^+$ K3

$HSO_4^- = SO_4^= + H^+$ K4 } S_{OX}

$H_2S + 2O_2(g) = HSO_4^- + H^+$ K7

write all species in terms of $[H_2S]$:

$$K1 = \frac{[HS^-][H^+]}{[H_2S]} \qquad [HS^-] = \frac{(K1)[H_2S]}{[H^+]} = \frac{(K1)}{[H^+]}[H_2S]$$

$$K2 = \frac{[S^=][H^+]}{[HS^-]} \qquad [S^=] = \frac{(K2)[HS^-]}{[H^+]} = \frac{(K1)(K2)}{[H^+]^2}[H_2S]$$

$$K7 = \frac{[HSO_4^-][H^+]}{[H_2S]f_{O_2}^2} \qquad [HSO_4^-] = \frac{(K7)(f_{O_2}^2)}{[H^+]}[H_2S]$$

$$K4 = \frac{[SO_4^=][H^+]}{[HSO_4^-]} \qquad [SO_4^=] = \frac{(K4)[HSO_4^-]}{[H^+]} = \frac{(K4)(K7)(f_{O_2}^2)}{[H^+]^2}[H_2S]$$

$$K3 = \frac{[HSO_4^-][H^+]}{[H_2SO_4]} \qquad [H_2SO_4] = \frac{[H^+][HSO_4^-]}{(K3)} = \frac{(K7)(f_{O_2}^2)}{(K3)}[H_2S]$$

derive f_{O_2}:

$$\Sigma S_R = [H_2S]\left[1 + \frac{(K1)}{[H^+]} + \frac{(K1)(K2)}{[H^+]^2}\right] = S_R$$

$$\Sigma S_{ox} = [H_2S]\left\{\frac{(K7)(f_{O_2}^2)}{(K3)} + \frac{(K7)(f_{O_2}^2)}{[H^+]} + \frac{(K4)(K7)(f_{O_2}^2)}{[H^+]^2}\right\} = S_{ox}$$

$$S_R / S_{ox} = \frac{[H_2S]\ \dfrac{[H^+]^2+(K1)[H^+]\ (K1)(K2)}{[H^+]^2}}{[H_2S]\ \dfrac{(K7)(f_{O_2}^2)[H^+]^2+(K7)(f_{O_2}^2)(K3)[H^+]+(K4)(K7)(f_{O_2}^2)(K3)}{[H^+]^2(K3)}}$$

$$S_R/S_{ox} = \frac{[H^+]^2+(K1)[H^+]+(K1)(K2)}{[H^+]^2} \times$$

$$\frac{[H^+]^2(K3)}{(K7)(f_{O_2}^2)[H^+]^2+(K7)(f_{O_2}^2)(K3)[H^+]+(K4)(K7)(f_{O_2}^2)(K3)}$$

$$= \frac{(K3)}{(K7)(f_{O_2}^2)} \cdot \frac{[H^+]^2+(K1)[H^+]+(K1)(K2)}{[H^+]^2+(K3)[H^+]+(K4)K(3)}$$

$$f_{O_2}^2 = \frac{1}{S_R/S_{ox}} \cdot \frac{(K3)}{(K7)} \cdot \frac{[H^+]^2+(K1)[H^+]+(K1)(K2)}{[H^+]^2+(K3)[H^+]+(K4)(K3)}$$

$$2 \log f_{O_2}^2 = \log K3 - \log K7 - \log({}^{S_R}/_{S_{ox}}) + \log \{ [H^+]^2 + (K1)[H^+] + (K1)(K2) \} - \log \{ [H^+]^2 + (K3)[H^+] + (K4)(K3) \}$$

define: $A = (H^+]^2 + (K1)[H^+] + (K1)(K2)$

$$B = [H^+]^2 + (K3)[H^+] + (K4)(K3)$$

$$\log f_{O_2}^2 = 1/2 \{ \log K3 - \log K7 - \log ({}^{S_R}/_{S_{ox}}) + \log A - \log B \}$$

derive f_{S_2}:

$$\Sigma S = [H_2S]\{1 + \frac{(K1)}{[H^+]} + \frac{(K1)(K2)}{[H^+]^2} + \frac{(K7)(f_{O_2}^2)}{(K3)} + \frac{(K7)(f_{O_2}^2)}{[H^+]} + \frac{(K4)(K7)(f_{O_2}^2)}{[H^+]^2} \}$$

$$[H_2S] = \Sigma S \; / \; \{ \; \frac{[H^+]^2(K3)+(K1)(K3)[H^+]+(K1)(K2)(K3)}{(K3)[H^+]^2}$$

$$+ \frac{(K7)(f_{O_2}^2)[H^+]^2+(K7)(f_{O_2}^2)(K3)[H^+]}{(K3)[H^+]^2}$$

$$+ \frac{(K4)(K7)(f_{O_2}^2)(K3)}{(K3)[H^+]^2} \; \} \; .$$

define: $C = [H^+]^2(K3)+(K1)(K3)[H^+]+(K1)(K2)(K3)$

$$+ (K7)(f_{O_2}^2)[H^+]^2+(K7)(f_{O_2}^2)(K3)[H^+]$$

$$+ (K4)(K7)(K3)(f_{O_2}^2)$$

$$\log [H_2S] = \log(\Sigma S) + \log(K3) + 2 \log [H^+] - \log C$$

$$H_2S + 1/2O_2(g) = 1/2S_2(g) + H_2O(l) \qquad KS_2$$

$$KS_2 = {f_{S_2}^{1/2}}[H_2O] / [H_2S]\ f_{O_2}^{1/2} = f_{S_2}^{1/2} / f_{O_2}^{1/2}[H_2S]$$

when $a_{H_2O} \approx 1$.

$$[H_2S] = f_{S_2}^{1/2} / (f_{O_2}^{1/2})(KS2)$$

$$\log [H_2S] = 1/2 \log f_{S_2} - 1/2 \log f_{O_2} - \log (KS2)$$

$$\log f_{S_2} = 2 \log [H_2S] + \log f_{O_2} + 2 \log (KS2)$$

For temperatures below 350°C, values for H_2S and $SO_4^{=}$ were calculated based on linear mixing curves between hydrothermal fluid at 350°C and seawater at 0°C. Both S_R and S_{OX} did vary linearly with temperature in mixed solutions collected at 21°N in 1979. However, better values for H_2S in the hot fluid were obtained from new samples collected in 1981 (K. von Damm, personal communication). Consequently, the values in the mixed solutions have been calculated based on the new data.

At 350°C, S_{OX} = "0". Since some undetectably small quantity of oxidized sulfur must be present, the possible range of conditions at 350°C has been simulated by varying the S_R/S_{OX} ratio. The f_{S_2} - f_{O_2} values obtained in this way define a line of constant S; the f_{S_2} - f_{O_2} conditions in the pure 350°C fluid should fall somewhere along that line. A likely location is the pyrite-pyrrhotite border, at $S_R/S_{OX} = \sim 10^{10}$,

as explained in the text.

This method of obtaining an f_{S_2} - f_{O_2} pair does assume that reaction takes place among reduced sulfur species and among oxidized sulfur species. However, because S_R/S_{OX} and ΣS are fixed, it also assumes that no exchange occurs between reduced and oxidized species.

	100°C	150°C	200°C	250°C	300°C
$[H_2S]$, mmol/kg	2.57	3.86	5.14	6.43	7.71
$[SO_4^{=}]$ mmol/kg	19.97	15.98	11.98	7.99	3.99
S_R/S_{ox}	0.129	0.242	0.429	0.805	1.932
ΣS mmol/kg	22.54	19.84	17.12	14.42	11.70
pH	5.625	5.176	4.85	4.5	4.23
log K1*	-6.48	-6.62	-7.00	-7.54	-8.22
log K2*	-11.48	-11.14	-11.11	-11.30	-11.65
log K7*	97.28	82.74	71.06	61.40	53.24
log K4*	-3.03	-3.70	-4.38	-5.06	-5.74
log K3*	3.10	2.12	1.20	0.33	-0.51
log KS2*	23.13	19.98	17.46	15.37	13.62
(1) log A	-11.19	-10.34	-9.70	-9.00	-8.46
log B	0.07	-1.566	-3.05	-4.06	-4.725
log f_{O_2}	-52.28	-44.39	-38.07	-32.96	-28.89
log C	-7.16	-7.51	-7.98	-8.32	-8.79
calculated log $[H_2S]$	-2.637	-2.42	-2.29	-2.19	-2.11
log f_{S_2}	-11.29	-9.27	-7.73	-6.60	-5.87

*from Drummond (1981)

350°C			
H_2S, mmol/kg	9	9	9
S_R/S_{OX}	$10^6/1$	$10^{10}/1$	$10^{20}/1$
ΣS mmol/kg	9	9	9
pH	3.4	3.4	3.4
log K1*	-8.98		
log K2*	-12.13		
log K7*	46.22		
log K4*	-6.42		
log K3*	-1.32		
log KS2*	12.11		
(1) log A	-6.80	-6.80	-6.80
log B	-4.72	-4.72	-4.72
log f_{O_2}	-27.81	-29.81	-34.81
log C	-8.12	-8.12	-8.12
calculated log $[H_2S]$	-2.046	-2.046	-2.046
log f_{S_2}	-7.68	-9.68	-14.68

(2) $\Delta: f_{O_2}$ based on $[CH_4], [CO_2]$

CH_4 given in cc(STP)/kg

molar volume of CH_4 at STP = 22.356 l/mol (Riley and Skirrow, 1975)

if 1 cc = 1 ml,

then 1 cc = 1 ml $\left(\frac{1c}{10^3 ml}\right)\left(\frac{1}{22.356}\right)\left(\frac{mol}{1}\right) = 4.473 \times 10^{-5}$ mol

$$CH_4 + 2O_2(g) = CO_2 + 2H_2O(l) \qquad K9$$

$$K9 = [CO_2][H_2O]^2 / [CH_4](f_{O_2}^2) \cong \frac{[CO_2]}{[CH_4](f_{O_2}^2)}$$

$$f_{O_2}^2 = [CO_2] / [CH_4](K9)$$

$$\log f_{O_2}^2 = 1/2 \{\log [CO_2] - \log [CH_4] - \log (K9)\}$$

CH_4 and CO_2 measurements are from Craig et al. (1980).

$CH_4 + 2O_2(g) = CO_2 + 2H_2O(l)$: Equilibrium constant from Drummond (1981)

(3) O: f_{O_2} based on $[H_2]$

$H_2 = H_2(g)$ K_H

$K_H = {}^{f_{H_2}}/_{[H_2]}$ f_{H_2} in atm, $[H_2]$ = molality

$$\ln K_H = 5.91+(0.01632)T+{}^{(-350.0)}/_{T}+(-2.769 \times 10^{-5})T^2$$

$$+ 0.1011$$ from Drummond (1981)

$f_{H_2} = (K_H)[H_2]$

$H_2O(l) = H_2(g) + 1/2O_2(g)$ K39 (from Drummond, 1981)

$$K39 = {}^{f_{H_2} \cdot f_{O_2}^{1/2}}/_{[H_2O]} = f_{H_2} \cdot f_{O_2}^{1/2}$$

$$f_{O_2}^{1/2} = {}^{K39}/_{f_{H_2}}$$

$$\log f_{O_2} = 2\{\log(K39) - \log(f_{H_2})\}$$

$[H_2]$ measured in cc(STP)/kg

$$\text{mol/kg} = \frac{\text{ccSTP}}{22{,}414} \text{ / kg}$$

H_2 measurements are from Craig et al. (1980).

(2) $[CH_4]$ cc(STP)/kg	0.36	0.748	1.138*	1.33*
$[CH_4]$ µmol/kg	16.10	33.46	50.90	59.49
$[CO_2]$ µmol/kg	3293	4262	5231	5716*
log K9	113.21	86.82	69.810	63.41
Δ: log f_{O_2}	-55.45	-42.36	-33.90	-30.71
(3) $[H_2]$ cc(STP)/kg	5.739	11.913	18.064*	21.17*
$[H_2]$ µmol/kg	256.1	531.5	805.9	944.5
log K_H	3.174	2.951	2.458	2.115
log f_{H_2}	-0.418	-0.324	-0.636	-0.910
log K39	-31.547	-23.193	-17.813	-15.79
○: log f_{O_2}	-62.26	-45.74	-34.35	-29.76

*extrapolated

CH_4, CO_2 and H_2 measurements were made by Craig et al. (1980) in mixed solutions collected at 21°N in november 1979; the only calculations involved are the extrapolations to the high temperature endmember solution.

Appendix C: Solubility of pyrite and pyrrhotite and construction of Mg-silicate diagrams

Pyrite Solubility, 350°C

at 350°C, Fe in solution is predominantly present as $FeCl_2$:

$$Fe^{++} + 2Cl^- = 2FeCl_2 \qquad \log K_{FeCl_2} = 4.5 \text{ (Crerar et al., 1978)}$$

$$K_{FeCl_2} = {}^{[FeCl_2]}/_{[Fe^{++}][Cl^-]^2}$$

$${}^{[FeCl_2]}/_{[Fe^{++}]} = (K_{FeCl_2})([Cl^-]^2)$$

The stoichiometric ion activity coefficient for Cl^- at 350°C is ca. 0.18 (Crerar and Barnes, 1976).

Therefore ${}^{[FeCl_2]}/_{[Fe^{++}]} = 10^{2.48}$

If all Fe is considered to occur as $FeCl_2$, then, for pyrite,

$$FeS_2 + 2H^+ + 2Cl^- + H_2O(l) = FeCl_2 + 2H_2S + \tfrac{1}{2}O_2(g)$$

$$K_1 = {}^{[FeCl_2][H_2S]^2 f_{O_2}^{1/2}}/_{[H^+]^2[Cl^-]^2}$$

$$\log K_1 = -9.4 \text{ (Crerar et al., 1978)}$$

However, in order to apply this relationship, an *in situ* pH is needed in place of the measured quench pH.

Crerar and Barnes (1976) and Crerar et al. (1978) calculated pH from the dissolved CO_2 concentration in their experimental fluids; a pH for 350°C will be calculated here

based on the dissolved CO_2 extrapolated from that measured by Craig et al. (1980), for use in this relationship and the pyrrhotite solvation reaction.

From the partial pressure of CO_2, pH can be obtained by using the relationship

$$(H^+)^2 = \frac{2K_{H_2CO_3}K_{HCl}[H_2CO_3]}{2K_{HCl}-K_{NaCl}+(K^2_{NaCl}+4K_{NaCl}\ \Sigma Na)^{\frac{1}{2}}} \times \left[\ 1.0 + \frac{-K_{NaCl}+(K^2_{NaCl}+4K_{NaCl}\Sigma Na)^{\frac{1}{2}}}{2K_{NaHCO_3}}\ \right]$$

derived in Crerar et al., 1978

K_{NaHCO_3} is approximated by K_{NaCl}; the maximum error in pH caused by this approximation is ca. 5% if K_{NaHCO_3} = infinity (Crerar et al., 1978).

at 350°C,

log $K_{H_2CO_3}$ = -8.27 (Drummond, 1981)

log K_{HCl} = -2.52 (Drummond, 1981)

log $NaHCO_3$ and log K_{NaCl} = -0.93 (Drummond, 1981)

$[H_2CO_3]$ = ca. 5.716 mmol/kg (Craig et al., 1980)

ΣNa = ca. 0.5 mol/kg (K. von Damm, personal communication)

therefore,

$\log (H^+)^2 = -11.9024$

and

pH = 5.95

Returning to the pyrite solvation reaction,

$$FeS_2 + 2H^+ + 2Cl^- + H_2O(l) = FeCl_2 + 2H_2S + \tfrac{1}{2}O_2(g),$$

$$K_1 = [FeCl_2][H_2S]^2 f_{O_2}^{\frac{1}{2}} / [H^+]^2[Cl^-]^2$$

Therefore, the Fe concentration in solution required for pyrite saturation is

$$[FeCl_2] = K_1[Cl^-]^2[H^+]^2 / [H_2S]^2 f_{O_2}^{\frac{1}{2}}$$

$[FeCl_2]$ = 1.5 mmol/kg when

$[Cl]$ = 0.5 mol/kg (K. von Damm, personal communication)

$[H_2S]$ = 9 mmol/kg (K. von Damm, personal communication)

$f_{O_2} = 10^{-30}$ (from Appendix A)

Since the measured Fe concentration at 350°C is ca. 1765 µmol/kg, pyrite apparently is saturated in the solutions

Pyrrhotite Solubility, 350°C

The equivalent reaction for pyrrhotite is:

$$FeS + 2H^+ + 2Cl^- = FeCl_2 + H_2S \qquad \log K_2 = 7.5$$

(Crerar et al., 1978).

$$K_2 = [FeCl_2][H_2S] / [H^+]^2[Cl^-]^2$$

and

$$[FeCl_2] = K_2[H^+]^2[Cl^-]^2 / [H_2S]$$

Substituting in the values above gives an Fe concentration at saturation of 1.1 mmol/kg.

Pyrrhotite is therefore also saturated in the fluid; the agreement between the Fe concentrations is a consequence of the pyrite-pyrrhotite equilibrium in the fluid.

An estimation of the concentration of Cu required in solution in order to achieve saturation with chalcopyrite can also be obtained using the approximate in situ pH of 6.8, and the conditions given above:

Cu is predominantly present as CuCl:

$$Cu^+ + Cl^- = CuCl \qquad \log K_{CuCl} = 2.7 \pm 0.6 \text{ at } 350°C$$

(Crerar and Barnes, 1976)

$$\frac{[CuCl]}{[Cu^+]} = K_{CuCl}[Cl^-] = 10^{1.65} \cong 45$$

therefore

$$CuFeS_2 + H^+ + \tfrac{1}{4}O_2(g) + Cl^- = FeS_2 + \tfrac{1}{2}H_2O(l) + CuCl$$

$$\log K_3 = 10 \text{ at } 350°C \quad \text{(Crerar and Barnes, 1976)}$$

$$K_3 = {}^{[CuCl]}/_{[H^+]\ f_{O_2}^{1/4}\ [Cl^-]}$$

$$[CuCl] = K_3(f_{O_2}^{1/4})\,[H^+]\ a_{Cl^-}$$

$$= 32 \quad \mu mol/kg.$$

The tentative determinations of total Cu in the vent fluids collected in 1979 fell in a range between 1 and 20 μmol/kg. It appears that chalcopyrite may also be saturated in the fluid at 350°C.

Mg-Silicate diagrams:

Brucite, chrysotile, and talc equilibrium constants were derived from ΔG_f° and ΔS_f° for brucite, talc, chrysotile, Mg^{++}, H_4SiO_4, H^+, and H_2O taken from Hemley et al. (1977).

Concentrations of Mg^{++} and SiO_2 (= H_4SiO_4) were calculated on the basis of a linear mixing trend, assuming that Mg^{++} in seawater = 53 mmol/kg, and SiO_2 in seawater = 0.048 mmol/kg (Holland, 1978), and that Mg^{++} in 350° fluid = 0 and SiO_2 in 350° fluid = 21.5 mmol/kg (Edmond et al. 1982)

(see Table II.1 for hydrothermal fluid compositions).

for talc: $Mg_3Si_4O_{10}(OH)_2 + 4H_2O + 6H^+ = 3Mg^{++} + 4H_4SiO_4$

$$K_{talc} = [Mg^{++}]^3[H_4SiO_4)^4 / [H^+]^6$$

for chrysotile: $Mg_3Si_2O_5(OH)_4 + 6H^+ = 3Mg^{++} + 2H_4SiO_4 + H_2O$

$$K_{chr} = [Mg^{++}]^3[H_4SiO_4]^2 / [H^+]^6$$

for brucite: $Mg(OH)_2 + 2H^+ = Mg^{++} + 2H_2O$

$$K_{br} = [Mg^{++}] / [H^+]^2$$

$\Delta G = -RT\ln K$

$$\Delta G^T_{reaction} = \Delta G_f^\circ(25°C)_{products} - G_f^\circ(25°C)_{reactants}$$

$$- \int_{25}^{T} \Delta S^\circ_{f,s} dT$$

calculating $\Delta G^T_{reaction}$ at each T allows calculation of K at each T.

Amorphous silica solubilities in 0.5 molar NaCl solution were taken from Chen and Marshall (1982);

Quartz solubilities in water were taken from Holland (1979). The difference in quartz solubility between water and 0.5 m NaCl solution were assumed to be very minor; the differ-

ence in amorphous silica solubility was minor.

	100°C	150°C	200°C	250°C	300°C
ΔG_{chr}	-41.780	-40.574	-39.369	-38.163	-36.958
$\log K_{chr}$	24.48	20.97	18.19	15.95	14.10
ΔG_{talc}	-27.119	-25.348	-23.577	-21.806	-20.035
$\log K_{talc}$	15.89	13.10	10.90	9.11	7.64
ΔG_{br}	-22.453	-22.209	-21.966	-21.722	-21.479
$\log K_{br}$	13.16	11.48	10.15	9.08	8.19
$\log [Mg^{++}]/[H^{+}]^2$	9.83	8.83	8.06	7.18	6.33
$\log [SiO_2]$	-2.21	-2.03	-1.91	-1.81	-1.73
log[Amorphous silica], saturated	-2.21	-2.00	-1.83	-1.70	-1.58
log[Quartz] saturated	-3.01	-2.63	-2.34	-2.08	-1.59

Acknowledgements

I would like to be able to thank all of the people who contributed to the development of this research and helped make it all happen, but I can only single out the major ones. The United States - Japan Cooperative Research Project on the Genesis of Volcanogenic Massive Sulfide Deposits, otherwise known as the Kuroko Project, provided funding for the work through NSF Grant EAR81-09270. The other members of the Kuroko Project were willing and eager to discuss any aspects of this work and to make comparisons with ore deposits with which they were familiar. In particular, Dr. Paul Barton of the U.S.G.S., Dr. Steven Scott of the University of Toronto, and Stewart Eldridge of the Pennsylvania State University contributed extensive discussions of sulfide geochemistry, ore textures, and comparisons between their samples and mine.

At Harvard University, where most of this work was done, the graduate students, staff, and faculty were generous and helpful. They taught me to use and helped me out of break-downs on the SEM at the Smithsonian Astrophysical Observatory and the ARL microprobe. After the arrival of the Cameca probe, Dave Lange both taught me how to use it and found me sufficient time to make all my analyses. Harvard also provid-ed me with room to work for two years. Dave Converse helped me develop and sharpen my concept of the formation of the 21°N

vents by discussion and by his writing and rewriting of our joint paper; he also drew figures illustrating chimney growth and the chimney-mound cycle which are far better than any of my attempts. Annetta Synar typed the manuscript both accurately and quickly, even when it grew much longer than anticipated.

At MIT, Dr. John Edmond helped me get involved in the work at 21°N in the first place. He and Karen von Damm were generous with their own information from the water samples they were studying, and Dr. Edmond also provided a range of information on each new area of hydrothermal activity discovered after 21°N.

I would like to thank my parents for their continual support, especially over the last year of this project.

This thesis would never even have been started without the help of Dr. Roger Burns of MIT and Dr. Heinrich Holland of Harvard University. Dr. Burns provided support and unfailing encouragement throughout. Dr. Holland found me a place in the 21°N project and guided me through the research. He provided advice and commentary on all aspects of the work, including several critical readings of the manuscript, and a considerable amount of useful debate as my ideas developed. Without these two advisors this thesis would not exist.

Finally, I would like to thank my husband, Rick, who lived through all the stages of graduate school and thesis-writing along with me, and always believed that I could do it all.